SSC-357

CARBON EQUIVALENCE AND WELDABILITY OF MICROALLOYED STEELS

SHIP STRUCTURE COMMITTEE

1991

SHIP STRUCTURE COMMITTEE

The SHIP STRUCTURE COMMITTEE is constituted to prosecute a research program to improve the hull structures of ships and other marine structures by an extension of knowledge pertaining to design, materials, and methods of construction.

RADM J. D. Sipes, USCG, (Chairman)
Chief, Office of Marine Safety, Security
  and Environmental Protection
U. S. Coast Guard

Mr. Alexander Malakhoff
Director, Structural Integrity
  Subgroup (SEA 55Y)
Naval Sea Systems Command

Dr. Donald Liu
Senior Vice President
American Bureau of Shipping

Mr. H. T. Haller
Associate Administrator for Ship–
  building and Ship Operations
Maritime Administration

Mr. Thomas W. Allen
Engineering Officer (N7)
Military Sealift Command

CDR Michael K. Parmelee, USCG,
Secretary, Ship Structure Committee
U. S. Coast Guard

CONTRACTING OFFICER TECHNICAL REPRESENTATIVES

Mr. William J. Siekierka
SEA 55Y3
Naval Sea Systems Command

Mr. Greg D. Woods
SEA 55Y3
Naval Sea Systems Command

SHIP STRUCTURE SUBCOMMITTEE

The SHIP STRUCTURE SUBCOMMITTEE acts for the Ship Structure Committee on technical matters by providing technical coordination for determinating the goals and objectives of the program and by evaluating and interpreting the results in terms of structural design, construction, and operation.

AMERICAN BUREAU OF SHIPPING

Mr. Stephen G. Arntson (Chairman)
Mr. John F. Conlon
Dr. John S. Spencer
Mr. Glenn M. Ashe

MILITARY SEALIFT COMMAND

Mr. Albert J. Attermeyer
Mr. Michael W. Touma
Mr. Jeffery E. Beach

MARITIME ADMINISTRATION

Mr. Frederick Seibold
Mr. Norman O. Hammer
Mr. Chao H. Lin
Dr. Walter M. Maclean

NAVAL SEA SYSTEMS COMMAND

Mr. Robert A. Sielski
Mr. Charles L. Null
Mr. W. Thomas Packard
Mr. Allen H. Engle

U. S. COAST GUARD

CAPT T. E. Thompson
CAPT Donald S. Jensen
CDR Mark E. Noll

SHIP STRUCTURE SUBCOMMITTEE LIAISON MEMBERS

U. S. COAST GUARD ACADEMY

LT Bruce Mustain

U. S. MERCHANT MARINE ACADEMY

Dr. C. B. Kim

U. S. NAVAL ACADEMY

Dr. Ramswar Bhattacharyya

STATE UNIVERSITY OF NEW YORK MARITIME COLLEGE

Dr. W. R. Porter

WELDING RESEARCH COUNCIL

Dr. Martin Prager

NATIONAL ACADEMY OF SCIENCES – MARINE BOARD

Mr. Alexander B. Stavovy

NATIONAL ACADEMY OF SCIENCES – COMMITTEE ON MARINE STRUCTURES

Mr. Stanley G. Stiansen

SOCIETY OF NAVAL ARCHITECTS AND MARINE ENGINEERS – HYDRODYNAMICS COMMITTEE

Dr. William Sandberg

AMERICAN IRON AND STEEL INSTITUTE

Mr. Alexander D. Wilson

Ship Structure Committee

An Interagency Advisory Committee
Dedicated to the Improvement of Marine Structures

January 31, 1991

CARBON EQUIVALENCE AND WELDABILITY OF MICROALLOYED STEELS

With the development of new technology steels, it is important that welding procedures used during fabrication are investigated and validated with regard to factors such as preheating, postweld heat treating, and heat affected zone hardness. This report presents the results of a project to determine the validity of carbon equivalent formulas used to predict the weldability of high yield strength, low carbon content, microalloyed steels. This information should be beneficial as we incorporate the new technology steels in the design of advanced marine structures.

J. D. SIPES
Rear Admiral, U.S. Coast Guard
Chairman, Ship Structure Committee

1. Report No.	2. Government Accession No.	3. Recipient's Catalog No.
SSC-357		XX

4. Title and Subtitle	5. Report Date
Carbon Equivalence and Weldability of Microalloyed Steels	October 25, 1989
	6. Performing Organization Code
	XX

7. Author's) C.D. Lundin, T.P.S. Gill, C.Y.P. Qiao, Y. Wang, K.K. Khan	8. Performing Organization Report No.
	WRG-8910

9. Performing Organization Name and Address	10. Work Unit No. (TRAIS)
Welding Research and Engineering Group Materials Science & Engineering Dept. The University of Tennessee Knoxville, TN 37996	
	11. Contract or Grant No.
	DTCG-23-87-C-20035

12. Sponsoring Agency Name and Address	13. Type of Report and Period Covered
Commandant U.S. Coast Guard Washington, DC 20593-0001	Final Report
	14. Sponsoring Agency Code
	G-M

15. Supplementary Notes

Sponsored by the Ship Structure Committee and its member agencies.

16. Abstract This is a final report of the effort to determine the validity of carbon equivalent formulae to predict weldability of low carbon microalloyed steels. The HAZ of a range of steels was characterized (HSLA 80-130, HY 130, DQ and AC types) and the formula of Yurioka was found to be most accurate in predicting HAZ hardness. The CE_1 carbon equivalent formula was also found to most accurately predict hardenability except that the effect of Copper is not linear above 0.5%. The Hydrogen sensitivity was evaluated by the Implant, Battelle and UT-Mod Hydrogen Sensitivity tests at two hydrogen levels. The Lower critical stress in the Implant test was utilized to define the critical preheat temperatures for the steels evaluated. The HSLA 80 type materials may require a preheat of 150°F under highly restrained conditions with hydrogen present. HSLA 130 was found to besuperior to HY 130 in regard to hydrogen cracking sensitivity. The high strength steels can be ranked in the order of increasing preheat required to prevent cracking as: HSLA 100--HSLA 130--DQ 125--HY 130 DQ 80 and AC 50 steels responded well to testing at high hydrogen levels (20ppm) and ambient temperature preheat. A soft zone was found in the HAZ of the HSLA, DQ and AC steels wich was a function of weld heat input. The soft zone in the copper bearing HSLA steels could be eliminated by PWHT. A probe study showed that the HSLA 80 steels are similar to A 710 grades with regard to PWHT/Reheat cracking and that the HAZ toughness decrease is also similar to the A 710 grades.

17. Key Words Weldability, Low Carbon Micro-Alloyed Steels, HSLA 80-130, HY-130, DQ, Effect of Hydrogen, Preheat, HAZ Micro-Structure, Soft Zone, Implant Testing Atlas of Micorstructures.	18. Distribution Statement This document is available through the National Technical Information Service Springfield, VA 22161

19. Security Classif. (of this report)	20. Security Classif. (of this page)	21. No. of Pages	22. Price
Unclassified	Unclassified	248	

Form DOT F 1700.7 (8-72)   Reproduction of completed page authorized

METRIC CONVERSION FACTORS

Approximate Conversions to Metric Measures

Symbol	When You Know	Multiply by	To Find	Symbol
		LENGTH		
in	inches	*2.5	centimeters	cm
ft	feet	30	centimeters	cm
yd	yards	0.9	meters	m
mi	miles	1.6	kilometers	km
		AREA		
in^2	square inches	6.5	square centimeters	cm^2
ft^2	square feet	0.09	square meters	m^2
yd^2	square yards	0.8	square meters	m^2
mi^2	square miles	2.6	square kilometers	km^2
	acres	0.4	hectares	ha
		MASS (weight)		
oz	ounces	28	grams	g
lb	pounds	0.45	kilograms	kg
	short tons (2000 lb)	0.9	tonnes	t
		VOLUME		
tsp	teaspoons	5	milliliters	ml
Tbsp	tablespoons	15	milliliters	ml
fl oz	fluid ounces	30	milliliters	ml
c	cups	0.24	liters	l
pt	pints	0.47	liters	l
qt	quarts	0.95	liters	l
gal	gallons	3.8	liters	l
ft^3	cubic feet	0.03	cubic meters	m^3
yd^3	cubic yards	0.76	cubic meters	m^3
		TEMPERATURE (exact)		
°F	Fahrenheit temperature	5/9 (after subtracting 32)	Celsius temperature	°C

*1 in = 2.54 (exactly). For other exact conversions and more detailed tables, see NBS Misc. Publ. 286, Units of Weights and Measures, Price $2.25, SD Catalog No. C13.10:286.

Approximate Conversions from Metric Measures

Symbol	When You Know	Multiply by
		LENGTH
mm	millimeters	0.04
cm	centimeters	0.4
m	meters	3.3
m	meters	1.1
km	kilometers	0.6
		AREA
cm^2	square centimeters	0.16
m^2	square meters	1.2
km^2	square kilometers	0.4
ha	hectares (10,000 m^2)	2.5
		MASS (weight)
g	grams	0.035
kg	kilograms	2.2
t	tonnes (1000 kg)	1.1
		VOLUME
ml	milliliters	0.03
l	liters	2.1
l	liters	1.06
l	liters	0.26
m^3	cubic meters	35
m^3	cubic meters	1.3
		TEMPERATURE (exact)
°C	Celsius temperature	9/5 (then add 32)

°F -40   0   32 40   80 98.6 120

°C -40 -20 0   20   37 40   60
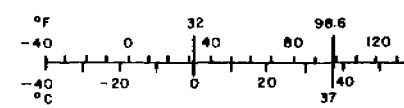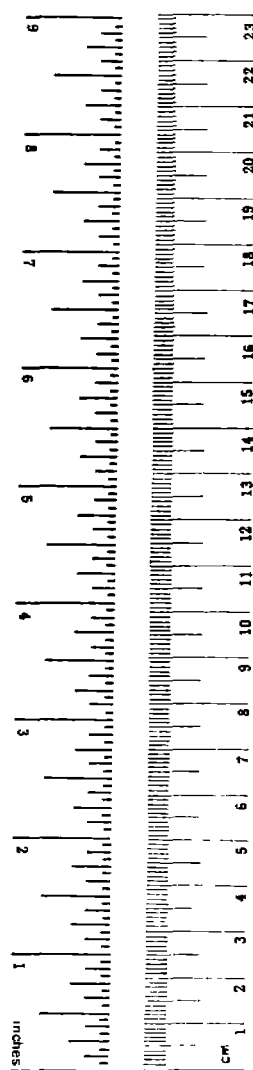
EXECUTIVE SUMMARY

Scope

This program to investigate the validity of conventional carbon equivalent formulae applicable to the weldability of nine low carbon micro-alloyed steels for marine structures included in its scope the determination of CGHAZ hardness as a function of cooling time from 800 to 500°C, measurement of cooling times/cooling rate as a function of welding conditions, validation of calculation methods, the categorization of HAZ microstructures and hydrogen assisted cracking by three different methods namely; the Battelle Underbead Cracking, UT-Modified Hydrogen Sensitivity and Implant Cracking tests. The steels tested were: HSLA-80-1, HSLA-80-2, HSLA-80M, HSLA-100, HSLA-130, HY-130, DQ-125, DQ-80, and AC-50.

Six steels, HSLA-80-1, HSLA-80-2, HSLA-80M, HSLA-100, HSLA-130, and DQ-80, contain copper (>1wt%) and were strengthened by the precipitation of epsilon-copper. Modern thermomechanical controlled processing (TMCP) was employed in the production of DQ-80, DQ-125 and AC-50, whereas the Navy HSLA steels were of quenched and aged variety. The literature review conducted at the inception of this program revealed the effects of TMCP and cleanliness of the "new" steels in reducing the hardenability of steels by providing more sites for ferrite nucleation. Therefore, the carbon equivalent formulae applicable to the conventional steels generally over estimate the hardenability of the TMCP steels.

Methods to Estimate Preheat Temperature

In order to estimate the preheat temperature for crack-free welding, two approaches-Hardness Control and Hydrogen Control-are in common use. In the Hardness Control approach, the hardenability of steels is represented by CE(IIW) carbon equivalent, whereas in the Hydrogen Control approach P_{cm} defines the hardenability. Neither method appears to be applicable to the steels in this program. The Hardness Control approach is based on the assumption that if the CGHAZ hardness is kept below a certain critical hardness, the risk of cracking is greatly reduced. Critical hardness is assumed to be independent of carbon equivalent (CE). However, it has been shown that critical hardness decreases with decreasing CE. Therefore, modern steels with low CE's may crack if the Hardness Control approach is used to estimate the preheat temperature. The steels in this program, with the exception of AC-50, lie outside the validity limits of P_{cm}, the composition characterizing parameter in the Hydrogen Control approach. Moreover, in this study it was found that P_{cm} is inadequate in representing the hardenability of the steels studied. Therefore, the Hydrogen Control approach may not be suitable for the present set of steels. Another method which is receiving cosiderable attention is the Critical Stress Control approach. In this method, a lower critical stress (LCS) is determined experimentally as a function of preheat temperature and hydrogen content. The risk of HAC is reduced if the LCS is greater than the intensity of restraint in the welded joint. The applicability of this approach to the steels of interest has been examined in detail in this report.

Characterization of the Heat Affected Zones

An extensive study was carried out to characterize the CGHAZ's as a function of heat input. The CGHAZ microstructures correlate well with the measured hardness. An Atlas of Microstructures is appended to this document.

Several published maximum hardness formulae were used to calculate the maximum HAZ hardness and compare these with the experimentally generated data. A recently proposed formula by Yurioka allowed an accurate determination of the maximum HAZ hardness in the steels studied. The CE_I formula was employed to define the hardenability in Yurioka's formula. A comparison of the influence of various alloying elements on the overall CE formulae; CE_I and P_{cm}, showed that the contribution of carbon and copper has been greatly reduced in CE_I as compared to that in P_{cm}, whereas the weightage of the other alloying elements is increased. The effect of copper in amounts greater than 0.50% does not appear to increase linearly with a further increase in copper content. The above data analysis resulted in the finding that the CE_I carbon equivalent is most applicable to the class of steels categorized in this investigation.

Hydrogen Assisted Cracking Studies

The evaluation of the susceptibility to hydrogen assisted cracking was carried out by the Battelle Underbead Cracking test, UT-Modified Hydrogen Sensitivity test and Implant Cracking test. The Battelle test was conducted using E 8010 electrodes to provide a high diffusible hydrogen content. No true CGHAZ hydrogen assisted cracking was observed in any of the steels. The cracks in the Battelle test appeared to have initiated in the weld metal and then propagated into the HAZ. In the UT-Modified HST test, cracking was confined to the CGHAZ and no cracks were observed in the fused zone. The CGHAZ cracks were intergranular in nature. The trend in the variation of critical preheat temperature to avoid cracking with CE's in these two tests was approximately the same, even though the location of cracking was different. It was found that the lower strength level steels (80 ksi) behaved differently from the higher strength level steels (100-130 ksi steels). The critical preheat temperature varied markedly with CE for the lower strength level steels but a relatively weak dependence of critical preheat temperature on CE was observed for the higher strength level steels. This implies that even though the carbon equivalent of higher strength steels is greater than the lower strength steels, their susceptibility to HAC may be equal or even lower than that of the lower strength steels. The CE_I formula provided a better data fit than P_{cm}.

The Implant Cracking tests were conducted at 75 and 150°F preheat temperatures and at two hydrogen levels. The diffusible hydrogen content was 5 and 20 ml/100g for the lower strength steels and 5 and 10 ml/100g for the higher strength steels. The AC-50 steel did not show any fracture in the CGHAZ and rupture occurred in the soft zone. A similar behavior was observed in DQ-80 when tested at a preheat temperature of 150°F. However, at 75°F preheat temperature hydrogen assisted rupture occurred in the CGHAZ. An appreciable drop in the LCS was observed in HSLA-80M and HSLA-100 when tests were conducted at the 75°F preheat temperature and high hydrogen level. This has been attributed to the presence of retained austenite or austenite-martensite packets in the CGHAZ which act as trapping sites for diffusible hydrogen and most likely assist in initiating cold cracking. The presence of fully or partly dissolved copper precipitates is believed to aid in the formation of austenite packets. This phenomenon becomes more pronounced at high hydrogen levels. HSLA-130 becomes slightly more susceptible to HAC than HY-130 at high hydrogen levels and at the 75°F preheat temperature, otherwise HSLA-130 was found superior to HY-130. A more detailed study is recommended to understand the influence of secondary

phases in the copper containing steels on the diffusivity of hydrogen, which may also lead to the optimization of mill heat treatment for HSLA steels.

In order to recommend a plan to establish weldability procedures for the steels in this study, the experimental LCS data from the Implant tests were compared with those calculated from six different formulae. These formulae had been developed using data from conventional steels, therefore, the comparison also provided an insight into the possible differences between the modern and the conventional steels when the resistance to hydrogen assisted cracking is considered. None of the published formulae were able to predict the LCS accurately. When the variation in the LCS was considered independently at 75 and 150°F preheat temperatures, it was possible to calculate the LCS with an acceptable degree of accuracy. Thus, a different thermal factor must be developed for use over a range of preheat temperatures.

Recommended Preheat Temperatures

An attempt was made to approximately estimate the critical preheat temperatures to avoid cold cracking in the steels under investigation from the data generated from the Implant Cracking and UT-Modified Hydrogen Sensitivity tests. It was found that AC-50 and DQ-80 can be welded safely at preheat temperatures below ambient and with high hydrogen electrodes. Under highly restrained conditions, HSLA-80-1 may require a preheat temperature of 150°F and the preheat temperature should be greater than 150°F for HSLA-80-2 and HSLA-80M. When the higher strength steels were considered, HSLA-130 was found to be superior to HY-130. The critical preheat temperature for HY-130 at the higher hydrogen content is reported to be 300°F. Therefore, the critical preheat temperature for HSLA-130 should be less than 300°F. The high strength steels can be arranged in the following order of increasing preheat temperature required to prevent cracking-
HSLA-100<HSLA-130<DQ-125<HY-130

The HY-130 and HSLA-80M were found to be the most susceptible to HAC among the higher strength and lower strength steels respectively. Further study is required to precisely define the critical preheat temperatures in the "nèw" steels.

Other Weldability Studies

Studies were carried out to characterize the occurrence of a HAZ soft zone. The width of the HAZ soft zone increased linearly with an increase in cooling time ($t_{8/5}$) and the extent of HAZ hardness decrease (with respect to the base metal level) as a function of cooling time was initially rapid and then tended to saturate as the cooling time increased. PWHT was found to eliminate the soft zone in the copper containing steels.

Optimum methods for calculating the $t_{8/5}$ time as a function of welding parameters for SMAW and SAW were investigated and the data developed show that highly accurate calculation methods are available.

A probe study to determine the sensitivity of the Navy HSLA-80 steel to reheat/PWHT cracking tendency and HAZ toughness response was conducted. While not reported within the work scope of this program the results showed that both the reheat/PWHT cracking tendency and HAZ toughness response parallel that of the ASTM A 710 material previously tested[2].

CONTENTS

1. WORK SCOPE

1.1. INTRODUCTION

High strength low alloy (HSLA) steels, also referred to as micro-alloyed steels, can be defined as steels possessing a yield strength of at least 43 ksi, achieved by micro-alloying or special thermomechanical processing or a combination of both. The more common of these steels are of the C-Mn type with additions of Nb (Cb) and / or V to increase the strength through grain refinement and precipitation hardening. The increase in strength is above that developed due to solid solution strengthening alone. Some of the steels that fall within the above strengthening mechanisms are ASTM A 572, A 808, A 633, A 588, A 131 and A 656. Several steels have been developed which use additions of Ti and B together with controlled rolling and controlled cooling which results in extremely fine grain sizes thus achieving high strength with low carbon content. Important to the processing of these steels is careful control of the nitrogen content and the aluminum level. Many of the developments originated with linepipe steels in the early 1970's. In addition to the high yield strengths these steels have good toughness and retain toughness in the HAZ during welding because of limited grain growth.

In general, HSLA steels are strengthened in four ways:

(a) As-rolled: Strengthening is achieved through the strain induced precipitation of carbides and carbo-nitrides during rolling.

(b) Controlled Rolled: Rolling is usually performed below 1800°F. Strain induced precipitation of carbo-nitrides prevent recrystallization of austenite. Very fine ferrite and pearlite result from transformation of the fine elongated austenite grains. The rolled product, however, can have extreme directional properties, and therefore low sulfur contents are advised.

(c) Normalizing: The presence of carbo-nitrides inhibits austenite grain growth, thus contributing to finer ferrite in the normalized microstructure. There is no contribution of precipitation hardening in the normalized condition.

(d) Quenching and Tempering: Quenching from austenite results in ferrite, bainite and martensite. Subsequent tempering gives a good combination of strength and toughness.

In practice, HSLA steels are rarely quenched and tempered. Since the strengthening mechanisms utilized in three of the four mechanisms described above do not utilize a low temperature phase transformation (austenite to martensite), the carbon content can be reduced significantly which implies a dramatic improvement in the weldability (i.e. cold cracking). Thus, the inherent utility of HSLA steels in marine environments stems from the excellent combination of strength and weldability that can be achieved by special metallurgical and mechanical processing and the concomitant reduction of the carbon content.

In addition to the class of HSLA steels described above, interest has recently been regenerated in a copper precipitation strengthened steel which is covered by ASTM specification A 710/A 786. These steels have a carbon content less than 0.10 % and achieve strength by copper precipitation and therefore obtain a good combination of strength and weldability. The U.S. Navy is currently using HSLA-80 for structural applications under its own designation MIL-S-24645 which applies to the steel similar to ASTM A 710. HSLA-100 was recently developed by the Navy and is soon to be added to this specification.

1

The weldability of HSLA steels has been widely investigated during the past fifteen years and salient features of the results of these investigations are presented below.

1.2. WELDABILITY OF NAVY HSLA STEELS

In considering the weldability of any steel, two important aspects need to be addressed; weldability for fabrication and weldability for service. The former relates primarily to cracking problems that may arise during welding and postweld heat treatment (PWHT) and the latter is concerned with potential problems after the weldment is placed in service and principally includes toughness of the weld HAZ and the corrosion behavior of the weldment. These two aspects are separately addressed briefly in the review presented below.

1.2.1. Weldability for Fabrication

Weldability aspects are concerned with cracking problems that might occur in a weldment, especially in the grain coarsened HAZ. The two most significant cracking problems are hydrogen assisted cracking (HAC) and postweld heat treatment (PWHT) cracking. Both occur in the grain coarsened region of the weld HAZ. In general, the prior treatment of the plate is not significant as far as the properties of the coarse grained HAZ are concerned whereas the properties of the grain refined HAZ can be affected by parent metal structure. The factors that govern the susceptibility of a steel to HAC can be broadly classified as:

(a) the composition of the steel and hence its hardenability,
(b) the presence of hydrogen during welding, dictated by the welding process, moisture in the electrode coating and environment, and
(c) the presence of stresses, residual or applied.

The carbon equivalent (CE) concept has evolved as a simple and convenient method to normalize the chemical composition to a single number to represent the hardenability of steels. Over the years many CE formulae have been developed to correlate the results of cracking tests or to relate the maximum HAZ hardness with composition. The CE formulae proposed by various researchers differ essentially in the weightage given to each of the elements present in the steel to represent its influence on hardenability and hence susceptibility to cracking. It is clear that in selecting a CE for a particular steel, one has to be extremely careful. For steels with a relatively high C and/or alloy content, the formulae based on maximum hardness are adequate. However, for steels where the strengths are not achieved through solid solution hardening or hardening through phase transformations, the applicability of CE formulae can lead to serious difficulties. This problem is exemplified in the case of an HSLA steel like ASTM A 710, which is strengthened by precipitation hardening. Earlier work at The University of Tennessee [1] has indicated a susceptibility of this material to cracking, in an augmented strain hydrogen cracking test, as compared to higher carbon steels.

PWHT cracking may be encountered when the weldment is postweld heat treated and is related to the precipitation processes that occur in the grain coarsened HAZ as well as the presence of certain tramp elements in the steel. The susceptibility to PWHT cracking has been never related to a CE type of formula although various parameters and indexes have been generated to relate the susceptibility to the extent of alloying and tramp elements present in the steel. Among the HSLA steels described earlier, A 710 appears to be highly susceptible to this type of cracking according to a recent work conducted at The University of Tennessee [2]. The conventional HSLA steels which are strengthened through the addition of Nb and/or V have been found to have little susceptibility to this type of cracking.

2

It should be noted that intergragular cracking in the HAZ can occur due to succeeding weld thermal cycle exposures in multipass welds by a mechanism identical to that of the PWHT cracking phenomenon.

The weldability of Navy HSLA steels with respect to hydrogen assisted cracking has been addressed in Section 4.

1.2.2. Weldability for Service

Carbon equivalent formula can be employed to assess the weldability of the HSLA steels, however, the toughness of the HAZ is very difficult to predict from a CE since the toughness can be affected by relatively minor compositional factors which are not included in the CE. This is especially true in the case of HSLA steels where small additions of Nb, V, Ti, B, N etc. are made to develop strength and toughness in the parent metal as well as in the HAZ. Consequently, the vast majority of work that has been conducted on HSLA steels has looked into the toughness of the HAZ especially the grain coarsened HAZ. Welding Research Council Bulletins 203 and 213 [3-5] provide good starting points for the evaluation of the influence of alloying elements on HAZ toughness. Cordea [3] determined that the toughness of the HAZ in micro-alloyed Nb containing steels was primarily governed by the heat input, higher heat inputs lowering the toughness. An embrittled zone developed in very high heat input welds. The embrittlement was related to the precipitation of NbC on the grain boundaries in the HAZ regions exposured above 2370°F. Similar results have been reported by Lundin and Eftekar [6] in Gleeble simulation tests conducted upon cooling from 2400°F. Dolby [7] also reports the embrittlement of HAZ's in Nb containing HSLA steels with increasing heat input. This was attributed to Nb inhibiting the nucleation and growth of proeutectoid ferrite and aiding the formation of upper bainitic structures in the HAZ as opposed to the formation of acicular ferrite. Acicular ferrite is reported to impart high toughness to the HAZ. Sawhill [8] on the other hand, reports a small improvement in the HAZ toughness with the addition of Nb. As Levine and Hill [5] report, specific compositions alone do not govern the HAZ toughness. The synergistic influence of composition and microstructure has to be taken into account. They state, contrary to Dolby's contention that an increase in proeutectoid ferrite does not necessarily mean improved toughness. The grain size of the grain coarsened HAZ, the microstructure and the composition all have contributions in determining the toughness of the HAZ. HSLA steels appear to have an advantage from the fact that the presence of carbonitrides restricts grain growth of austenite during high temperature exposure such as welding. However, V and Nb carbo-nitrides can only restrict grain growth up to temperatures of 2000°F, which is considerably lower than what is experienced in the region immediately adjacent to the fusion boundary. A significant effort in the Japanese development of HSLA [9-11] steels has been in the ways and means, primarily through compositional control, to improve the toughness of the grain coarsened HAZ. The addition of critical amounts of Ti, Al, B and N have resulted in the development of steels that possess excellent notch toughnesses in the HAZ when welded with heat inputs as high as 250 kJ/in. A cautionary note here is that free N will deteriorate the HAZ toughness.

In summary, it can be said that the prediction of HAZ toughness from gross microstructure and CE is difficult. Restrictions of grain growth and the presence of larger fractions of acicular ferrite as opposed to lower temperature transformation products are desirable. However, the compositional factors, have to be taken into account to adequately assess toughness.

3

1.2.3. Weldability of A710 Type Precipitation Strengthened Steel

The weldability of the A 710 type steels has to be considered in a different vein than for the other HSLA steels discussed herein, primarily because the composition and heat treatment used to develop strength in these steels are quite different from that for the other HSLA steels. A 710 steel is usually extremely low in carbon content (< 0.10%) but contains up to 1.25 % Cu as a precipitation hardening element. The steel is either rolled, normalized or quenched prior to aging. The steel possesses excellent notch toughness at low temperatures and due to its low carbon content is regarded to have minimal problems as far as HAC is concerned. Although relatively few problems have been reported to date as far as welding the A 710 type steels is concerned, recent work at The University of Tennessee [2] portends a potential problem with regard to PWHT cracking. Another, aspect of the weldability of this steel is the loss in HAZ toughness in the intercritically heated HAZ as well as the loss of toughness upon PWHT.

In order to evaluate the validity of the CE approach to the weldability of Navy HSLA steels a work plan consisting of (a) Characterization of CGHAZ's and (b) Cold cracking tests (the Battelle Underbead Cracking, UT-Modified Hydrogen Sensitivity, and Implant Cracking tests), was proposed. A total of nine different steels were selected for evaluation. The program tasks to achieve the above objectives are outlined as follows.

1.3. PROGRAM TASKS

1.3.1. Task 1 - Literature Review

Published information about the weldability of low carbon microalloyed steels was reviewed with particular emphasis on the validity of conventional carbon equivalents used to define hardenability of steels, applicability of various approaches practiced, such as Hardness Control and Hydrogen Control, to predict safe welding conditions, and suitability of using different formulae to calculate the maximum heat-affected zone hardness. Actual data, where available, have been analyzed to ascertain if it is applicable to the class of micro-alloyed steels being considered for marine applications. The survey has been carried out by both computer and hand search of the international and U.S. literature.

The published data has been critically evaluated and state-of-the-art reviews of the information included in this report in the appropriate sections.

1.3.2. Task 2 - Microstructural Studies

Detailed microstructural analysis of the HAZ's of bead-on-plate welds in the steels in this program has been carried out as a function of cooling time between 800 and 500°C ($t_{8/5}$). The $t_{8/5}$ was varied either by changing the heat input or by employing different plate thicknesses. This analysis aided in understanding the hardenability behavior of these steels, and provided useful information for interpreting the effect of microstructure on HAC. Moreover, a knowledge of the microconstituents also aided in rationalizing the maximum HAZ hardness data obtained to assess the applicability of the formulae selected to calculate the maximum HAZ hardness as a function of $t_{8/5}$ and carbon equivalent (see Task 3A for details). Additionally, extensive metallographic and fractographic examination of the samples tested for susceptibility to the hydrogen assisted cracking constituted an important part of this task (see Task 3B for details).

An atlas of microstructures was prepared and correlated with the type of steel and the cooling time. The hardness of the various microstructures

accompany the description of the microstructures and is used to further describe the characteristics of the HAZ.

1.3.3. Task 3 - Testing of Candidate Materials

The testing of materials for verification of the CE with maximum HAZ hardness and hydrogen assisted cracking susceptibility was accomplished on seven steels selected in consultations with the Project Technical Committee. In addition to the initial seven steels, two steels were added to the program because additional funding was made available by the Department of the Navy and Lukens Steel Co. The addition of these steels permitted the range of strength levels to be increased to 130 ksi. Thus the present program consisted of the following nine steels for weldability evaluations:

    (1) HSLA-80 (C-0.044%)
    (2) HSLA-80 (C-0.062%)
    (3) HSLA-80 Modified (C-0.057%)
    (4) DQ-80 (C-0.032%)
    (5) HSLA-100 (C-0.072%)
    (6) DQ-125 (C-0.11%)
    (7) AC-50 (C-0.079%)
    (8) HY-130 (C-0.12%)
    (9) HSLA-130 (C-0.070%)

(A) <u>Testing for Validity of CE for Determining Maximum HAZ Hardness</u>

Determination of maximum HAZ hardness (H_{max}) provides information on the susceptibility of the HAZ microstructure to HAC. The presence of various microconstituents in the HAZ depends on the hardenability of a steel, which in turn is defined by a composition characterizing parameter (CE-carbon equivalent). There are various CE's suggested in the published literature which are applicable to different classes of steels. There is no universal CE formula which can define the hardenability of all the steels. However, there have been continuous efforts to evolve more accurate CE's applicable to a wider range of steels. The conventional CE's are not valid for describing the hardenability of thermo-mechanically control processed low carbon micro-alloyed steels because in such steels it appears the hardenability is not a simple function of the chemistry alone but metallurgical factors like austenite grain size, and amount and distribution of non-metallic inclusions play an important role. The effect of these factors on the hardenability of steels has been of less importance in the past as hardenability of conventional steels was fully described by their chemistries and any effect of the metallurgical factors was not discernible. However, thus far, no detailed study has been carried out to completely quantify the effects of metallurgical factors and therefore, incorporation of these effects in the approaches to predict safe welding conditions has to await results of detailed investigations. While the influence of metallurgical factors on the hardenability may be of importance, a dominant role is played by the chemistry of steel. In the present investigation where the "new steels" are of the low carbon variety (C≤0.12%), a suitable CE from literature has been chosen to fully describe hardenability. In the event a suitable CE was not available, an attempt was to be made to modify the existing CE's to fit the data generated in the present study.

There are a number of formulae available to calculate the maximum HAZ hardness and a literature review was carried out to provide the most suitable formula to calculate H_{max}. (The formulae for calculating H_{max} derive from a relationship between the CE and $t_{8/5}$). To verify different formulae the hardness response of all steels was determined from bead-on-plate welds. The heat input was selected as to give $t_{8/5}$ values between 2 and 100 sec. The

cooling time, $t_{8/5}$, was measured during the actual welding operation. The data thus generated was used to analyze the suitability of the formulae extracted from the literature. This exercise not only validated the CE's but also provided the possibility of predicting H_{max} from a knowledge of welding parameters and chemistry. The basis of determining safe welding condition in the hardness control approach is to define a critical HAZ hardness below which no cracking takes place and once the HAZ hardness can be calculated with a significant degree of confidence, it should be possible to validate this approach for materials of interest.

(B) Testing for Susceptibility to Hydrogen Assisted Cracking

Susceptibility of the candidate materials to hydrogen assisted cracking was studied utilizing three different tests; The first test is the Battelle Underbead Cracking test in which crack/no-crack behavior of the steels was evaluated as a function of preheat temperature. The electrodes was chosen to match the strength levels of different steels to be characterized. Normally high hydrogen electrodes are employed to deposit bead-on-plate welds, however, since for the high strength steels employed in this study high hydrogen consumables are not available commercially, the diffusible hydrogen content of the deposits was increased by exposing the electrodes to a controlled humidity level. The Battelle test usually provides a reasonable determination of preheat temperatures which are normally conservative in actual fabrication practices. Results from this test can be used to rank various steels as to their susceptibility to HAC.

The second test to asses the HAC of the steels was the UT-Modified Hydrogen Sensitivity test. This test was conducted as a function of preheat temperature and augmented strain. Three strain levels namely, 1, 2, and 4% were employed. This test enabled various steels to be ranked in accord with the carbon equivalency criteria. A major advantage in conducting this test is that diffusible hydrogen content is kept constant at the saturation level, unlike in other HAC tests where hydrogen content depends on the type of electrode used, baking conditions, welding conditions, and atmospheric relative humidity.

Thirdly, the cracking tendency of the steels was also evaluated by the Implant Cracking test. The test evaluates the effect of preheat temperature and hydrogen content. In the present program, the lower critical stress (LCS), below which no cracking takes place during the interval of the test has been determined at two preheat temperatures and at each preheat temperature, samples with two different hydrogen levels were tested. To obtain a consistently uniform level of diffusible hydrogen in the HAZ's of the implant samples, the welding parameters and storage conditions of the consumables were fully standardized. Additionally, the maximum HAZ hardness of the implant samples was also determined to analyze the applicability of recently proposed equations for calculating LCS from a knowledge of HAZ hardness, and hydrogen content. Finally, the data from implant cracking tests were used to check the suitability of predictive equations for calculating preheat temperature for safe welding conditions.

1.3.3. Task 4 - Validation of Carbon Equivalent Formulae

Based upon the literature review, the test results obtained from this program, and the information gathered from a survey of the fabricators and producers of the low carbon micro-alloyed steels under consideration, the different approaches used to predict safe welding conditions were assessed and a CE formula is recommended to characterize the hardenability. An attempt was also to be made to analyze the use of conventional approaches by

6

incorporating the "new" carbon equivalent. The above evaluation formed the basis for complete analysis.

This final report outlines the direction for future work to determine specific weldability correlations and the potential for fabrication related and serviceability related problems with low carbon micro-alloyed steels.

The work scope of this program can be summarized as below:

Fabrication procedures and commonly accepted criteria relating to preheats, heat-affected zone (HAZ) hardness and hydrogen assisted cracking should be investigated and validated for these new classes of steels, and their companion consumables by doing the following:

(1). Review existing micro-alloy steels and fabrication practices, procedures and testing. Include published literature in the United States and overseas.

(2). Identify the microstructures and other properties that are detrimental to good quality welds.

(3). Identify types of microstructures or other weld/HAZ properties that are desirable for a good weld.

(4). Investigate the validity and conceptual basis of the carbon - equivalent approach and the methods of correlating alloy composition and microstructure to weld cracking for the new steels.

(5). Identify one or more approaches for characterizing weldability in these steels and recommend a plan for establishing proper procedure or analytical techniques to support these new classes of steels.

(6). Extend and enhance testing for hydrogen assisted cracking using the Implant test.

All the above aspects have been described in detail in the subsequent Sections of this report. In addition preliminary investigations were also carried out to study the occurrence of "soft" zones in the HAZ and their behavior as a result of postweld heat treatment.

2. MATERIALS

2.1. INTRODUCTION

Some steels in this program are modern low carbon micro-alloyed steels and incorporate the advantages brought about by the application of thermomechanical controlled processing (TMCP) in production of these "new" steels. TMCP is a generic name and represents a number of steel making routes. The main advantage derived from using TMCP is in terms of improving the strength and toughness by grain size and microstructural control. The enhancement in these properties is achieved either at the same carbon content or at reduced carbon level. The decrease in the carbon content increases the resistance to HAC by decreasing the carbon equivalent. The Navy HSLA steels (HSLA-80 to -130) achieve their properties by quenching and aging to develop a copper containing precipitate. HY-130 steel is a conventional low carbon alloy steel and derives its strength from a tempered martensite structure.

The set of low carbon steels include five Navy HSLA steels namely, HSLA-80 (C-0.044%), HSLA-80 (C-0.062%), HSLA-80 Modified (C-0.057%), HSLA-100 (C-0.072%), and HSLA-130 (C-0.070%). In order to identify HSLA steels of 80 ksi category, the steels containing C-0.044% and C-0.062% are referred to as HSLA-80-1 and HSLA-80-2 respectively and the modified version of HSLA-80 is referred as HSLA-80M.

The chemical composition of the steels investigated is provided in Table 2.1. The chemical composition range for the steels under study varies as follows.

C -0.032 to 0.12%	Nb-<0.001 to 0.034%
Mn-0.48 to 1.37%	Al-0.015 to 0.054%
Si-0.10 to 0.37%	Ti-0.001 to 0.009%
Ni-0.02 to 4.68%	S -0.001 to 0.004
Cr-0.02 to 0.74%	P -0.003 to 0.008%
Mo-<0.01 to 0.58%	B -<0.001 to 0.002%
Cu-0.01 to 1.72%	N -0.002 to 0.014%
V -0.002 to 0.089%	O -0.002 to 0.006%

The chemical composition of these steels was analyzed by a second laboratory as given in Table 2.2. There was little difference between the analyses except that the boron content was consistently lower in the analysis from the second laboratory. In this study all data analysis has been carried out using chemical compositions reported in Table 2.1

The values of carbon equivalents (P_{cm}, CE(IIW), CEN, and CE_I)are given in Table 2.3 and the tensile properties (UTS, YS, % elongation, and %reduction in area), and hardness for all nine steels are given in Table 2.4. The yield strength varies from 64 for AC-50 to 135.9 ksi for HY-130. The mechanical properties show a well-known linear relationship with the base metal hardness as indicated for UTS and YS in Figs 2.1 and 2.2 respectively. The chemistry of HSLA-100 and HSLA-130 is essentially identical because they were derived from the same heat. However, the difference in UTS and YS is appreciable. This is primarily due to the use of different aging treatments.

The values of only four carbon equivalents are provided in Table 2.3. The CE's P_{cm} and CE(IIW) were chosen because of their world-wide recognition, and not necessarily for their applicability to the class of steels under investigation. CE(IIW) is widely used in Europe and characterizes the hardenability of steels in British Standard BS-5135 [12]. The composition characterizing parameter, P_{cm}, was first proposed by Ito and Bessyo [13] and is used in the hydrogen control approach to estimate the preheat temperature for safe welding. Both formulae are also recommended in the AWS structural welding code D1.1-86 in

Table2.1. **Chemical Composition of Steels**

Composites Materials	C	Mn	P	S	Si	Ni	Cr	Mo	V	Cb	Ti	Co	Cu	Al	B	W
HSLA-80-1	0.044	0.48	0.007	0.001	0.37	1.02	0.68	0.22	0.003	0.028	0.004	0.008	1.26	0.015	0.002	<.0
HSLA-80-2	0.062	0.50	0.004	0.002	0.26	0.84	0.74	0.20	0.005	0.034	0.002	0.015	1.28	0.031	0.001	<.0
HSLA-80M	0.057	0.96	0.006	0.001	0.32	1.76	0.60	0.49	0.003	0.029	0.002	0.010	1.29	0.018	0.001	<0.
HSLA-100	0.072	0.75	0.005	0.001	0.34	3.30	0.56	0.54	0.004	0.018	0.002	0.011	1.70	0.022	0.001	<.0
HSLA-130	0.070	0.79	0.007	0.001	0.37	3.33	0.57	0.58	0.005	0.023	0.003	0.011	1.72	0.023	0.002	<.0
DQ-80	0.032	0.93	0.007	0.001	0.26	0.47	0.05	<0.01	0.002	0.034	0.009	0.005	1.14	0.030	0.001	<.0
DQ-125	0.11	0.79	0.003	0.001	0.10	1.46	0.52	0.52	0.066	0.001	0.001	0.008	0.03	0.049	0.001	<.0
HY-130	0.12	0.74	0.004	0.004	0.23	4.68	0.59	0.38	0.089	0.002	0.002	0.045	0.17	0.021	<.001	<.0
AC-50	0.079	1.37	0.008	0,002	0.27	0.02	0.02	<0.1	0.003	<.001	0.007	0.006	0.01	0.054	0.001	<.0

Table 2.2. **Chemical Composition of Steels**

Composites Materials	C	Mn	P	S	Si	Ni	Cr	Mo	V	Cb	Ti	Co	Cu	Al	B
HSLA-80-1	0.041	0.50	0.009	0.002	0.38	1.02	0.69	0.22	0.003	0.032	0.005	0.009	1.18	0.017	0.0006
HSLA-80-2	0.060	0.53	0.007	0.002	0.29	0.88	0.74	0.21	0.004	0.041	0.003	0.016	1.15	0.033	0.0004
HSLA-80M	0.053	1.02	0.009	0.002	0.35	1.78	0.61	0.50	0.003	0.037	0.003	0.011	1.24	0.022	0.0004
HSLA-100	0.066	0.83	0.010	0.002	0.38	3.42	0.58	0.58	0.005	0.028	0.004	0.013	1.57	0.025	0.0004
HSLA-130	0.067	0.85	0.011	0.002	0.39	3.48	0.58	0.58	0.005	0.029	0.004	0.013	1.59	0.026	0.0005
DQ-80	0.031	0.95	0.009	0.001	0.26	0.48	0.05	0.01	0.002	0.038	0.009	0.005	1.03	0.029	0.0001
DQ-125	0.092	0.85	0.005	0.001	0.11	1.40	0.53	0.55	0.069	0.001	0.002	0.008	0.02	0.051	0.0004
HY-130	0.107	0.78	0.008	0.004	0.25	4.84	0.60	0.39	0.101	0.003	0.003	0.048	0.19	0.023	0.0004
AC-50	0.077	1.42	0.009	0.003	0.26	0.02	0.02	0.01	0.002	0.001	0.007	0.006	0.01	0.052	0.0004

Table 2.3- Carbon Equivalents of the Steels

Steel	P_{cm}[1]	$CE(IIW)$[2]	CEN[3]	CE_I[4]
HSLA-80-1	0.22	0.46	0.35	0.49
HSLA-80-2	0.23	0.48	0.37	0.49
HSLA-80-M	0.28	0.64	0.47	0.69
HSLA-100	0.33	0.75	0.57	0.85
HSLA-130	0.34	0.77	0.59	0.86
HY-130	0.32	0.78	0.61	0.87
DQ-125	0.25	0.56	0.41	0.65
DQ-80	0.16	0.31	0.23	0.40
AC-50	0.16	0.32	0.23	0.41

1. $P_{cm} = C + \dfrac{Si}{30} + \dfrac{Mn+Cu+Cr}{20} + \dfrac{Ni}{60} + \dfrac{Mo}{15} + \dfrac{V}{10} + 5B$

2. $CE(IIW) = C + \dfrac{Si}{6} + \dfrac{Mn}{6} + \dfrac{Cu+Ni}{15} + \dfrac{Cr+Mo}{5} + \dfrac{V}{5}$

3. $CEN = C + A(C)\left(\dfrac{Si}{24} + \dfrac{Mn}{6} + \dfrac{Cu}{15} + \dfrac{Ni}{20} + \dfrac{Cr+Mo+Nb+V}{5} + 5B \right)$

   Where $A(C) = 0.75 + 0.25\tanh[20(C-0.12)]$

4. $CE_I = C + \dfrac{Si}{24} + \dfrac{Mn}{6} + \dfrac{Cu}{15} + \dfrac{Ni}{40} + \dfrac{Cr}{6} + \dfrac{Mo}{4} + \dfrac{V}{5} + 10B$

Table 2.4 Transverse tensile properties and hardness of steel plates

Material	UTS (ksi)	YS (ksi)	%Elongation	RA(%)	Hardness[+] (DPH)	Plate Thickness (inch)
HSLA-80-1	92.0	83.0	36.0	67.8	220	3/4
HSLA-80-2	100.5	91.7	53.0	61.5	244	1
HSLA-80-M	104.0	95.0	26.0	77.6	242	1 1/4
HSLA-100	123.2	118.3	21.0	71.1	272	2 1/4
HSLA-130	131.0	130.0	21.5	71.1	303	1 1/4
HY-130	141.8	135.9	19.0	67.0	326	1
DQ-80	93.0	83.0	26.5	79.4	221	1 1/2
DQ-125	138.0	131.0	20.0	*	321	2
AC-50	76.8	64.0	36.0	*	172	1 1/4

* not reported

+ measured on R_c Scale but converted to DPH
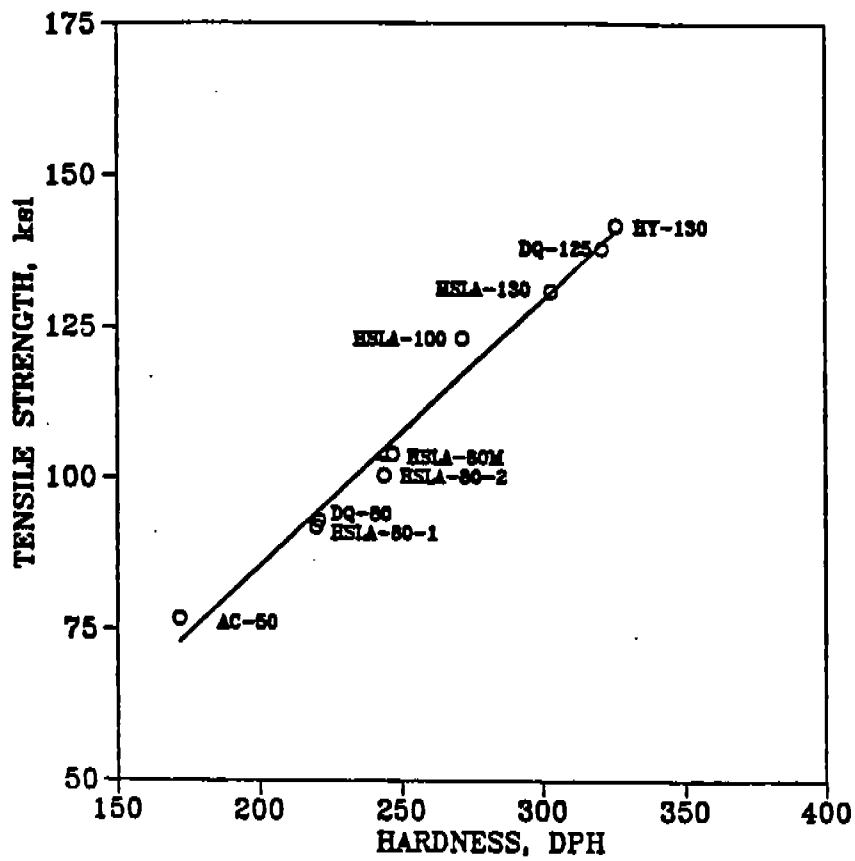
Fig.2.1. Variation of UTS with base metal hardness
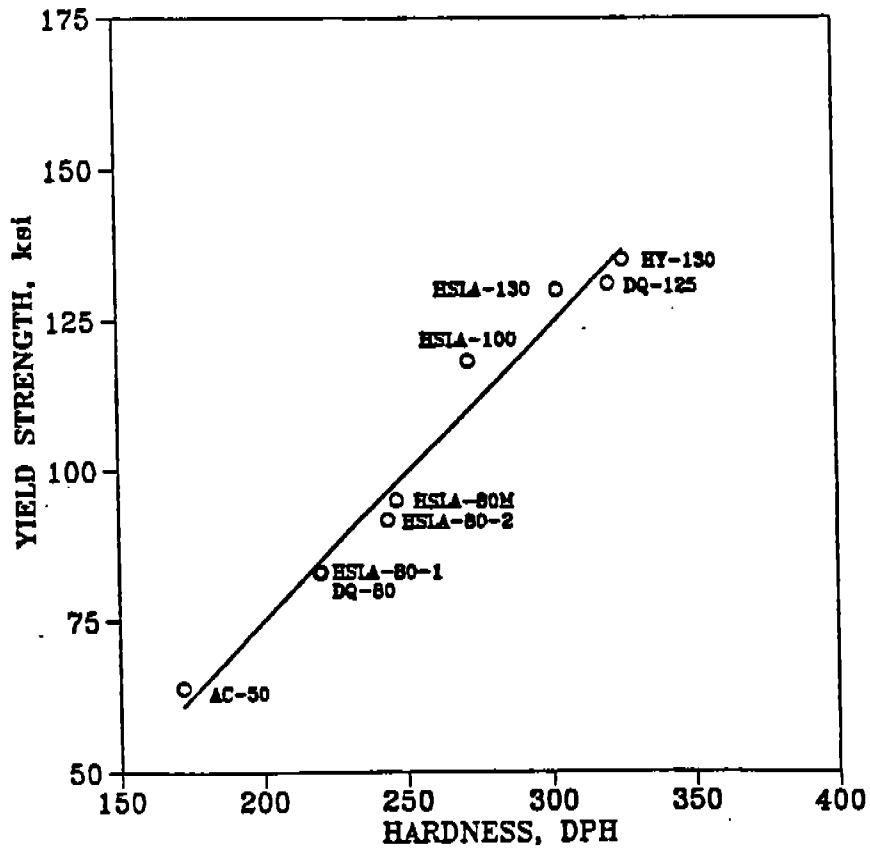
Fig. 2.2. Variation of yield strength with base metal hardness

14

the Guidelines on Alternative Methods for Determining Preheat [14]. The formula CEN was proposed by Yurioka [15] and combines both P_{cm} and CE(IIW) into one CE formula. CEN approaches CE(IIW) at higher carbon contents and P_{cm} at lower carbon contents. The carbon equivalent formula, CE_I, was also proposed by Yurioka [16]. He used CE_I along with two other carbon equivalents for the calculation of maximum CGHAZ hardness in steels of chemical composition varying over a wide range. Yurioka's formula for estimating maximum CGHAZ hardness was found to allow accurate prediction of maximum HAZ hardness for the steels investigated herein (Section 3).

The location of all nine steels in the Graville diagram [17] is shown in Fig.2.3. All steels (because of low carbon content) except HY-130 lie in Zone I of the diagram thus indicating a high resistance to hydrogen assisted cracking. HY-130 lies in Zone III and, according to Graville, is prone to HAC. Therefore, for all nine steels, the hydrogen approach for estimating the preheat temperature for safe welding should be applicable.

2.2. NAVY HSLA STEELS

All five Navy HSLA steels in this study contain copper in amounts greater than 1wt%. These steels are first austenitized, rolled, quenched and then aged to obtain optimum strengthening from epsilon-copper precipitation. The above mill treatment parameters may vary slightly from steel to steel depending on the properties desired and the final plate thickness.

Steels HSLA-80-1 and HSLA-80-2 are almost similar in composition except carbon content in the former is 0.044% and in the latter it is 0.062%. The HSLA-80-1 and HSLA-80-2 were soaked at 1660°F for 108 and 60 min. respectively and subsequently aged for 60 min. at 1160 and 1100°F. Base metal microstructures in the as-polished and etched conditions for HSLA-80-1 and HSLA-80-2 are shown in Figs A-1 and A-5 respectively (the micrographs with prefix A are given in Appendix A). The base plate microstructure in these steels consists of a mixture of polygonal and acicular ferrite. Some dark etching regions are also shown in the micrographs. These regions have been shown to be areas where granular bainite is present [18]. Granular bainite consists of packets of ferrite laths with non-cementite, interlath, second phase particles [19]. The particles have been identified as retained austenite or retained austenite-martensite. The copper precipitates in these steels are too fine to be resolvable with the optical microscope. However, using electron microscopy it is possible to identify these particles. It has been reported [20] that epsilon-copper preferentially nucleates at dislocations, grain boundaries, and sub-grain boundaries. The coherency of copper precipitates with the surrounding matrix depends on aging temperature and time.

HSLA-80M steel contains higher amounts of Mn and Ni than HSLA-80-1 and HSLA-80-2 and thus possesses higher hardenability. It is of an intermediate composition between the HSLA-80 and HSLA-100 steels and is being considered for Navy applications. Wilson et al [18] in their review of copper-added steels have shown that in the CCT diagram for modified versions of A 710 steels, the granular bainitic region is enlarged when compared to HSLA-80-1 or HSLA-80-2. Therefore, the microstructure of the base plate is predominantly granular bainite. However, martensite may also be present, particularly in thin plates. The micrographs of the as-polished and etched samples from HSLA-80M are shown in Fig. A-9.

Figs. A-13 and A-17 show the base plate microstructures of HSLA-100 and HSLA-130 respectively. These steels contain about 3.3% Ni and 1.7% Cu. Therefore, the hardenability of these steels is much higher than most of the HSLA-80 steels. The dominant phase in these steels is martensite, as granular
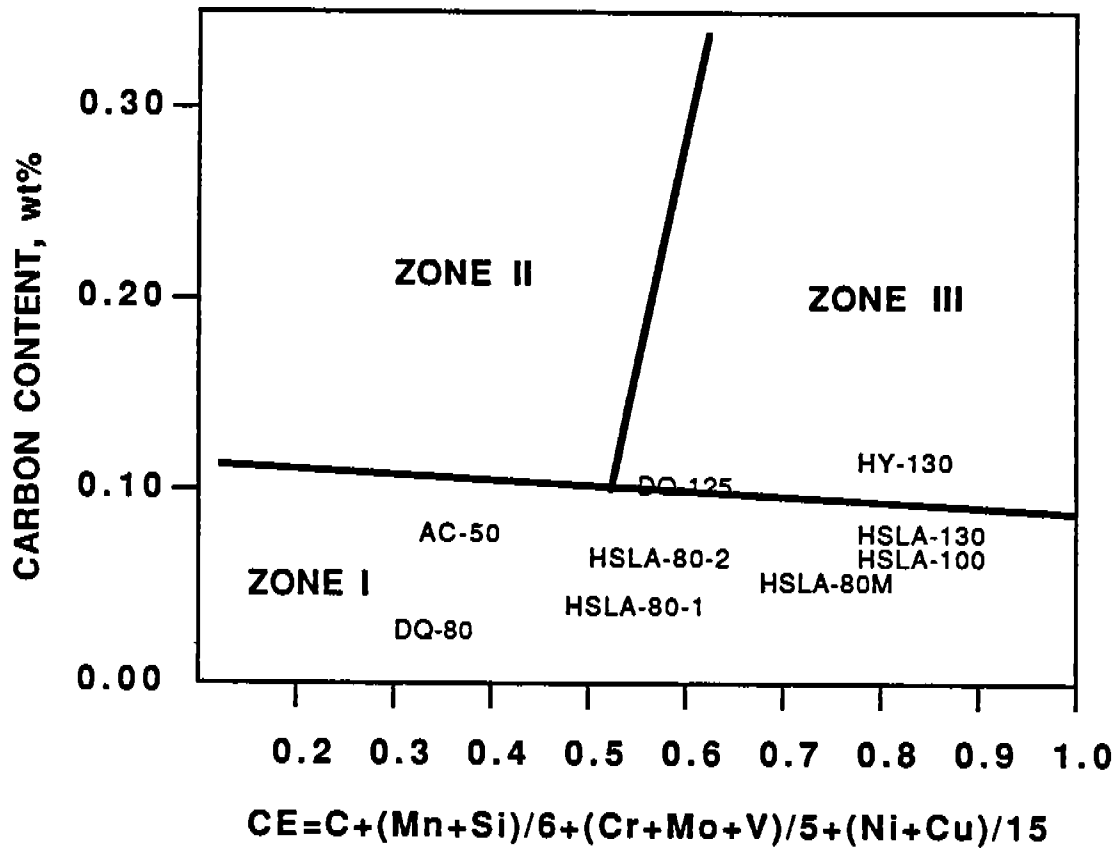
15

Fig. 2.3 Position of steels in this program in the Graville diagram[17].

bainite is formed upon much slower cooling. In lower carbon versions of these steels, however, granular bainite may form depending on the cooling rate. The aging treatment in HSLA-130 is carried out at 1150°F as contrasted to 1200°F in HSLA-100 to obtain higher strength levels while maintaining the chemistry nearly identical.

2.3. DQ STEELS

The Direct Quench (DQ) process recently has been developed in Japan to produce low carbon micro-alloyed steels. Little is known of the actual TMCP parameters employed to produce the DQ-80 and DQ-125 investigated herein. However, a direct quench process, in principle, consists of rapid quenching of steel to a temperature below the martensite transformation temperature after controlled rolling. DQ-80 has the lowest carbon content (0.032%) and carbon equivalent among all steels. It contains 1.14% copper, thus indicating that after controlled rolling and quenching, this steel has undergone aging for the precipitation of epsilon-copper. On the other hand DQ-125 does not contain copper but the carbon content in this steels is higher (0.11%) than in DQ-80. The strength of DQ-125 is mainly achieved by carbon content and microstructure. The base plate microstructure of DQ-125 is shown in Fig. A-25. It is difficult to identify finer microstructural features from the optical micrographs, however, the base plate microstructure consists mainly of martensite and bainite. On the other hand the DQ-80 microstructure (Fig. A-29) consists of ferrite and bainite.

2.4. HY-130

HY-130 is a conventional quenched and tempered steel and like HSLA-100 and HSLA-130 contains higher amounts of Ni (4.68%) to improve low temperature toughness. It may be pointed out that in HSLA steels nickel plays a dual role; it not only improves low temperature toughness properties but is also beneficial in avoiding hot shortness in copper containing steels. The mill treatment of HY-130 consisted of soaking at 1660°F for 60 min. and water quenching followed by a second heat treatment at 1550°F for 60 min. and water quenching. Subsequent to the solutionizing treatment the steel was tempered at 1180°F for 62 min. and water quenched. The base plate microstructure of the as-received plate is shown in Fig. A-21. The microstructure consists of tempered martensite. This steel shows the highest hardness (326 HV) among all steels in this program. This is achieved not only from carbon content (0.12%) but also from other alloying elements in addition to hardening due to the presence of martensite constituent.

2.5. AC-50

AC-50 steel is a low-carbon, manganese steel that has been control rolled and control cooled to produce a fine grain size and higher toughness than for a control rolled only process. Fig. A-33 shows the base metal microstructure of AC-50. It is characterized by the presence of banded structure of ferrite and fine pearlite.

The present set of steels also differs in the amount and type of micro-alloying elements added to control the grain size. The HSLA steels and DQ-80 are micro-alloyed mainly with Nb and Al, whereas DQ-125 and HY-130 contain V and Al. AC-50 contains Al as the major micro-alloying element. The amount of Nb has steadily decreased in micro-alloyed steels from about 0.06% in 1970's to about 0.03% in 1980's [21]. This has resulted from the observations about the detrimental effect Nb exerts on the CHGAZ toughness especially after stress relief treatment. It has been shown that similar to TiN, Nb(CN) has the maximum beneficial effect in controlling grain size [22]. The efficiency of

17

grain pinning by AlN also comes close to that of Nb(CN) and that is why in the modern steels Nb is partly replaced by Al. But the pinning efficiency of VC and VN is least among all the micro-alloy carbides and nitrides. It appears that in DQ-125 (V-0.066%; Al-0.049%) the AlN is the main precipitate controlling the grain growth particularly in high heat input welding as the VC or VN dissolution with increasing heat input is much greater than for AlN.

3. CHARACTERIZATION OF THE HEAT AFFECTED ZONE

3.1. INTRODUCTION

Welding of a material affects the microstructure of the base metal adjacent to the weld deposit and thus the heat affected zone (HAZ) has different mechanical and corrosion properties than that of the weld deposit and base metal. In the HAZ alone there is a point-to-point variation in microstructure and hence properties (microstructural gradient). In the following sections the- (a) HAZ Thermal Cycles and Microstructures, (b) Calculation of Cooling Time, (c) CGHAZ Hardness, and (d) Calculation of Maximum HAZ Hardness are discussed.

3.1.1. HAZ Thermal Cycles and Microstructures

During a welding process the heat affected zone in the base metal adjacent to the fusion zone does not undergo melting but experiences complex thermal and stress alterations. The HAZ consists of several sub-zones which are normally defined by the peak temperature of the welding thermal cycle. Predicting or interpreting metallurgical transformations at a point in the HAZ requires some knowledge of the peak temperature reached at a specific location. Several relationships are available in literature to permit the calculation of peak temperature as a function of distance from the fusion line in a weldment from a knowledge of thermal properties of the material, plate thickness, weld geometry, preheat temperature, welding process and welding parameters [23-26]. The following equation represents a typical example of the predictive equations derived from the heat flow equations for a weldment:

$$1/(T_p - T_0) = 4.13. \, p. \, C. \, t. \, Y/H_{net} + 1/(T_m - T_0) \quad \dots\dots\dots\dots\dots\dots(3.1)$$

where-

T_p = peak temperature (°C) at a distance Y (mm) from the weld fusion boundary,

T_0 = initial plate temperature (°C)

T_m = melting temperature (°C)

H_{net} = net energy input (J/mm)

p = density of material (g/mm^3)

C = specific heat of solid material (J/g.°C)

t = plate thickness, mm

A knowledge of variation in peak temperature with distance can provide useful information regarding the location of a specific zone in the HAZ, estimating the width of the HAZ, and evaluating the influence of preheat temperature on the peak temperature distribution and thus microstructure. The effect of energy input and preheat temperature on the variation of peak with distance from the weld center line for a SMA weld on 1/2" thick plate is shown in Fig.3.1 [25]. A steeper distribution of peak temperatures in the HAZ results when either the energy input or the preheat temperature is decreased.

Each sub-zone in the HAZ is characterized by a different microstructure and hence different mechanical properties. Fig.3.2 illustrates, by a series of optical micrographs, the various zones in the HAZ of a shielded metal arc welded normalized pearlitic steel [22]. This Figure also includes the microstructure of the unaffected base metal for comparison. The zone immediately adjacent to the fusion zone experiences the highest peak temperature and austenite grain growth takes place. This zone is referred as the coarse grained HAZ region (CGHAZ) and corresponds to an average peak temperature of 2400°F. The CGHAZ is of paramount importance not only from the point of view of mechanical properties such as strength and toughness but

19
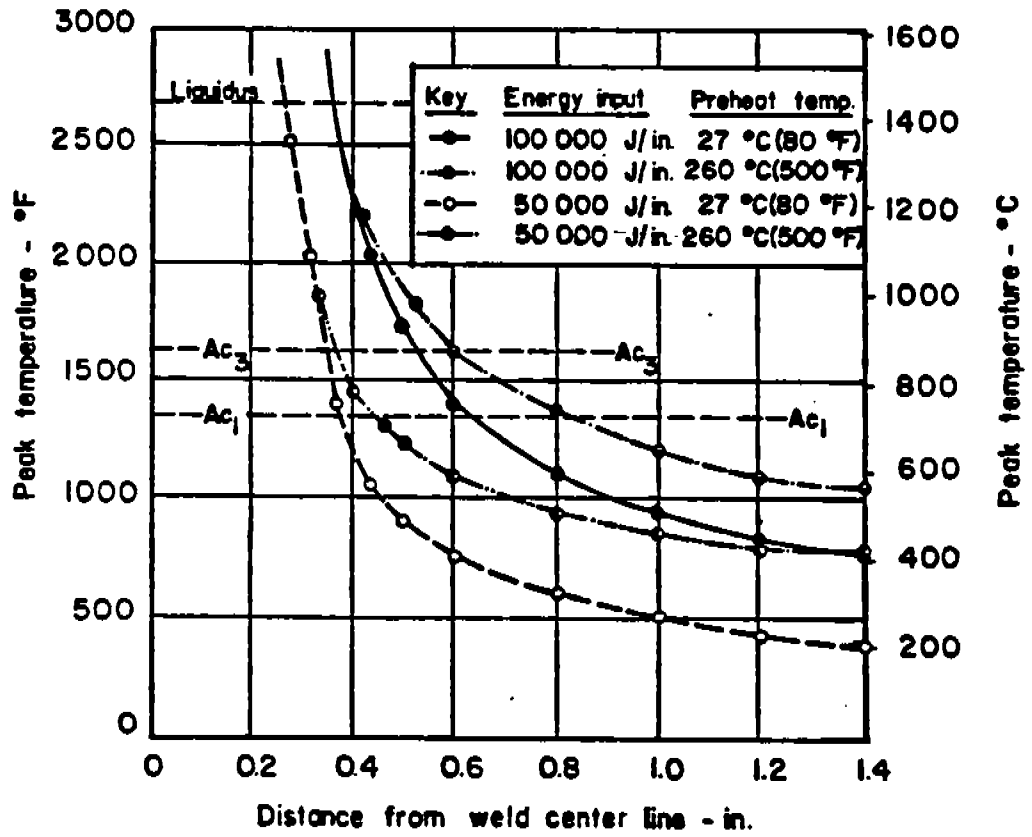
Fig.3.1. Effect of energy Input and preheat temperature on peak temperature distribution. [25]
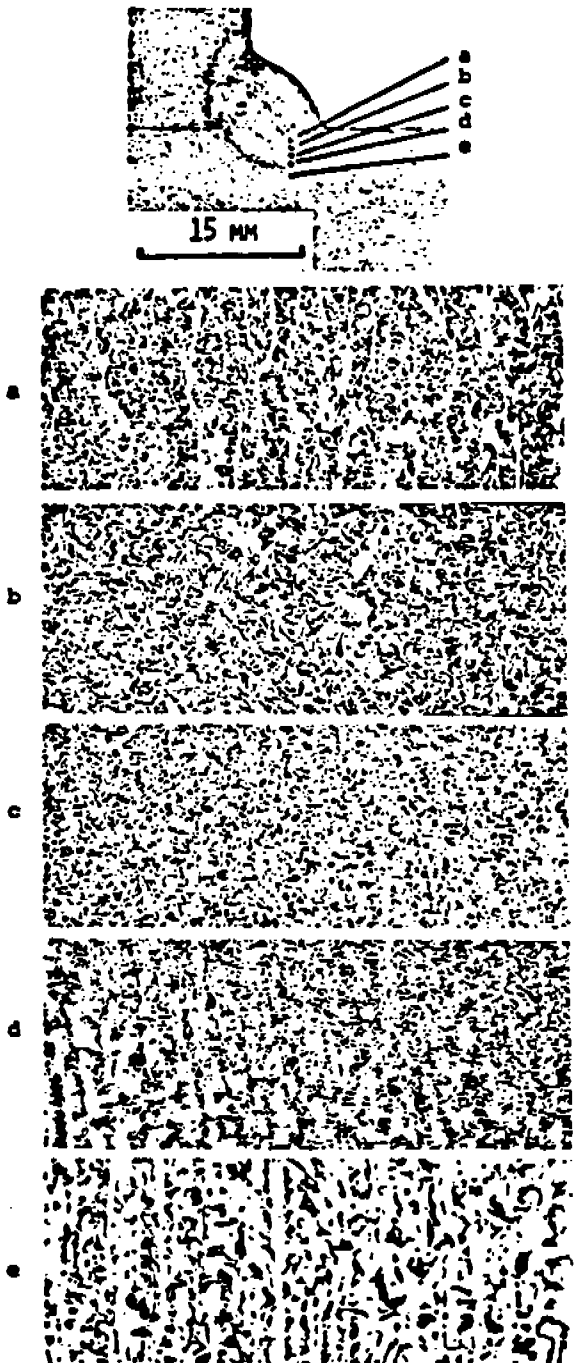
Fig.3.2. (a) Fusion zone
          (b) CGHAZ
          (c) FGHAZ
          (d) ICHAZ
          (e) Unaffected base metal [22]

also for its susceptibility to cold cracking and reheat cracking. The 2400°F peak temperature is commonly used to represent the CGHAZ, but in many investigations peak temperatures ranging from 2300 to 2650°F have been employed to simulate the CGHAZ. Ronningen et al [27] quantitatively measured the amounts of various micro-constituents present in the HAZ. It was found that a "soft" zone in the base metal existed very close to the fusion when the weld deposit carbon content was less than in the base metal. Fig.3.3 shows variation in the carbon content and fraction of martensite as a function of distance from the fusion zone in a 0.17 wt.% carbon micro-alloyed steel. The "soft" zone closely corresponds to a decrease in the carbon content. However, the martensite content beyond the "soft" zone remains constant for considerable distance. Therefore, the embrittling effect of martensite is evidenced more at some distance from, rather than immediately adjacent to the fusion zone. Since in most cases the weld deposit carbon content is less than the base metal content, it is not surprising that underbead cracks are formed a short distance away from the fusion line. In view of the above, the choice of 2400°F peak temperature (representing a HAZ region slightly away from the fusion zone) appears to be based on the fact that the microstructure represents the most severe metallurgical condition in the CGHAZ.

During the on-heating portion of a thermal cycle for an average peak temperature of 1750°F, ferrite transforms to austenite and sufficient time is not available for the austenite grains to grow, therefore, the grain size in this zone remains small. Consequently during the austenite to ferrite transformation for the on-cooling portion of the cycle, a fine grained microstructure results, and the corresponding zone is called the fine grained HAZ (FGHAZ). In micro-alloyed steels the FGHAZ is quite wide because of more effective grain boundary pinning as the carbides and nitrides present do not completely dissolve at these temperatures. A thermal cycle with a peak temperature of 1450°F represents the HAZ heated between the critical temperatures (A$_1$ - A$_3$) and is known as the intercritical HAZ (ICHAZ) or partially refined zone. Thermal cycles with peak temperatures less than the A$_1$ temperature represent subcritical HAZ exposures (SCHAZ).

The HAZ properties depend not only on the thermal cycle but also on the prior thermal and mechanical history of the material. For example, recrystallization behavior during a thermal cycle is affected by whether the original material was cold rolled, cold rolled and control cooled, or in the annealed condition. The onset and extent of grain growth is influenced by the presence of precipitates such as carbides and nitrides of the micro-alloying elements and their solubility at high temperatures.

A HAZ thermal cycle is defined by a steep heating portion, peak temperature, and cooling portion. The heating and cooling portions of the thermal cycle are important and exert different influences on the HAZ. According to Easterling [22] the following metallurgical alterations can occur during the heating and cooling portions of the weld thermal cycle. However, the extent of these changes depends on the welding process used, the geometry of the weld joint, plate thickness, preheat temperature, and the composition of the material.

(a) During the heating cycle:
- recrystallization
- ferrite to austenite transformation
- pearlite/cementite to austenite transformation
- carbon distribution in austenite
- carbonitride coarsening

22
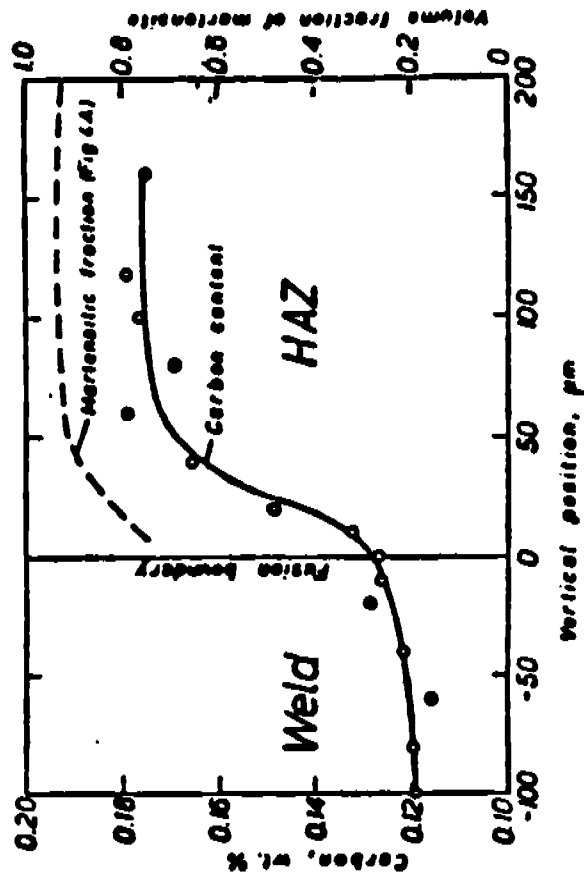
Fig.3.3. Variation in carbon content and martensite fraction in a SMA weldment. [27]

23

- carbonitride dissolution
- austenite grain growth

(b) During the cooling cycle:
- continued austenite grain growth
- austenite transformation to ferrite and cementite
- reprecipitation
- continued coarsening

Fig.3.4 presents a typical family of thermal cycles for an arc welding process (plate thickness - 1/2") [25]. The following three characteristics are apparent:

(a) the peak temperature decreases rapidly with increasing distance from the fusion boundary

(b) the time required to reach peak temperature increases with increasing distance from the fusion boundary

(c) the rate of heating and the rate of cooling both decrease with increasing distance form the fusion boundary

The HAZ thermal cycles are also affected by the heat input of welding and the preheat temperature. This is illustrated in Fig.3.5 for a SMA weld in 1/2" thick plate [25]. The following changes take place when the energy input or preheat temperature is increased:

(a) For a given preheat temperature, increasing the energy input causes an increase in the time of exposure to temperature near the peak temperature and causes a decrease in cooling rate

(b) For a given energy input, increasing the preheat temperature decreases the cooling rate, but does not significantly influence the time of exposure to temperatures near the peak temperature.

The thickness of the plate influences the thermal cycle in a complex way as shown in Fig.3.6 for a 1/2" thick 40 kJ/in SMA weld with an 80°F preheat temperature [25]. The cooling rate tends to increase with an increase in plate thickness. With increasing thickness the heat flow pattern changes from two to three dimensional. The critical thickness where the heat flow changes from 2 to 3-D mode is a function of welding parameters, joint geometry, and plate thickness. For example, for a given set of welding parameters and plate thickness, the heat flow may be 2-D for a butt weld but 3-D for a fillet weld. To distinguish between thick and thin plates a dimensionless quantity, t, is defined, which is the relative plate thickness.

$$t = h\sqrt{\{[pC\,(T_c - T_0)]\,/\,H_{net}\}} \qquad \text{.......................................(3.2)}$$

where;

h = thickness of the base metal, mm
H_{net} = net energy input, J/mm
p = density of base metal, g/mm3
C = specific heat of base metal, J/g.°C
T_0 = the initial plate temperature, °C
T_c = the temperature at which the cooling rate is calculated, °C

The plate is "thin" if t is less than 0.6 and "thick" if t is greater than 0.9. The relative plate thicknesses between 0.6 and 0.9 are referred as showing 2 1/2 - D behavior.

The presence of a susceptible microstructure in the CGHAZ is one of the factors besides stress and diffusible hydrogen responsible for hydrogen assisted cracking. The chemical composition of a steel along with the peak temperature attained during welding, and cooling rate or cooling time through the austenite transformation temperature range determines the

24
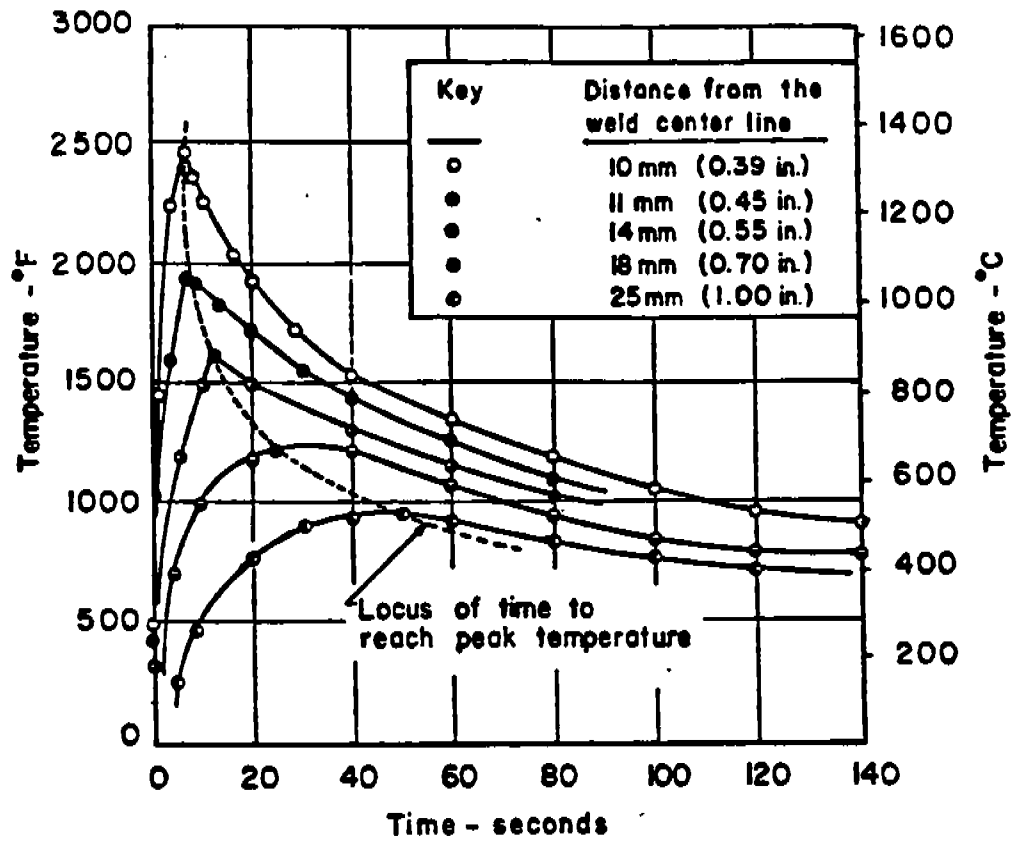
Fig.3.4. Thermal cycles experienced by indicated locations in the heat-affected zone of an arc weld. [25]
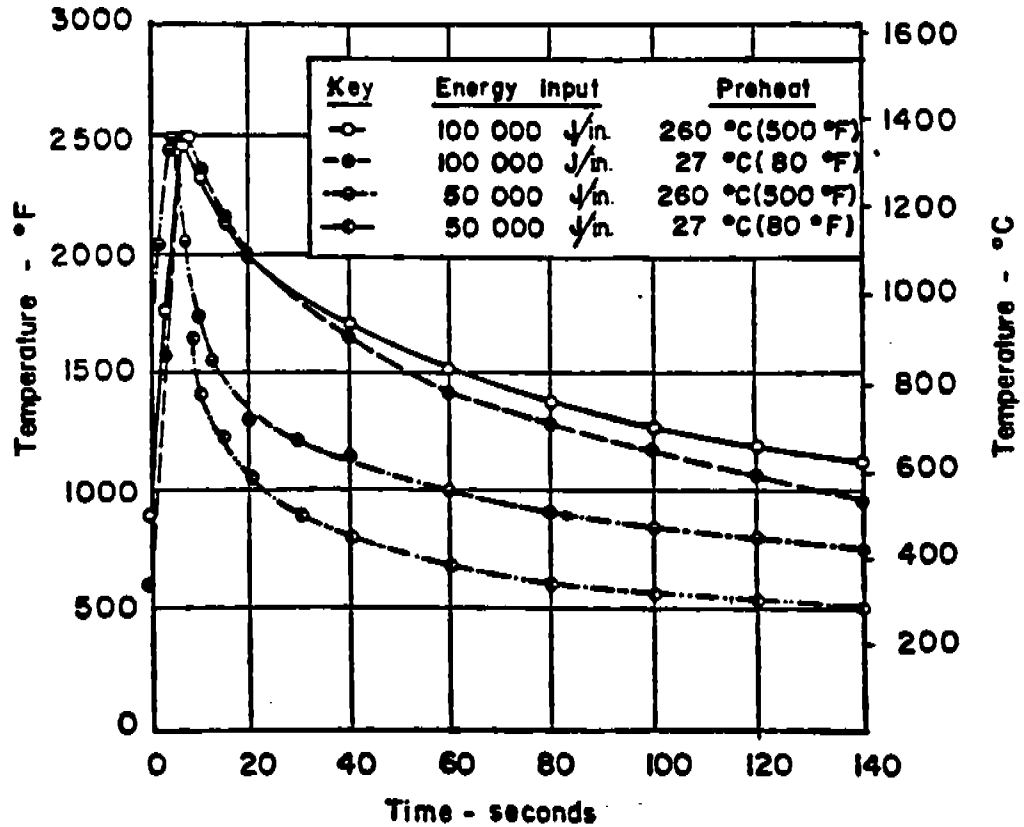
Fig.3.5. Effect of initial plate temperature on thermal cycles in the heat-affected zone of an arc weld. [25]

25
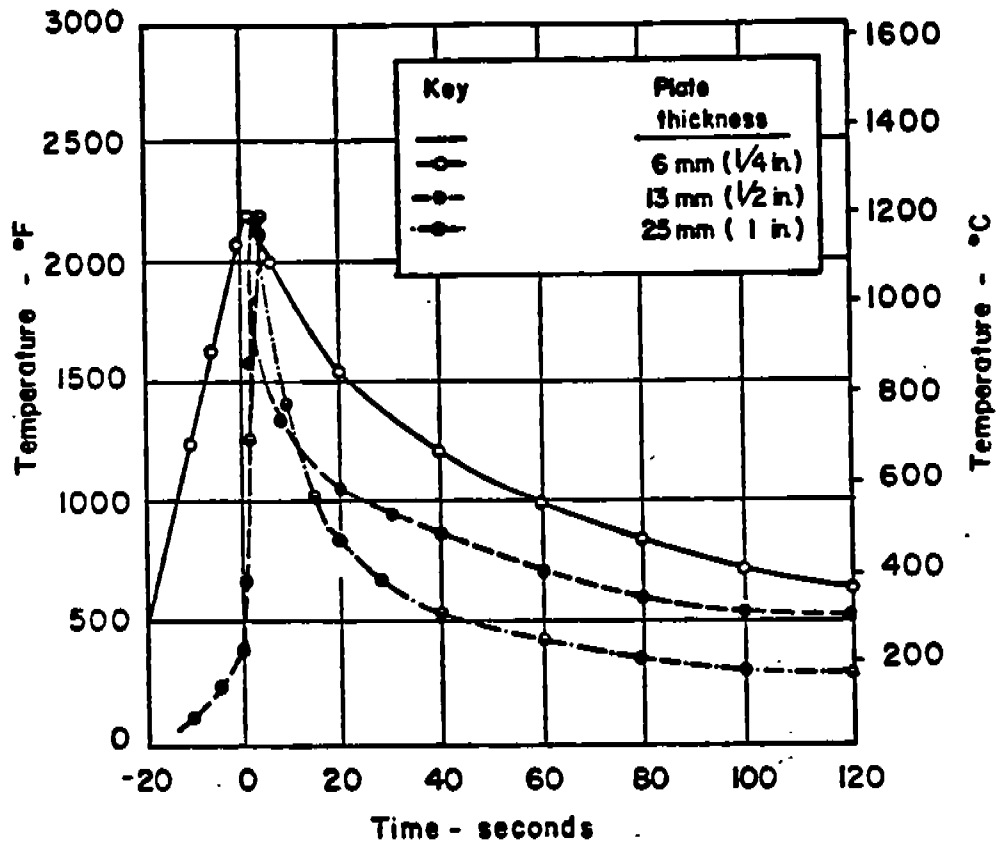
Fig.3.6. Effect of plate thickness on the thermal cycles in the weld HAZ of SMA welds in steel plate [25]

Energy Input: 47 kJ/in.
Initial plate temperature: 80°F.

microstructure developed in the HAZ. The effect of chemical composition on the HAZ microstructure is represented by a carbon equivalent (CE), which normalizes the composition to a single number. There are several carbon equivalents available depending on the type of weldability approach and kind of steel. There is no universal CE formula applicable to all classes of steels. Most of the formulae have limited validity (in terms of chemical composition, cooling time from 800 to 500°C, and plate thickness) and are applicable to the class of steels for which they were devised, though there are claims to the contrary. The reason for disagreement appears to result from the fact the "derivation" of CE formulae is still empirical in nature and experimental errors in determining cooling time, hardness and chemical composition may cause significant scatter when comparing data from different sources. Moreover, predictive utility of the CE's has come into question, especially with respect to modern HSLA steels, which have a significantly reduced carbon content. In conventional steels with higher CE's, the weldability and metallurgical response are totally dictated by the carbon content and CE values. As C and CE levels have progressively decreased, the importance of other metallurgical factors, such as austenite grain size, which hitherto was negligible as compared to the dominant effect of the overall chemistry, has increased. The controlled addition of micro-alloying elements to steels and the application of the TMCP during production stage have reduced the tendency of austenite grain size coarsening, thereby increasing the grain boundary area and hence sites for nucleating ferrite. The enhancement in the density of inclusions in the shape controlled steels and the presence of boron are believed to play a similar role. The main effect of these parameters is to decrease the hardenability of steels for a constant chemical composition. The influence of such effects was not taken into consideration in the conventional CE formulae. Recently some attempts have been made to rationalize the predictive models on the basis of metallurgical factors, but considerably more data are needed to develop a workable model [28].

3.1.2. Calculation of Cooling Time

To obtain an accurate and reproducible prediction of the maximum HAZ hardness, the cooling rate or cooling time between 800 to 500°C should either be measured or calculated by available nomograms and predictive equations. Many attempts have been made to develop a suitable model to calculate a HAZ thermal cycle, however, since the thermal cycle for an actual welding process depends on a number of parameters, some of which are not known or are estimated with certain assumptions, the prediction of $t_{8/5}$ is still based largely on semi-empirical equations. One of the first attempts to theoretically calculate a welding thermal cycle was made by Rosenthal [29,30]. Though the basic form of the equation has remained unchanged over the years, the accuracy of the model has been improved by incorporating the following modifications [31-38]: the point heat source has been replaced by a finite source size used in practice to give a better measure of the shape of the temperature field about the moving electrode, the Rosenthal equation was further refined by using experimental measurements to adjust for unknown effects of alloying additions on the thermal properties of the steels, arc efficiency, and latent heat of fusion and transformation. However, the effect of latent heat of transformation of various transformed products on the thermal cycle is difficult to incorporate in the heat flow equation as it depends on a number of factors like chemical composition, grain size, and prior thermal history of the steel. Therefore, a heat flow equation modified for a particular steel may not be appropriate for another class of steel. The

27

empirical-analytical approach has been found to be of limited use for calculating complete thermal cycles, but these can be, nevertheless, employed for calculating cooling time/cooling rate and the variation in peak temperature with distance from the fusion boundary. The cooling time and cooling rate have been shown to describe the hardenability behavior of steels and has been used successfully to compute maximum HAZ hardness from carbon equivalent of steel. The HAZ thermal cycle has been variously characterized by cooling rates at 570°F (300°C), 1000°F (540°C), and 1300°F (704°C), but recently the cooling time between 1472°F (800°C) and 932°F (500°C) has found universal acceptance because of ease and accuracy in its determination.

Several authors have published nomograms for the determination of cooling time, $t_{8/5}$. Inagaki and Sekiguchi [39] constructed a nomogram based on experimental data from actual bead-on-plate and T-fillet-joint SMA welds. The nomogram is shown in Fig.3.7. This nomogram also provides the effect of preheat temperature on $t_{8/5}$. It is applicable for a maximum plate thickness of 34 mm, and between 20 and 117 kJ/in. heat input. Within the applicable heat input range $t_{8/5}$ for thicknesses greater than 34 mm will be similar to that for 34 mm. The cooling time from the nomogram is obtained where the tie line connecting the heat input and plate thickness intersects the cooling time line.

Two nomograms were proposed respectively by Berkhout and van Lent (Fig. 3.8) [40] and De Fourny and Bragard (Fig. 3.9) [41]. Both nomograms were based on heat flow theory as opposed to Inagaki's nomogram which is based on experimental observations. The De Fourny and Bragard nomogram provides separate charts for determining mode of heat flow and different charts for calculating $t_{8/5}$ depending on whether the operating mode is 2-D or 3-D.

The cooling time from the Berkhout and van Lent nomogram is determined by following the procedure described below-

(a) Connect the plate thickness and energy input, read a cooling time from 800 to 500°C when tie line does not touch or cross the 3-D line. If the tie line touches or crosses the 3-D line, connect 0 of the 3-D line with energy input and read cooling time on 2-D line.

(b) Preheat temperature correction is made using the preheat temperature scale. The transition point between 2-D and 3-D heat flow must also be shifted on the 3-D line.

The cooling time from the De Fourny and Bragard nomogram can be determined by using the following operating instructions-

(a) Find the heat flow pattern at given nominal energy input and plate thickness using Fig. 3.9 (1). Use preheat levels as indicated in the Figure.

(b) For 3-D heat flow, the cooling time can be read from Fig. 3.9 (2).

(c) For intermediate or 2-D heat flow cooling time must first be read from Figs. 3.9.(3) and 3.9 (5) respectively and a correction for thickness is then necessary. The correction factor is read from Figs. 3.9. (4) and 3.9. (6), for intermediate and 2-D heat flow respectively, and the cooling time value read from Figs. 3.9. (3) or 3.9. (5) is divided by the correction factor to arrive at the "correct" cooling time.

Though a number of equations are available in literature to calculate $t_{8/5}$ from welding parameters, only two equations have been considered in this investigation. The basis of selection for the equations was dictated by the type of steel for which they were developed, and convenience in calculating cooling times. The following equation for calculating $t_{8/5}$ was proposed by Uwer and Degenkolbe [42] for normalized, normalized and tempered, and quenched and tempered low alloy high strength steels:

28

HEAT INPUT   COOLING TIME   PLATE THICKNESS

KILOJOULES PER INCH	FROM 1472 F TO 932 F	FOR CARBON AND ALLOY STEELS
KJI	SECONDS	INCHES

```
200                               1/8
175          600                    5/32
150   200    500                         3/16
             400
125   175    300
      150    200               1/4
100          150
90    125    100               5/16
80    115    80
             60                3/8
70    100    50
      90     40
60    80     30                7/16
             25
50    70     20
45    60     15
40    55                       1/2
35    50     10
      45     8                 9/16
30    40     6                 5/8
25    35     4                   11/16   3/4
      30     3                 1
20           2
      25
15    20
```

FILLET WELD IN TEE JOINT
BEAD-ON-PLATE CONDITIONS

Fig.3.7. Nomograph for calculating cooling time which elapes between 1472 and 932 °F when the base metal heat-affected zone cools from an arc-welding operation. [39]

PLATE THICKNESS

CT 800-500

PREHEAT TEMPERATURE

NOMINAL ENERGY INPUT kJ/cm
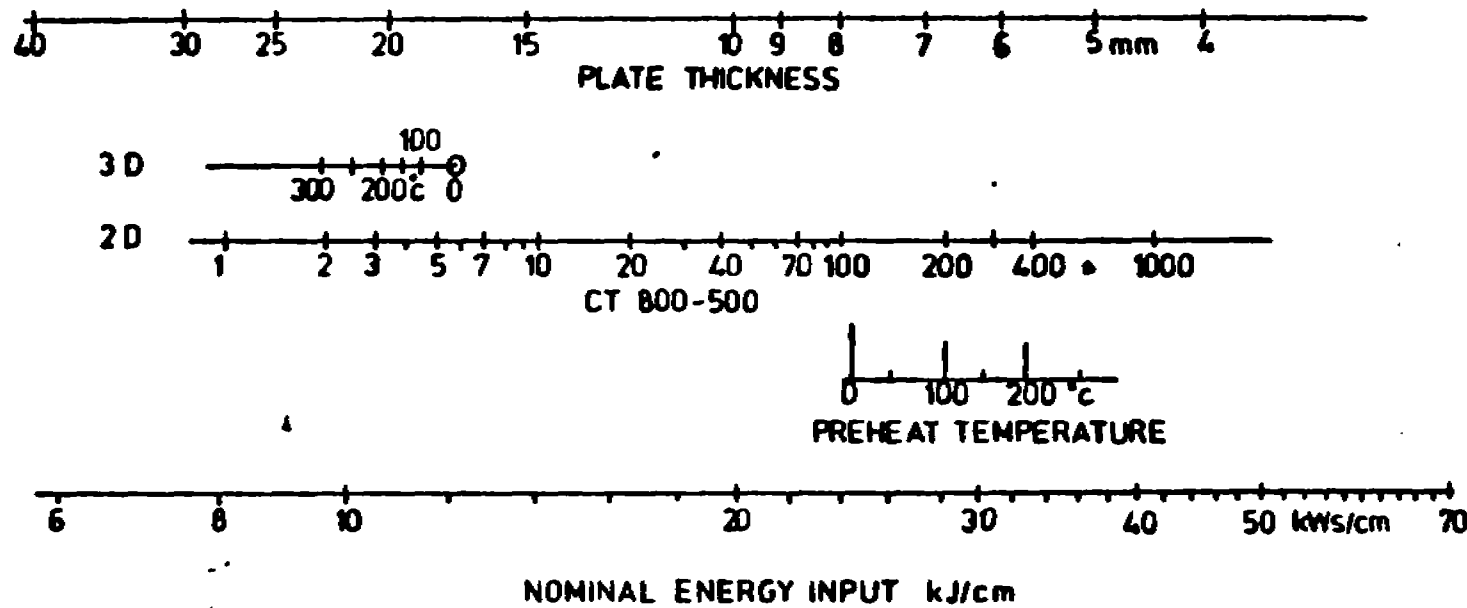
Fig.3.8. Berkhout and van Lent nomogram for estimation of cooling time. [40]

30
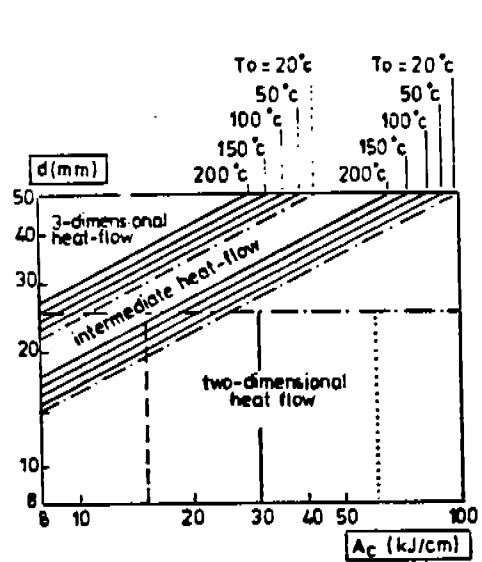
Fig.3.9(1). Charts for the determination of t 8/5. Type of heat-flow.
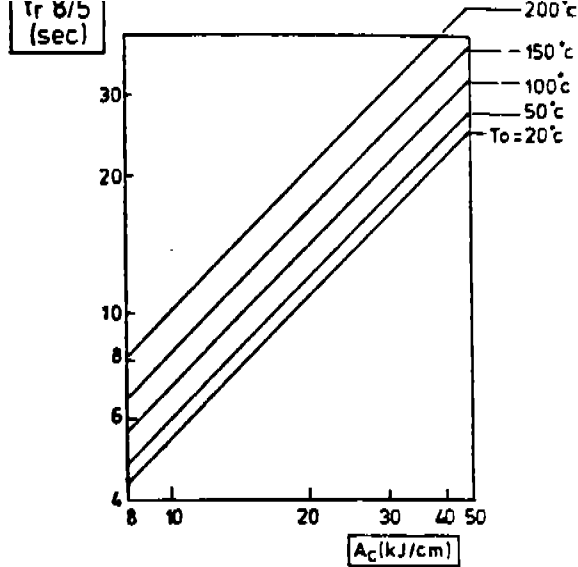
Fig.3.9(2). Charts for the determination of t 8/5. Three-dimensional heat-flow.
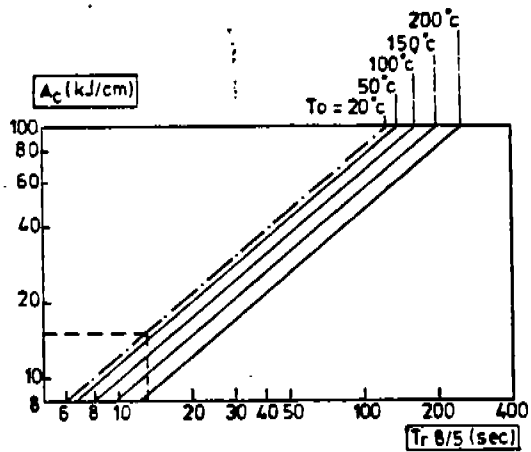
Fig.3.9(3). Charts for the determination of t 8/5. Intermediate heat-flow. Cooling time for d: 10 mm.
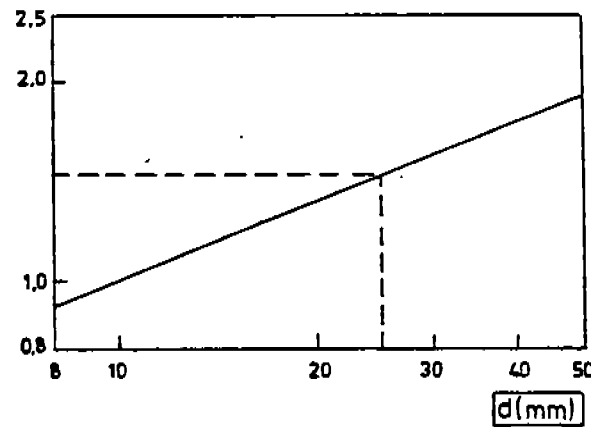
Fig.3.9(4). Charts for the determination of t 8/5. Intermediate heat-flow. Correction for thickness.
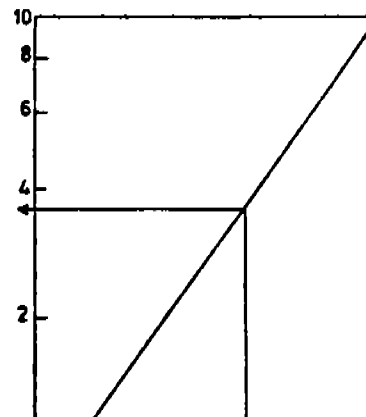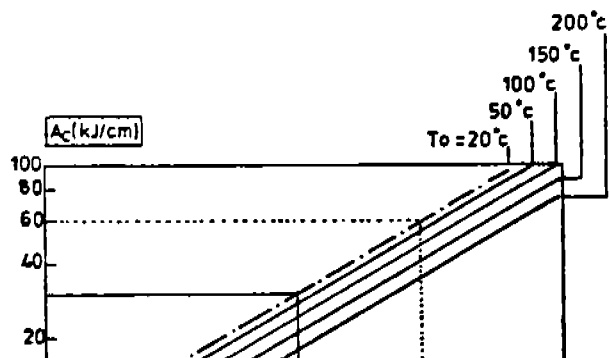
$$t_{8/5}(3-D)=K_3.n.E.[(500-T_o)^{-1}-(800-T_o)^{-1}].F_3 \quad ....(3.3)$$

$$t_{8/5}(2-D)=K_2.[(n^2.E^2)/d_k^2].[(500-T_o)^{-2}-(800-T_o)^{-2}].F_2 \quad .....(3.4)$$

$$d_k=[(K_2/K_3).n.E.\{(500-T_o)^{-1}+(800-T_o)^{-1}\}]^{1/2} \quad ....(3.5)$$

where-

$K_2 = 0.043 - 4.3 \times 10^{-5} \times T_o$

$K_3 = 0.670 - 5.0 \times 10^{-4} \times T_o$

T_o = preheat temperature in °C

n = arc efficiency

E = heat input in kJ/cm

d_k = critical plate thickness in cm

F_2 and F_3 are weld factors for 2-D and 3-D heat flow respectively.

The Uwer and Degenkolbe equation is applicable to several welding processes, and different joint geometries.

Suzuki [43] recently proposed the following simplified equation for determining $t_{8/5}$:

$$t_{8/5} = F[\gamma/(600-T_p)^\delta].Q^{(\alpha+ \beta T_p)} \quad ....(3.6)$$

where-

Tp = preheat temperature in °C

F = 1 for bead-on-plate long welds

F = 0.9 for groove weld (first pass)

F = 0.67 for fillet weld (first pass) on plate thicker than 20 mm

F = 0.45 to 0.67 for fillet weld on plate thinner than 20 mm

The values of γ, δ, α and β depend on plate thickness and welding parameters (Table 3.1).

The above nomograms and equations provide a single $t_{8/5}$ for a given set of conditions. However, it is observed that even in the HAZ of a single pass weld the cooling time, $t_{8/5}$, and hence the microstructure is not the same at all the locations. Kohno and Jones [44] measured the CGHAZ thermal cycles at three different locations in a submerged arc bead-on-plate deposit. Fig. 3.10 shows the thermal cycles recorded at the root (R), re-entrant (B), and surface (S) locations of the weld deposit. The position of the thermocouple is shown schematically in the inset. It is clearly observed that there is a significant difference in the three thermal cycles. The cooling time, $t_{8/5}$, and retention time above 1050°C (which determines the time available for austenite grain coarsening) at the surface of the weld are appreciably longer than that at the root.

Therefore, the prior austenite grain size and microconstituents in the CGHAZ will vary depending on the location. In the nomograms and equations for determining $t_{8/5}$ there is no mention about the location of HAZ where $t_{8/5}$ was determined.

3.1.3. CGHAZ Hardness

The coarse grained HAZ experiences the maximum peak temperature and is often represented by a thermal cycle with 2400°F peak temperature. The type of microstructure obtained and thus hardness in the CGHAZ depends on $t_{8/5}$ and chemical composition of the steel (carbon equivalent). Fig. 3.11 illustrates the variation of maximum hardness as a function of cooling time [45]. Also shown are the microstructures typically obtained as a function of hardness. It is noticed that the hardness curve is represented by three distinct regions. There are two plateaus - upper and lower. The upper plateau, at shorter

Table 3.1 Parameters for calculating $t_{8/5}$ from Suzuki's equation [43].

Plate Thickness (mm)	Heat Input (kJ/cm)	Preheat Temp. (°C)	γ	δ	α	β
>20	6-15	20-200	993	1.22	0.94	0.0007
20	15-50	do.	966×10^{-5}	3.30	1.61	-0.00068
25	do.	do.	1.31	0.274	1.15	0.00111
30	do.	do.	3.51	0.345	0.97	0.00103
>40	do.	do.	63200	1.87	0.96	-0.00004

33
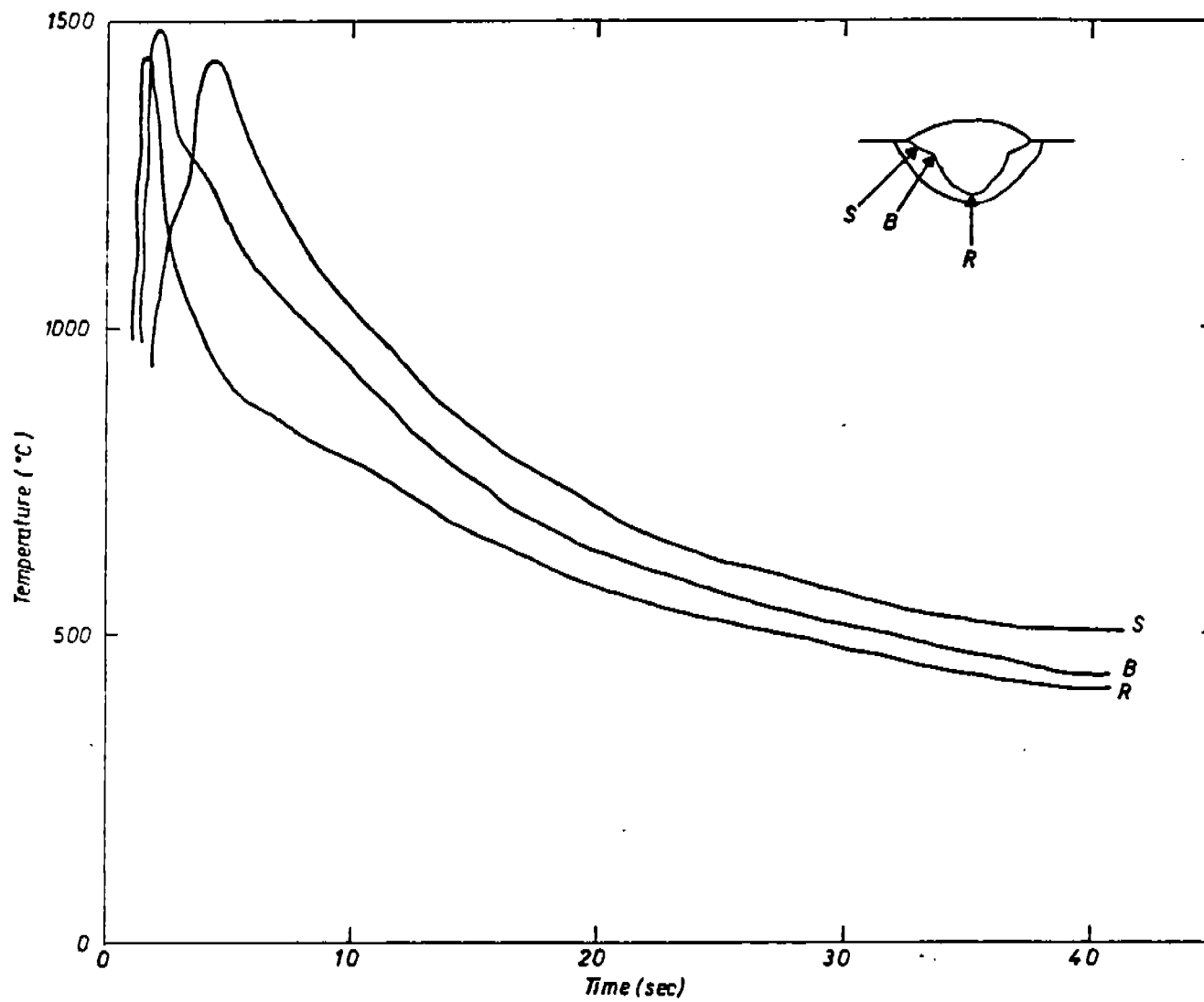
Fig.3.10. Variation in thermal cycle with thermocouple position. [44]
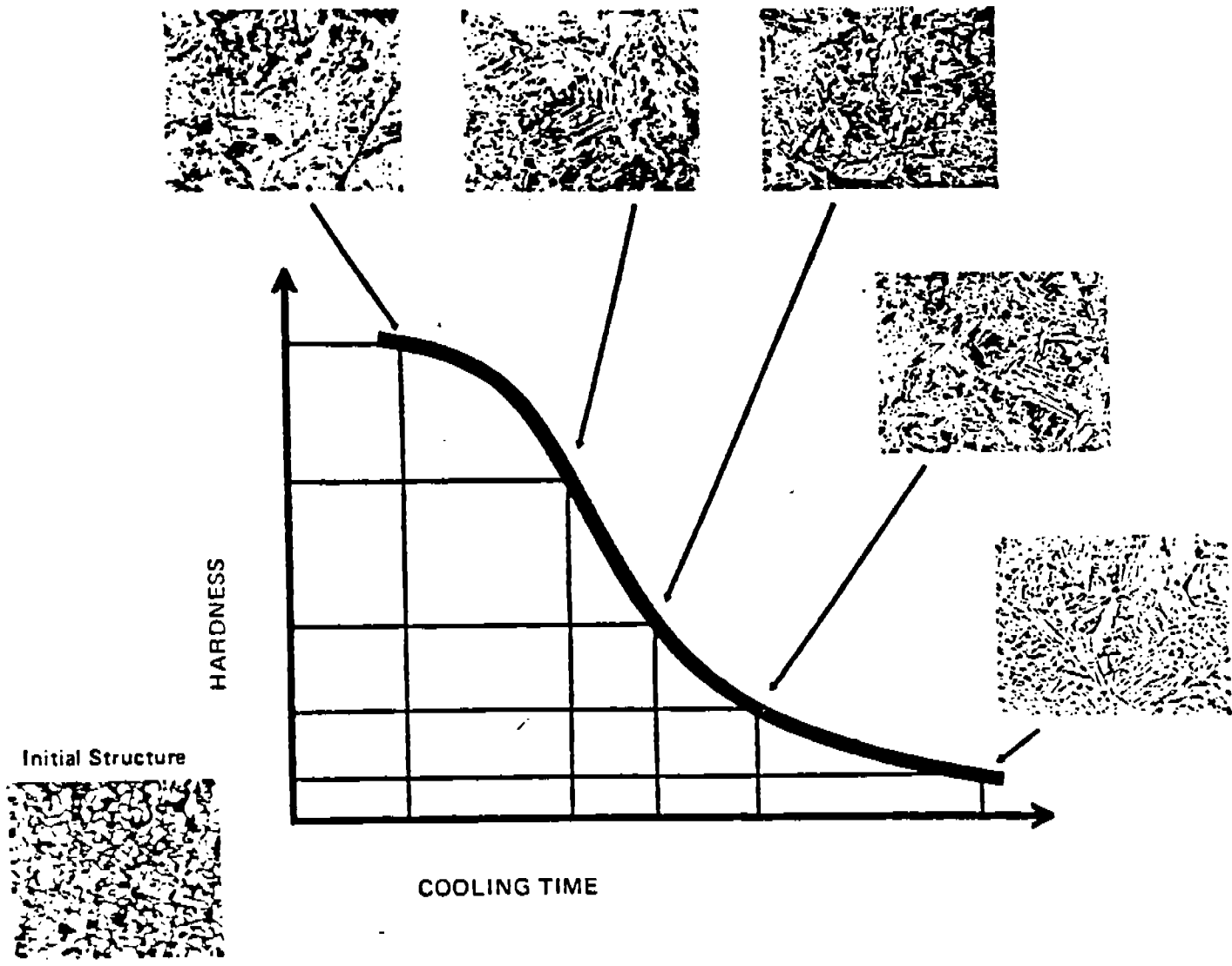
Fig.3.11. Typical hardness versus cooling time curve with HAZ microstructures corresponding to different hardness values superimposed. [45]

cooling times, represents the hardness of 100% martensite, which is essentially a function of carbon content, and the lower plateau, at longer cooling times, defines the hardness of non-martensitic constituents such as bainite and ferrite and depends on the carbon equivalent. Between these two regions the hardness drops rapidly as a transition occurs from martensite to upper and lower bainite microconstituents. The hardness of martensite (H_M) depends mainly on the carbon content as shown in Fig.3.12 [46]. The maximum hardness (HV) can be represented by the following empirical relationships:

$$H_M = 812\ C + 293\ \ [47] \ \dots\dots\dots(3.6)$$

$$H_M = 802\ C + 305\ \ [48] \ \dots\dots\dots(3.7)$$

$$H_M = 939\ C + 284\ \ [49] \ \dots\dots\dots(3.8)$$

$$H_M = 1667\ C - 926\ C^2 + 150\ \ [50] \ \dots\dots(3.9)$$

$$H_M = 884\ C - 265.2\ C^3 + 294\ \ [16] \ \dots\dots(3.10)$$

Maynier et al [51] have provided the formula for estimating H_M. In this relationship the effect of alloying elements and cooling rate is also incorporated, which is not taken into account by formulae (3.6) to (3.10). The alloying elements (other than carbon) should exert a weak effect on the martensite hardness by solid solution strengthening. The cooling rate effect takes into account the decrease in H_M due to auto-tempering when the cooling rate (R °C/h) is decreased.

$$H_M = 127 + 949\ C + 27\ Si + 11\ Mn + 8\ Ni + 16\ Cr + 21\ \log R \ \dots\dots(3.11)$$

The hardness at the lower shelf for non-martensitic constituents (H_B) has also been quantified by the following empirical relationships. A linear increase in H_B with CE is shown in Fig. 3.12

$$H_B = 350\ C_{EB} + 101\ \ [48] \ \dots\dots\dots(3.12)$$

$$(C_{EB} = C + Si/11 + Mn/8 + Cu/9 + Ni/17 + Mo/6 + V/3)$$

$$H_B = 145 + 130\ \tanh(2.65\ CE_{II} - 0.69)\ \ [16] \ \dots\dots(3.13)$$

$$(CE_{II} = C + Si/24 + Mn/5 + Cu/10 + Ni/18 + Cr/5 + Mo/2.5 + V/5$$
$$+ Nb/3)$$

$$H_B = -323 + 185\ C + 330\ Si + 153\ Mn + 65\ Ni + 144\ Cr + 191\ Mo$$
$$+ (98 + 53\ C - 55\ Si - 22\ Mn - 10\ Ni - 20\ Cr - 33\ Mo)\ \log R\ \ [51]\dots(3.14)$$

where R in °C/h represents the CGHAZ cooling rate.

The hardness response of a steel can be computed from a knowledge of the presence of various microconstituents as a function of $t_{8/5}$. Fig. 3.13 shows a typical diagram developed to provide fractions of various phases present in the HAZ as a function of cooling time [39]. The HAZ hardness, as a function of distance from the fusion line, can be calculated by assigning hardness to each constituent and applying the rule of mixtures approach. However, such diagrams may not be applicable to all classes of steel and therefore, the use of a CE to describe the hardenability of steels is preferred and in the literature a number of CE's are available, which essentially differ from one another in the weightage given to different alloying elements. The concept of carbon equivalent was devised to assess the susceptibility of steels to hydrogen assisted cracking. However, these CE's are also increasingly being used to calculate the maximum HAZ hardness.

3.1.4. Calculation of Maximum HAZ Hardness

The cold cracking susceptibility of steels can be assessed by using a hardness control approach (BS:5135) [12]. This approach is based on the observation that the occurrence of HAZ cracking is greatly reduced when the

36
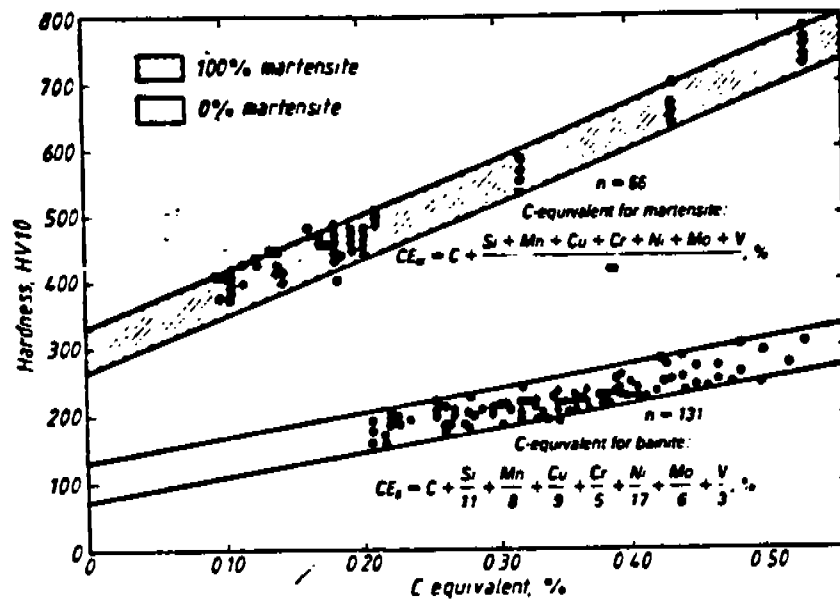
Fig.3.12. Hardness of the martensite and bainite in the HAZ as a function of their carbon equivalent. [46]

Within figure 1:
- 100% martensite
- 0% martensite
- n = 66
- C-equivalent for martensite:
$$CE_m = C + \frac{Si + Mn + Cu + Cr + Ni + Mo + V}{6} \, \%$$
- n = 131
- C-equivalent for bainite:
$$CE_b = C + \frac{Si}{11} + \frac{Mn}{8} + \frac{Cu}{9} + \frac{Cr}{5} + \frac{Ni}{17} + \frac{Mo}{6} + \frac{V}{3} \, \%$$

Axes: Hardness, HV10 (vertical); C equivalent, % (horizontal)
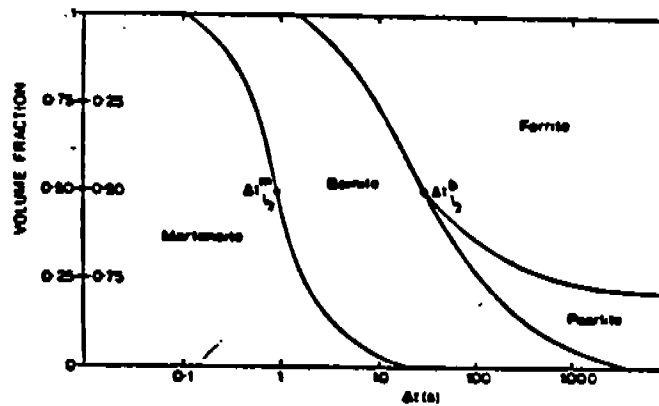
Fig.3.13. Relationship between the amount of various eutectoidal decomposition products in the HAZ and the cooling time of the weld thermal cycle. [39]

37

maximum HAZ hardness is below a certain value. An accurate knowledge of CGHAZ hardness is also necessary in order to be able to predict the critical stress (in implant cracking tests) to determine the susceptibility of steels to hydrogen assisted cracking. Therefore, the ability to calculate the maximum HAZ hardness (H_{max}) accurately from the steel composition and cooling time provides a valuable tool by which the ultimate prediction of welding conditions can be achieved for crack-free welds.

Several formulae have been developed to determine H_{max} from $t_{8/5}$ and CE. Some of the formulae claimed to provide accurate determination of H_{max} are described below:

(a) Maynier's Formula [51]

Hardness of fully martensitic and fully bainitic structures is given by equations (3.11) and (3.14) respectively. The hardness for a mixed structure is provided by the following relationship:

$$H_{max} = 42 + 223\ C + 53\ Si + 30\ Mn + 12.6\ Ni + 7\ Cr + 19\ Mo$$
$$+ (10 - 19\ Si + 4\ Ni + 8\ Cr + 130\ V)\ \log R \qquad \text{................(3.15)}$$

where R is the cooling rate measured in °C/h

(b) Beckert's Formula [49]

$$H_{max} = B + (A - B)\ \exp[-(bt_{8/5})^2] \qquad \text{...................(3.16)}$$

where-

A = 939 C + 284

B = 167 $(CE_B)^{2.42}$ + 137

b = exp(-0.013 B + 0.8)

CE_B = C + Si/11 + Mn/2.9 + Cu/3.9 + Ni/17 + Cr/3.2 + Mo/3.4

(c) Duren's Formula [48]

For $t_M < t_{8/5} < t_B$

$$H_{max} = 2019\ [C(1 - 0.5\ Y) + 0.3(CE_D - C)] + 66(1 - 0.8\ Y) \qquad \text{......(3.17)}$$

For $t_{8/5} < t_M$

H_{max} = 802 C + 305   (hardness of fully martensitic structure)

For $t_{8/5} > t_B$

H_{max} = 350 CE_D + 101   (hardness of microstructure containing 0% martensite)

where

Y = log $t_{8/5}$

t_M = Cooling time below which 100% martensite is retained

t_B = Cooling time above which no martensite is formed

CE_D = C + Si/11 + Mn/8 + Cu/9 + Ni/17 + Cr/5 + Mo/6 + V/3

Duren's formula is based on data from steels with chemical composition in the range: C - 0.10 to 0.33%, Si - 0.35%, Mn - 1.45%, Cu - 0.03%, Ni - 0.05%, and Cr - 0.05%

(d) Terasaki's Formula [52]

For $t_M \leq t_{8/5} \leq t_B$

$$H_{max} = H_B + (H_M + H_B)\exp[-0.2(t_{8/5}/t_M - 1)] \qquad \text{..................... (3.18)}$$

For $t_{8/5} \leq t_M$

H_{max} = 812 C + 293

For $t_{8/5} \geq t_B$

H_{max} = 164(C + Si/2 + Cr/7 + Mo/2 + V + Nb + 7 B)

where

t_M can be calculated from the following relationship

$\log t_M = 2.5 P_V - 1.27$

$P_V = C + Mn/3 + Cu/4 + Ni/8 + Cr/10 + Mo/3 + 5 B$

The validity range of Terasaki's formula is: C - 0.08 to 0.20%, Si - 0.21 to 0.34%, Mn - 0.48 to 1.57%, Cu - 0 to 0.26%, Ni - 0 to 0.61%, Cr - 0 to 0.95%, Mo - 0 to 0.48%, V - 0 to 0.04%, Nb - 0 to 0.04%, and Ti - 0 to 0.02%

(e) Yurioka-1 Formula [15]

(Yurioka et al have reported three formulae to estimate the maximum HAZ hardness. In this report these formulae will be referred as Yurioka-1, Yurioka-2, and Yurioka-3.)

$$H_{max} = 406 C + 164 CE_I + 183 - (369 C - 149 CE_I + 100) \arctan (x) \quad ......(3.19)$$

where-

$x = (Y - 2.822 CE_{II} + 0.262)/(0.526 - 0.195 CE_{II})$

$Y = \log t_{8/5}$

$CE_I = C + Si/24 + Mn/6 + Cu/15 + Ni/40 + Cr/6 + Mo/4 + V/5 + Nb/5 + 10 B$

$CE_{II} = C - Si/30 + Mn/5 + Cu/5 + Ni/20 + Cr/4 + Mo/6 + 10 B$

The Yurioka-1 formula is based on the steels with the following composition:

C - 0.03 to 0.25%, Si - 0.15 to 0.45%, Mn - 0.87 to 2.06%, Cu - 0 to 0.23%, Ni - 0 to 0.81%, Cr - 0 to 0.85%, Mo - 0 to 0.33%, V - 0 to 0.06%, Nb - 0 to 0.06%, Ti - 0 to 0.018%, and B - 0 to 0.0018%

(f) Suzuki's Formula (BL Formulae) [43]

Suzuki compared the above formulae (Beckert, Duren, Terasaki, and Yurioka-1) using H_{max} data from 70 steels. He assumed the H_{max} curve to be a backward logistic (BL) curve. The general equation of the BL-curve can be represented by:

$$H_{max} = H_B + K/[1 + \exp\{a(Y - Y_5)\}] \quad ....(3.20)$$

where-

$K = H_M - H_B$

H_B, K, a, and Y_5 are BL constants depending on the steel chemical composition.

The value of material constants K, a, and Y_5 were determined for each of seventy steels by simple regression analysis for six $t_{8/5}$ values namely 3, 4, 6, 8, 10, and 20 sec. Stepwise multiple regression analysis was performed for the material constants on eleven alloying elements as independent variables. Based on the above calculations Suzuki proposed the following formulae for calculating H_{max}. The validity limit of these formulae is:

C - 0.017 to 0.33%, Si - 0.05 to 0.65%, Mn - 0.54 to 2.06%, Cu - 0 to 0.26%, Ni - 0 to 2.09%, Cr - 0 to 1.06%, Mo - 0 to 0.66%, V - 0 to 0.07%, Nb - 0 to 0.06%, Ti - 0 to 0.02%, and B - 0 to 0.0023%.

(i) BL-70 Formula

$H_{max} = H_B + K/[1 + \exp\{a(Y - Y_5)\}]$

where-

$K = 269 + 454 C - 36 Si - 79 Mn - 57 Cu - 12 Ni - 53 Cr - 122 Mo - 169 Nb - 7089 B$

$H_B = 884 + 287 - K$

$aK = 478 + 3364 C - 256 Si + 66 Ni - 408 Mo - 1321 V - 1559 Nb$

$Y_5 = - 0.085 + 2.07 C + 0.459 Mn + 0.655 Cu + 0.122 Ni + 0.222 Cr + 0.788 Mo+30 B$

Stepwise multiple regression analysis of the BL constants on two independent variables, C and P_{cm}, yielded BL-70S (P_{cm}) formula with the following values for constants:

$K = 237 + 1633 C - 1157 P_{cm}$

$$aK = 566 + 5532 \ C - 2280 \ P_{cm}$$

$$Y_5 = -0.03 - 6 \ C + 7.77 \ P_{cm}$$

where P_{cm} is the chemical composition parameter proposed by Ito and Bessyo [13].

$$P_{cm} = C + Si/30 + Mn/20 + Cu/20 + Ni/60 + Cr/20 + Mo/15 + V/10 + 5 \ B$$

Suzuki compared BL-70 and BL-70S (P_{cm}) formulae with those proposed by Beckert, Duren, Terasaki, and Yurioka using data from 70 steels and at six $t_{8/5}$. The formulae were rated in terms of accuracy of prediction as:

BL-70 > Yurioka-1 > BL-70S (P_{cm}) > Terasaki > Duren

It was found that BL-70 formula allowed the greatest accuracy of prediction and Duren's the least. However, in a subsequent report Duren contested Suzuki's claim and maintained that his formula was more accurate than both the BL-70 and BL-70S (P_{cm}) when applied to the steels for which it was evolved. The correlation coefficient for Duren's formula was 0.98 as compared to 0.91 and 0.96 for BL-70 and BL-70S (P_{cm}) respectively. Since the BL-70 formulae are based on data from Beckert's, Duren's, Terasaki's and Yurioka's results it is not surprising that Duren's formula predicted H_{max} with a slightly better accuracy over that of the BL formulae.

Two additional simplified versions of BL-70 were obtained by the multiple regression analysis of the BL constants of two independent variables, C and CE_m, and C and CE, yielding respectively BL-70S (CE_m) and BL-70S (CE).

(ii) **BL-70S (CE_m) Formula**

$$K = 233 + 811 \ C - 355 \ CE_m$$

$$aK = 574 + 3918 \ C - 732 \ CE_m$$

$$Y_5 = 0.005 - 0.472 \ C + 2.37 \ CE_m$$

w h e r e -

$$CE_m = C + Si/24 + Mn/6 + Cu/15 + Ni/15 + Cr/5 + Mo/5 + V/5 + 15 \ B$$

(iii) **BL-70S (CE)**

$$K = 231 + 838 \ C - 376 \ CE$$

$$aK = 571 + 3975 \ C - 778 \ CE$$

$$Y_5 = 0.0202 - 0.652 \ C + 2.5 \ CE$$

w h e r e -

$$CE = C + Mn/6 + Cu/15 + Ni/15 + Cr/5 + Mo/5 + V/5$$

Suzuki compared the validity of the above formulae for data from independent sources and found the following order of prediction accuracy:

BL-70S (P_{cm}) > BL-70S (CE_m) > Yurioka-1 > Duren > BL-70S (CE) > BL-70 > Terasaki

(iv) **BL-70SM (P_{cm})**

This formula is applicable to low-C low-Mn low strength steels. Y_5 in modified to Y_{5m} as follows-

$$Y_{5m} = -0.03 - 6 \ C + 7.77 \ P_{cm} + 0.22 \ (Mn - 1.5)$$

The other material constants remain the same as in BL-70S (P_{cm}).

(g) **Yurioka-2 and Yurioka-3 Formulae [16]**

Recently Yurioka has proposed two formulae for calculating H_{max}. These are applicable to a much wider chemical composition range as compared to all the formulae described above. The general equation of Yurioka's formula is:

$$H_{max} = (H_M + H_B)/2 - [(H_M - H_B)/2.2] \ arctan \ (x) \quad \quad\dots\dots\dots\dots(3.21)$$

w h e r e -

$$x \ (rad.) = [4\{(log \ t_{8/5})/t_M\}/log(t_B/t_M)] - 2$$

The data from 40 steels was employed to calculate H_M, H_B, and x. The following formulae resulted from data analysis:

(i) Yurioka-2 Formula

$$H_{max} = 220 + 442\ C\ (1 - 0.3\ C^2) + 65\ \tanh\ (y) + \{68 + 402\ C\ (1 - 0.3\ C^2)$$
$$- 59\ \tanh\ (y)\}\ \arctan\ (x) \qquad \qquad ....(3.22)$$

where-

$x = [\log\ t_{8/5} - 2.3\ CE_I - 1.35\ CE_{III} + 0.882]/[1.15\ CE_I - 0.673\ CE_{III} - 0.6]$

$y = 2.65\ CE_{II} - 0.69$

$CE_I = C_p + Si/24 + Mn/6 + Cu/15 + Ni/12 + Cr(1 - 0.16\ \sqrt{Cr})/8 + Mo/4 + \Delta H$

$CE_{II} = C + Si/24 + Mn/5 + Cu/10 + Ni/18 + Cr/5 + Mo/2.5 + V/5 + Nb/3$

$CE_{III} = C_p + Mn/3.6 + Cu/20 + Ni/9 + Cr/5 + Mo/4$

$C_p = C$, when $C \leq 0.3\%$

$C_p = C/6 + 0.25$, when $C > 0.3\%$

This formula is applicable to steels with the chemical composition in the following range:

C < 0.8%, Si < 1.2%, Mn < 2%, Cu < 0.9%, Ni < 10%, Cr < 10%, and Mo < 2%

(ii) Yurioka-3 Formula

A simplified version of Yurioka-2 is derived for steels with C < 0.3%, Ni < 5%, and Cr < 1%.

$$H_{max} = 442\ C + 99\ CE_{II} + 206 + (402\ C - 90\ CE_{II} + 80)\ \arctan\ (x) \qquad ......(3.23)$$

where-

$x = [\log\ t_{8/5} - 2.3\ CE_I - 1.35\ CE_{III} + 0.882]/[1.15\ CE_I - 0.673\ CE_{III} - 0.601]$

$CE_I = C + Si/24 + Mn/6 + Cu/15 + Ni/12 + Cr/8 + Mo/4 + \Delta H$

$CE_{II} = C + Si/24 + Mn/5 + Cu/10 + Ni/18 + Cr/5 + Mo/2.5 + V/5 + Nb/3$

$CE_{III} = C + Mn/3.6 + Cu/20 + Ni/9 + Cr/5 + Mo/4$

$\Delta H = 0$ when $B \leq 1$ ppm

$\Delta H = 0.03\ f_N$ when $B = 2$ ppm

$\Delta H = 0.06\ f_N$ when $B = 3$ ppm

$\Delta H = 0.09\ f_N$ when $B \geq 4$ ppm

$f_N = (0.02 - N)/0.02$

The formulae proposed by Yurioka et al (Yurioka-2 and Yurioka-3) are applicable to cooling times $t_{8/5}$ up to 100 sec. These are valid not only for common structural steels but also alloy steels.

In the present study the above described formulae for estimating cooling time ($t_{8/5}$) and maximum HAZ hardness (H_{max})) were validated for the steels employed.

3.2 EXPERIMENTAL PROCEDURES

3.2.1. Bead-on-plate Tests

Bead-on-plate welds were deposited on each steel by shielded metal arc and submerged arc welding processes on plates dimensioned 6" x 12" (to provide an infinite cooling geometry for the desired heat input range). Thicknesses for different steels were those of the as-received plates (Table 2.4). Welding was carried out at ambient temperature (75°F) and the heat input was varied by either changing the current or welding speed or both. For obtaining different heat inputs by SMAW, electrodes of diameters 3/32", 1/8", 5/32", and 1/4" were employed, while filler wires of 1/8" and 5/32" diameter were used when depositing welds by SAW. The SMA welding was performed in a semi-

automatic mode. A submerged arc welding unit was modified to hold the welding consumable and the welding parameters changed to obtain the desired heat input. The semi-automatic facility shown in Fig. 3.14, helped to achieve consistent weld quality and it enabled accurate monitoring of welding parameters.

The welding parameters were varied for plates of different thicknesses to ensure that cooling times, $t_{8/5}$, were evenly spaced on a log scale. In order to choose a suitable equation and/or nomogram to calculate $t_{8/5}$ from welding parameters, plate thickness, and preheat temperature, thermal cycles were recorded during the welding process by plunging the tip of tungsten - 5% rhenium and tungsten - 26% rhenium thermocouple into the molten weld metal. The cooling time between 800 to 500°C was measured from the cooling portion of the thermal cycle. (Cooling time in the weld deposit is very close to that of in the CGHAZ near the weld surface) On-cooling thermal cycles were recorded only on two plates namely HSLA-80-2 (1" thick) and DQ-125 (2" thick).

The bead-on-plate welds were sectioned transverse to the welding direction and cross-sections were polished and etched in 2% nital. The microhardness (HV) of the CGHAZ under the weld bead was determined using a 5 kg load. A minimum of five readings were taken and the maximum HAZ hardness reported is the average of the five readings.

The microstructural changes taking place in the CGHAZ as a function of heat input were also examined using optical microscopy. Microstructural features at three different cooling times were documented for all nine steels. The austenite grain size in the CGHAZ for the above samples from each steel was measured using ASTM comparison method.

3.3. RESULTS AND DISCUSSION

3.3.1. Validation of Equations for Calculating Cooling Time

Hardenability of steels can be characterized by investigating the variation of maximum hardness developed in the coarse grained HAZ as a function of cooling time. Therefore, it is essential to have the capability of accurately estimating the cooling time from welding parameters before validating H_{max} formulae.

Since there are many equations and nomograms available in literature to determine cooling time from 800 to 500°C from a knowledge of heat input, plate thickness, preheat temperature, and type of weld (Section 3.1.2) several methods were evaluated in this study: three nomograms (Inagaki and Sekiguchi [39], Berkhout and van Lent [40], and De Fourny and Bragard [41]) and two equations (Suzuki [43], and Uwer and Degenkolbe [42]) to determine the cooling time. The calculated values were compared to the experimental data obtained from the thermocouple plunge technique.

Figs. 3.15 to 3.19 illustrate the comparison between the actual and calculated cooling times using different nomograms and equations. It should be noted that the nomograms are only valid for the shielded metal and not for the submerged arc welding process. Any attempt to use these nomograms for SAW will result in an underestimation of cooling time as the arc efficiency of the SA process is greater than that of SMA process. Suzuki's equation is applicable to a maximum heat input of 127 kJ/in., therefore, it was not possible to estimate cooling time from this equation for SA welds. The Uwer and Degenkolbe equation is valid over a much wider energy input range and for SMA, SA, and GTA welding. When the experimental data from this study was compared with the calculated cooling times the following equations resulted:

$$t_{8/5} \text{ (exp)}=0.44+1.06 \ t_{8/5} \text{ (cal)} \quad R^2=0.998 \quad \text{(Inagaki \& Sekiguchi)} \quad \ldots\ldots(3.24)$$
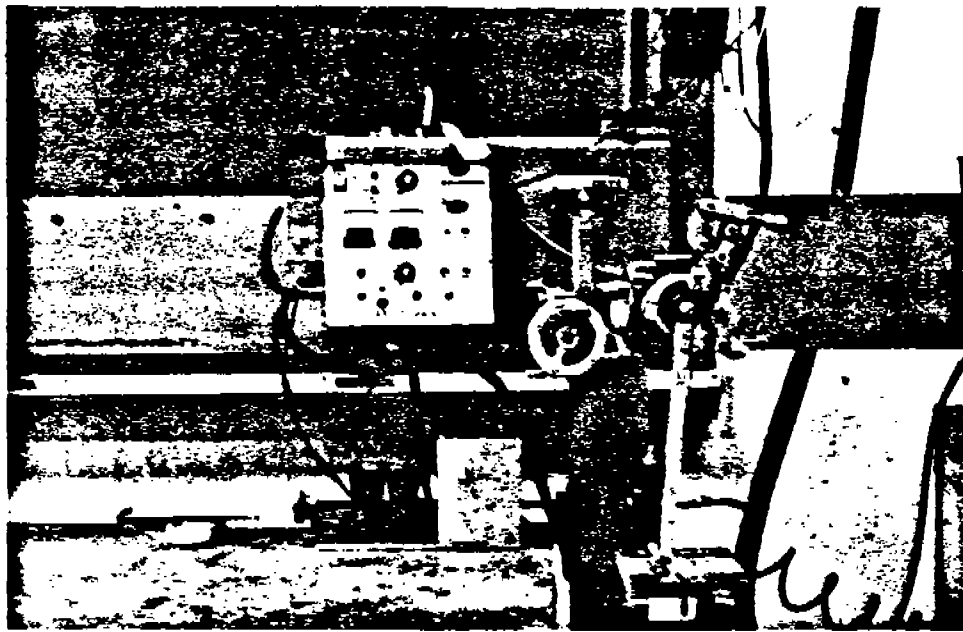
Fig.3.14. Submerged arc welding unit modified to deposit welds by
the shielded metal arc welding.
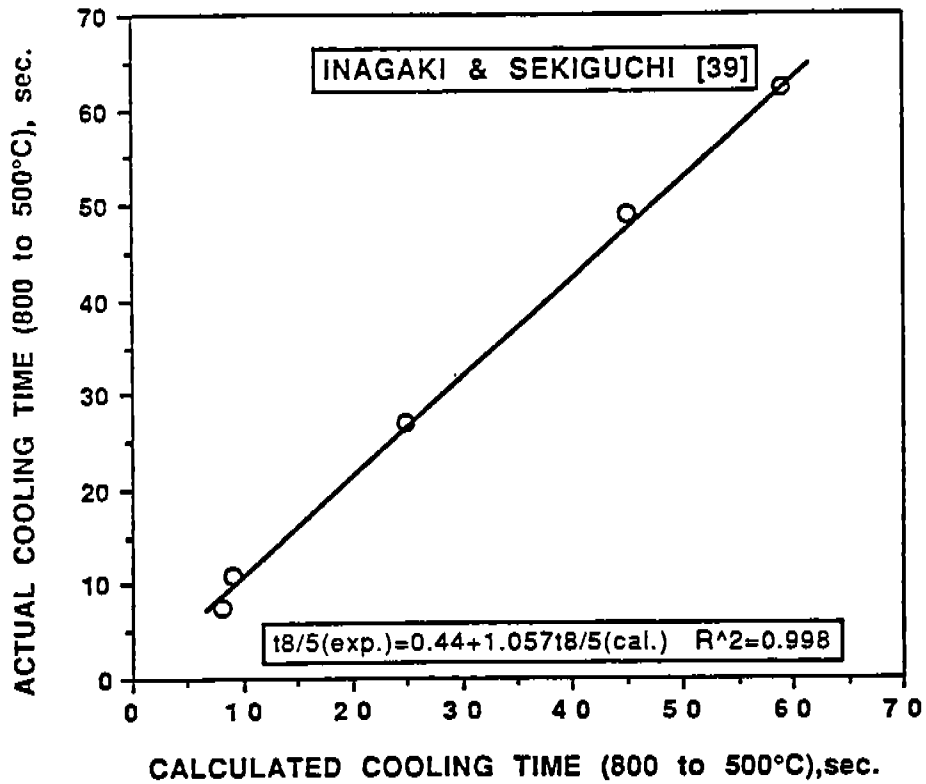
Fig.3.15. Comparison between the experimental and calculated
cooling time using Inagaki and Sekiguchi nomogram.

43
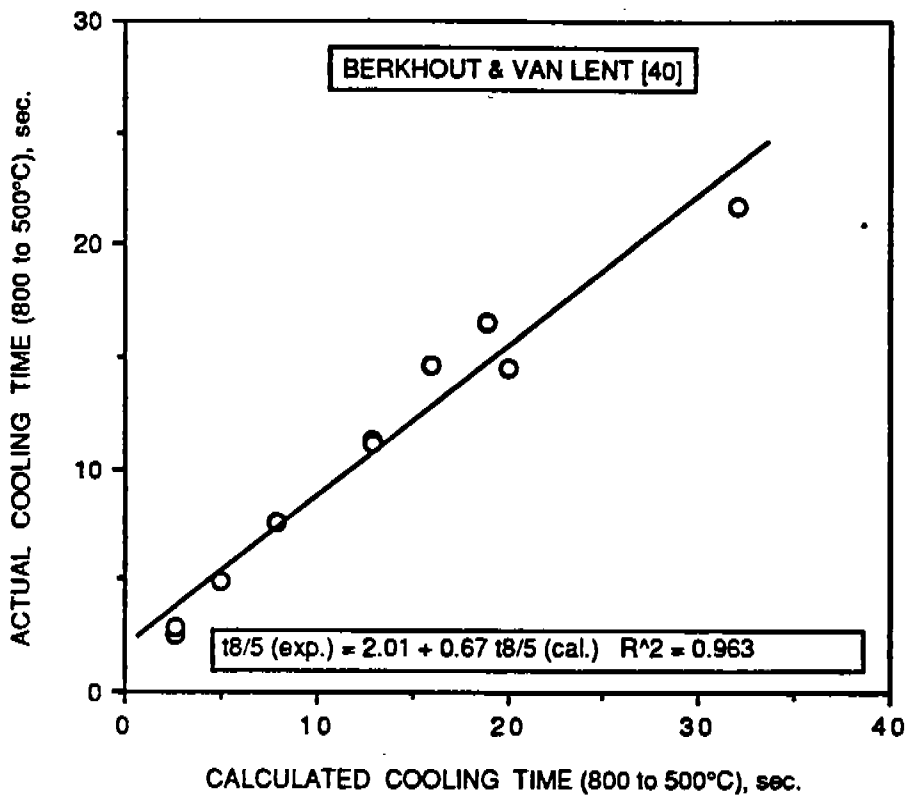
Fig.3.16. Correlation between experimental and calculated cooling time using Berkhout and van Lent nomogram.
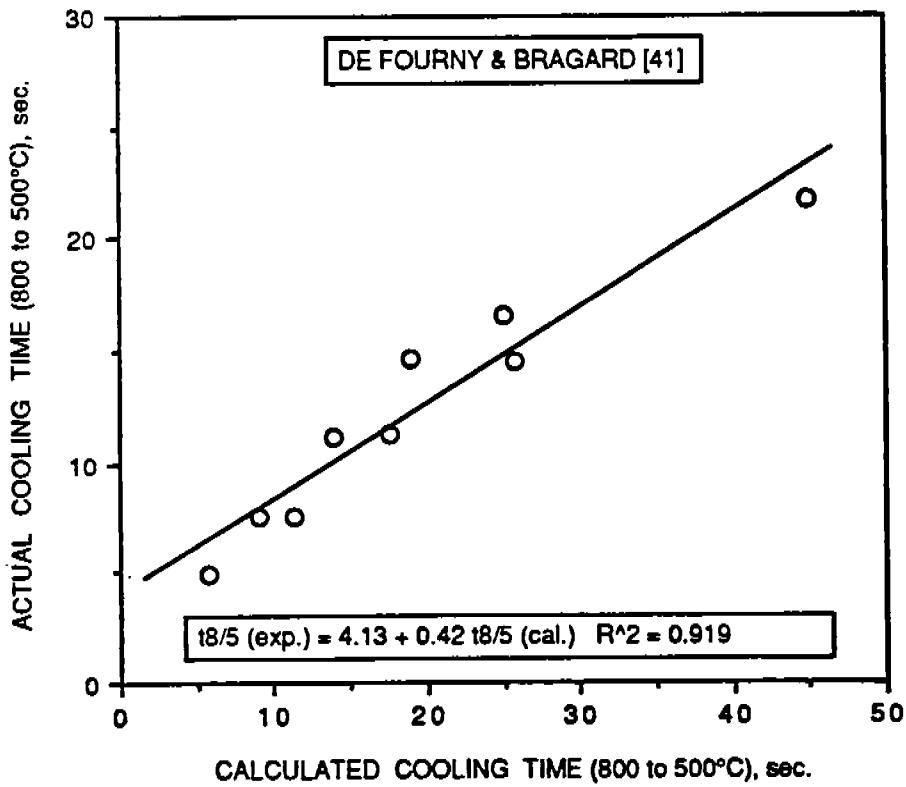
Fig.3.17. Correlation between experimental and calculated cooling time from De Fourny and Bragard nomogram.

44
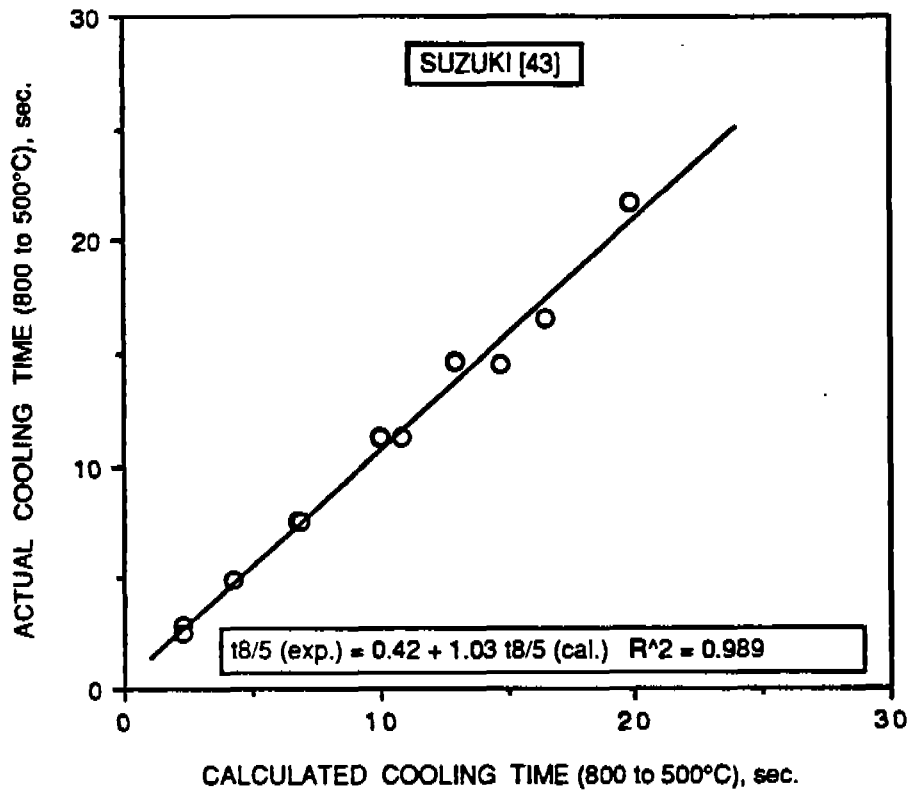
Fig.3.18. Comparison of experimental and calculated cooling time using Suzuki's equation.

t8/5 (exp.) = 0.42 + 1.03 t8/5 (cal.)   R^2 = 0.989
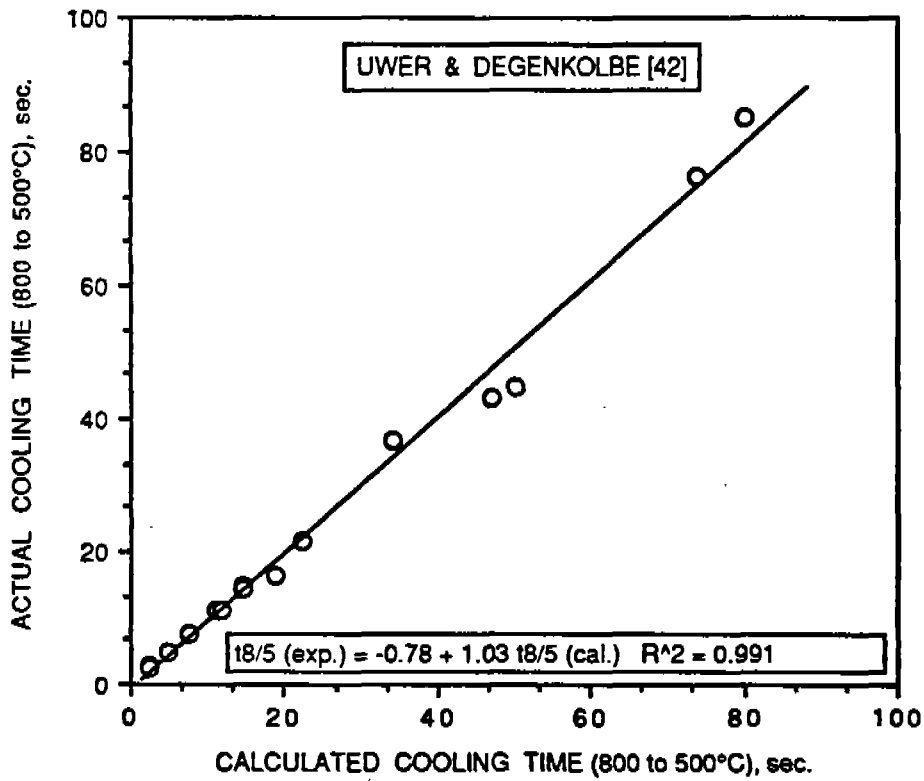
Fig.3.19. Correlation between actual and calculated cooling time from Uwer and Degenkolbe equation.

t8/5 (exp.) = -0.78 + 1.03 t8/5 (cal.)   R^2 = 0.991

45

$t_{8/5}$ (exp)=4.13+0.42 $t_{8/5}$ (cal) R^2=0.919   (De Fourny & Bragard)   ......(3.25)

$t_{8/5}$ (exp)=2.01+0.67 $t_{8/5}$ (cal) R^2=0.963   (Berkhout & van Lent)   ......(3.26)

$t_{8/5}$ (exp)=0.42+1.03 $t_{8/5}$ (cal) R^2=0.989   (Suzuki)   ....(3.27)

$t_{8/5}$(exp)=-0.78+1.03$t_{8/5}$(cal) R^2=0.991   (Uwer & Degenkolbe)   ....(3.28)

All the nomograms over estimate the cooling time as shown by the values of slope and intercepts, however, a good correlation exists between the calculated and experimental cooling times. Inagaki, Suzuki and the Uwer and Degenkolbe equations are very close to the 45° line and also show good correlations with the experimental results. The Uwer and Degenkolbe equation is preferred over Suzuki's equation in this study as it applicable over a wider range of parameters and welding processes. This is also corroborated by comparing data from the published literature in Fig. 3.20. Both, published data and results from this investigation, are predicted with excellent accuracy by the Uwer and Degenkolbe equation. Therefore, this equation was employed to calculate cooling times for the welding conditions and steel thicknesses for which actual $t_{8/5}$ were not measured.

3.3.2 Microstructure and Hardness of CGHAZ

In the following sections the results for CGHAZ microstructural changes and consequent variation in the maximum HAZ hardness with increasing heat input are discussed. The microhardness values determined in the CGHAZ have been correlated with the corresponding microstructural changes. The Yurioka-3 formula [16] for estimating maximum HAZ hardness has been found to allow accurate determination of H_{max} in the present set of steels under study. This formula, in turn, is based on the determination of volume fraction of martensite and its hardness from empirical equations. It is presumed that if Yurioka-3 formula is applicable to the low carbon micro-alloyed steels in this study, the formulae for estimating volume fraction of martensite and martensite hardness should also be applicable.

The following formula to estimate the vol% martensite in the CGHAZ was employed.

    Vol% Martensite = 0.5 - 0.455 arctan (x)   ....(3.29)
    where-

$$x \text{ (rad)} = [4\{\log (t_{8/5})/t_M\}/[\log (t_B/t_M)] - 2$$

3.3.2.1. HSLA-80-1 Steel

The variation in maximum HAZ hardness with cooling time for HSLA-80-1 steel is shown in Fig. 3.21. The hardness response shows typical behavior marked by two plateaus corresponding to 100% martensite and 0% martensite. The maximum hardness generated at the minimum heat input (15 kJ/in., $t_{8/5}$ = 2.5 sec.) is 312 HV5. The microstructure (Fig. A-2) (Figures with prefix A are given in Appendix A) for this condition shows the presence of a predominant martensitic constituent. This also correlates well with the estimated vol% of martensite (89%). However, as the heat input and hence cooling time is increased, there is a decrease in the martensite fraction in the CGHAZ with a corresponding hardness decrese. This is illustrated in Figs A-3 to A-4 corresponding to cooling times of 14 and 90 sec. The CGHAZ of weldments with a 14 sec. cooling time shows the presence of a small amount of martensite (estimated - 28%) while the 90 sec. $t_{8/5}$ the CGHAZ is fully bainitic. The estimated martensite was 0% for this condition. Fig. 3.21 also compares the difference in the hardness of the CGHAZ and base metal. The CGHAZ hardness remains above the base metal hardness even at the longest cooling times. In
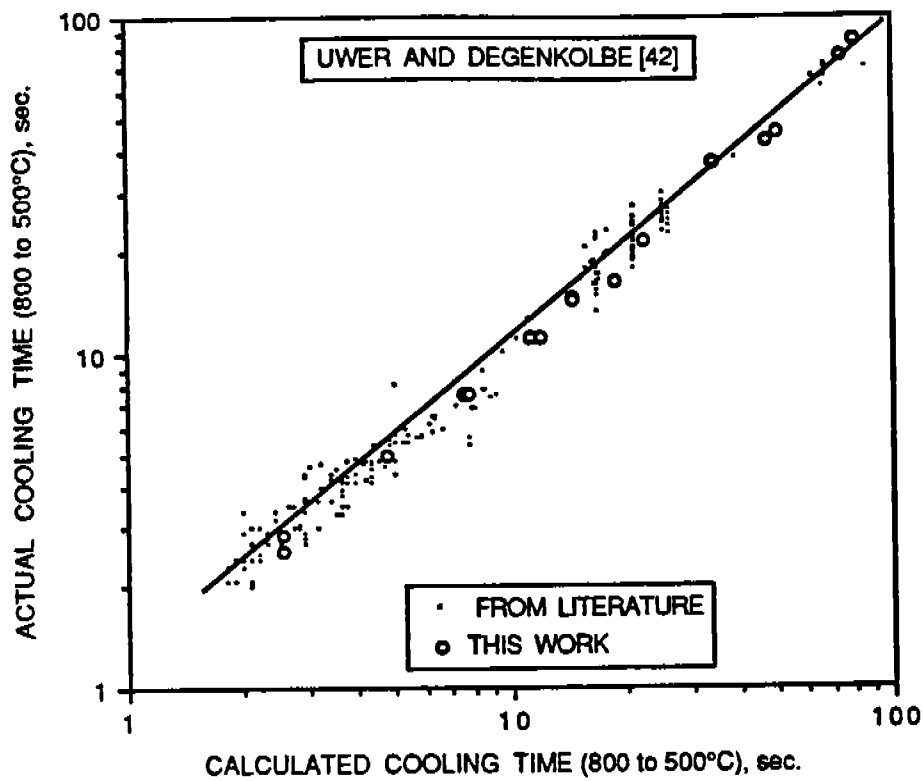
Fig.3.20. Comparison between the experimental (from this study and from literature) and calculated cooling time employing Uwer and Degankolbe equation.
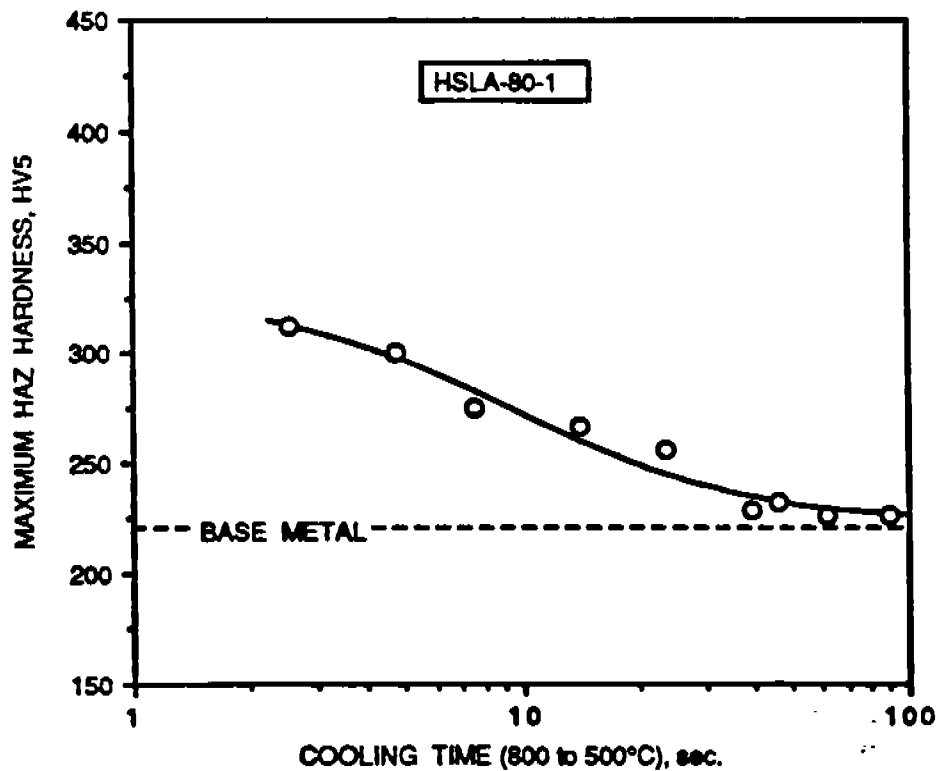
Fig.3.21. Variation of the maximum HAZ hardness with cooling time for HSLA-80-1 steel.

47

some of the steels in this program it was found that the CGHAZ becomes softer than the base metal thus increasing the soft zone width significantly (to be discussed in detail in Section 5).

The validity of Suzuki's formulae (BL-70, BL-70S (P_{cm}), BL-70S (CE_m), BL-70 (CE), and BL-70SM (P_{cm})) and Yurioka's formulae (Yurioka-1 and Yurioka-3) has been evaluated for HSLA-80-1. The linear regression equation for the relationship between experimental and calculated hardness values has been derived for all formulae. The accuracy of the prediction has been checked further by calculating the coefficient and standard error of determination, R^2 and P respectively. The standard error is defined as-

$$P = \sqrt{\sum [H_{max}(exp) - H_{max}(cal)]^2 / n}$$ ....(3.30)

where n is the number of readings. The following regression equations were obtained by using the above formulae for calculating H_{max}-

BL-70 H_{max} (exp.) = -67.59 + 1.09 H_{max}(cal.)
                 $R^2 = 0.805$;   P = 43.60 HV5

BL-70S (P_{cm}) H_{max} (exp.) = -162.7 + 1.40 H_{max} (cal.)
                 $R^2 = 0.899$;   P = 44.17 HV5

BL-70S (CE_m) H_{max} (exp.) = - 5.27 + 0.96 H_{max} (cal.)
                 $R^2 = 0.962$;   P = 16.62 HV5

BL-70S (CE) H_{max} (exp.) = 10.56 + 0.92 H_{max} (cal.)
                 $R^2 = 0.965$;   P = 12.02 HV5

BL-70SM (P_{cm}) H_{max} (exp.) = -149.6 + 1.39 H_{max} (cal.)
                 $R^2 = 0.943$;   P = 37.18 HV5

Yurioka-1 H_{max} (exp.) = 18.3 + 0.82 H_{max} (cal.)
                 $R^2 = 0.873$;   P = 36.52 HV5

Yurioka-3 H_{max} (exp.) = 24.39 + 0.89 H_{max} (cal.)
                 $R^2 = 0.954$;   P = 8.21 HV5

The CGHAZ hardness calculated from BL-70, BL-70S (P_{cm}), BL-70SM (P_{cm}), and Yurioka-1 provided the poorest correlation and greater standard error. Since the R^2 values for the remaining formulae do not vary significantly from one another, these formulae can be ranked on the basis of standard error of determination -

Yurioka-3 > BL-70S (CE) > BL-70S (CE_m)

Therefore, the Yurioka-3 formula can be employed to calculate the maximum HAZ hardness in HSLA-80-1.

3.3.2.2. HSLA-80-2 Steel

The change in the H_{max} with cooling time for HSLA-80-2 is shown in Fig. 3.22. The hardness response of this steel is similar to that of HSLA-80-1. The maximum hardness obtained in the lowest heat input weld, however, is higher (350 HV5) than the corresponding value in HSLA-80-1. This is because of the fact that HSLA-80-2 contains a higher carbon content- 0.062 wt % - as opposed 0.044 wt % in HSLA-80-1, but the carbon equivalents do not differ significantly. As expected the predominant phase in the CGHAZ corresponding to a 2.5 sec. cooling time is martensite (Fig. A-6). The estimated vol.% of martensite is 90, very close to that calculated for HSLA-80-1. The amount of martensite decreases as the cooling time is increased, as shown in Figs. A-7 and A-8 for cooling times 11 and 140 sec. respectively. The hardness of the lower plateau (fully bainitic structure) is almost the same for both HSLA-80-1 and

48

HSLA-80-2, because of a very small difference in their carbon equivalents. However, unlike in HSLA-80-1, the CGHAZ in HSLA-80-2 becomes softer than the base metal at longer cooling times. The HSLA-80-2 base metal hardness is higher than that of HSLA-80-1 because of a higher carbon content and a different aging treatment. The hardness of a bainitic structure is directly proportional to the carbon equivalent, therefore, the CGHAZ hardness for longer cooling times becomes lower than the base metal.

The comparison of measured H_{max} with those calculated from different formulae yielded the following regression equations-

BL-70 H_{max} (exp.) = - 17.84 + 0.93 H_{max} (cal.)

$$R^2 = 0.581; \quad P = 46.88 \text{ HV5}$$

BL-70S (P_{cm}) H_{max} (exp.) = -121.93 + 1.27 H_{max} (cal.)

$$R^2 = 0.737; \quad P = 43.21 \text{ HV5}$$

BL-70S (CE_m) H_{max} (exp.) = -33.47 + 1.08 H_{max} (cal.)

$$R^2 = 0.913; \quad P = 16.46 \text{ HV5}$$

BL-70S (CE) H_{max} (exp.) = -37.32 + 1.09 H_{max} (cal.)

$$R^2 = 0.907; \quad P = 17.54 \text{ HV5}$$

BL-70SM (P_{cm}) H_{max} (exp.)=-169.59 + 1.47 H_{max} (cal.)

$$R^2 = 0.911; \quad P = 33.16 \text{ HV5}$$

Yurioka-1 H_{max} (exp.) = 27.01 + 0.80 H_{max} (cal.)

$$R^2 = 0.649; \quad P = 44.17 \text{ HV5}$$

Yurioka-3 H_{max} (exp.) = -23.28 + 1.09 H_{max} (cal.)

$$R^2 = 0.971; \quad P = 8.08 \text{ HV5}$$

Formulae BL-70, BL-70S (P_{cm}), BL-70SM (P_{cm}), and Yurioka-1 provided poor correlation between the actual and calculated values. However, the remaining three formulae gave acceptable regression parameters and the standard error was also low. These can be ranked in the following order:

Yurioka-3 > BL-70S (CE_m) > BL-70S (CE)

Therefore, after HSLA-80-1, the Yurioka-3 formula can be employed for an accurate estimation of maximum HAZ hardness in HSLA-80-2.

3.3.2.3. HSLA-80M Steel

HSLA-80M belongs to the same category as HSLA-80-1 and HSLA-80-2 steels. However, the amount of Mn and Ni has been increased thus increasing its hardenability. The carbon content is almost the same (0.057 wt%) as that of HSLA-80-2 (0.062 wt%) but the carbon equivalent is increased (P_{cm} = 0.28) by the intentional addition of Mn and Ni. These changes are also reflected in the CGHAZ hardness variation with cooling time (Fig. 3.23). The H_{max} drops gradually with cooling time instead of exhibiting a typical hardness response as seen in Figs 3.21 and 3.22 for HSLA-80-1 and HSLA-80-2 respectively. By virtue of having almost the same carbon content as that in HSLA-80-2, the maximum HAZ hardness (353 HV5) at the shortest cooling time is close to that of HSLA-80-2. The coarse grained HAZ (Fig. A-10) consists of a fully martensitic structure, which is also confirmed by a 100% martensite estimation. The fully martensitic microstructure persists even at an 11 sec. cooling time (Fig. A-11), however, martensite is mostly replaced by bainite in the CGHAZ of the highest heat input weldments studied (cooling time - 90 sec., Fig. A-12). As shown in Fig. 3.23, the CGHAZ hardness always remains above the base metal hardness level. It is expected that the CGHAZ hardness may not drop below the base metal hardness even if the CGHAZ is fully bainitic. This becomes obvious when steels HSLA-80M and HSLA-80-2 are compared. The
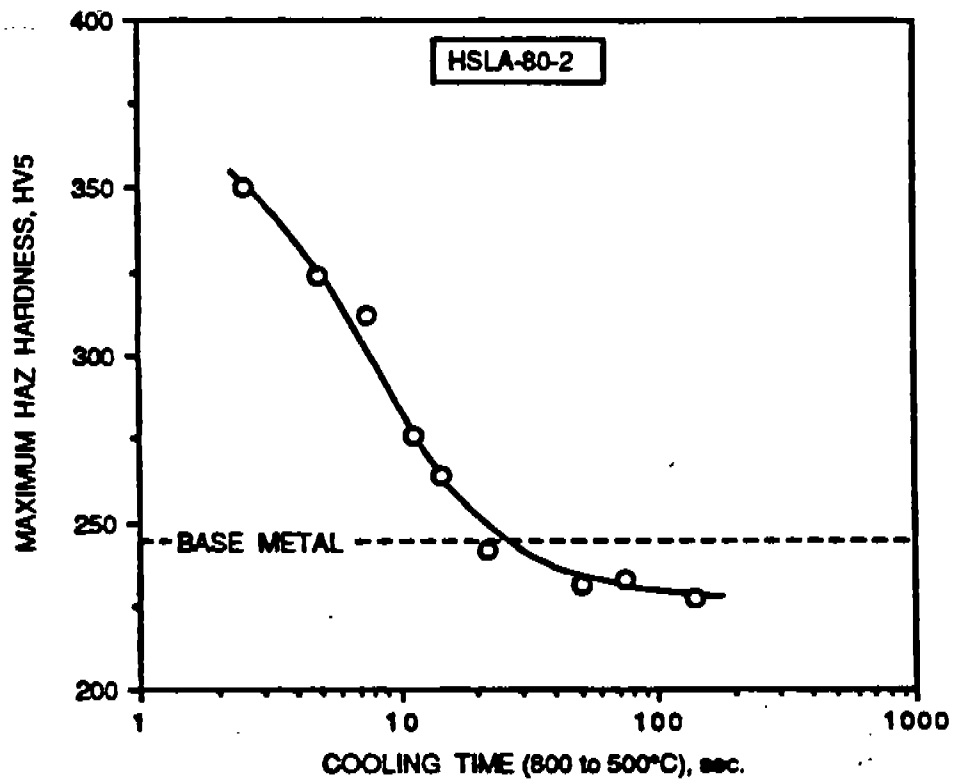
Fig.3.22. Maximum HAZ hardness variation with cooling time for
HSLA-80-2 steel.
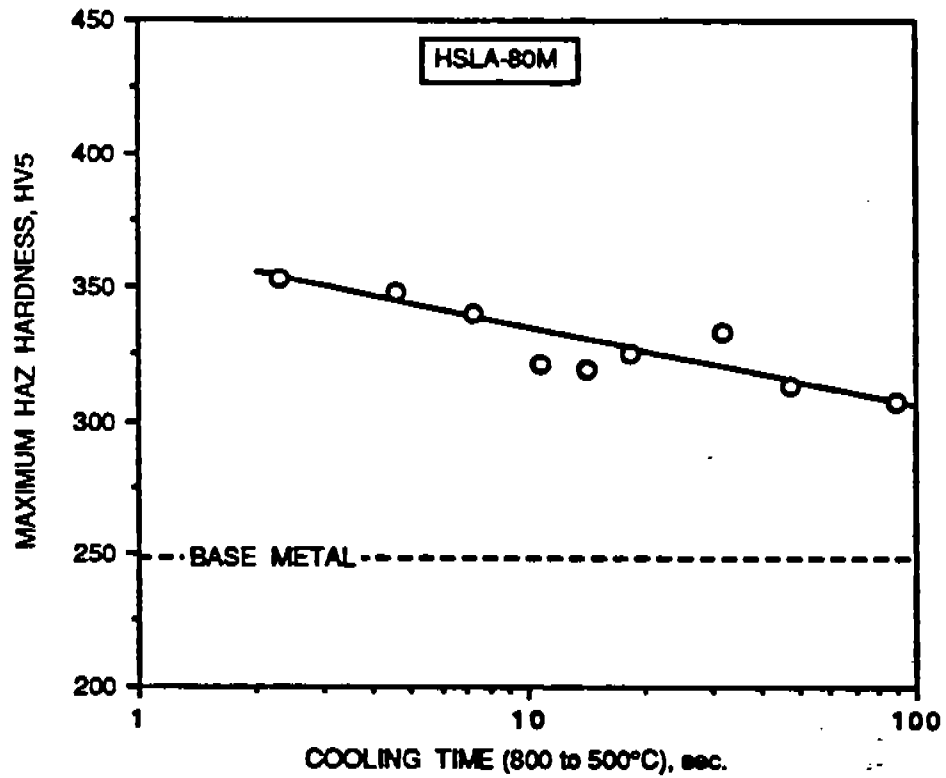
Fig.3.23. Change in the maximum HAZ hardness with cooling time
for HSLA-80M steel.

50

base metal hardness of HSLA-80M (248 HV) is only slightly higher than that of HSLA-80-2 (244 DPH) while there is an appreciable difference in their carbon equivalents (P_{cm})- 0.23 for HSLA-80-2 and 0.28 for HSLA-80M. Since the hardness of a bainitic structure is a direct function of the carbon equivalent, the minimum CGHAZ hardness in HSLA-80M should be greater than 248 HV (the base metal hardness). This view is also confirmed from the fact that the CGHAZ corresponding to 90 sec. predominantly contains bainitic constituentS and its hardness is about 60 HV higher than the base metal.

None of the formulae for estimating H_{max} showed good correlation between the measured and calculated values. This was also found to be true for the other steels in this program with higher hardenability such as HSLA-100, HSLA-130 and HY-130. The reason for poor correlation with the experimental data is that in the martensitic CGHAZ usually a large scatter in the measured hardness values was observed because of the non-uniform distribution of martensite laths in the grains adjacent to the fusion boundary [27]. The regression line for BL-70 formula could not be obtained as it predicts a constant value of CGHAZ hardness at all the cooling times and consequently the magnitude of slope becomes indeterminate. The following equations for best-fit lines were obtained-

BL-70	indeterminable	$P = 17.54$ HV5
BL-70S (P_{cm})	H_{max} (exp.) $= -516.6 + 2.51\ H_{max}$ (cal.)	
	$R^2 = 0.221$;	$P = 16.09$ HV5
BL-70S (CE_m)	H_{max} (exp.) $= 110.3 + 0.67\ H_{max}$ (cal.)	
	$R^2 = 0.395$;	$P = 12.78$ HV5
BL-70S (CE)	H_{max} (exp.) $= 86.1 + 0.74\ H_{max}$ (cal.)	
	$R^2 = 0.385$;	$P = 12.32$ HV5
BL-70SM (P_{cm})	H_{max} (exp.) $= -673.8 + 2.99\ H_{max}$ (cal.)	
	$R^2 = 0.365$;	$P = 15.36$ HV5
Yurioka-1	H_{max} (exp.) $= -33.8 + 1.07\ H_{max}$ (cal.)	
	$R^2 = 0.494$;	$P = 14.78$ HV5
Yurioka-3	H_{max} (exp.) $= 99.4 + 0.68\ H_{max}$ (cal.)	
	$R^2 = 0.515$;	$P = 13.86$ HV5

Although the correlation of calculated vs. measured values was poor because of the reasons explained above, it is possible to rank these formulae in terms of the standard errors:

BL-70S (CE) > BL-70S (CE_m) > Yurioka-3 > Yurioka-1 > BL-70SM (P_{cm}) > BL-70S (P_{cm}) > BL-70

Unlike in HSLA-80-1 and HSLA-80-2, in HSLA-80M the difference obtained in the standard errors are small when different formulae are employed to correlate the H_{max} data from HSLA-80M is small. Therefore, any one of the above formulae can be used to calculate the H_{max} in HSLA-80M with acceptable accuracy. However, the best accuracy can be obtained by employing BL-70S (CE), BL-70S (CE_m) and Yurioka-3.

3.3.2.4. HSLA-100 and HSLA-130 Steels:

The results for HSLA-100 and HSLA-130 are discussed together in this section because of the similarity in their chemistry, the only difference is in the mill heat treatment to strengthen these steels with copper precipitation. The effect of any prior thermomechanical treatment is erased in the CGHAZ due to high temperature thermal excursions during welding. This becomes apparent when the hardness behavior of these steels is compared (Figs. 3.24

and 3.25). Both show a similar hardness response. The CGHAZ microstructures at three different heat input levels are shown in Figs A-14 to A-20. The microstructures are characterized by a fully martensitic structure at all the cooling times. This is expected as the hardenability of these steels is the highest among all steels in this program except for HY-130. Despite the presence of 100% martensite in the CGHAZ, there is a definite decrease in the hardness because of auto-tempering. The maximum HAZ hardness obtained at the shortest cooling time (2.5 sec.) is about 388 HV5. This is in accord with the expected trend as the carbon content in these steels is ~ 0.07 wt%. The ranking of the prediction accuracy of various formulae for calculating CGHAZ hardness for these steels was found to be the same as obtained for HSLA-80M.

3.3.2.5. HY-130 Steel

HY-130 has the highest P_{cm} value (0.35) among all steels in this program. A higher amount of nickel (4.68 wt%) is intentionally added to enhance low temperature toughness. The variation in CGHAZ hardness with cooling time is shown in Fig. 3.26. The CGHAZ hardness (419 HV5) achieved for a cooling time of 2.5 sec. is quite high because of the higher carbon content (0.12 wt%). The CGHAZ contains 100% martensite at all cooling times, as shown in Figs A-22 to A-24. None of the formulae for predicting hardness allowed good correlation among predicted and measured hardness data. The reasons for this have been described in Section 3.3.2.3. Based on the magnitude of standard error the following ranking can be considered adequate-

BL-70S (CE) > BL-70S (CE_m) > Yurioka-3 > BL-70S (P_{cm}) > BL-70SM (P_{cm}) > Yurioka-1 > BL-70

It is noticed that the ranking of various formulae for estimating maximum HAZ hardness in steels of higher hardenability such as HSLA-80M, HSLA-100, HSLA-130, and HY-130 show a similar trend. BL-70S (CE) is found to be superior to both BL-70S (CE_m) and the Yurioka-3, whereas the BL-70 formula is found to be the least accurate.

3.3.2.6. DQ-125 Steel

DQ-125 contains 0.11 wt% carbon and is produced by the direct quenching process. Strength in this steel is obtained by a combined effect of carbon and the presence of a martensitic structure. The base metal hardness, therefore, is quite high (321 HV), although its carbon equivalent is relatively low (P_{cm} = 0.25). In fact, its carbon equivalent is the lowest among all steels in the 130 ksi category. Therefore, the DQ-125 CGHAZ should become softer than the base metal at longer cooling times as opposed to the other steels in the same category, where the CGHAZ hardness was well above the base metal level. The hardness response of the CGHAZ with cooling time is shown in Fig. 3.27. The maximum hardness was 399 HV5 for 2.5 sec. cooling time and is due to the presence of a fully martensitic HAZ (Fig. A-26). On increasing the cooling time the HAZ hardness drops rapidly and it becomes lower than that of the base metal at cooling times greater than about 30 sec. The CGHAZ microstructures corresponding to 11 and 80 sec. are shown in Figs. A-27 and A-28. It is clear that martensite is progressively replaced by bainite as the cooling time is increased.

The following regression equations were obtained for formulae to estimate the maximum HAZ hardness-

BL-70 H_{max} (exp.) = 114.6 + 0.72 H_{max} (cal.)

$$R^2 = 0.947; \quad P = 27.24 \text{ HV5}$$

BL-70S (P_{cm}) H_{max} (exp.) = 100.7 + 0.75 H_{max} (cal.)

$$R^2 = 0.940; \quad P = 22.97 \text{ HV5}$$
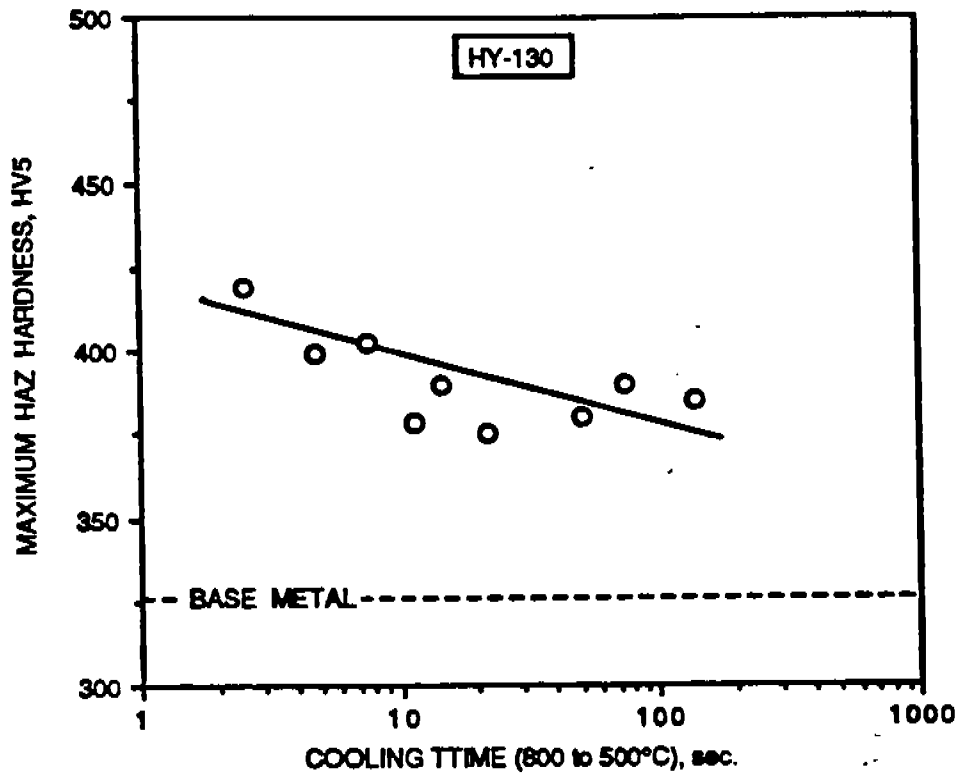
Fig.3.26. CGHAZ hardness relationship with cooling time for HY-130 steel.
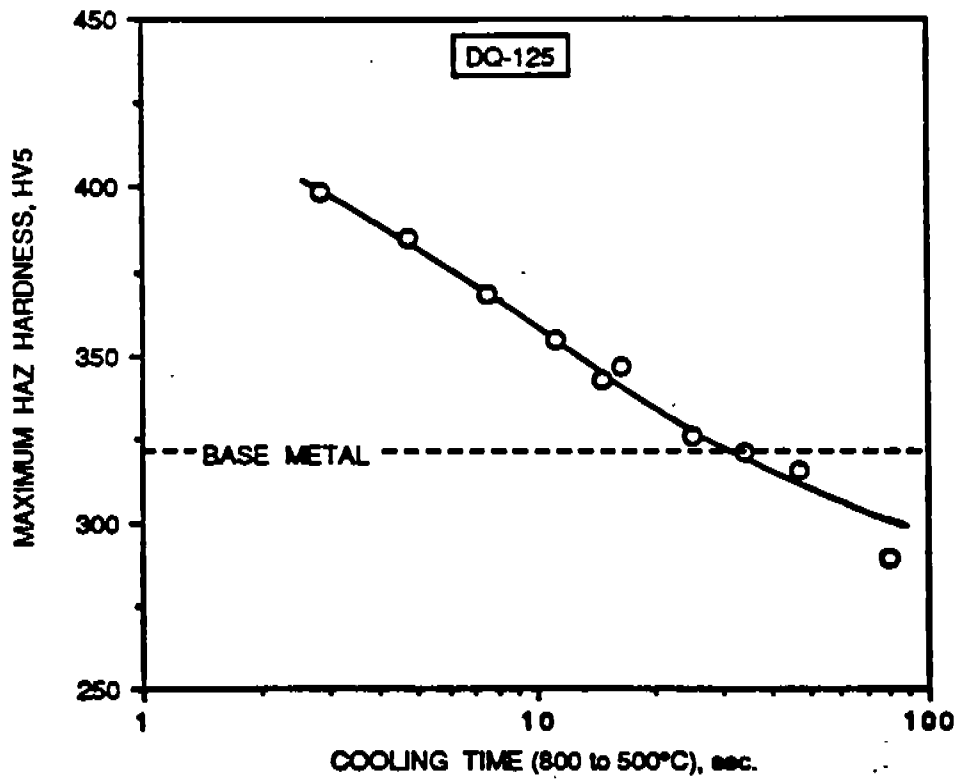
Fig.3.27. Relationship between CGHAZ hardness and cooling time for DQ-125 steel.

53

BL-70S (CE$_m$) H_{max} (exp.) = 74.1 + 0.80 H_{max} (cal.)

$$R^2 = 0.919; \quad P = 14.37 \text{ HV5}$$

BL-70S (CE) H_{max} (exp.) = 62.3 + 0.83 H_{max} (cal.)

$$R^2 = 0.910; \quad P = 12.32 \text{ HV5}$$

BL-70SM (P$_{cm}$) H_{max} (exp.) = 110.4 + 0.75 H_{max} (cal.)

$$R^2 = 0.947; \quad P = 34.50 \text{ HV5}$$

Yurioka-1 H_{max} (exp.) = 108.1 + 0.72 H_{max} (cal.)

$$R^2 = 0.946; \quad P = 22.36 \text{ HV5}$$

Yurioka-3 H_{max} (exp.) = 89.3 + 0.74 H_{max} (cal.)

$$R^2 = 0.927; \quad P = 13.84 \text{ HV5}$$

All formulae provide good correlation with experimental data. However, when the standard error of determination is used for comparing different formulae. The following order of accuracy is obtained:

BL-70S (CE) > Yurioka-3 > BL-70S (CE$_m$) > Yurioka-1 > BL-70S (P$_{cm}$) > BL-70 > BL-70SM (P$_{cm}$)

3.3.2.7. DQ-80 Steel

DQ-80, like DQ-125, is produced by the direct quench process, but the strength level of this steel is achieved by a subsequent aging treatment at elevated temperature to precipitate epsilon-copper. This steel contains the lowest carbon (0.032 wt%) among all steels in this program and consequently has the lowest carbon equivalent (P$_{cm}$ = 0.16). The variation of H_{max} with cooling time is shown in Fig. 3.28. The hardness response shows a typical curve marked by two shelves - the upper shelf because of the presence of martensite and the lower due to the presence of bainite. It should be noted that the upper shelf is not very well defined as the CGHAZ is not fully martensitic even at the shortest cooling time (2.5 sec.) as shown in Fig. A-30. However, the martensite constituent is rapidly replaced by bainite as the cooling time is increased. This is illustrated in Figs. A-31 and A-32 for cooling times of 14.6 and 140 sec. Because of a very low value of carbon equivalent and an aging treatment to strengthen the base metal, the CGHAZ hardness decreases for cooling times greater than 14 sec.

The validation of various formulae to estimate the maximum CGHAZ yield the following regression equations-

BL-70 H_{max} (exp.) = 111.4 + 0.42 H_{max} (cal.)

$$R^2 = 0.914; \quad P = 46.75 \text{ HV5}$$

BL-70S (P$_{cm}$) H_{max} (exp.) = 87.5 + 0.53 H_{max} (cal.)

$$R^2 = 0.951; \quad P = 34.29 \text{ HV5}$$

BL-70S (CE$_m$) H_{max} (exp.) = 122.1 + 0.47 H_{max} (cal.)

$$R^2 = 0.910; \quad P = 20.56 \text{ HV5}$$

BL-70S (CE) H_{max} (exp.) = 122.6 + 0.47 H_{max} (cal.)

$$R^2 = 0.910; \quad P = 21.25 \text{ HV5}$$

BL-70SM (P$_{cm}$) H_{max} (exp.) = 84.8 + 0.56 H_{max} (cal.)

$$R^2 = 0.931; \quad P = 27.58 \text{ HV5}$$

Yurioka-1 H_{max} (exp.) = 140.1 + 0.34 H_{max} (cal.)

$$R^2 = 0.952; \quad P = 35.92 \text{ HV5}$$

Yurioka-3 H_{max} (exp.) = 94.5 + 0.60 H_{max} (cal.)

$$R^2 = 0.852; \quad P = 15.85 \text{ HV5}$$

The following ranking of the formulae is based on the standard error-
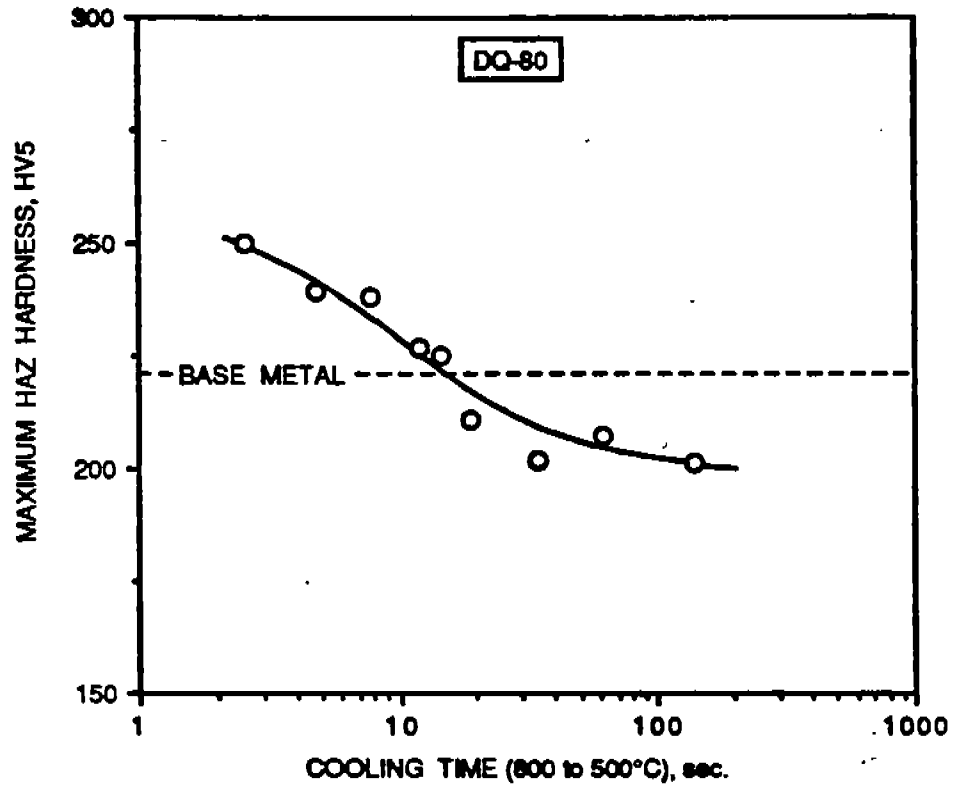
Fig.3.28. Variation of CGHAZ hardness with cooling time for DQ-80 steel.

Yurioka-3 > BL-70S (CE) > BL-70S (CE_m) > BL-70SM (P_{cm}) > BL-70S (P_{cm}) > Yurioka-1 > BL-70

3.3.2.8. AC-50 Steel

The carbon equivalent of AC-50 is the same as that of DQ-80 but its carbon content is higher (0.079wt%). The strength of this steel is the lowest among all steels in this study. The effect of increasing cooling time on the maximum HAZ hardness is shown in Fig. 3.29. The CGHAZ hardness corresponding to 2.5 sec. cooling time is only 300 HV5 as compared to 388 HV5 for HSLA-100 and HSLA-130, which also contain carbon in the same range. This is due to the fact that (a) the CGHAZ in AC-50 is not fully martensitic (estimated martensite-70% see Fig. A-34) while it is 100% martensite in HSLA steels, and (b) AC-50 is a lean steel while in the HSLA steels alloying elements are intentionally added to optimize certain mechanical properties, which can increase the hardness by providing solid solution strengthening. The CGHAZ microstructures corresponding to 12 and 90 sec. cooling times are shown in Figs. A-35 and A-36. The hardness corresponding to the lower shelf (bainitic microconstituent) is almost the same (207 HV5) as obtained in DQ-80 because of similarity in carbon content.

The AC-50 steel falls within the validity limits of all the formulae considered for calculating H_{max}. Therefore, excellent correlations are observed for all the formulae as given below-

BL-70 H_{max} (exp.) $= 75.7 + 0.68\ H_{max}$ (cal.)
$$R^2 = 0.983; \quad P = 14.92\ HV5$$

BL-70S (P_{cm}) H_{max} (exp.) $= 76.2 + 0.68\ H_{max}$ (cal.)
$$R^2 = 0.983; \quad P = 14.57\ HV5$$

BL-70S (CE_m) H_{max} (exp.) $= 77.6 + 0.68\ H_{max}$ (cal.)
$$R^2 = 0.984; \quad P = 14.89\ HV5$$

BL-70S (CE) H_{max} (exp.) $= 78.6 + 0.68\ H_{max}$ (cal.)
$$R^2 = 0.982; \quad P = 15.22\ HV5$$

BL-70SM (P_{cm}) H_{max} (exp.) $= 75.3 + 0.69\ H_{max}$ (cal.)
$$R^2 = 0.982; P = 14.31\ HV5$$

Yurioka-1 H_{max} (exp.) $= 86.2 + 0.65\ H_{max}$ (cal.)
$$R^2 = 0.982; \quad P = 17.24\ HV5$$

Yurioka-3 H_{max} (exp.) $= 56.6 + 0.82\ H_{max}$ (cal.)
$$R^2 = 0.975; P = 18.28\ HV5$$

The magnitude of the slope and intercept indicate that all the formulae underestimate the hardness values. According to the standard error, these formulae can be ranked as:

BL-70SM (P_{cm}) > BL-70S (P_{cm}) > BL-70S (CE_m) > BL-70 > BL-70S (CE) > Yurioka-1 > Yurioka-3.

The H_{max} vs. $t_{8/5}$ response for copper containing and non-copper containing steels are compared in Figs. 3.30 and 3.31 respectively.

3.3.3. Applicability of Carbon Equivalent Formulae

The discussion of the results presented above indicates that no single H_{max} formula allows for precise determination of the maximum HAZ hardness for all the steels in this program. The following is a summary of the ranking of the different formulae in order of their accuracy of prediction. Only the three best formulae have been listed.

HSLA-80-1   Yurioka-3 > BL-70S (CE) > BL-70S (CE_m)
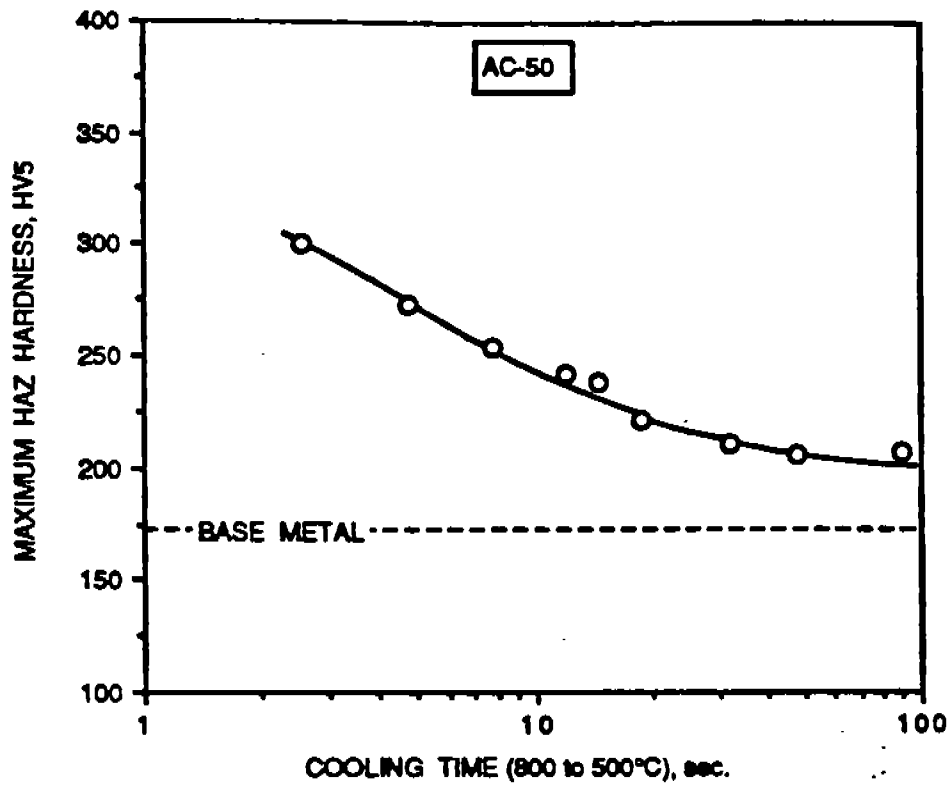
Fig.3.29.   Change in CGHAZ hardness with cooling time for
AC-50 steel.
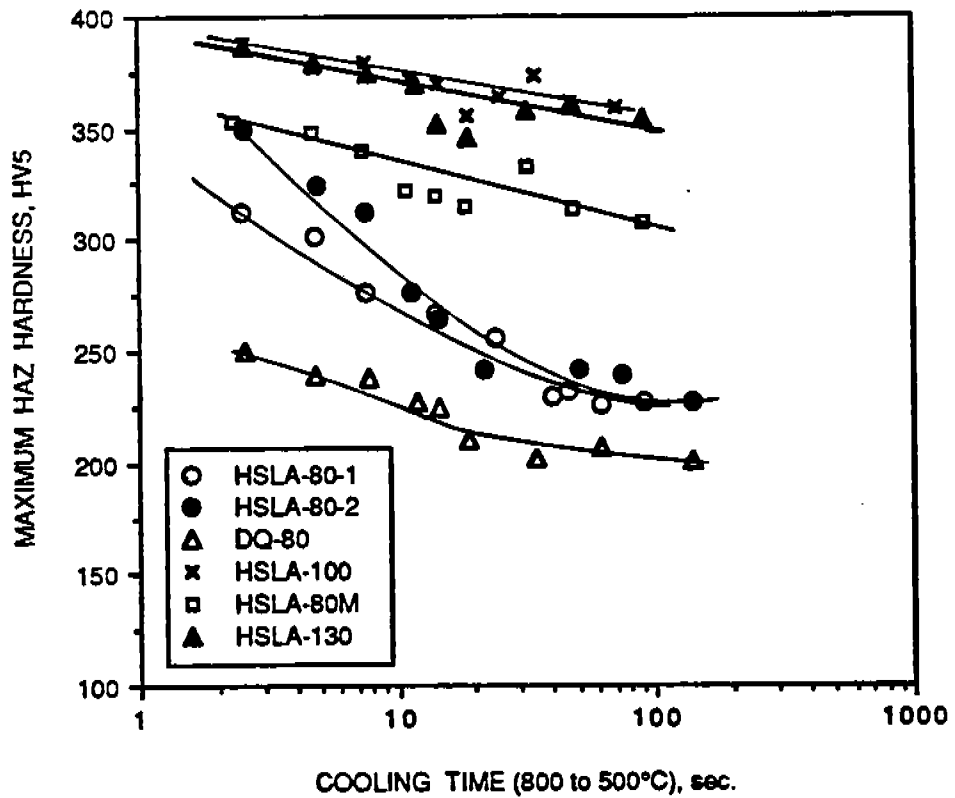
Fig.3.30.   Change in CGHAZ hardness with cooling time for all of the
copper containing steels.
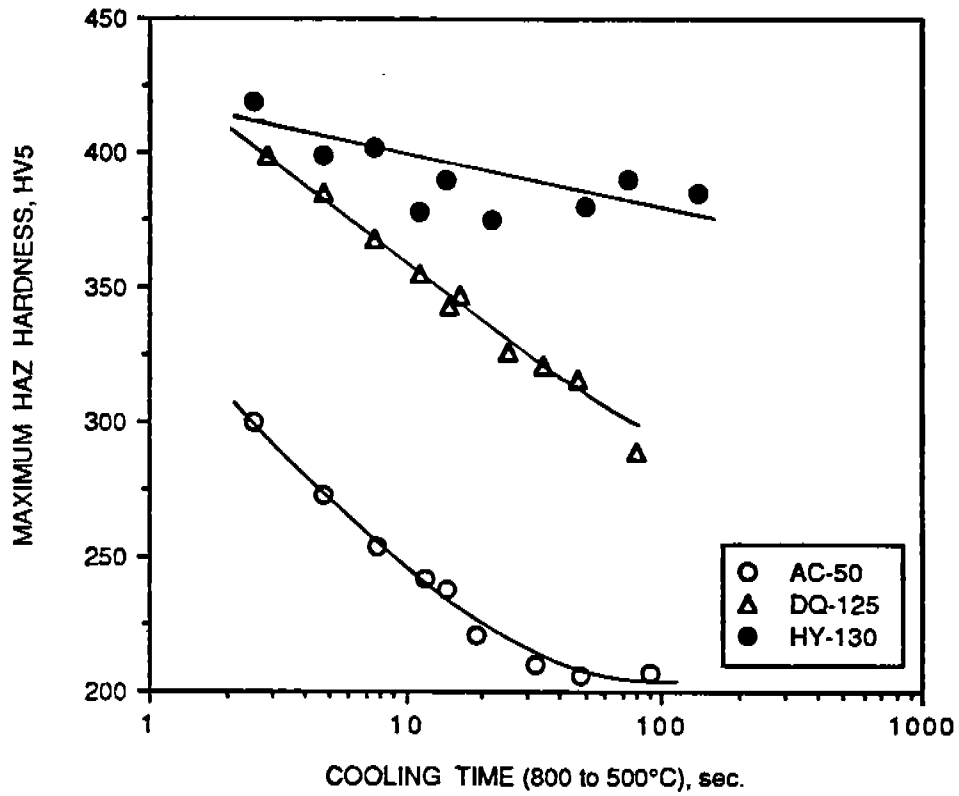
Fig.3.31. Change in CGHAZ hardness with cooling time for all of the non-copper containing steels.

HSLA-80-2	Yurioka-3 > BL-70S (CE_m) > BL-70S (CE)
HSLA-80M	BL-70S (CE) > BL-70S (CE_m) > Yurioka-3
HSLA-100	BL-70S (CE) > BL-70S (CE_m) > Yurioka-3
HSLA-130	BL-70S (CE) > BL-70S (CE_m) > Yurioka-3
HY-130	BL-70S (CE) > BL-70S (CE_m) > Yurioka-3
DQ-125	BL-70S (CE) > Yurioka-3 > BL-70S (CE_m)
DQ-80	Yurioka-3 > BL-70S (CE) > BL-70S (CE_m)
AC-50	BL-70SM (P_{cm}) > BL-70S (P_{cm}) > BL-70S (CE_m)

Steels DQ-125 and AC-50 fall within the validity limits of all the formulae. The chemistry of HY-130 lies within the applicable limits of Yurioka-3 only. The remaining steels are outside the scope of all the H_{max} formulae considered. However, for copper containing steels (Cu > 1 wt%), the limit of Yurioka-3 formula is violated only with respect to Cu content. Yurioka-3 is applicable to steels with a maximum 0.90 wt% copper. It gives the best results when applied to HSLA-80-1, HSLA-80-2 and DQ-80 followed by either BL-70S (CE) or BL-70S (CE_m). But when Yurioka-3 is applied to steels with higher hardenability such as HSLA-80M, HSLA-100, HSLA-130, and HY-130, it is found inferior to BL-70S (CE) and BL-70S (CE_m). It should be noted that in these steels none of the formulae provided an acceptable coefficient of determination (because of the reasons discussed earlier) and the formulae were ranked in terms of the standard error of determination. The difference in the standard errors for these three formulae is small, therefore, all the three formulae may be considered to provide almost the same accuracy of prediction for quench hardenable steels.

Formula BL-70S (CE) was found superior to Yurioka-3 for DQ-125, although the difference in the accuracy of prediction was negligibly small. However, Yurioka-3 predicted the CGHAZ hardness with the least accuracy when applied to AC-50, the best prediction was provided by BL-70SM (P_{cm}). BL-70SM (P_{cm}) was developed to predict CGHAZ hardness in low-C low-Mn low strength steels. Once again the magnitude of difference between the best and the least accurate formulae is small.

Therefore, it appears that the Yurioka-3 formula will allow acceptable prediction of H_{max} for all steels in this program.

The formulae for estimating the CGHAZ hardness were also applied to the data from all nine steels in this study in order to assess their applicability to this class of steels. The comparisons are illustrated in Figs. 3.32 to 3.39. The following regression equations for best-fit lines were obtained-

BL-70
$$H_{max} \text{ (exp.)} = -14.47 + 1.02 \ H_{max} \text{ (cal.)}$$
$$R^2 = 0.741; \quad P = 33.78 \ HV5$$

BL-70S (P_{cm})
$$H_{max} \text{ (exp)} = -18.64 + 1.02 \ H_{max} \text{ (cal)}$$
$$R^2 = 0.835; \quad P = 28.83 \ HV5$$

BL-70S (CE_m)
$$H_{max} \text{ (exp)} = -1.28 + 1.02 \ H_{max} \text{ (cal)}$$
$$R^2 = 0.928; \quad P = 17.68 \ HV5$$

BL-70S (CE)
$$H_{max} \text{ (exp)} = 5.16 + 1.0 \ H_{max} \text{ (cal)}$$
$$R^2 = 0.933; \quad P = 17.00 \ HV5$$

BL-70SM (P_{cm})
$$H_{max} \text{ (exp)} = -7.03 + 1.0 \ H_{max} \text{ (cal)}$$
$$R^2 = 0.835; \quad P = 27.01 \ HV5$$

Yurioka-1
$$H_{max} \text{ (exp)} = -0.06 + 0.99 \ H_{max} \text{ (cal)}$$
$$R^2 = 0.799; \quad P = 28.76 \ HV5$$
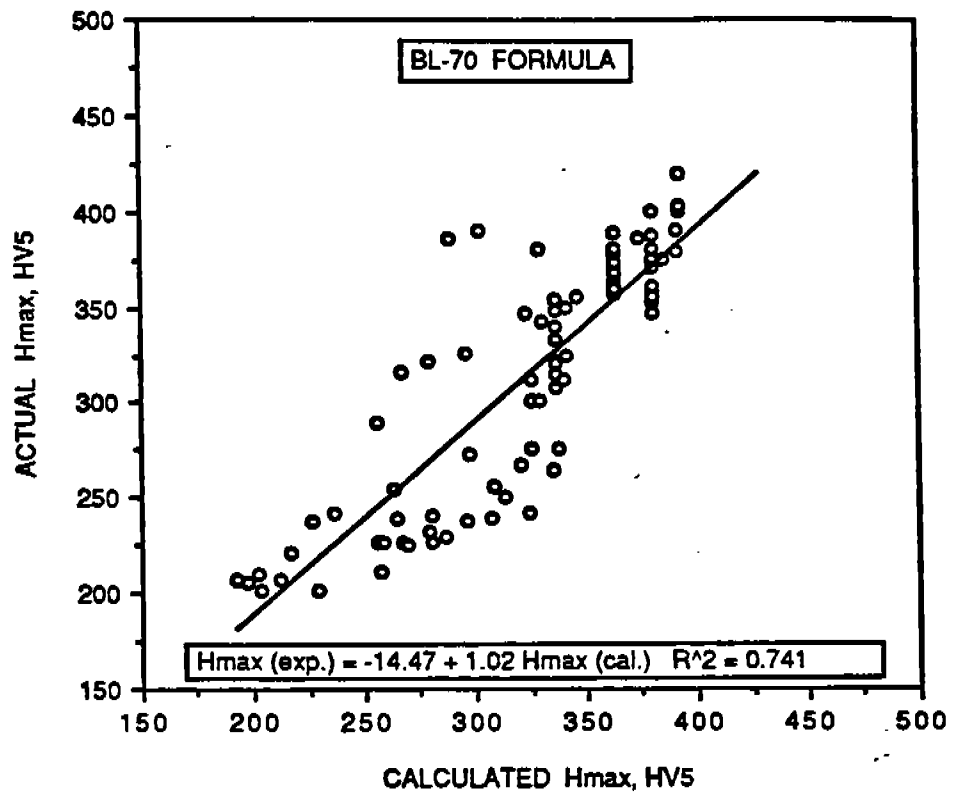
Fig.3.32. Comparison between experimental and calculated maximum HAZ hardness from BL-70 formula for all steels.
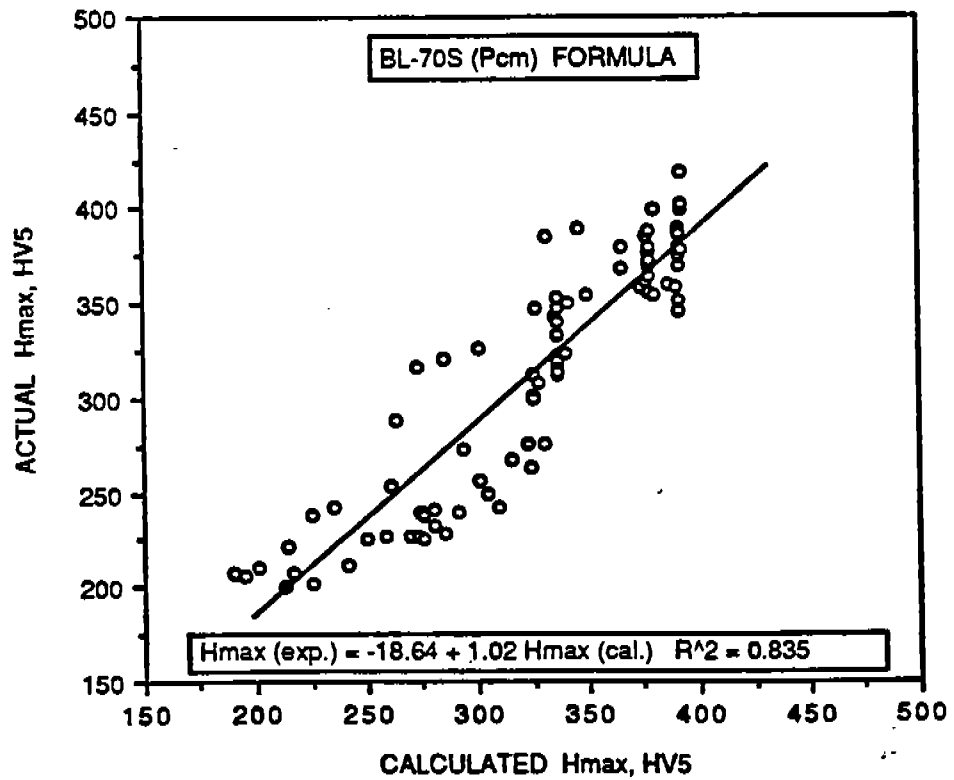
Fig.3.33. Correlation between experimental and calculated CGHAZ hardness from BL-70S (P_{cm}) formula for all steels.

60
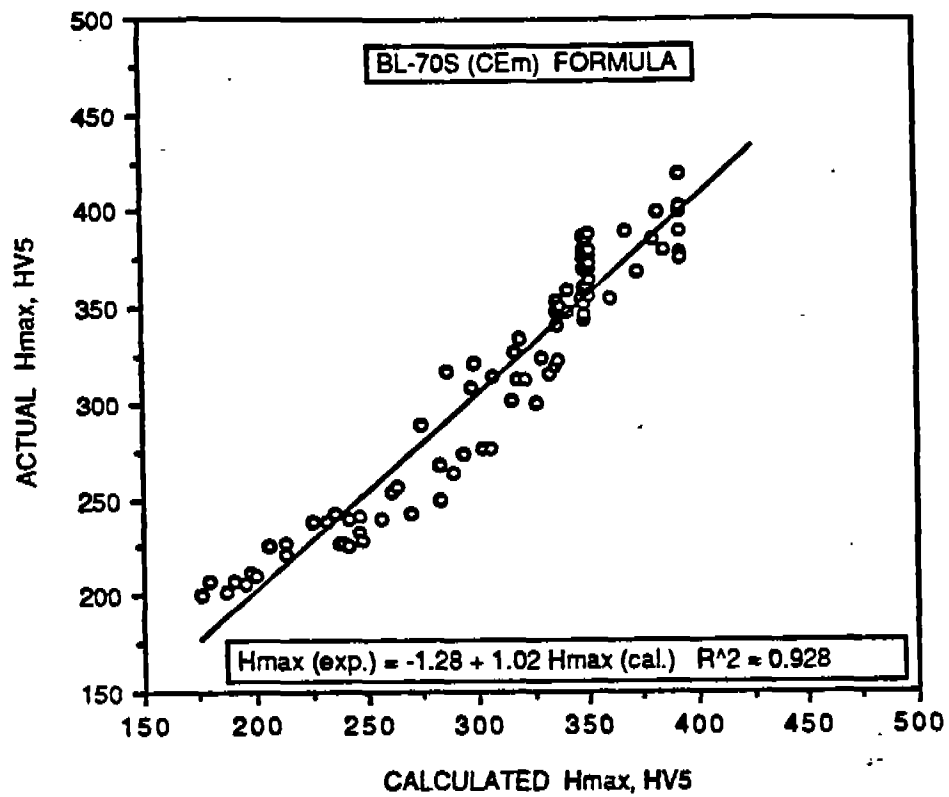
Fig.3.34. Comparison between experimental and calculated maximum HAZ hardness from BL-70S (CE_m) for all steels.
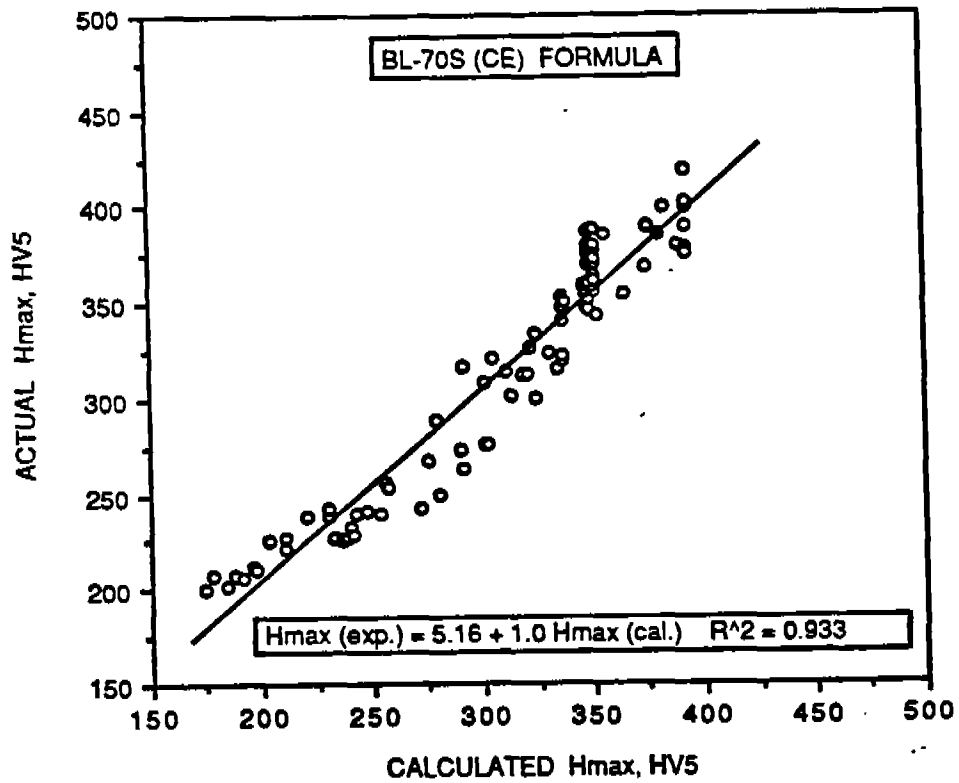
Fig.3.35. Comparison between experimental and calculated CGHAZ hardness by BL-70S (CE) formula.

61
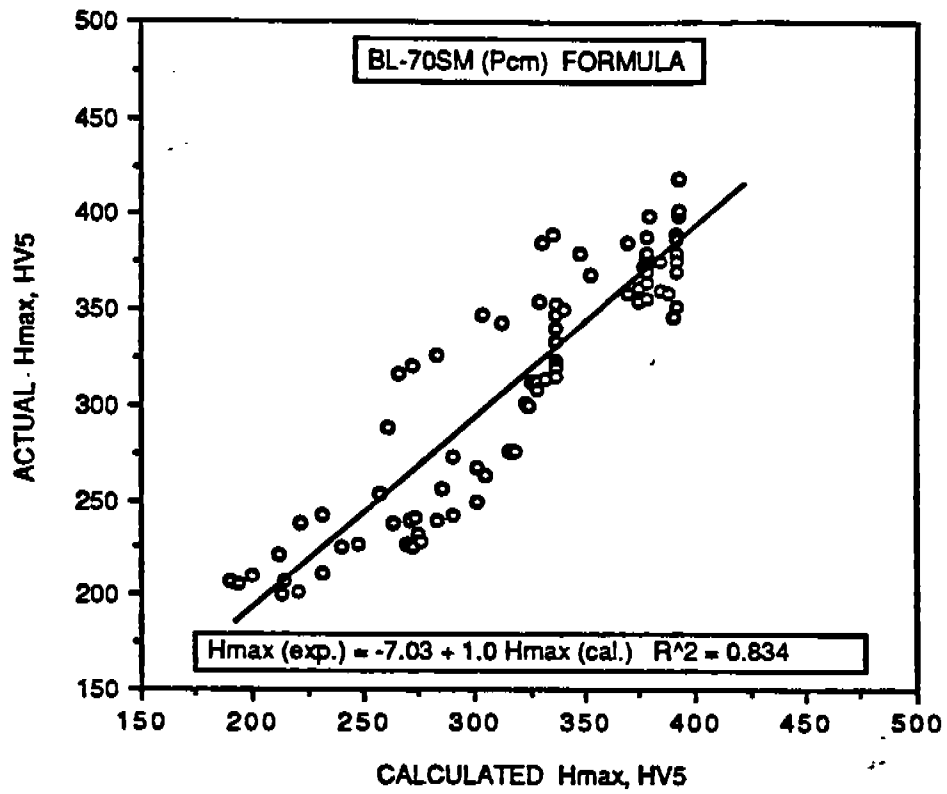
Fig.3.36. Correlation between actual and calculated CGHAZ hardness from BL-70SM (P_{cm}) for all steels.
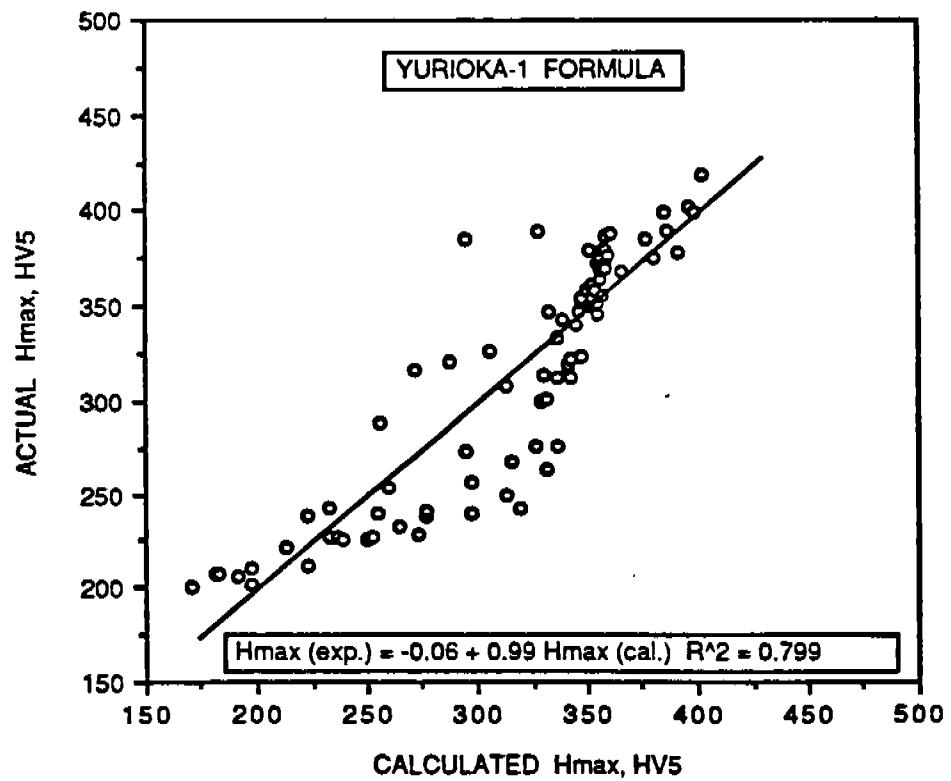
Fig.3.37. Results of comparison between actual and calculated CGHAZ hardness using Yurioka-1 formula for all steels.

62
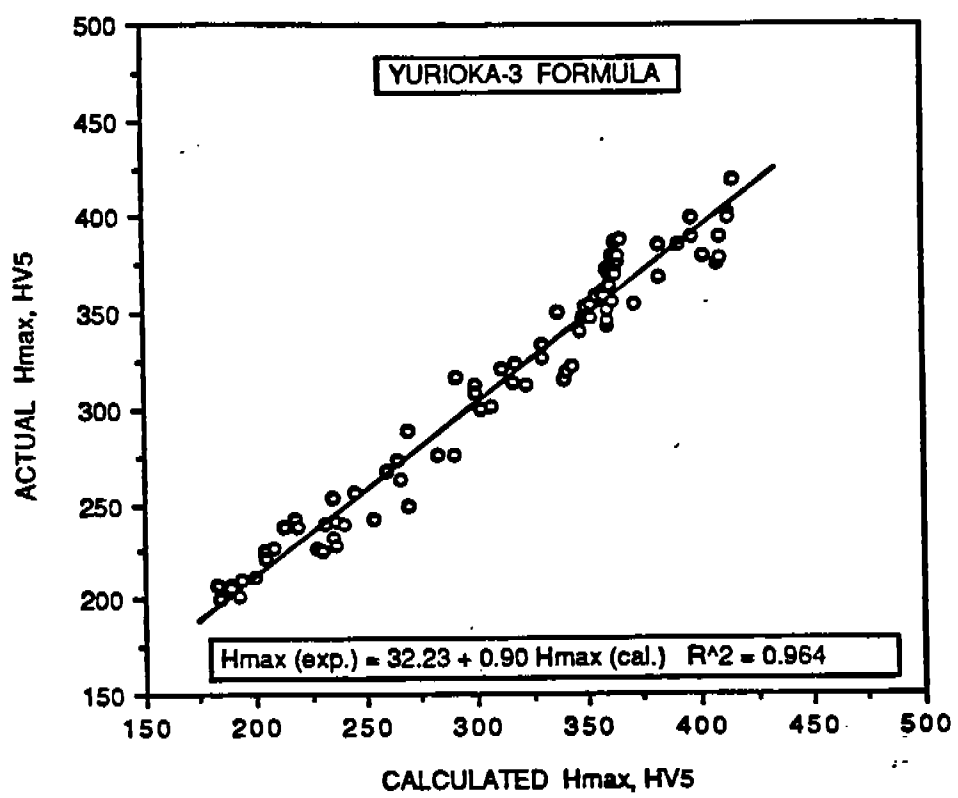
Fig.3.38. Correlation between actual and calculated CGHAZ hardness using Yurioka-3 formula for all steels.
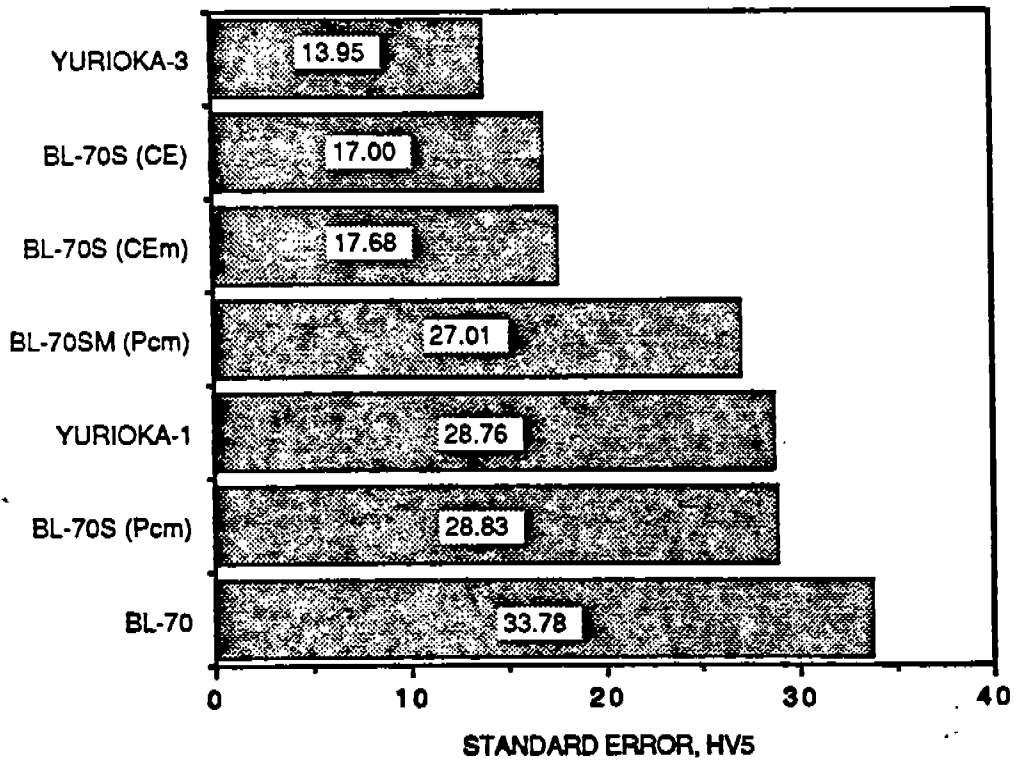
Fig.3.39. Ranking of various formula to calculate maximum HAZ hardness based on standard error of determination.

63

Yurioka-3 H_{max} (exp) = 32.23 + 0.90 H_{max} (cal)

$$R^2 = 0.964; \quad P = 13.95 \text{ HV5}$$

The accuracy of prediction in terms of standard error for all the formulae is shown in the bar chart in Fig. 3.39. The formulae Yurioka-3, BL-70S (CE) and BL-70S (CE_m) allow acceptable prediction of H_{max} data determined in this study.

It is interesting to note that among all the formulae proposed by Suzuki, BL-70S (CE) and BL-70S (CE_m), were able to predict H_{max} with an acceptable level of accuracy in the present steels, as contrasted to other formulae based on P_{cm} such as BL-70S (P_{cm}) and BL-70SM (P_{cm}). The carbon equivalents P_{cm}, CE, and CE_m are given below for ready comparison. The carbon equivalent CE_I (from Yurioka-3) representing hardenability is also compared with the other three CE's.

P_{cm} = C + Si/30 + Mn/20 + Cu/20 + Ni/60 + Cr/20 + Mo/15 + V/10 + 5 B

CE (IIW) = C + Mn/6 + Cu/15 + Ni/15 + Cr/5 + Mo/5 + V/5

CE_m = C + Si/24 + Mn/6 + Cu/15 + Ni/15 + Cr/5 + Mo/5 + V/5 + 15 B

CE_I = C + Si/24 + Mn/6 + Cu/15 + Ni/12 + Cr/8 + Mo/4 + ΔH

where

ΔH = 0 when B ≤ 1 ppm

ΔH = 0.03 f_N when B = 2 ppm

ΔH = 0.06 f_N when B = 3 ppm

ΔH = 0.09 f_N when B ≥ 4 ppm

and f_N = (0.02 - N)/0.02

Suzuki developed CE_m as a modified version of CE (IIW) by including the effects of Si and B on the hardenability of micro-alloyed steels. Both the formulae are related by-

CE_m = CE + Si/24 + 15 B

CE_m and P_{cm} relationship is given below-

P_{cm} = 0.0039 + 0.702 C + 0.310 CE_m

In order to compare the contribution of each element to the overall carbon equivalent, (a typical example) HSLA-80-1 steel is considered. The coefficients of various elements in the four carbon equivalent formulae described above have been normalized and denote the percentage contribution toward a carbon equivalent of 100.

P_{cm} = 20 C + 5.61 Si + 10.91 Mn + 28.64 Cu + 7.28 Ni + 15.45 Cr
           + 6.67 Mo + 0.14 V + 4.54 B

CE (IIW) = 9.56 C + 17.39 Mn + 18.26 Cu + 14.78 Ni + 29.56 Cr
           + 9.56 Mo + 0.13 V

CE_m = 8.8 C + 3.08 Si + 16 Mn + 16.8 Cu + 13.6 Ni + 27.2 Cr
           + 8.8 Mo + 0.12 V + 6 B

CE_I = 8.98 C + 3.15 Si + 16.33 Mn + 17.14 Cu + 17.35 Ni + 17.35 Cr
           + 11.22 Mo + 9.18 ΔH

The comparison of the contribution of different elements to CE value reveals that in the P_{cm} formula carbon and copper were given maximum weightage, while in the remaining three formulae the carbon contribution has been reduced substantially (from 20 to about 9%) and copper weightage has been decreased from 28.64 to about 17.%. The P_{cm} formula is based on steels with a minimum carbon content of 0.07 wt% and a maximum Cu content of 0.50 wt%. This implies that when copper is present in amounts greater than

0.50 wt% its influence on hardenability no longer increases in proportion to its content, but becomes appreciabally smaller. Another striking feature among the CE (IIW), CE_m and CE_I is the similarity of weightages given to some of the other alloying elements such as Mn, Ni, and Mo. In general, it is found that the percentage contribution of C, Si and Cu to carbon equivalents has decreased and that of Mn, Ni, Cr, Mo, and B has increased since P_{cm} was developed (in 1968). In the modern low carbon steels, it is recognized that the effect of other alloying elements on the hardenability has become more important as compared to carbon. The effect of boron is recognized in CE_m and its interaction with nitrogen is given due consideration in CE_I. Boron inhibits the nucleation of ferrite by segregating to the grain boundaries, thus increasing hardenability. However, the presence of nitrogen decreases this effect by fixing boron. The interaction of nitrogen with boron is affected when strong nitride formers like Al and Ti are present.

In order to assess the contribution of elements to various CE's in non-copper containing steel that falls within the validity limit of P_{cm} and the other three CE's, the results from AC-50 are discussed below. It should be noted that all H_{max} formulae allowed accurate determination of maximum HAZ hardness in this steel, thus implying that all four CE's described above may be suitable to define the hardenability of AC-50.

$$P_{cm} = 49.37\ C + 5.62\ Si + 42.8\ Mn + 0.31\ Cu + 0.21Ni + 0.62\ Cr + 4.17\ Mo + 0.19\ V + 3.12\ B$$

$$CE\ (IIW) = 23.94\ C + 69.2\ Mn + 0.20\ Cu + 0.40\ Ni + 1.21\ Cr + 6.06\ Mo + 0.18\ V$$

$$CE_m = 21.94\ C + 3.12\ Si + 63.42\ Mn + 0.18\ Cu + 0.37\ Ni + 1.11\ Cr + 5.56\ Mo + 0.17\ V + 4.17\ B$$

$$CE_I = 18.37\ C + 2.62\ Si + 53.1\ Mn + 0.15\ Cu + 0.39\ Ni + 0.58\ Cr + 5.81\ Mo + 18.83\ \Delta H$$

Comparison of the above equations reveals that in AC-50 the hardenability is primarily controlled by C and Mn and it is evident in all the CE formulae, though the relative contributions of C and Mn are different. However, in HSLA-80-1 the alloying elements other than C and Mn become of increasing importance in determining hardenability.

The improved correlation obtained with H_{max} formulae based on CE, CE_m, and CE_I may not be trivial, but may reflect the changing role of different alloying elements (e.g. C, B, N, and Cu) when present in amounts not customary in conventional steels and their relative effect on hardenability in the modern low carbon micro-alloyed steels. Therefore, it appears from the above that the hardenability of steels in this program can be represented adequately by CE_I. The applicability of CE_I will be further evaluated in Section 4 where the results of susceptibility of these steels to hydrogen assisted cracking are discussed.

3.4. CONCLUSIONS

The following main conclusions can be drawn from the results presented in this Section-

(1) Three nomograms and two equations to estimate the cooling time from 800 to 500°C were evaluated for the experimental data on two steels - HSLA-80-2 (1" thick) and DQ-125 (2" thick) - from this study. The equation proposed by Uwer and Degenkolbe was found to provide accurate determination of cooling time for both SMA and SA weldments. The remaining nomograms and equation were also suitable for predicting cooling time in SMA welds but were of limited

validity to SA welds. On the other hand the Uwer and Degenkolbe equation was applicable to SMA, SA, and GTA welding and to a much wider range of energy inputs and joint geometries. Therefore, the Uwer and Degenkolbe method was employed to calculate the cooling times for welding conditions employed on all steels in this program.

(2) The maximum HAZ hardness variation with cooling time was investigated for all nine steels. The cooling time (800 to 500°C) was varied from 2.5 sec. to a maximum of 140 sec. by employing both the SMA and SA welding processes. This range of cooling time allowed the study of an array of different CGHAZ microstructures ranging from fully martensitic to fully bainitic. An equation recently proposed by Yurioka to estimate % martensite in the CGHAZ was evaluated qualitatively for the steels under study. This equation appears to be valid for all steels. The reason for selecting the above equation was also based on the fact that Yurioka's formula to calculate maximum HAZ hardness is derived from this equation and it allowed accurate determination of hardness in all steels.

(3) Seven formulae to calculate maximum HAZ hardness were selected for comparison with experimental data from this study. Five of these formulae were proposed by Suzuki (BL-70 formulae) and two by Yurioka. Suzuki's formulae represented an improvement over the predecessor formulae which were widely used to estimate CGHAZ hardness before 1985 including one by Yurioka - Yurioka-1 formula. Another formula - Yurioka-3 was published in 1987, and has applicability to not only low carbon low alloy steels but also to high alloy steels. When these hardness formulae were applied to the steels in this study, the Yurioka-3 formula, followed by BL-70S (CE) and BL-70 (CE_m), allowed the most accurate prediction of CGHAZ hardness. The BL-70 formulae based on P_{cm} were found inadequate for estimating maximum hardness.

(4) A comparison of different carbon equivalent formulae - P_{cm}, CE (IIW), CE_m, and CE_I, used in H_{max} equations to describe the hardenability of steels revealed that in CE(IIW), CE_m and CE_I, while the carbon and copper contribution to the overall carbon equivalent has been appreciably reduced, the weightage of Mn, Ni, Cr, Mo, and B has been increased as compared to that in P_{cm}. This implies that in low carbon micro-alloyed steels the influence of alloying elements (other than carbon) on hardenability has been given more influence when compared to conventional C-Mn steels. The effect of copper (in amounts > 0.50 wt%) on the hardenability does not increase linearly with increase in content and thus in CE's valid for the steels in this investigation its weightage has been reduced appreciably. Therefore, from the CGHAZ hardness data, it appears that the CE_I carbon equivalent formula may be considered to best represent the hardenability of steels in this program.

4. HYDROGEN ASSISTED CRACKING

4.1. INTRODUCTION:

The concept of weldability encompasses many diverse areas, however, for the last 50 years hydrogen assisted cracking (HAC) has been synonymous with the weldability of steels. Consequently, it has received considerable attention from steel users, manufacturers, fabricators and researchers alike. As a result of these sustained efforts, superior grades of steels have been made available to the user with greatly reduced susceptibility to cold cracking and which can be welded with lower preheat temperatures and over wider heat input ranges than was possible in years past. A chronological illustration in Fig. 4.1 shows the improvement brought about in the quality of linepipe steels over the years [53]. The weldability of structural steels has been improved by (a) the introduction of steels with lower carbon content and thus a lower carbon equivalents, (b) the application of various thermomechanical treatments to enhance strength and toughness by grain size and microstructure control, (c) lower sulfur content and inclusion shape control, and (d) the availability of high quality low hydrogen welding consumables.

The main advantage derived from the above developments is in terms of improving the heat affected zone properties with respect to hardenability, cold cracking, lamellar tearing, reheat cracking, toughness and stress corrosion cracking. Moreover, it has become technically possible to weld steels over a wider range of heat inputs with limited preheat. One of the important advantages of preheating and holding the preheat temperature during welding is the removal of hydrogen introduced into the weld and HAZ. For the case where there is no preheating or inadequate preheating, hydrogen cannot effectively diffuse and escape from the weldment, but remain trapped and stress concentration, thus increasing the risk of cold cracking. Moisture contained in consumables has been generally less important in the past, since welding was carried out at carefully defined preheat levels. Recently, however, there have been significant efforts to minimize preheat as a cost reduction measure, therefore, the hydrogen introduced into the weldment through consumables has become of greater importance. Though considerable work has been carried out to understand the phenomenon of hydrogen assisted cracking, there are still many attributes of the phenomena that are not fully understood.

HAC commonly occurs in the grain coarsened region of the HAZ and is frequently described as toe cracking, root cracking, or underbead cracking depending on crack location. It is also known as delayed cracking or cold cracking because cracking usually occurs after an incubation period, which can vary from a few hours to days, and generally does not initiate until the weldment has cooled to below 200°C. The three most important factors responsible for HAC in a steel weldment are: (a) the chemical composition and hence hardenability, which in turn determines the HAZ microstructure, (b) the hydrogen content of the weld deposit, and (c) the restraint associated with the welded geometry and the attendant residual stresses.

4.1.1 Effect of Chemical Composition

The chemical composition of a steel, along with the peak temperature attained during welding, and the cooling rate through the austenite transformation temperature range determines the microstructure developed in the HAZ. The carbon content defines the maximum hardness obtained in the HAZ, whereas the carbon and other alloying elements (carbon equivalent) determine the hardenability. The addition of micro-alloying elements to resist

67
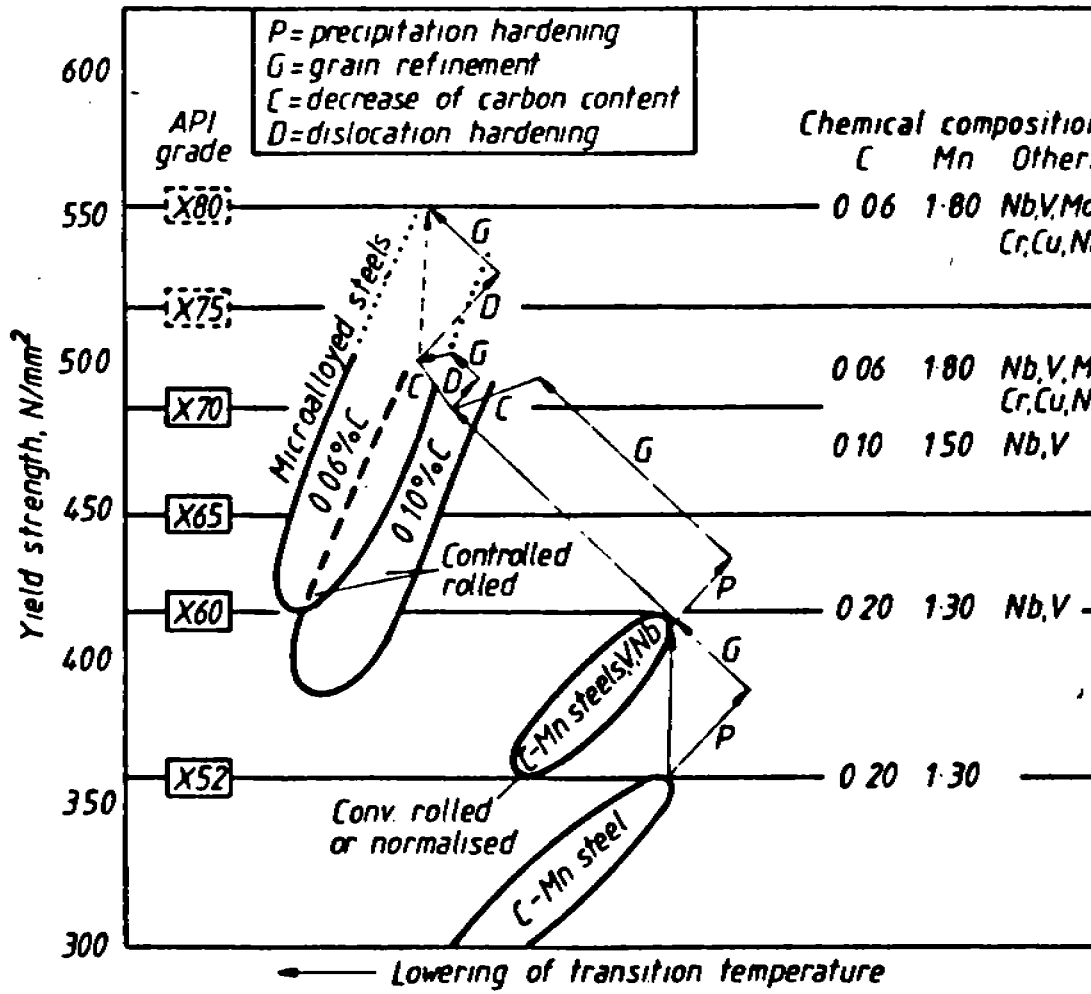
Fig.4.1. Chronological development in linepipe steels.[53]

the grain growth in the HAZ by a pinning effect not only improve toughness but also reduce susceptibility to HAC, as the transformation kinetics of austenite to non-martensitic constituents in a fine grained structure is comparatively rapid and the critical cooling time, below which 100% martensite forms, decreases almost linearly with austenite grain size (Fig. 4.2) [21]. Therefore, the net effect of the addition of micro-alloying elements is to shift the CCT diagram to shorter times and thereby decrease the amount of martensite in the HAZ. Recently, computation of austenite grain growth in the HAZ's of micro-alloyed steel weldments has been achieved as illustrated in Fig. 4.3 [28] and it is suggested that the hardenability of steels can be fully represented by a composition characterizing parameter and austenite grain size. For conventional steels, however, the transformation behavior of HAZ's during welding has been successfully quantified by composition characterizing parameters alone, because in such steels hardenability is totally dictated by the chemical composition and any effect of the austenite grain size is not discernible.

Reduced sulfur levels in "clean" steels are reported to enhance susceptibility to cold cracking. This is attributed to a decrease in the density of inclusions and thus a reduction in the number of hydrogen trapping sites. However, Kirkwood [21] in his review of the data on the cold cracking susceptibility of offshore structural steels containing sulfur levels in the range 0.002 to 0.009% concluded that "while there is indeed evidence that lower sulfur steels may have an increased tendency to produce higher hardness levels, this does not necessarily imply increased hardenability in the classical context. The "sulfur effect" appears to increase in magnitude as carbon equivalent decreases, and is of maximum importance when considering the ability of a steel to generate hardness levels above 375 HV. There is no evidence that the lower sulfur steels in this (sic) study are more susceptible to hydrogen induced cold cracking". A similar conclusion was also espoused by Yurioka et al [54] in the case of C-Si-Mn-Nb-V-B-N steels containing 0.002 to 0.021 % sulfur. However, Hart [55,56] in a survey found that 70 % of reports stated that decrease in the sulfur content increases the susceptibility of steels to HAC. The reason for such conflicting views on the role of sulfur may be due to the fact that the analyses have been carried out taking into account the total impurity content whereas a parameter involving the shape, size, and distribution of non-metallic inclusions would appear to be more appropriate. It is now becoming increasingly evident that non-metallic inclusions act as sites for intragranular ferrite nucleation and any reduction in sulfur content should act in a way such as to increase the hardenability of "clean" steels. Attempts are underway to decrease S to as low a level as possible and form CaO rather than CaS to act as sites for trapping diffusible hydrogen.

Controlled additions of boron in modern steels is a relatively new development. Boron contents less than 10 ppm are quite effective in elevating the hardenability of steels as free boron segregates to the grain boundaries and retards the nucleation of ferrite [16]. However, boron reacts with nitrogen to form boron nitride, thus free boron becomes unavailable to retard the nucleation of ferrite. Therefore, the use of strong nitride formers, such as Ti and Al, is resorted to fix nitrogen and exploit the effect of boron on the hardenability.

4.1.2. Effect of Hydrogen

Hydrogen in a weldment exists in combined (molecular) and diffusible (atomic) forms. It is the diffusible hydrogen which is responsible for cold crack initiation. The main sources for the introduction of hydrogen into a
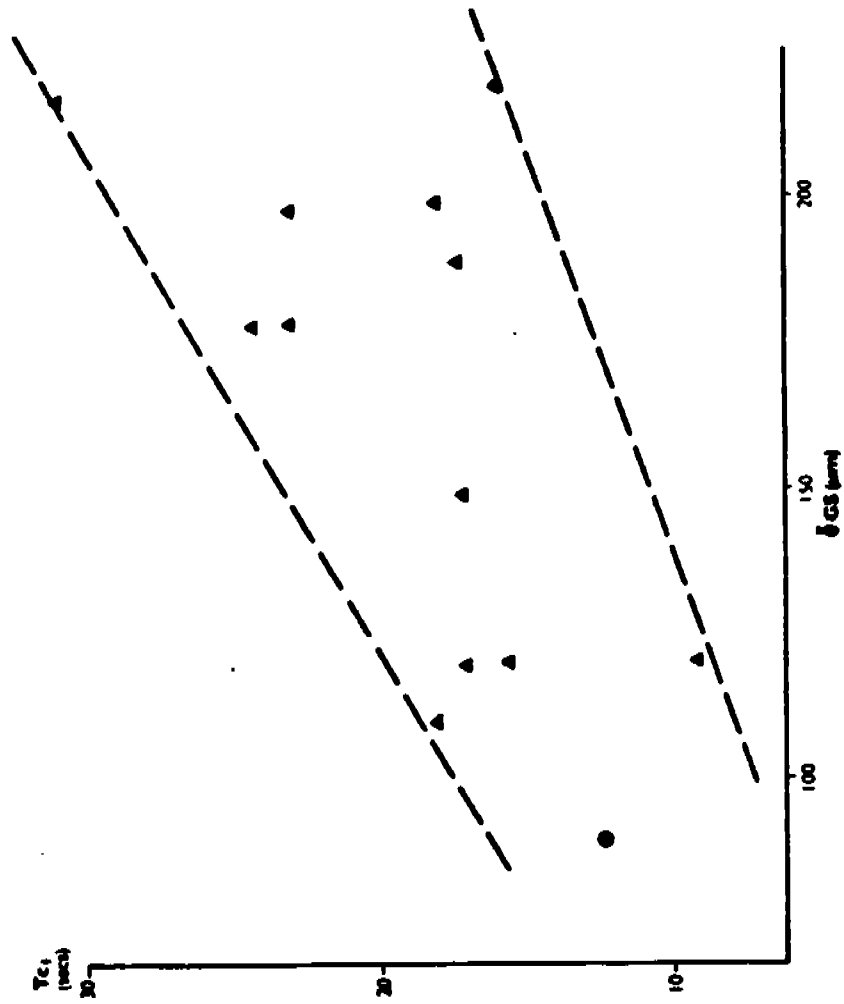
Fig.4.2. Variation in critical cooling time for martensite formation with austenite grain size [21]
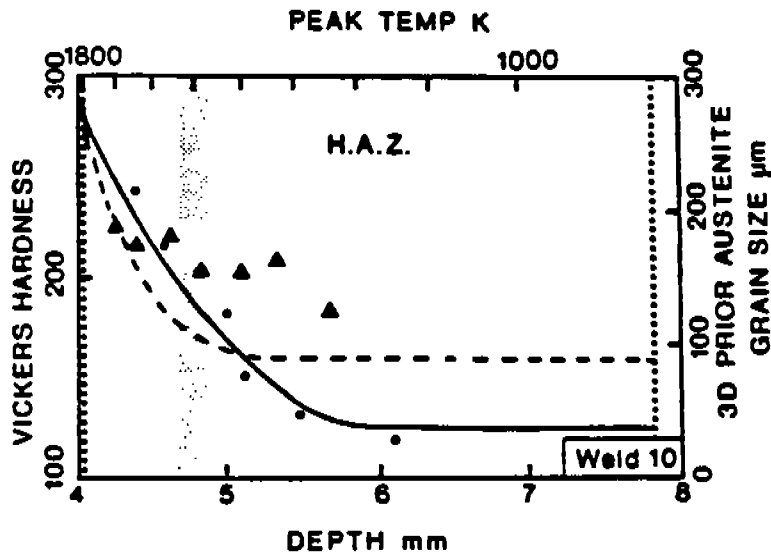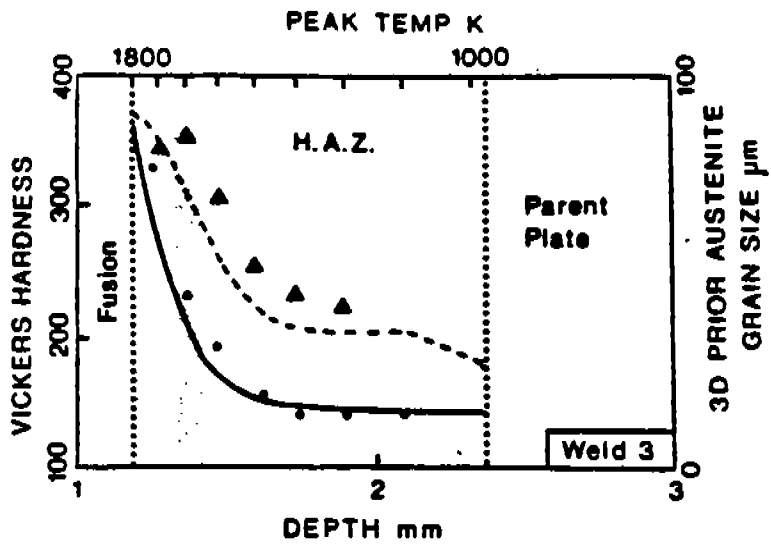
Fig.4.3. Computation of austenite grain growth in HAZ's of microalloyed steel weldments [28]

weldment are: (a) chemically bonded and absorbed water in the electrode coatings and fluxes, (b) moisture in shielding gas from GMA and GTA welding processes, and atmospheric humidity and (c) surface contaminants. Typical diffusible hydrogen contents in the weldments may vary from 1 to 40 ml/100g depending on the type of consumables and fluxes used, their storage conditions and atmospheric humidity. Fig. 4.4 shows range of hydrogen contents expected in a weldment when different welding processes are employed [57].

The trend of linear variation of lattice diffusivity coefficient of hydrogen at temperatures above 150-200°C is not followed at lower temperatures, as shown in Fig. 4.5 [58]. In the lower temperature range the apparent diffusivity becomes progressively smaller than the "ideal" diffusivity with decrease in temperature. This figure has been constructed from data taken from various sources. It is apparent that the deviation in the observed diffusivity coefficient from expected values depends on the impurity content of the weld metal. This phenomenon is attributed to the trapping or delaying of hydrogen as it moves through the lattice. The resistance to hydrogen movement through lattice becomes less pronounced at high temperatures as trapped hydrogen can escape with greater ease at these temperatures. Trapping efficiency differs with the type of lattice discontinuity. Microvoids created either by cold work or plastic deformation have been found to be the most efficient sites for hydrogen trapping. Other trapping sites such as dislocations, grain boundaries, inclusions, and precipitates also have varying degrees of trapping efficiencies.

Diffusible hydrogen content is recognized to play a crucial role in initiating cracks and at present significant work is underway to understand the mechanism of hydrogen distribution as a function of microstructure and stress. In Fig. 4.6 [28] the results of one such study to compute hydrogen distribution in the HAZ of steel welds are shown. At present, sites for hydrogen segregation have not been completely defined and the role of stress is not fully understood. However, with some simplified assumptions it is possible to estimate the hydrogen distribution in the HAZ.

4.1.3. Effect of Stress

Strains are developed by thermal contraction during cooling of the weld. Stresses approach yield in most instances. The presence of hydrogen appears to lower the stress level at which cracking will occur. In rigid structures the natural contraction stresses are intensified because of the restraint imposed on the weld by the different parts of the structure. These stresses are concentrated at the toe and the root of the weld and also at notches constituted by inclusions and other defects. Higher degree of restraint produces higher risks of cracking for a given microstructure hardness.

Very little can be done to modify the welding stresses as they depend mainly on restraint, however, models have been recently developed to precisely calculate the distribution of local stresses by judicious selection of the design and welding process [59]. In an extensive study at MIT [60], to calculate the stress distribution in welds, a good correlation between theory and experimental results was obtained.

The residual stress acting upon a weld is a function of weld size, joint geometry, fitup, external restraint, and the yield strength of the base plate and weld metal. Judicious selection of joint geometry, welding parameters, and stress-relief treatment may aid in mitigation of cold cracking in a welded joint.
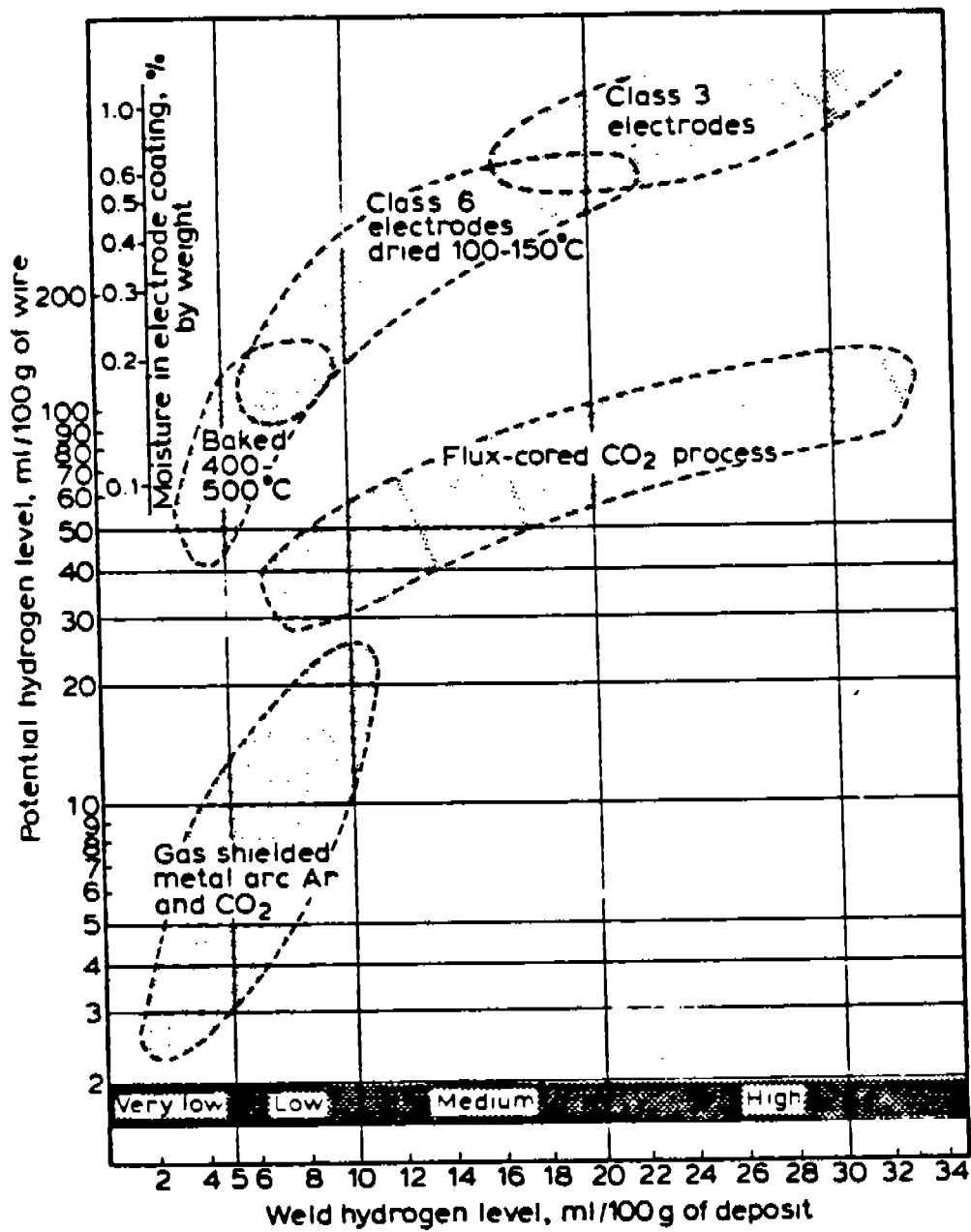
Fig.4.4. Range of hydrogen contents expected in various welding processes [57]
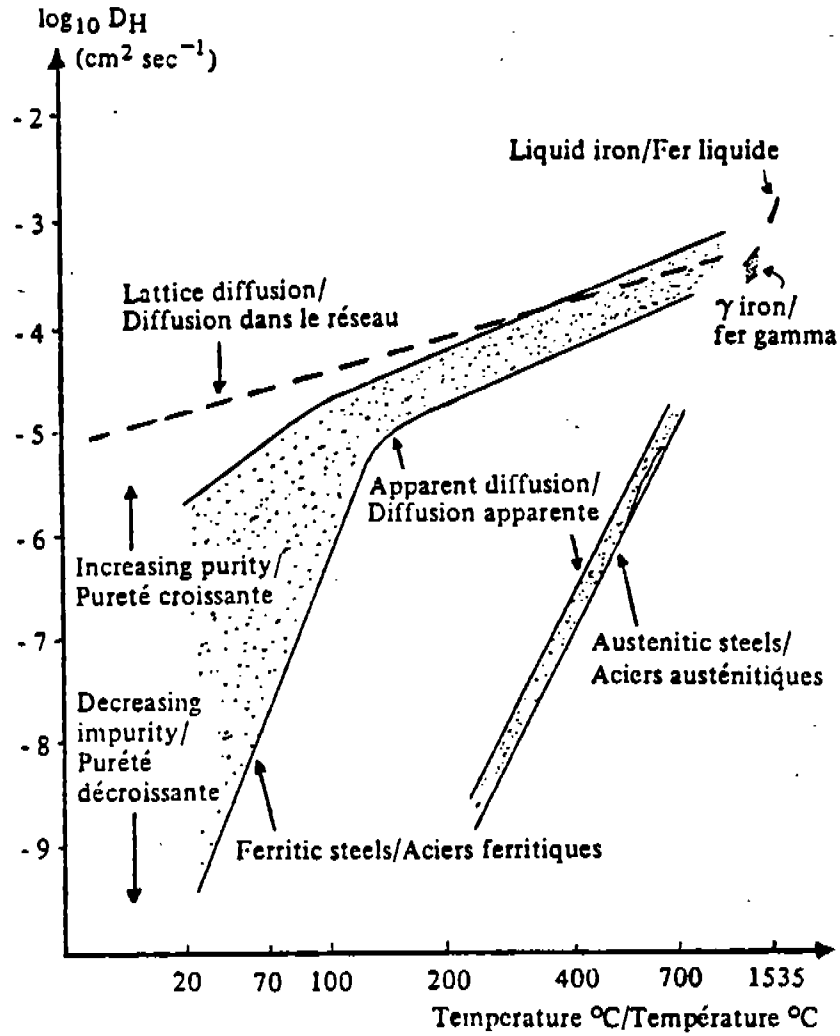
Fig.4.5. Variation in the hydrogen diffusivity coefficient in austenite and ferrite lattices [58]
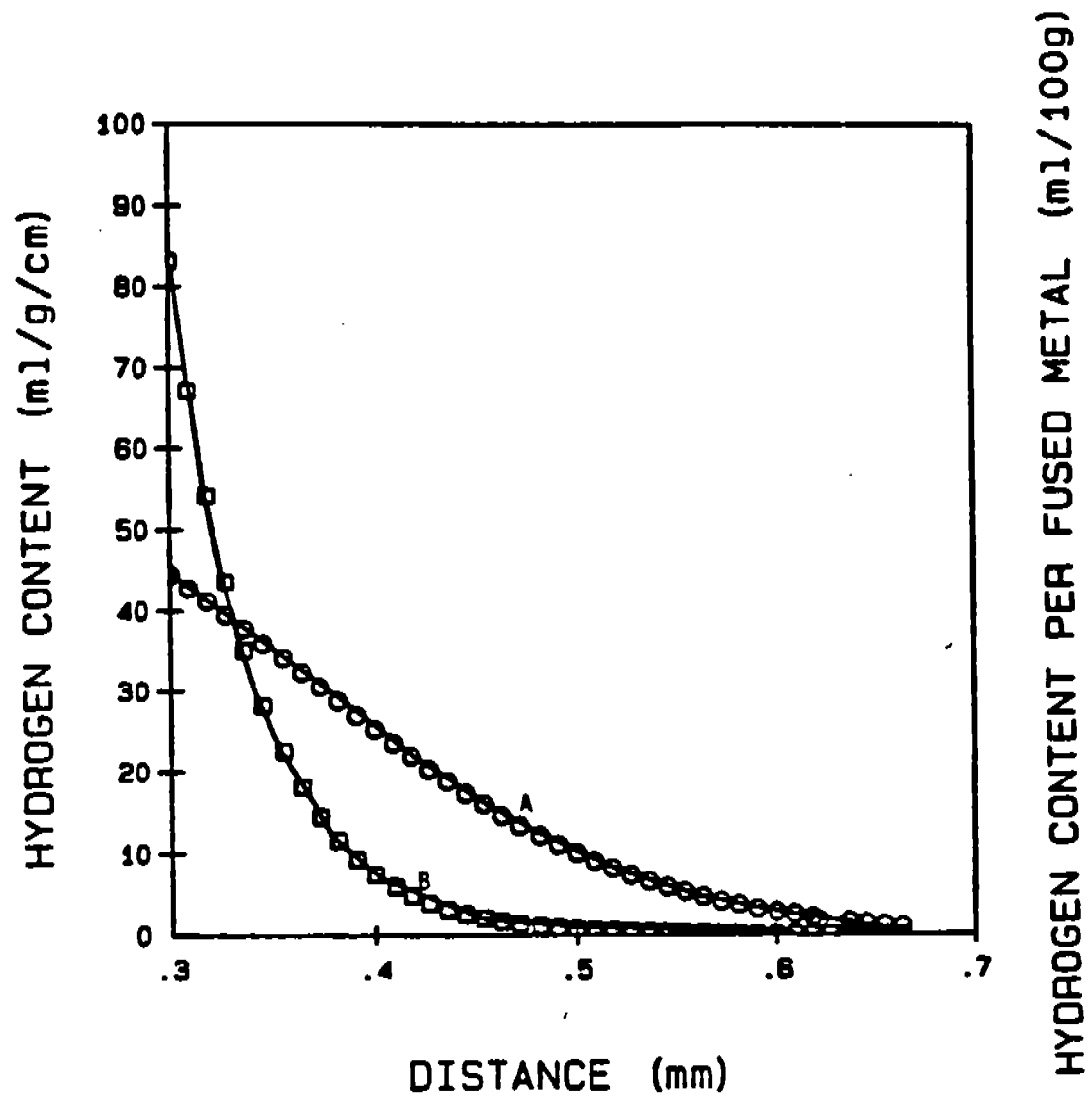
Fig.4.6. Modelling of diffusible hydrogen in the HAZ [28]

4.1.4. Concept of Carbon Equivalent

From the above it is clear that if the effects of chemical composition, diffusible hydrogen level, and stress on a weld deposit on its cold cracking susceptibility can be quantified, it is possible to predict safe welding conditions. Many attempts have been made in this direction and met with varied degrees of success . The effect of chemical composition on the weldability of a steel is described by a carbon equivalent, which normalizes the composition to a single number. There are many CE's available depending on type of approach and class of steel. Table 4.1 lists various CE's proposed thus far. There is no universal CE formula applicable to all classes of steels. Most of the formulae have limited validity (in terms of chemical composition, cooling time from 800 to 500°C, and plate thickness) and are applicable to the class of steels for which they were devised, though there are claims to the contrary. The reason for disagreement appears to result from the fact that the "derivation" of CE formulae is still empirical in nature and experimental errors in determining $t_{8/5}$, hardness and chemical composition may cause significant scatter when comparing data from different sources. Moreover, the predictive utility of the CE has come into question especially with regard to HSLA steels which have a significantly reduced carbon content. In the case of conventional steels with higher CE's, the weldability and metallurgical response is totally dictated by the carbon content and CE values. As C and CE levels have progressively decreased, the importance of other metallurgical factors, such as prior austenite grain size, which hitherto was negligible as compared to the dominant effect of the overall chemistry, has increased. Recently some attempts have been made to rationalize the predictive models on the basis of metallurgical factors, but considerably more data are needed to develop a workable model. In the following sections two of the widely used models for predicting preheat temperatures are briefly described and their applicability to HSLA steels is discussed.

4.1.5. Hardness Control Approach

A considerable extent of the early development of CE formulae was based on work conducted on C-Mn steels with relatively high carbon content ($\geq 0.20\%$). These models were developed at The Welding Institute and form the basis of the requirements in BS 5135 [12]. It is based on the observation that the incidence of HAZ cracking is greatly reduced when the HAZ hardness is below a certain critical value. The hardness of the HAZ is controlled by limiting the cooling rate to a certain value below which the critical HAZ hardness is never achieved. The selection of the critical hardness will depend on a number of factors such as type of steel, hydrogen level, restraint and service conditions. For example, the maximum hardness in the HAZ of high strength structural steels for offshore application is restricted to 325 HV to safeguard against cold cracking, whereas a critical hardness of 245 HV is considered an upper limit in aggressive environments to avoid stress corrosion cracking. Therefore, as a first step toward defining the welding conditions, the maximum critical HAZ hardness (H_{max}) should be selected. The minimum preheat temperature is then determined from a nomogram available in BS 5135 (e.g. Fig.4.7). In this approach the following carbon equivalent is used as a chemical composition characterizing parameter:

$$CE(IIW) = C + Mn/6 + (Cr + Mo + V)/5 + (Ni + Cu)/15$$

76

Table 4.1 Carbon Eqivalent Coefficient*

S. No.	Reference	Year	C	Mn	Si	Cu	Ni	Cr	Mo	Nb	V	B	Co
1	Deardent & O'Neill	1940	1	6	-	13	15	5	4	-	5	-	150
2	Edson	1942	1	7.3	-	47	16.4	8.8	-	-	-	-	-
3	Nehrenberg	1946	1	9	27	-	18	14	27	-	-	-	-
4	Voldrich et al	1947	1	4	-	-	-	-	-	-	-	-	-
5	Voldrich et al	1947	1	4	4	-	-	-	-	-	-	-	-
6	Heuschkel	1949	1	10	9	99	99	10	3	-	6	-	-
7	Heuschkel	1949	1	10	5	28	28	7	3	-	6	-	-
8	Sims & Banta	1949	1	7	25	-	-	510	31	-	13	-	-
9	Bradstreet	1956	1	20	-	-	15	10	10	-	10	-	-
10	Kihara et al	1959	1	6	24	-	-	-	-	-	-	-	-
11	Winterton	1961	1	6	-	40	20	10	(-50)	-	(-10)	-	-
12	Ito & Bessyo	1968	1	20	30	20	60	20	15	-	10	-	-
13	Beckert	1973	1	2.9	11	3.9	17	3.2	3.4	-	-	-	-
14	Stout	1976	6	6	-	40	20	10	10	-	-	-	-
15	Stout	1976	1	6	-	40	20	10	10	-	-	-	-
16	Graville	1976	1	16	-	-	50	23	7	8	9	-	-
17	Harasawa	1977	1	6	-	15	15	5	5	-	5	-	-
18	Duren	1980	1	16	25	16	60	20	40	-	15	-	-
19	Yurioka	1982	1	6	24	15	40	6	4	5	5	X10	-
20	Yurioka	1980	1	6	(-30)	15	20	4	6	-	-	-	-
21	Duren	1982	1	8	11	9	17	5	6	-	3	-	-
22	Terasaki	1984	1	3	-	4	8	10	3	-	-	X5	-
23	Cottrell	1984	1	6	-	-	-	5	5	4XC	3	-	-
24	Suzuki	1985	1	6	24	15	15	5	5	-	5	X15	-
25	Yurioka	1987	1	6	24	15	12	8	4	-	-	-	-
26	Yurioka	1987	1	5	24	10	18	5	2.5	3	5	-	-
27	Yurioka	1987	1	3.6	-	20	9	5	4	-	-	-	-

* Coefficient for various elements are denominators to the wieght percent of the
elements unless otherwise specified

77
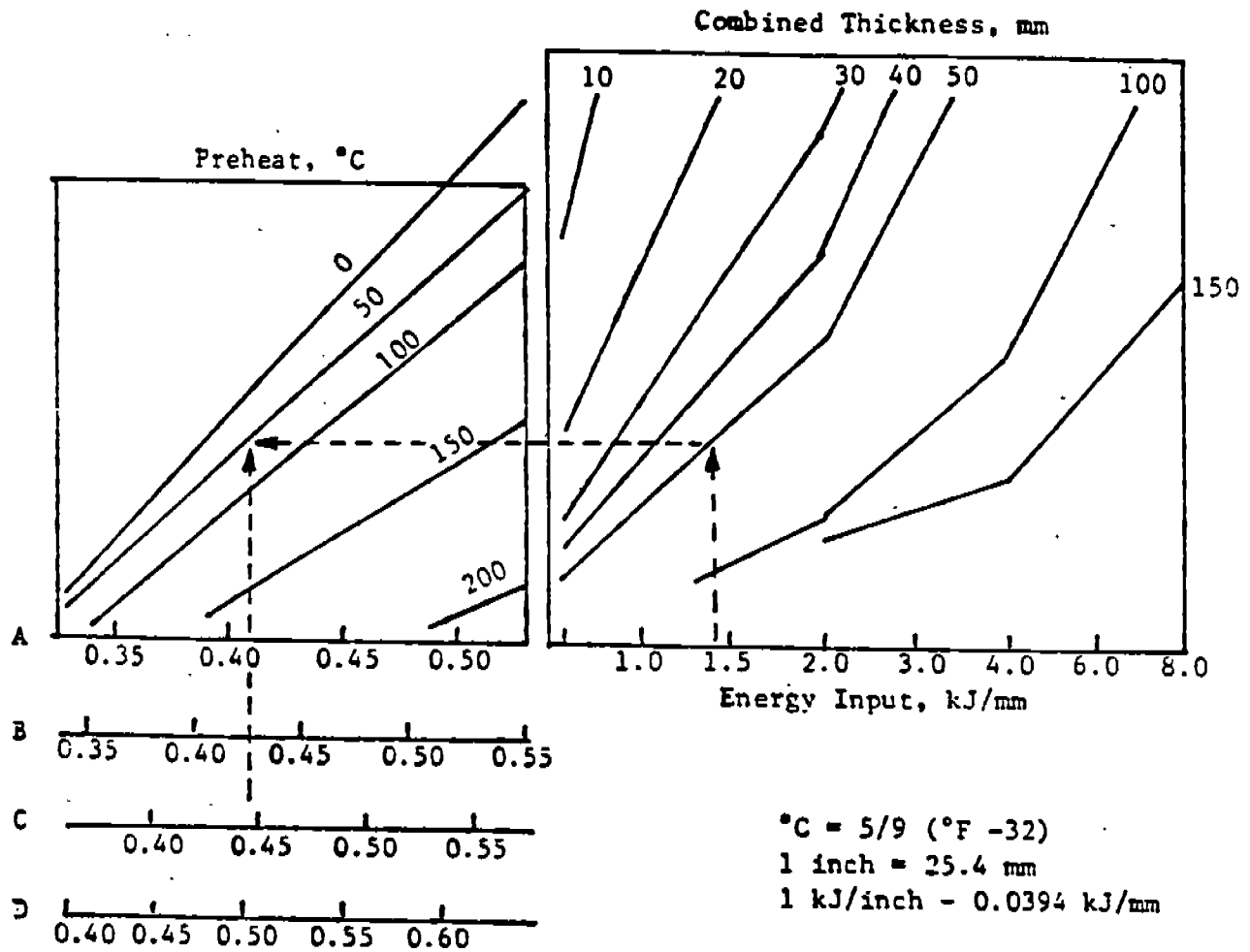
Fig.4.7. A typical nomogram to determine the preheat temperature using the Hardness
Control approach [12]

The Hardness Control method is applicable to steels with carbon equivalents in 0.46 to 0.58 range. The approach is based on the assumption that the critical hardness is independent of carbon equivalent. Kirkwood [21] analyzed the published data from the "new" steels and arrived at the conclusion that the critical hardness decreases dramatically with decreasing carbon equivalent (Fig.4.8). Thus implying that the Hardness Control approach should be employed to the modern steels with caution.

4.1.6. Hydrogen Control Approach

This model was developed in response to the recognition that cracking did not always occur when the critical hardness was exceeded. Preheated welds tolerated higher hardness than unpreheated. This is due to enhanced diffusion of hydrogen out of HAZ in the preheated welds. Ito and Bessyo [13] carried out a large number of groove weld experiments (more than 200) using the Tekken Test for a wide range of low alloy steels, (carbon content ranging from 0.07 to 0.22 wt%). They proposed the cracking parameter, P_w, which includes a composition characterizing parameter, P_{cm}, diffusible hydrogen content, H_{JIS} (ml/100g), and intensity of restraint, K (kg/mm^2):

$$P_w = P_{cm} + H_{JIS}/60 + K/(40 \times 10^3) \quad \text{.................................(4.1)}$$

where:

$$P_{cm} = C + Si/30 + (Mn + Cu + Cr)/20 + Ni/60 + Mo/15 + V/10 + 5B$$

The critical P_w is related to the time for the weld to cool to 100°C as shown in Fig. 4.9. The cooling time to 100°C is a measure of the amount of time available for hydrogen to diffuse out of the weldment. The cooling time can be measured experimentally or a preheat temperature related to a given cooling rate can be estimated from various empirical diagrams that have been developed based upon P_w, heat input, and plate thickness [61-65], such as shown in Fig.4.10. If the actual cooling time is greater than the calculated critical cooling time, cold cracking will not be expected to occur. Several formulae for the weld cracking parameter, P_w, have been proposed but they are essentially similar to the hydrogen control approach differing only in the degree of refinement of the hydrogen diffusion equation and the method of determining the stress in the weld [13,61,66]. Some of these formulae are given below:

$$P_w = P_{cm} + H_{JIS}/60 + h/600 \quad [13] \quad \text{.................................(4.2)}$$

$$P_w = P_{cm} + A \log H_{JIS} + \alpha \, \kappa K/[160,000(1 + C \, \gamma^2)] \quad [66] \quad \text{................(4.3)}$$

$$P_w = CEN + 0.15 \log H_{JIS} + 0.30 \log (0.017 \, K_t \, \sigma_w) \quad [61] \quad \text{................(4.4)}$$

where h is the plate thickness, A, α, κ, C, and γ are coefficients that are dependent upon heat input, restraint, and joint geometry, Kt is the theoretical elastic stress concentration factor at the weld root or toe, $_w$ is the mean stress acting on the weld metal, and CEN is Yurioka's carbon equivalent -

$$CEN = C + A(C) \times (Si/24 + Mn/6 + Cu/15 + Ni/20$$
$$+ Cr/5 + Mo/5 + V/5 + Nb/5 + 5B)$$

where

$$A(C) = 0.75 + 0.25 \tanh [20 (C - 0.12)]$$

The accommodation factor, A(C), increases with an increase in the carbon content. It approaches 0.5 at carbon contents below 0.08 wt% and 1 above 0.18 wt% (Fig. 4.11). Yurioka also compared the validity of his formula with those proposed by others. He performed Stout's line pipe cold cracking test on 20 steels and determined the critical preheat temperatures. His steels also included low carbon micro-alloyed steels. The carbon ranged from 0.018 to
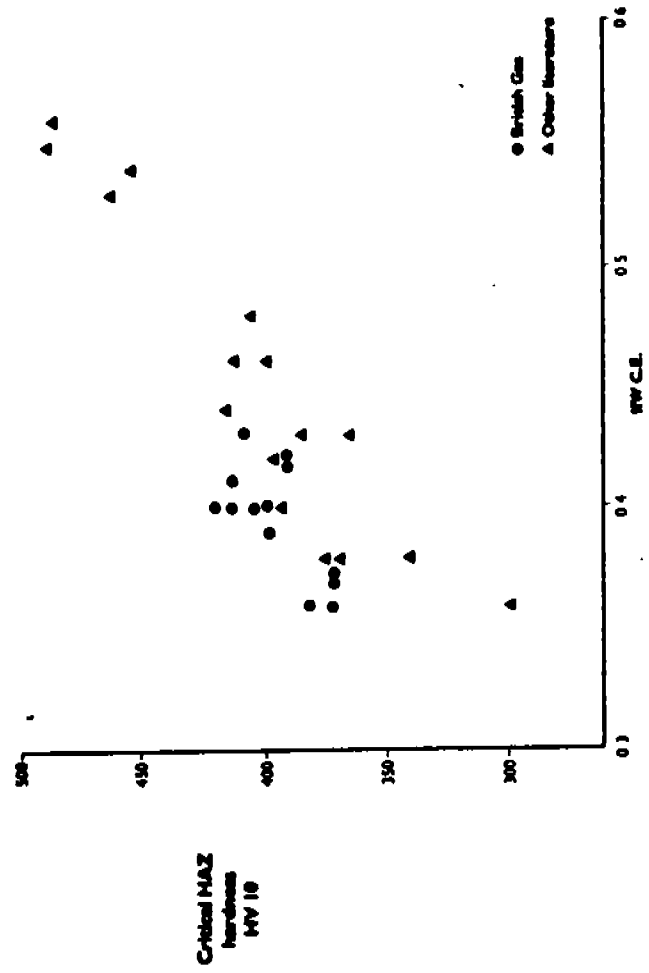
Fig.4.8. Dependence of critical HAZ hardness for cracking on carbon equivalent [21]
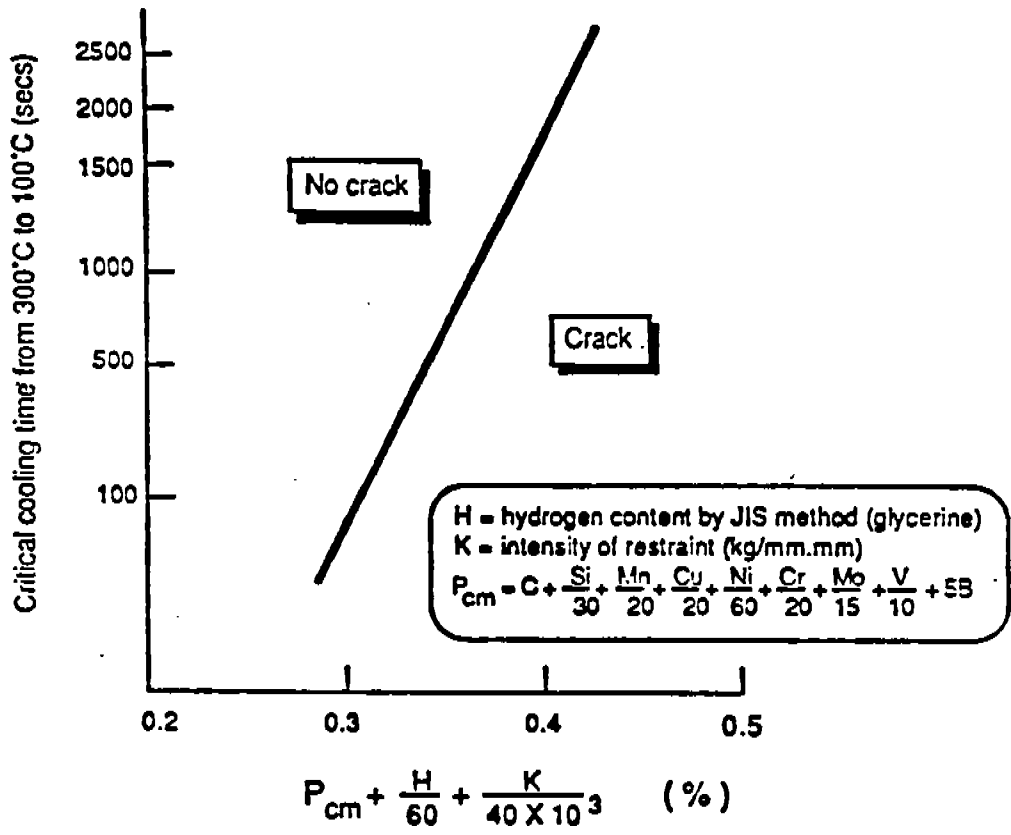
Fig.4.9. Relation between cracking parameter P_W and critical cooling time [13]

The figure shows a plot with the y-axis labeled "Critical cooling time from 300°C to 100°C (secs)" with values 100, 500, 1000, 1500, 2000, 2500. The x-axis is labeled $P_{cm} + \dfrac{H}{60} + \dfrac{K}{40 \times 10^3}$ (%) with values 0.2, 0.3, 0.4, 0.5. Regions labeled "No crack" and "Crack" are separated by a line.

A legend box reads:

H = hydrogen content by JIS method (glycerine)
K = intensity of restraint (kg/mm.mm)
$P_{cm} = C + \dfrac{Si}{30} + \dfrac{Mn}{20} + \dfrac{Cu}{20} + \dfrac{Ni}{60} + \dfrac{Cr}{20} + \dfrac{Mo}{15} + \dfrac{V}{10} + 5B$

81

Fig.4.10. Empirical diagram for estimating preheat temperature [66]
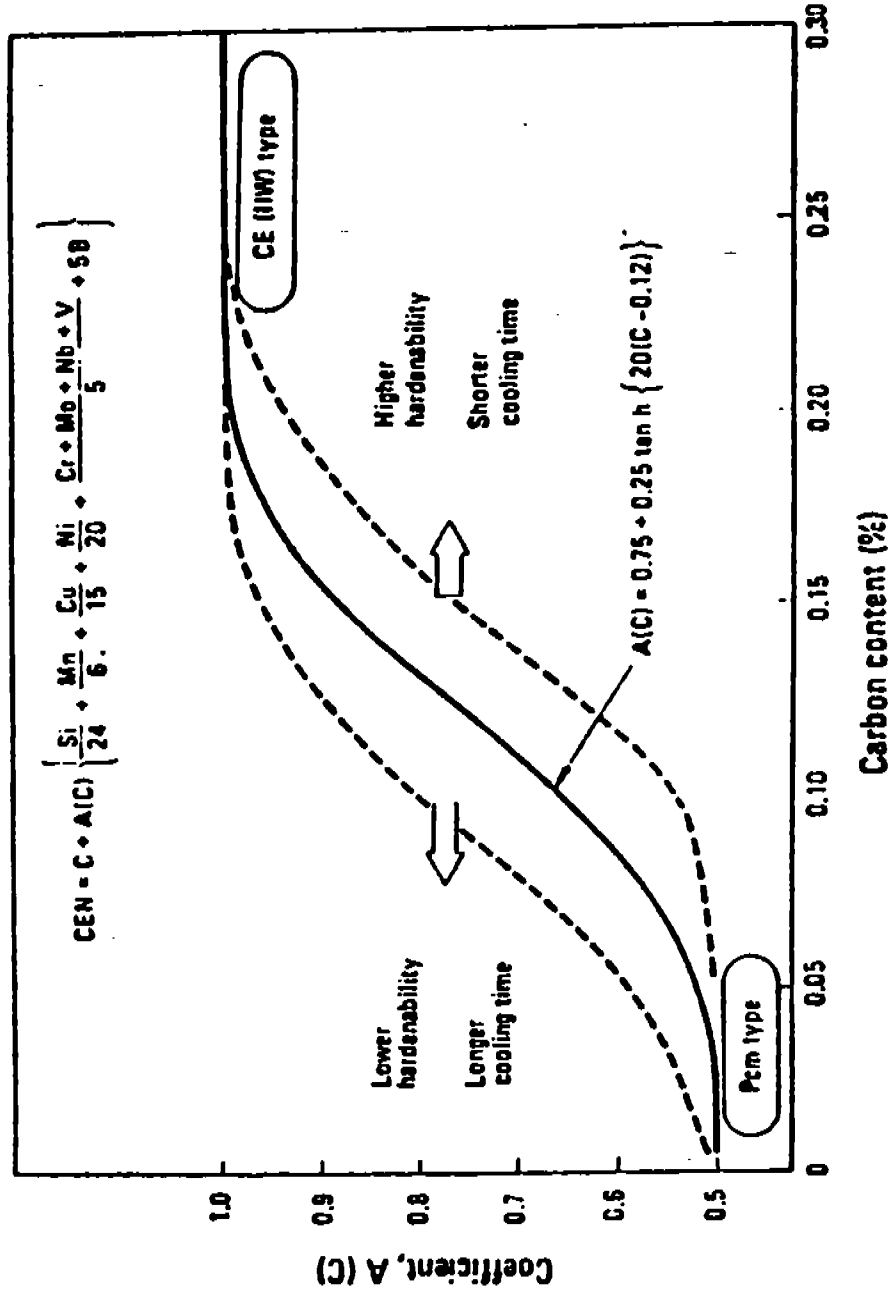
Fig.4.11. Relationship between CEN and CE(IIW) and Pcm [61]

0.25 wt%. He rated various CE's in order of decreasing correlation coefficients. The CEN carbon equivalent showed the highest correlation coefficient.

Suzuki et al have published a number of predictive formulae for assessing the cold cracking susceptibility of steels. The latest formula proposed by Suzuki [67] is given below. It is claimed to predict the preheat temperature more accurately than those formulae previously proposed by him.

$$(0)_{cr} = 68 \log (h) + 97 \log (H_D) + 459 \tan^{-1} (3C)$$

$$+ 44 \text{ Si} + 67 \text{ Mn} + 23 \text{ Cu} + 12 \text{ Ni} + 151 \tan^{-1} (0.7 \text{ Cr})$$

$$+ 29 \tan^{-1} (3 \text{ Mo}) + 139 \text{ V} + 24 \tan^{-1} (300 \text{ B}) -354 \qquad ....(4.5)$$

where $(0)_{cr}$ is the critical preheat temperature, h is the thickness of the plate and H_D is the amount of diffusible hydrogen (ml/100g) of the deposited weld metal. This formula is also applicable to very low carbon steels (C≥ 0.037 wt%). Based on standard error in predicting critical preheat temperatures while using equation (4.1) and (4.5), Suzuki's formula is shown to be more accurate and convenient to use. However, when the values are compared with those obtained for steels used in the Ito-Bessyo study, the accuracy is almost the same.

Graville [17,68] proposed a more generalized approach by assuming that cracking occurred only if a critical hydrogen level remained in the weld after it had cooled to 50°C. The amount of hydrogen diffusing out was represented by a diffusion parameter ßt. ß is a geometry factor and $t = \sum D\Delta t$ integrated over the cooling cycle of the weld where D is the diffusivity coefficient for hydrogen and t is time. For a given material, t is related directly to the cooling time to 50°C. Critical values of ßt for the onset of cracking were empirically related to the composition and the hydrogen content:

$$\text{ßt} = 12 \text{ P}_{cm} + \log H_{IIW} + \text{constant} \qquad ....(4.6)$$

where P_{cm} is Ito-Bessyo carbon equivalent, H_{IIW} is the hydrogen content in ml/100g of deposited metal and the constant term depends on the restraint level (Fig. 4.12). The minimum preheat temperature required to avoid cold cracking is obtained from standard Tables [68] giving values of preheat temperature for various thicknesses, restraint levels, and susceptibility indexes.

In the Ito-Bessyo cracking parameter, P_w, the diffusible hydrogen content is measured by the JIS (glycerine) method, whereas in the Graville cracking parameter, ßt, it is by the IIW (mercury) method. These methods are related by the following equation:

$$H_{JIS} = 0.67 \text{ } H_{IIW} - 0.8 \qquad ....(4.7)$$

Graville [68] while discussing the suitability of the above two approaches notes that "hardness control is most appropriate for carbon steels with limited alloy content. Such steels have a steep hardening curve (i.e. curve of HAZ hardness vs cooling rate) allowing a precise determination of critical cooling rate. The hydrogen control method is more appropriate for lower carbon steels with significant alloy and micro-alloy element present. These steels have flatter hardening curves and thus reducing the cooling rate has less of an effect on the hardness".

To assist in deciding which method is appropriate the diagram (Fig. 2.3) developed by Graville allows one to place a steel in a particular zone on the basis of carbon and carbon equivalent. Zone I steels have low carbon and a low risk of cracking in the HAZ but cracking may occur with high hydrogen and high restraint. The hydrogen control method should be used to determine preheat for steels in this zone. Steels in Zone II have steep hardening curves

84
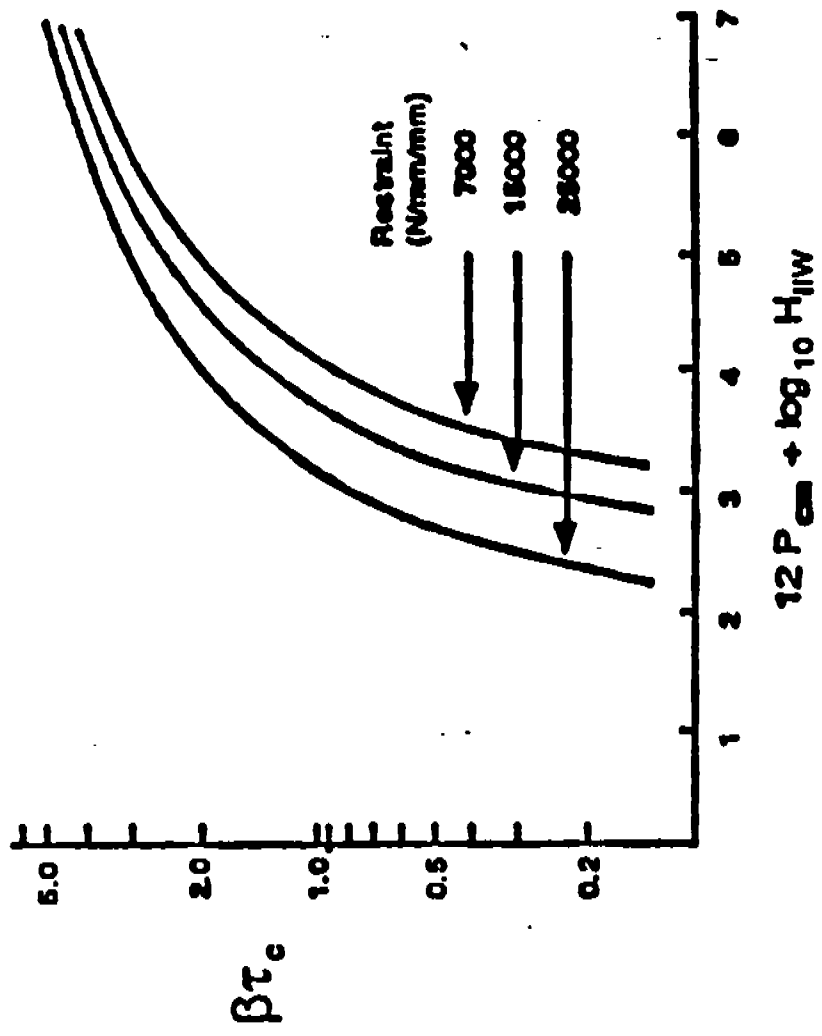
Fig.4.12. Determination of preheat temperature from βt parameter [68]

and hardness control is possible. Those in Zone III have higher hardenability and flat hardening curves for which hydrogen control is more appropriate.

Both the Hardness and Hydrogen Control approaches take into account all three parameters, namely chemistry, diffusible hydrogen content, and stress, to estimate the preheat temperature for crack-free welding. However, the degree of emphasis placed on different parameters is not the same. For example, in the hydrogen control approach greater emphasis is placed on hydrogen diffusion and restraint, while in the hardness control approach these two factors are not significantly represented and greater attention is paid to the microstructural factor by defining a critical HAZ hardness above which HAC can occur.

The suitability of these two approaches in estimating safe welding conditions for low carbon micro-alloyed steels has come into question, mainly because of the fact that these approaches are empirical in nature and data for "new" steels were not available for consideration and inclusion in developing formulae. Although these methods for assessing preheat temperature are based on data from a large number of steels of different types, the predicted conditions for safe welding of low carbon HSLA steels are more often overly conservative. The reason for this behavior is not readily apparent. However, one or more of the following factors may be responsible for the anomalous behavior;

(a) Inadequate characterization of hardenability by the existing carbon equivalents,

(b) Lower critical hardness above which cracking may occur than that for conventional steels (Fig. 4.8),

(c) The effect of austenite grain size on the hardenability of steels is not included, and

(d) The effect of non-metallic inclusions on the hardenability of "clean" steels is not rigorously defined.

In the literature there are no clear guidelines regarding the applicability of a particular approach for the low carbon micro-alloyed steels of Zone I. These steels show a flatter hardness vs cooling time behavior, as compared to the steels of Zone II, where the rate of change of hardness is rapid and the critical cooling rate determined will not vary appreciably with the hardness chosen so long as it is on the steep part of the curve. Graville recommends that for Zone II steels, the hardness approach is suitable but for Zone III steels with shallow hardness behavior, the hydrogen model will be optimum. However, when discussing the behavior of Zone I steels he states that "these steels have a fairly flat hardening curve and even the hardest microstructure that can be produced during welding is not very susceptible to cracking". He does not specifically suggest the use of the hydrogen approach for these steels but based on the hardness response it is implied that the hydrogen model will also be applicable for Zone I steels.

The hardness model has been in use for the last five decades and it has been successful in predicting the weldability of steels. Its applicability to low carbon HSLA steels cannot be ruled out mainly because- (a) long-standing successful use of this approach, and (b) the availability in recent years of more accurate maximum hardness predictive formulae (discussed in Section 3) upon which the method relies. It has now become possible to estimate the HAZ hardness with greater degree of confidence for a wide range of compositions because of the introduction of a number of predictive formulae.

86

4.1.7. Critical Stress Control Approach

The Critical Stress Control approach is based on the assumption that if the lower critical stress obtained in tests like implant cracking test is not exceeded in a welded structure, the chances of cracking associated with hydrogen embrittlement are greatly reduced. The laboratory tests are conducted as a function of heat input, preheat temperature, and diffusible hydrogen content. In case of the implant cracking test, generally a bead-on-plate geometry is used but some Japanese workers have also employed single and/or double V-groove welds to more closely simulate the actual conditions. Various predictive parameters from the cracking tests are related to the lower critical stress and predictive equations are derived by regression analysis. Several investigators have proposed relationships to calculate the lower critical stress in the implant cracking test. Some of these empirical equations are described in detail in Section 4.3.4.

4.2. EXPERIMENTAL PROCEDURES

All steels in this program were tested with respect to their resistance to the hydrogen assisted cracking employing three different methods namely; the Battelle Underbead Cracking Test, UT-Modified Hydrogen Sensitivity Test, and Implant Cracking Test.

4.2.1. Battelle Underbead Cracking Test:

This test, developed at Battelle, is a simple bead-on-plate test, and involves the deposition of a weld bead on a block of the test material, the dimensions of the block being 3" x 2" x 1" (Fig. 4.13). The weld bead is approximately 1 1/4" long and is usually deposited using a 1/8" E 6010 (high hydrogen) electrode. Low hydrogen electrodes can also be used. The welding parameters used are a current of approximately 100 amps. at 24 to 26 volts and a travel speed of 10 inches per minute. These parameters result in a heat input of approximately 15 kJ/in. The cooling rates attained in the coarse grained HAZ's of plain carbon steels with the use of this heat input are usually sufficient to enable the formation of martensite. Hydrogen is introduced into the weldment through the arc; the amount of hydrogen introduced can be low or high, depending on whether low or high hydrogen electrodes are used. The strain developed in this test is only that due to the self restraint of the block. After welding, the block is held at room temperature (70 to 75°F) for 24 hours to allow underbead cracks to develop. The block is then sectioned longitudinally, as shown in Fig. 4.13, to expose the cracks. The cut section is polished to 1 micron, etched and then examined metallographically to detect underbead and/or weld metal cracks. The extent of cracking is reported as the ratio of the sum of the length of the underbead cracks (overlapping cracks counted as one) to the length of the weld, expressed in percent.

No high hydrogen electrodes are commercially available at strengths above 90 ksi. Therefore, all steels were welded using E 8010 electrodes. This electrode has a cellulosic coating and its nominal composition approximately is: C - 0.14%, Mn - 0.45%, Si - 0.15%, Mo - 0.17%, Ni - 1.50%, P - 0.015%, S - 0.01%. The diffusible hydrogen content in the E 8010 weld deposit may lie in the range 40 to 60 ml/100g of deposited metal. The electrodes used were stored at 165°F and for each test a new electrode was employed. The HSLA-80-1 steel used for this investigation was available in 3/4" thickness and thus not within the size recommended for standard test conditions. The reduced thickness will result in slightly less self restraint and thus the results will be less conservative than the 1" thickness recommended. However, the difference is not great and

87

UNDERBEAD CRACKS

CUT SECTION

SMAW WELD

$1\frac{1}{4}"$

VOLTAGE   24-26v
CURRENT   100 amps
TRAVEL SPEED   10 ipm
ELECTRODE   E 8010 1/8"dia

R.D.

BATTELLE SAMPLE
3"x2"x1"
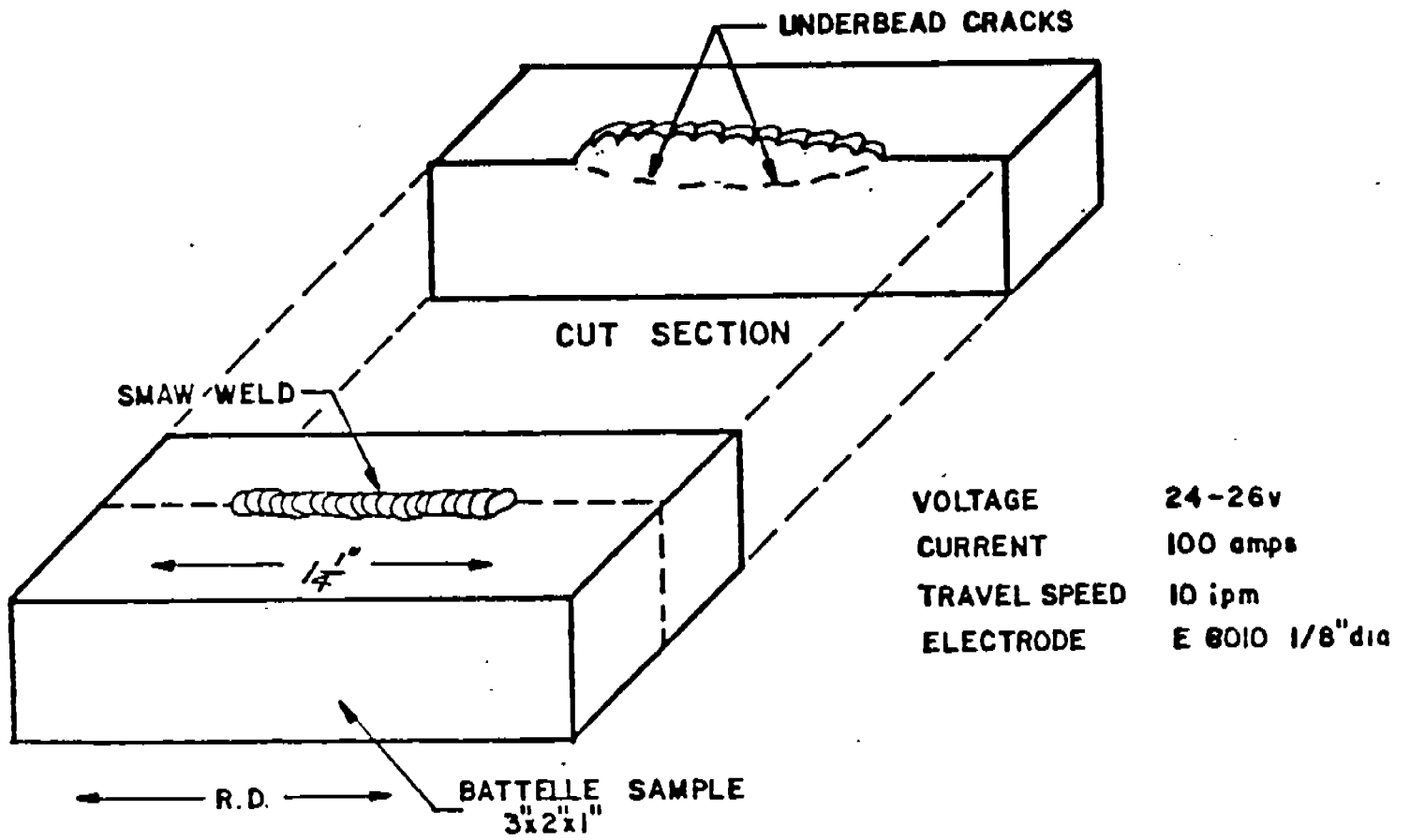
Fig.4.13. Schematic diagram of the Battelle underbead cracking test

88

Battelle UBC tests were conducted on 3/4" test block for HSLA-80-1, but for the remaining steels, the standard 1" test block thickness was employed.

4.2.2. UT-Modified Hydrogen Sensitivity Test:

The UT-Modified Hydrogen Sensitivity Test (UT-Mod. HST) has been employed to evaluate the hydrogen assisted cracking susceptibility of carbon and low alloy cast and wrought steels as well as Cr - Mo steels. The UT - Mod. HST is a variation of the RPI augmented strain test [69-71] and includes the following modifications:

(a) Reduced specimen size
(b) Autogenous GTA weld
(c) Hydrogen introduced directly into weld pool
(d) Materials evaluated on a pass - fail basis
(e) Effect of preheat, hold time and straining temperature determined
(f) Acoustic emission determination of crack initiation
(g) No cutting or polishing steps required for crack observation.

Fig. 4.14 shows a schematic sketch of the experimental details of the test. The specimen is held in a copper fixture which can be preheated to any desired temperature. An autogenous gas - tungsten arc (GTA) weld is made along the length of the sample employing the following parameters:

Current	90 amps
Voltage	10 volts
Travel Speed	5 in/min.
Shielding Gas	5 vol% H_2-Ar
Energy Input	11 kJ/in.

Hydrogen is added directly to the argon shielding gas (5 vol %) saturating the fusion zone. After welding the sample is allowed to cool to 90°F and then strained in the fixture shown in Fig. 4.14. The nominal augmented strain on the surface is given by the approximation:

$$e \cong t/2R$$

where e is the nominal augmented strain, t is the specimen thickness (0.125") and R is the bending radius. Die blocks are available to produce strain levels of 1, 2, and 4%. Susceptibility to cracking is determined by observing if cracks form on the specimen face strained in tension. Cracking can be evaluated as a function of preheat temperature, straining temperature, and strain level.

After straining, the specimen and fixture are placed in a padded vice and an acoustic emission (AE) sensor attached to the die block. The output of the AE instrument is recorded on a strip chart recorder. The time of crack initiation is the time at which sustained AE bursts above the background level are recorded. The presence of cracks are also verified by optical microscopic examination. If the specimen does not crack within 24 hours, the test is terminated. For any strain level the preheat temperature at which two of three tests remain crack-free is designated as the preheat required to prevent cracking.

The UT-Mod. HST is intended to provide a comparative relative ranking of the cold cracking sensitivity of steels based on nominal strain, hydrogen content, microstructure, preheat and welding conditions. Although the nominal strain levels employed in the sensitivity test have no direct correlation with actual measurable restraint encountered during welding, the 4% strain level is analogous to the restraint encountered when weld thick multipass joints while the lower strain levels (2 and 1%) are analogous to restraint produced during the welding of thinner joint sections.

89

Autogenous GTA weld

Specimen 1⅝ x ⅝ x ⅛

R.D
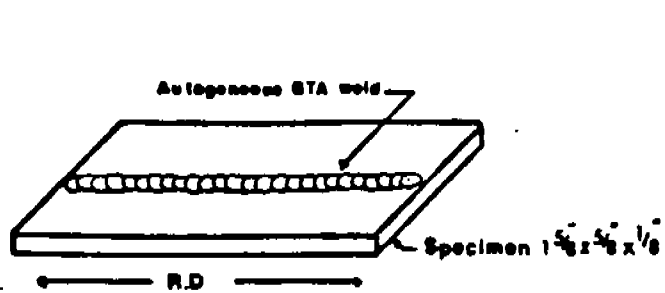
Current	80 - 100 amps
Voltage	10 v
Travel Speed	5 ipm
Shielding gas	5% H, 95% Ar, flow rate 30 CFH
Electrode	2% thoriated tungsten 1/16 dia.

UT– MODIFIED
HYDROGEN SUSCEPTIBILITY TEST
SPECIMEN

Specimen

Die Block

R
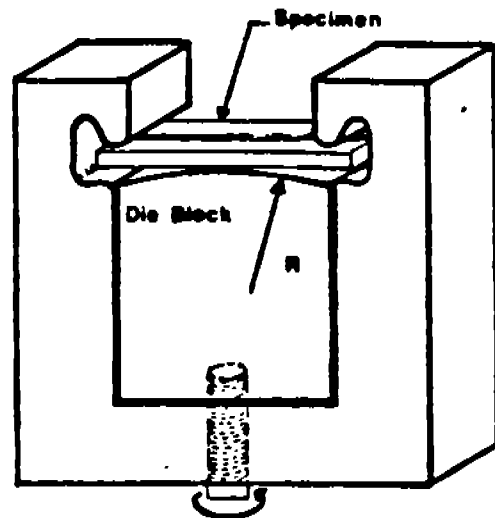
SCHEMATIC DIAGRAM OF
APPARATUS USED TO
STRAIN SPECIMEN

Fig.4.14. Schematic sketch of the experimental details of the UT-Modified hydrogen
sensitivity test

In the present study UT-Mod. HS tests were conducted at 4, and 2% strain levels and the preheat temperature was varied to obtain crack/no-crack behavior. Since no hydrogen assisted cracking was observed at 2% strain and 32°F preheat temperature for any of the steels, the results pertaining only to 4% strain are presented.

4.2.3. Implant Cracking Test:

The implant cracking tests were conducted for all the steels at two preheat temperatures and at two hydrogen levels. In order to determine the diffusible hydrogen content in the weld deposit the procedure outlined in the AWS A4.3 - 86 standard "Standard Method for Determination of the Diffusible Hydrogen Content of Martensitic, Bainitic, and Ferritic Weld Metal Produced by Arc Welding" was followed. The test specimen (from A 36 bar stock) dimensioned 3 1/8" x 1" x 1/2". The specimen is degassed at 500°C for one hour and the scale is removed by dry grinding. The sample is cleaned in acetone and weighed to the nearest 0.1g. The sample is then held in a pneumatic copper clamping fixture along with starting and run off tabs. Welding is carried out semi-automatically (SMAW using the modified submerged arc unit, Fig. 3.14). The arc is initiated on the starting weld tab at a point such that the leading edge of the deposit is approximately 1" from the leading edge of the test specimen. The welding is terminated on the run off weld tab at a position such that the trailing edge of the crater is on the run off tab but within 1" of the trailing edge of the test assembly.

After welding the weld test assembly is released from the copper clamping fixture and plunged into ice water within 5 sec. of extinguishing the arc. The weld test assembly is agitated vigorously in the ice water for 20 sec. and then quickly transferred to a liquid nitrogen bath. After about two minutes in the liquid nitrogen bath, the test assembly is removed from the bath and the tabs are broken by a hammer impact on the unwelded side. The test specimen is then once again immersed in the liquid nitrogen bath. For each condition four test assemblies are prepared. Before samples are loaded in the sampler for collecting diffusible hydrogen, the weld bead surface is cleaned with a wire brush to remove the surface scale. At any time during cleaning the test assembly is not allowed to remain out of the liquid nitrogen bath for more than one minute. If the cleaning is not complete within one minute, the weld test assembly is returned to the bath for at least two minutes before proceeding further with cleaning of the weld bead. After the samples are cleaned they are loaded into the sampler and the sample chambers are purged with high purity argon gas at 1.5 bar pressure for a minimum of 30 sec. Then the sampler is placed in an oven maintained at 45°C. Hydrogen is allowed to diffuse out of the weld assembly for 72 hours at 45°C. Then the diffusible hydrogen content is measured by gas chromatography. The gas chromatograph measures ml of hydrogen at standard temperature and pressure. After the gas analysis the samples are again weighed to the nearest 0.1 g. The diffusible hydrogen content in ml/100g of deposited metal is then calculated.

The diffusible hydrogen content in the weld metal was measured using electrodes in the (a) as-received (stored at 165°F), (b) baked (400°C/1h) and (c) exposed (to controlled humidity chamber) conditions. To increase the moisture content of the electrode coating and hence the amount of diffusible hydrogen in the weld metal, the electrodes were exposed to a humid environment. The relative humidity of the environment was controlled (80 % at 75°F) by maintaining a saturated solution of ammonium sulfate at the bottom of the

humidity chamber. Tests were conducted as a function of exposure time to the humid environment.

The implant specimens were extracted from the steel plates in a direction parallel to the rolling direction. Although no standard exists for implant geometry and testing procedure, the IIW guidelines were followed in this study [72]. An "I 65" (6 mm diameter, 0.5 mm deep notch) geometry was chosen to conduct the implant cracking tests. The implant sample (Fig. 4.15) with a helical notch at one end was inserted into a hole drilled in a support plate (12" x 8" x 1") so that the notched end was flush with the plate surface. In the present investigation support plates of A 515 steel were employed. The chemical composition of the support plate is:

C - 0.26%,   Mn - 0.70%, Si - 0.20%,   Ni - 0.15%,   Cr - 0.15%,
Cu - 0.11%, Mo - 0.02%, P - 0.016%,   S - 0.026%,   V - 0.003%,
Ti - 0.002%, Al - 0.002%, Cb - 0.001%, B - 0.0003%, N - 0.0072%

A 6" long weld bead was deposited on the plate surface in one pass under carefully controlled conditions, passing over the center of the implant. The welding parameters employed were:

Current	150 amps.
Voltage	25 volts
Travel speed	4.5 ipm
Electrode diameter	1/8"
Heat Input	50 kJ/in.
Preheat temp.	75 and 150°F

The width of the weld bead was such as to cover the implant adequately. After welding the implant assembly was allowed to cool for 5 minutes before applying the static tensile load. If fracture occurred within 24 hours, rupture time was noted. The maximum stress at which no rupture took place was taken as the lowest critical stress (LCS).

The length of the helical notch region in the implant sample (recommended in the IIW document) employed for the present study was increased from 1/2" to 1" so that each sample could be used twice. After the first test, 1/2" of the notched length was removed. Proper care was taken to avoid overheating of the sample during cutting operation. After cutting, the sample was degassed at 165°F for 24 hours before reusing. These procedures allow the retesting of material in its virgin form thus reducing test costs significantly. Other investigators have employed the reuse technique without any complications [73].

The implant cracking tests for HSLA-80-1, HSLA-80-2, HSLA-80M, and DQ-80 were conducted using E 11018 M electrodes. The two hydrogen levels in the weld metal were obtained by baking the as-received electrodes at 400°C/1h (5ml/100g diffusible hydrogen) and exposing the as-received electrodes to 80%/75°F for 230 hours to provide the higher hydrogen level (20 ml/100g). The higher strength steels such as HSLA-100, HSLA-130, HY-130, and DQ-125 were tested using E 14016 electrodes. In the as-received condition the weld deposit provided 5ml/100g diffusible hydrogen and after exposure to humid environment the maximum diffusible hydrogen level obtained was 10 ml/100g. In case of AC-50, the as-received electrode E 7018 gave a diffusible hydrogen level of 5ml/100g which did not increase further after exposure to humid environment. Therefore, it was decided to employ E 7010 electrode to provide a higher hydrogen content.

In order to determine the cooling time from 800 to 500°C in the CGHAZ, the thermal cycle for the welding parameters, plate thickness, and two preheat temperatures employed to carry out implant cracking tests were recorded during welding under implant test conditions by plunging the tip of a
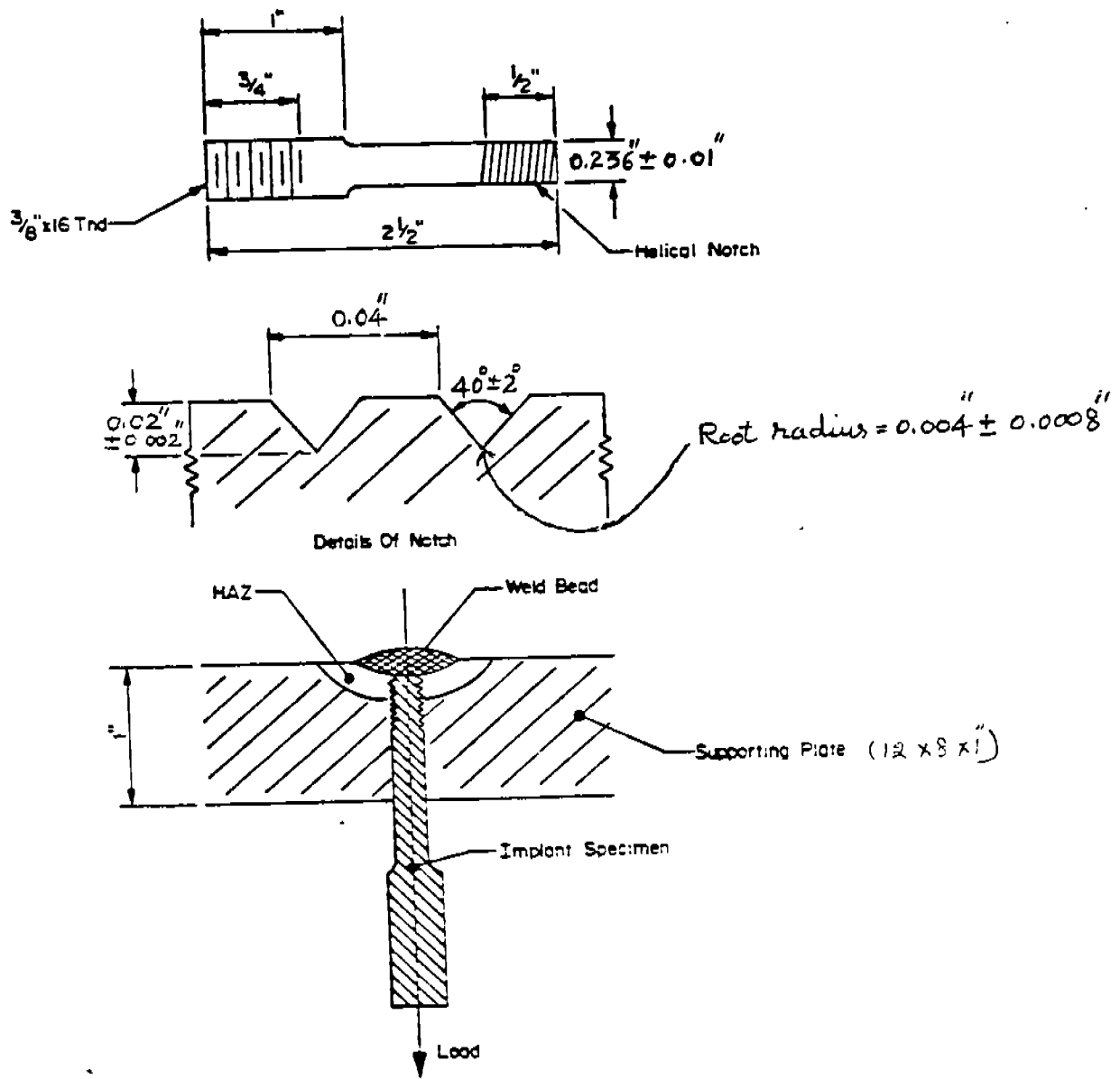
Fig.4.15. Geometry of the implant sample employed in this study

tungsten - 5% rhenium and tungsten - 26% rhenium thermocouple into the molten weld metal. The cooling time (800 to 500°C) in the weld deposit is very close to that in the CGHAZ near the plate surface.

For some of the implant samples that did not rupture in 24 hours, cross - sections along the length of the implant samples were examined and microhardness profiles across the HAZ were measured as a function of preheat temperature to determine the effect of preheat temperature on the HAZ softening and CGHAZ hardness. Mode of fracture in the tested samples was also studied using SEM.

In order to calculate the Susceptibility Index (SI) to rank the steels in this program, the notched tensile strength of the simulated CGHAZ was determined. The CGHAZ thermal cycle corresponding to 50 kJ/in. and a plate thickness of 1" (cooling time from 800 to 500°C = 7.5 sec.) was simulated in the Gleeble in 1/4" diameter specimens extracted in a direction parallel to the rolling direction. A tensile sample with a circular notch in the CGHAZ was then machined from the simulated sample. The tensile tests were carried out at a nominal strain rate of 4×10^{-4} s^{-1} at room temperature. The ultimate tensile strength thus obtained was referred as the notched tensile strength.

4.3. RESULTS AND DISCUSSION

In the following sections the results of the investigation to examine the susceptibility of steels to hydrogen assisted cracking by three methods (Battelle Underbead Cracking Test, UT-Modified Hydrogen Sensitivity Test and Implant Cracking Test) are discussed and the applicability of various published formulae to the implant test data evaluated.

4.3.1. Battelle Underbead Cracking Test

Results of the Battelle Underbead Cracking Test are listed in Table 4.2. As shown, majority of the cracks occurred in the weld deposit only and very few cracks were found in the HAZ's. The HAZ cracks were invariably associated with the weld metal cracks, indicating that the weld cracks propagated into the HAZ. Table 4.2 also provides qualitative information about the extent of cracking in the weld metal. The extent of cracking decreased when preheat temperature was increased. Increase in the preheat temperature may have a slight effect on the cooling time from 800 to 500°C but the time from 300 to 100°C is increased appreciably. The main effect of an increase in the cooling time between 300 to 100°C is to provide more time for the diffusible hydrogen to escape from the weld. For all tests conducted the same electrode type (E 8010) was used, and with preheat temperature required to obtain crack-free welds was different for different steels. This could be due to the fact that during welding the weld deposit becomes diluted with the base metal. Therefore, the observed preheat temperature is that for the resultant chemistry of the diluted weld deposit. A typical weld metal/HAZ crack is shown in Fig. 4.16. The predominant mode of cracking in the weld deposit was in the direction transverse to the weld axis, however, a few cracks were also observed in the longitudinal direction. The morphology of cracks suggests that cracking was not continuous but occurred in isolated locations along the weld and link-up occurred during the propagation stage. The HAZ cracks were transgranular in nature with a wavy tail and, in most of the cases, were associated with inclusions - either initiating or terminating at an inclusion or propagating along it. Thus it appears that the presence of inclusions probably assisted in the propagation of cracks by trapping diffusible hydrogen and acting as a stress concentration site. In the present set of steels, the inclusion distribution varies from steel to steel and the scope of this program did not

94

Table 4.2: Results of Battelle Underbead Cracking test

Preheat Temperature (^{0}F) Steel	32	85	130	180
HSLA-80-1	WM & HAZ (H)	WM & HAZ (M)	NC	*
HSLA-80-2	*	WM (M)	WM (L)	NC
HSLA-80-M	*	WM & HAZ (M)	WM (L)	NC
HSLA-100	*	WM & HAZ (M)	NC	*
HSLA-130	*	WM & HAZ (M)	WM (L)	NC
HY-130	*	WM (M)	WM (L)	NC
DQ-80	WM & HAZ (L)	NC	*	*
DQ-125	*	WM (L)	NC	*
AC-50	WM (L)	NC	*	*

* tests not conducted
WM: weld metal
HAZ: heat affected zone
NC: no cracks
H: high degree of cracking in the weld metal
M: medium degree of cracking in the weld metal
L: low degree of cracking in the weld metal
Note: The degree of cracking in the heat affected zones was always low, typically one or two cracks transverse to the fusion line were observed.

95

Fig.4.16. A typical weld metal/HAZ crack observed in the Battelle test. Steel
HSLA-80-2; 400X

include a detailed study of the shape, size, and distribution of inclusions and their potential influence on HAC susceptibility. Some investigators are of the opinion that the presence of non-metallic inclusions decreases the hardenability of steels by providing nucleation sites for ferrite and hence enhanced resistance to HAC. However, many other researchers have not found any effect of inclusions on hardenability. The difference between the two opposing viewpoints may lie in the interpretation of results. The effect of inclusions should be interpreted in terms of number of inclusions and not in terms of sulfur content as for the same sulfur level the inclusion density may be higher in the shape controlled steels as opposed to that in the conventional steels.

The presence of HAZ cracking in this study appears to be random. Not all cracks in the weld metal propagated in the CGHAZ. Most of the cracks terminated inside the weld deposit or at the fusion line. A steel was listed as cracked in the HAZ when at least two of three samples tested showed HAZ cracks. In steels like AC-50, DQ-125, HY-130, and HSLA-80-2, HAZ cracks were either not present or were found in only one sample of the three tested. Moreover, in samples designated as cracked in the HAZ, typically one or two cracks were observed.

The critical preheat temperature required to avoid cracking in the weldment is plotted in Figs. 4.17 to 4.19 as a function of P_{cm}, CE_I, and H_{max} respectively. The overall results do not show any correlation, however, if the data are categorized into two classes depending on tensile strength namely, lower strength (50 and 80 ksi) and higher strength (100 and 130 ksi), it is possible to draw straight lines indicating an increase in the critical preheat temperature with CE's and H_{max}. The CE's show good linear correlation with critical preheat temperature for the lower strength steels but correlate poorly for the higher strength steels. On the other hand when the Battelle test data are plotted as a function of H_{max}, both types of steel show good linear correlations. It is difficult to establish general predictive equations involving CE formulae, or H_{max}, or hydrogen content, and critical preheat temperature from the Battelle test data because (a) the tests were conducted at a fixed hydrogen level, (b) the weld beads were deposited using E 8010 electrodes irrespective of the base plate strength level, and (c) no true hydrogen assisted HAZ cracks were observed. However, since the weld deposit becomes diluted with the base metal chemistry, it should be possible to rank the steels based on the Battelle test results. Steels DQ-80 and AC-50 were the least susceptible to HAC. HSLA-80-2, HSLA-80M, HSLA-130, and HY-130 were most prone to cold cracking, whereas HSLA-80-1, DQ-125, and HSLA-100 susceptibilities were intermediate to these two extremes. For the steel HSLA-80-1, a sub-size sample was employed as the plate thickness was only 3/4" against standard requirement of 1" thickness. This would decrease the self-restraint in the weldment and is likely to give a lower critical preheat temperature.

In the standard Battelle test the bead is deposited using E 6010 electrode, but in the present study the tests were carried out with E 8010 in order to more nearly match the strength of the weld fusion zone to that of the base metal. However, the results indicate that the susceptibility of the weld fusion zone to HAC in all cases is higher than that of the base metal HAZ. Therefore, it was considered that by employing E 6010 electrodes the weld deposit cracking susceptibility would be reduced and cracking similar to the traditional underbead morphology might be obtained. Steel HSLA-80-2 was chosen to carry out the exploratory investigations as this steel (along with HSLA-80M, HY-130, and HSLA-80-1) showed the highest critical preheat temperature

97
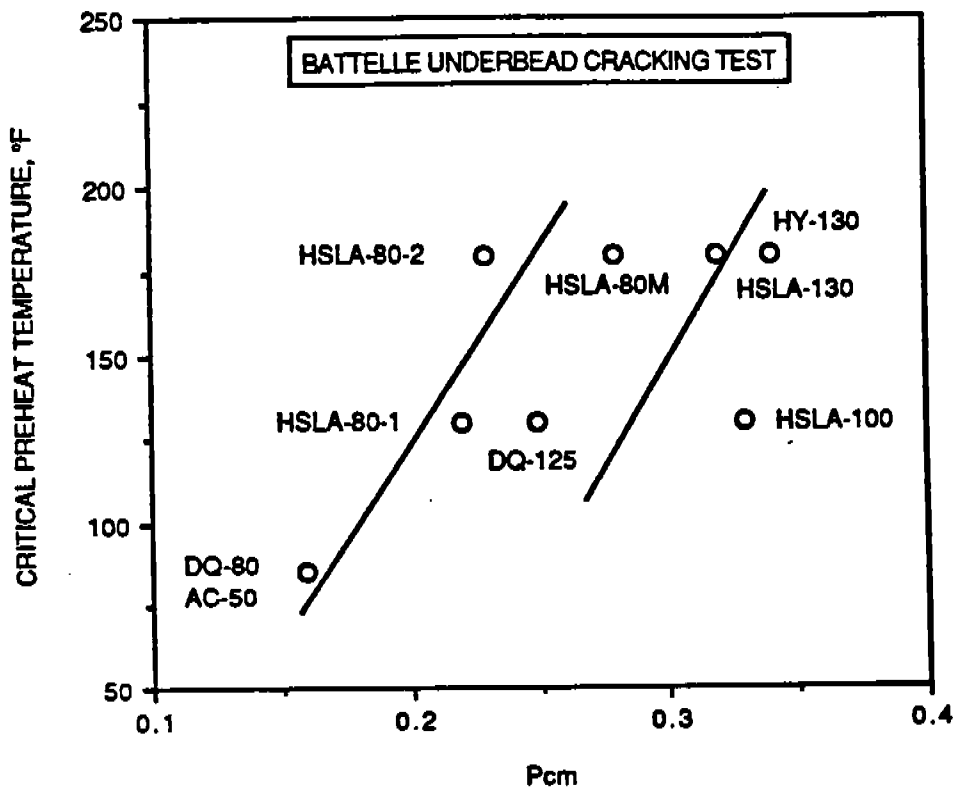
Fig.4.17. Variation of the critical preheat temperature with Pcm
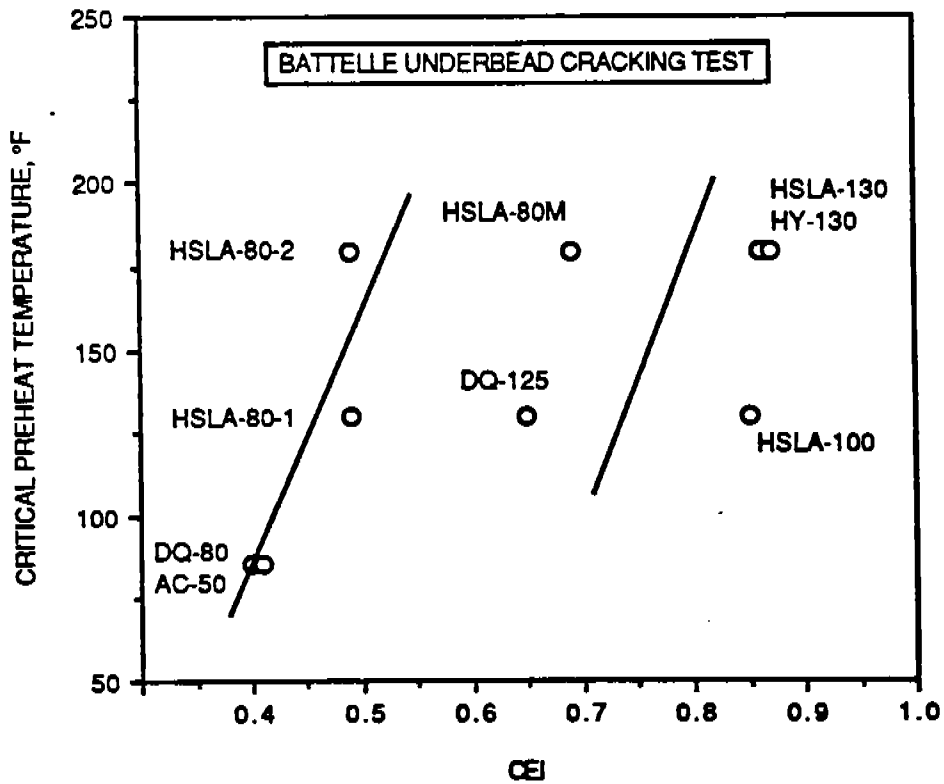
Fig.4.18. Variation of the critical preheat temperature with CE₁

98
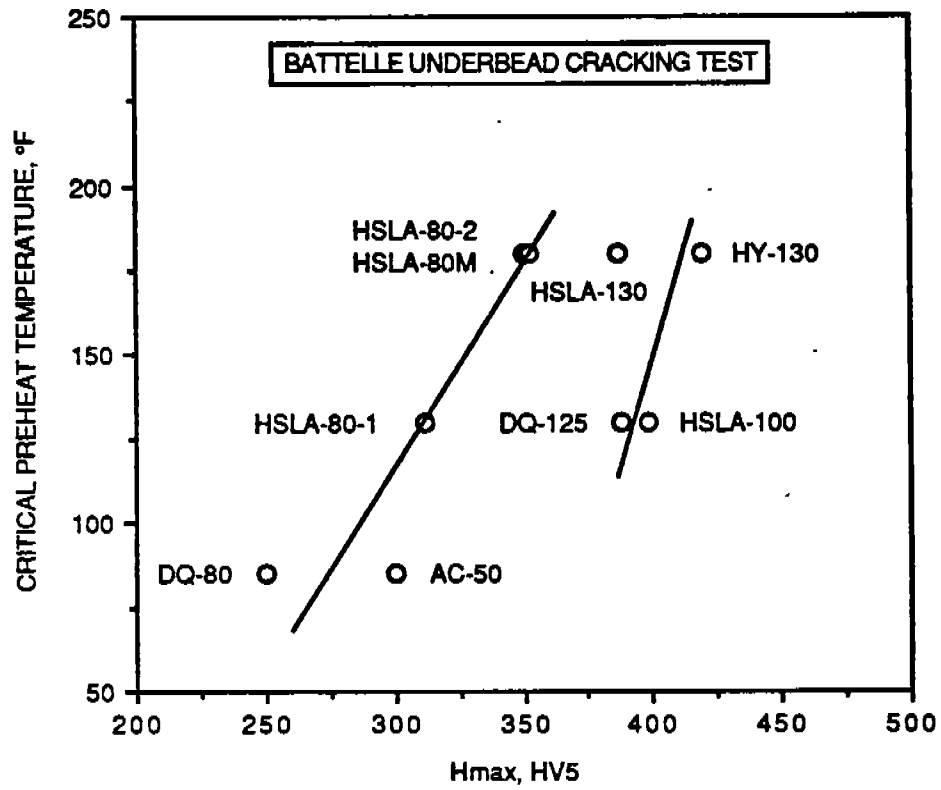
Fig.4.19. Variation of the critical preheat temperature with H_{max}

(180°F) among all steels, thus indicating that E 8010 weld deposit when diluted with the HSLA-80-2 chemistry becomes significantly prone to HAC.

Battelle tests were carried out under standard conditions using E 6010 electrodes. However, the crack location and morphology remained the same as that obtained when the E 8010 electrode was used. Fig. 4.20 shows a typical HAZ crack in a sample welded at 32°F preheat temperature. Several of the cracks in the weld metal propagated into the HAZ. The HAZ cracks were transgranular in nature and propagated in a direction transverse to the fusion line. The critical preheat temperature was found to be 130°F as contrast to 180°F when E 8010 electrodes were used. This is not surprising as the hardenability of the E 6010 deposit is expected to be considerably lower than that of the E 8010 deposit. This is also brought out clearly when the hardness of the weld deposit is compared. The E 8010 weld metal hardness was 428 HV5 as compared to 288 HV5 for the E 6010 deposit.

4.3.2. UT-Modified Hydrogen Sensitivity Test

None of the steels showed HAZ cracking when tested at 2% strain and a minimum preheat temperature of 32°F. Results of hydrogen sensitivity tests conducted at 4% strain on all nine steels are given in Table 4.3 and the variation in the critical preheat temperature as a function of P_{cm}, CE_I and H_{max} are shown in Figs. 4.20 to 4.22 respectively. No clear advantage was evident by using CE_I over P_{cm}. This could be due to the fact that the preheat temperature was generally varied in steps of 50°F and the data points are not sufficiently closely spaced to differentiate between any possible advantage in interpreting results by employing CE_I. However, it is possible to rank the different steels in terms of their susceptibility to HAC from this test. Steels AC-50, DQ-80, DQ-125, and HSLA-80M did not show HAZ cracking when tested at 4% strain and 32°F temperature and thus have the least susceptibility to HAC. Whereas steels like HSLA-80-1, and HSLA-80-2 were the most prone to cold cracking. HSLA-100, HSLA-130, and HY-130 showed an intermediate behavior between these two extremes. When the UT-Mod. HST data are plotted as a function of Hmax, a greater scatter was observed as compared to when CE's are considered.

In all the steels which showed cracking, intergranular cracks occurred only in the HAZ's and no cracks were observed in the weld fusion zone. Typical HAZ cracks (in HSLA-80-1 tested at 4% strain and at room temperature preheat) observed in the UT-Mod. HST are shown in Fig. 4.23

On comparing results from the Battelle UBCT and UT-Mod. HST, it is noted that there is a general agreement between these two tests if it is recognized that cracking in the Battelle test has occurred in the weld deposit as contrasted to that in the HAZ in the UT-Mod. test. The steels in this program can be ranked based on their susceptibility to HAC as below-

Battelle Test - Lower strength steels:
HSLA-80-2 = HSLA-80M > HSLA-80-1 > DQ-80 = AC-50
Battelle Test - Higher strength steels:
HSLA-130 = HY-130 > HSLA-100 = DQ-125
UT-Mod. Test - Lower strength steels:
HSLA-80-1 = HSLA-80-2 > DQ-80 = AC-50
UT-Mod. Test - Higher strength steels:
HSLA-100 > HSLA-130 = HY-130 > DQ-125 = HSLA-80M

Despite the obvious differences between the two tests, there is a remarkable similarity in ranking the steels. It appears that HSLA steels, in general, show more susceptibility to HAC as compared to steels such as DQ-80 and HY-130. This

Fig.4.20. A typical weld metal/HAZ crack in the Battelle test. Steel HSLA-80-2; Preheat temp. 32°F; E6010 electrode; 200X

Table 4.3: Results of UT-Modified hydrogen sensitivity test at 4% augumented strain

Preheat Temperature (^{o}F) Steel	32	75	100	120	150
HSLA-80-1	*	C	C	C	NC
HSLA-80-2	*	C	C	C	NC
HSLA-80-M	NC	NC	*	*	*
HSLA-100	*	C	NC	*	*
HSLA-130	C	NC	*	*	*
HY-130	C	NC	*	*	*
DQ-80	NC	NC	*	*	*
DQ-125	NC	NC	*	*	*
AC-50	NC	NC	*	*	*

* tests not conducted

C =cracks present in the heat affected zone

NC=no cracks present in either HAZ or weld metal

102
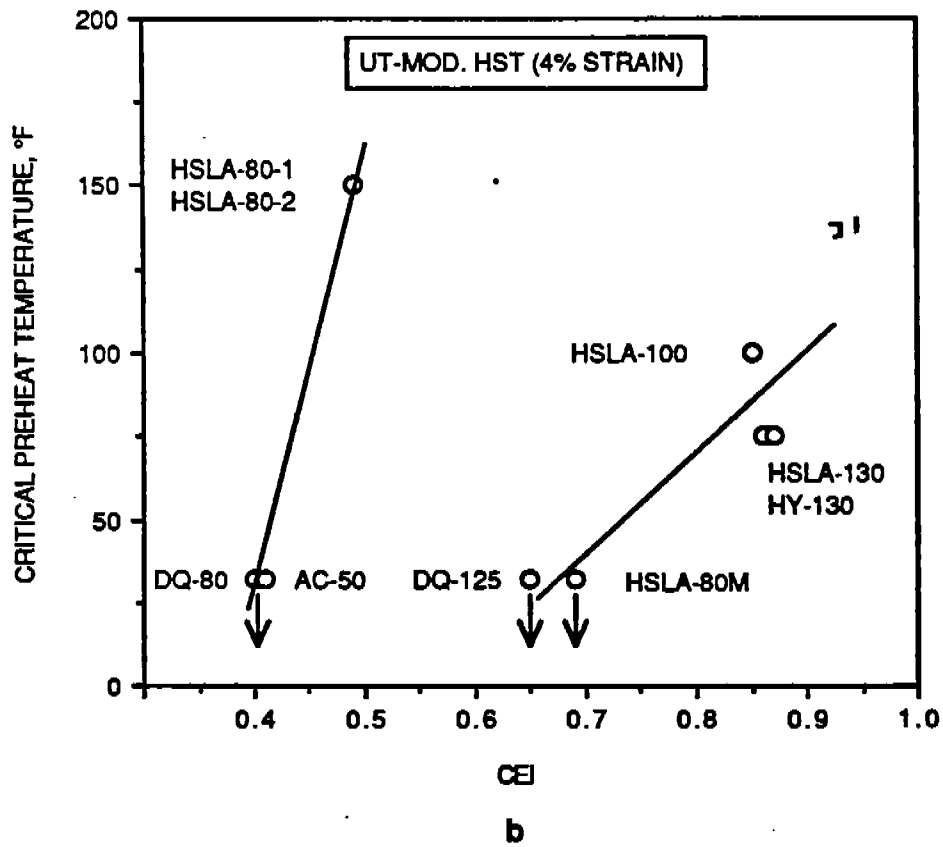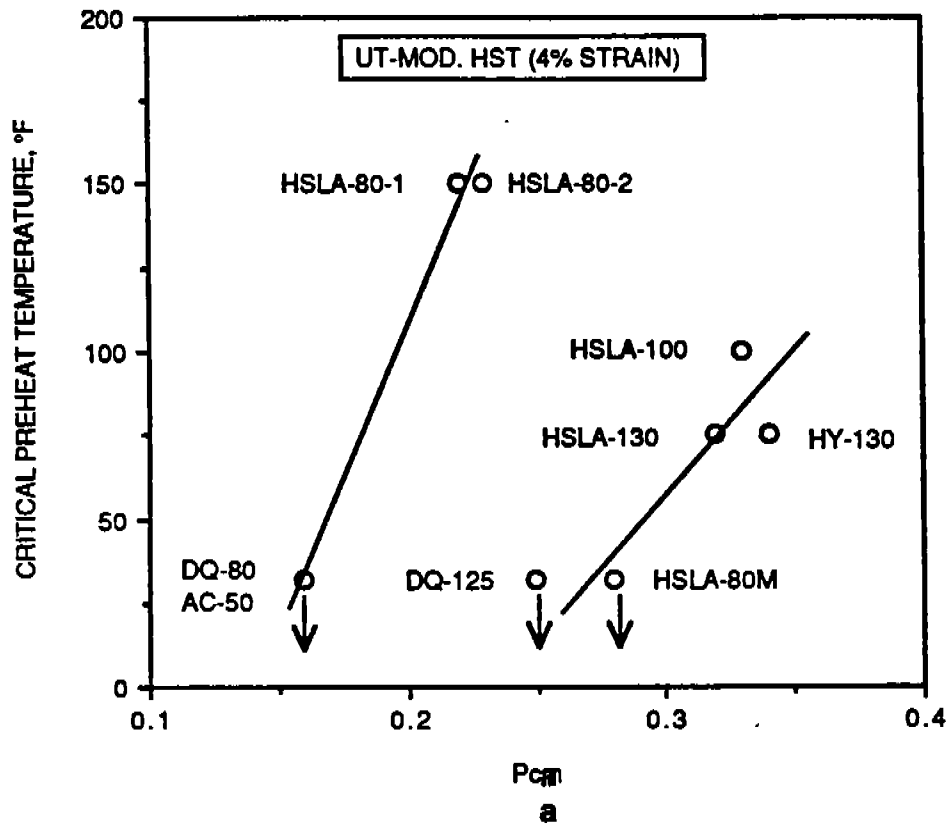
Fig.4.21. Variation of critical preheat temperature with (a)P_{cm} and (b)CE_I
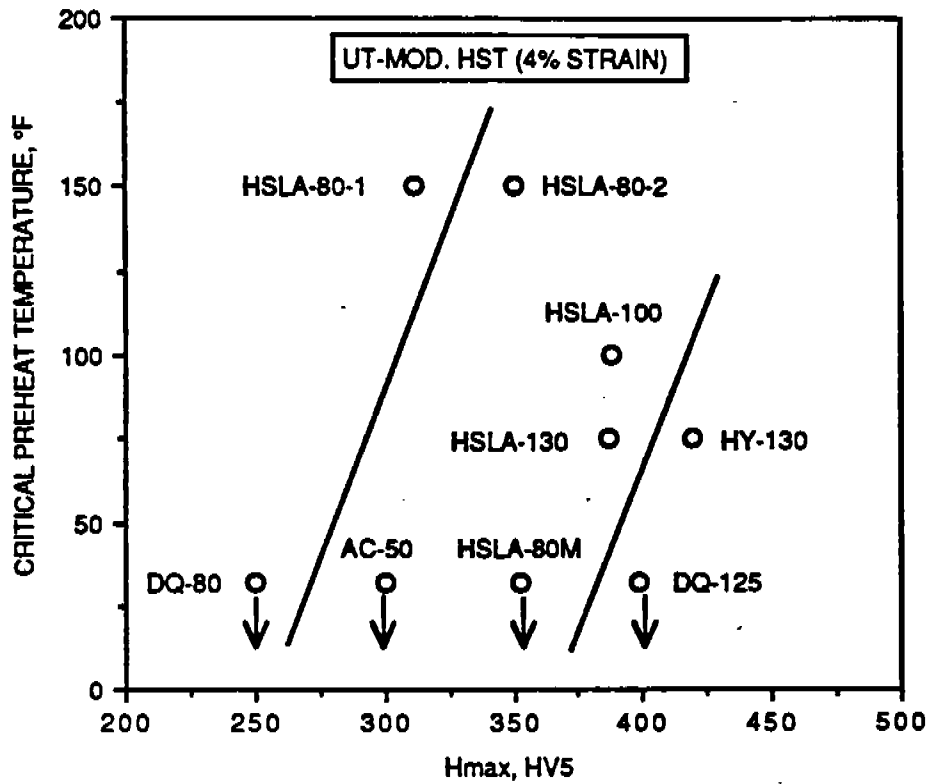
Fig.4.22. Variation of critical preheat temperature with H_{max}
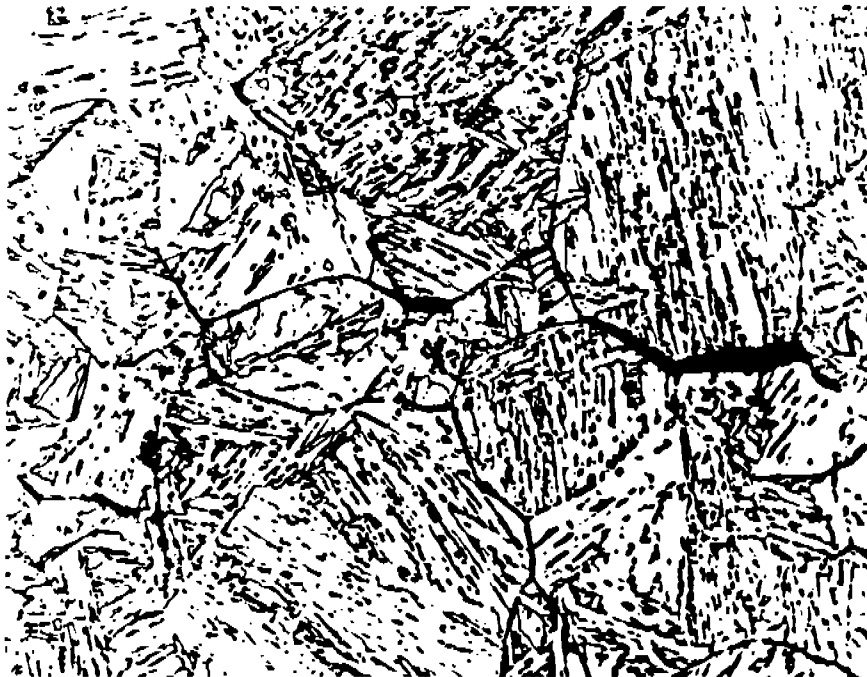
Fig.4.23. Typical HAZ cracks in HSLA-80-1 tested at 4% strain and 75°F preheat temperature; 1000X

trend in the ranking of materials is further discussed with regard to the Implant Cracking test data below.

4.3.3. Implant Cracking Test

The implant cracking tests for all the nine steels were conducted at two diffusible hydrogen contents and two preheat temperatures - 75 and 150°F. Two hydrogen levels chosen were 5 ml/100g and the higher level of hydrogen content was selected as the diffusible hydrogen content corresponding to a value obtained when the electrode coating was saturated with moisture picked up on exposure to 80% RH/75°F environment. The time of exposure to controlled humidity (for obtaining a hydrogen content value independent of exposure time) varied with the type of electrode coating. For example, the hydrogen content in the weld deposit made from exposed E 11018 M electrodes yielded about 20 ml/100g hydrogen after exposure for 230 hours and the diffusible hydrogen content increased only slightly for exposures beyond this time, but in E 14016 weld deposit the hydrogen content increased from 4.9 ml/100g (as-received condition) to about 10 ml/100g in 160 hours and there was no significant further increase in the diffusible hydrogen content for exposures greater than 160 hours. The E 7018 coating did not appear to pick up moisture on exposure to humid environment as the hydrogen content in the deposited weld beads increased only slightly from 4.5 ml/100g to 5.3 ml/100g after exposure for 240 hours. Figs. 4.24 and 4.25 illustrate the variation of diffusible hydrogen content with exposure time to controlled humidity environment for welds deposited by E 11018M, E 14016 and E 7018 electrodes respectively. Therefore, steels HSLA-80-1, HSLA-80-2, HSLA-80M, and DQ-80 were tested to determine their lower critical stress by implant cracking test using E 11018 M in two conditions - the lower hydrogen content, 5 ml/100g, was obtained by baking the as-received electrodes at 400°C/1h, and the higher hydrogen content, 20ml/100g, by exposing the electrodes to humid environment for 230 hours. The steels of the higher strength category - HSLA-100, HSLA-130, HY-130, and DQ-125 - were tested using E 14016 electrodes at two hydrogen levels (a) 5 ml/100g obtained in the as-received condition, and (b) 10 ml/100g obtained after exposure for 160 hours. Since the hydrogen content in the E 7018 weld deposits did not increase significantly even after exposure to high humidity for long durations, it was decided to employ E 7010 electrode to obtain higher hydrogen contents (in the range 40 to 60 ml/100g).

Results of implant testing for eight steels are shown in Figs. 4.26 to 4.33. Steel AC-50 did not rupture in the CGHAZ during the implant cracking test at low (4.5 ml/100g) as well as high (40 to 60 ml/100g) hydrogen contents but fracture occurred in the "soft" zone adjacent to the CGHAZ. The samples fracturing in the "soft" zone fail immediately when the stress reaches the fracture strength as contrasted to samples failing due to HAC. The failure in the "soft" zone occurred in tests carried out both at 75 and 150°F preheat temperatures. When the preheat was increased from 75 to 150°F, the stress to rupture in the "soft" zone decreased, thus indicating a further decrease in "soft" zone hardness at higher preheat temperatures. A typical sample that failed in the "soft" zone is shown in Fig. 4.34. The distance of fracture surface from the fusion boundary (about 5 mm) compares very well with the distance obtained between fusion boundary and the point of minimum HAZ hardness (4 mm) in a bead-on-plate weld corresponding to 45 kJ/in. (Section 5). The failure in the "soft" zone in preference to CGHAZ even at very high levels of hydrogen indicates the excellent resistance of AC-50 to HAC. This is also evident from its very low carbon equivalent ($P_{cm} = 0.16$, and $CE_I = 0.41$).
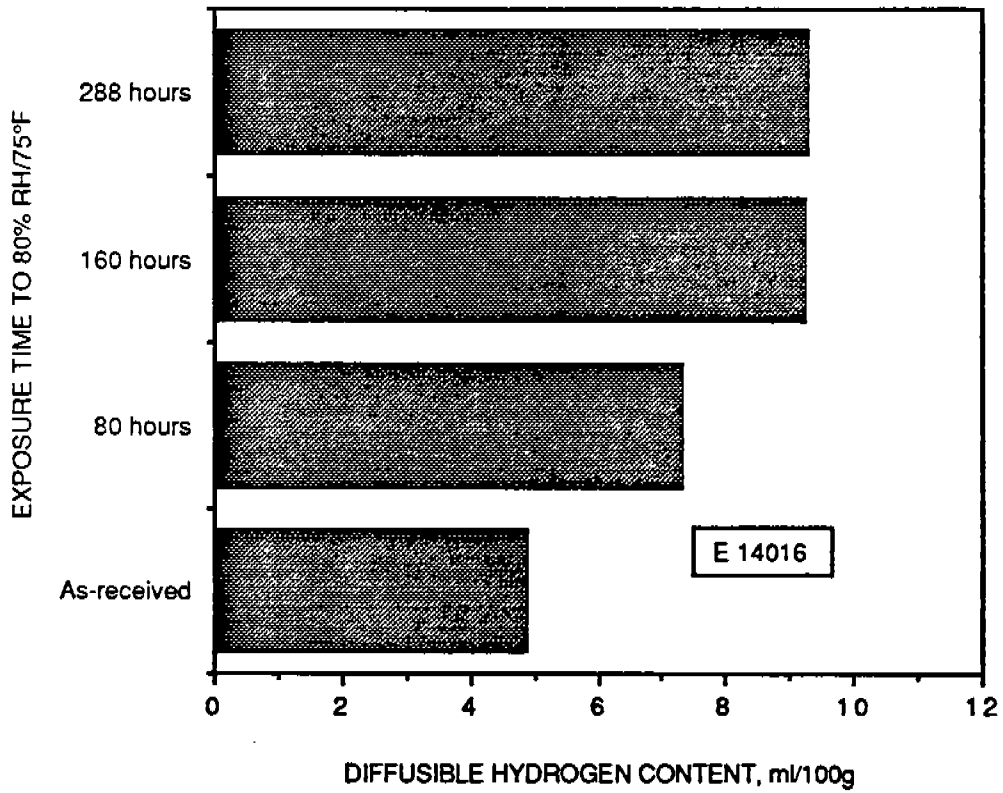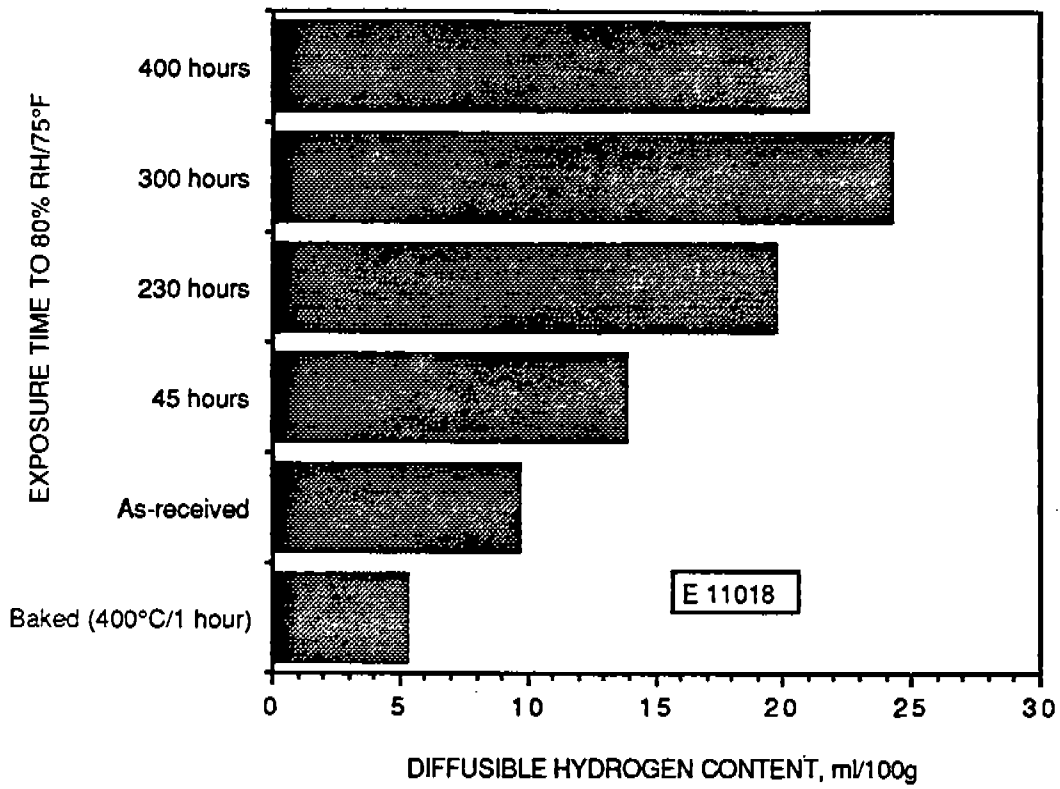
Fig.4.24. Increase in the diffusible hydrogen content with exposure time to controlled humidity environment for (a) E11018M and (b) E14016 electrodes

106
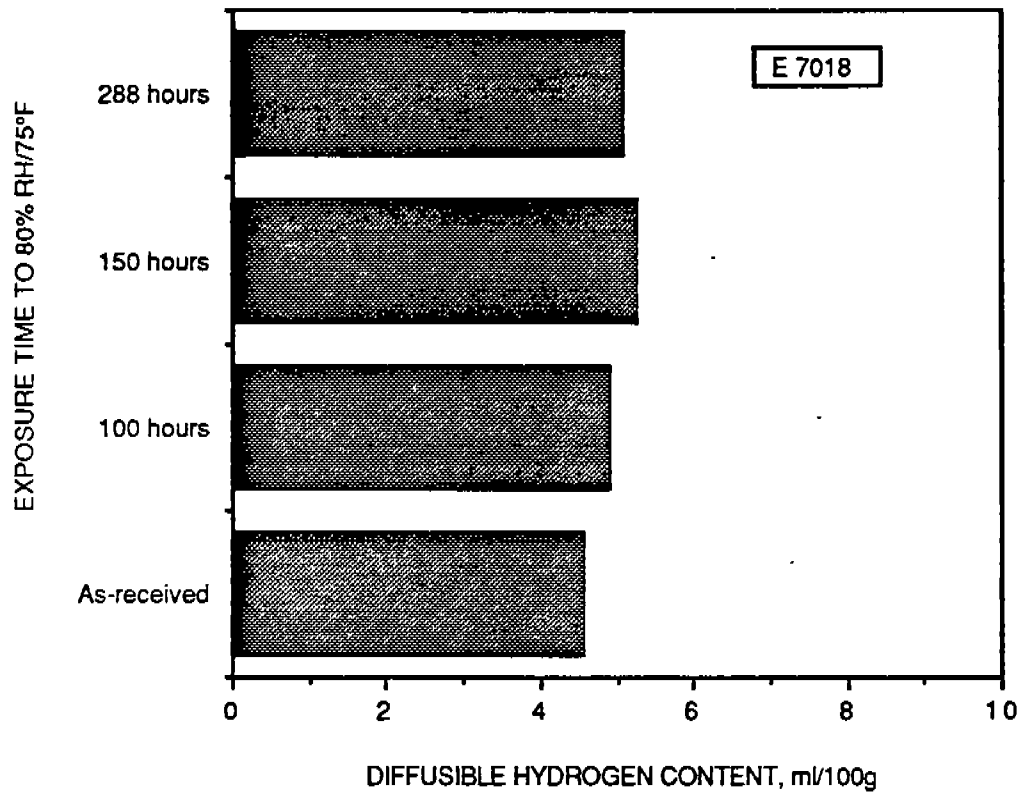
Fig.4.25. Increase in the diffusible hydrogen content with exposure time to controlled humidity environment for E7018
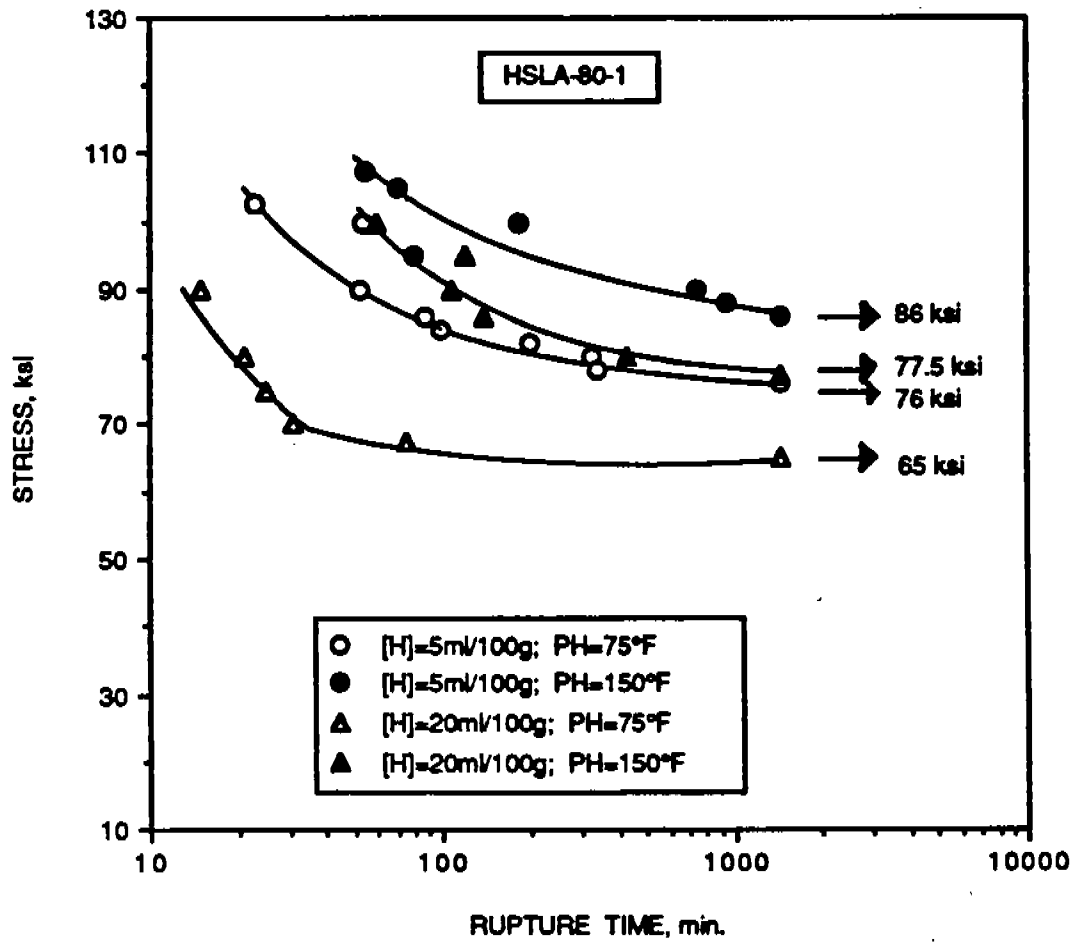
Fig.4.26. Implant cracking test results for HSLA-80-1
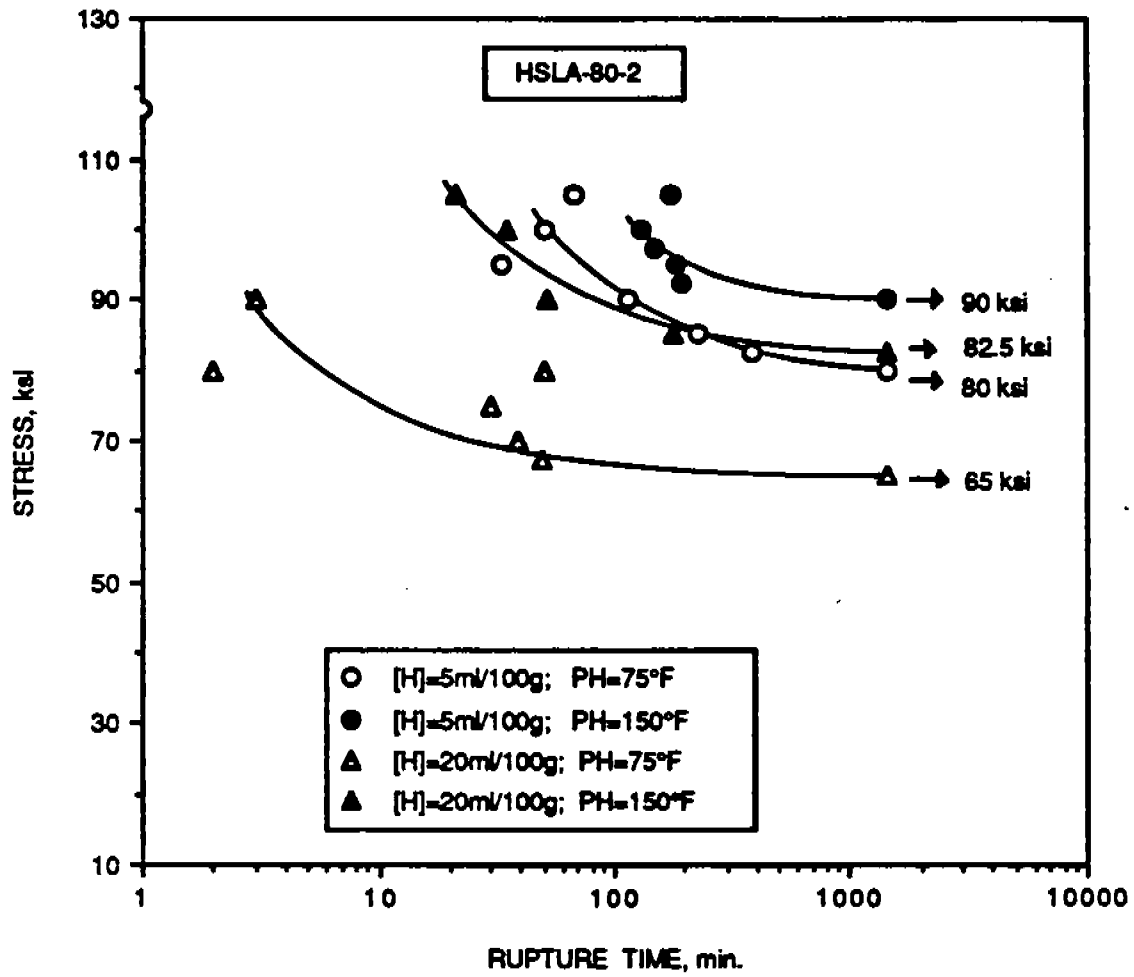
Fig.4.27. Implant cracking test results for HSLA-80-2
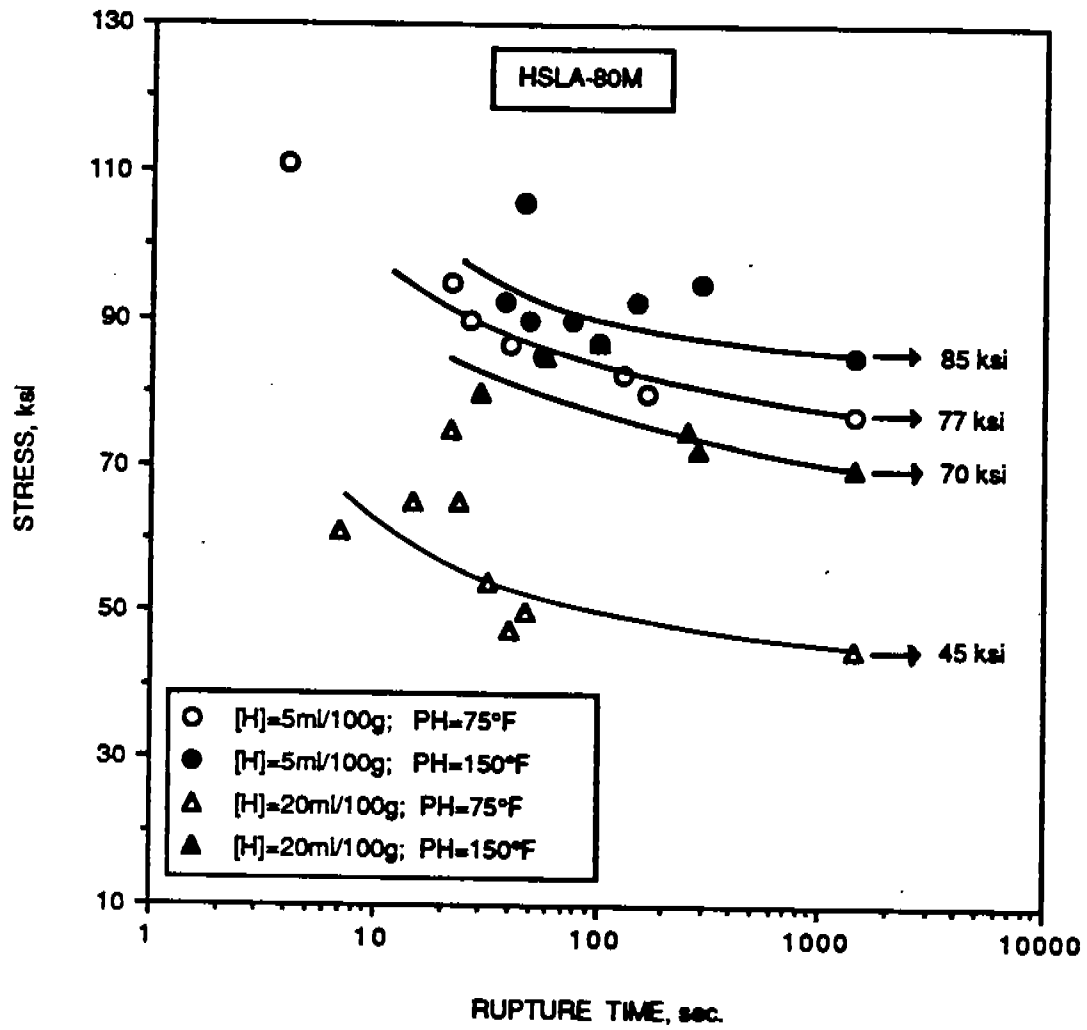
Fig.4.28. Implant cracking test results for HSLA-80M
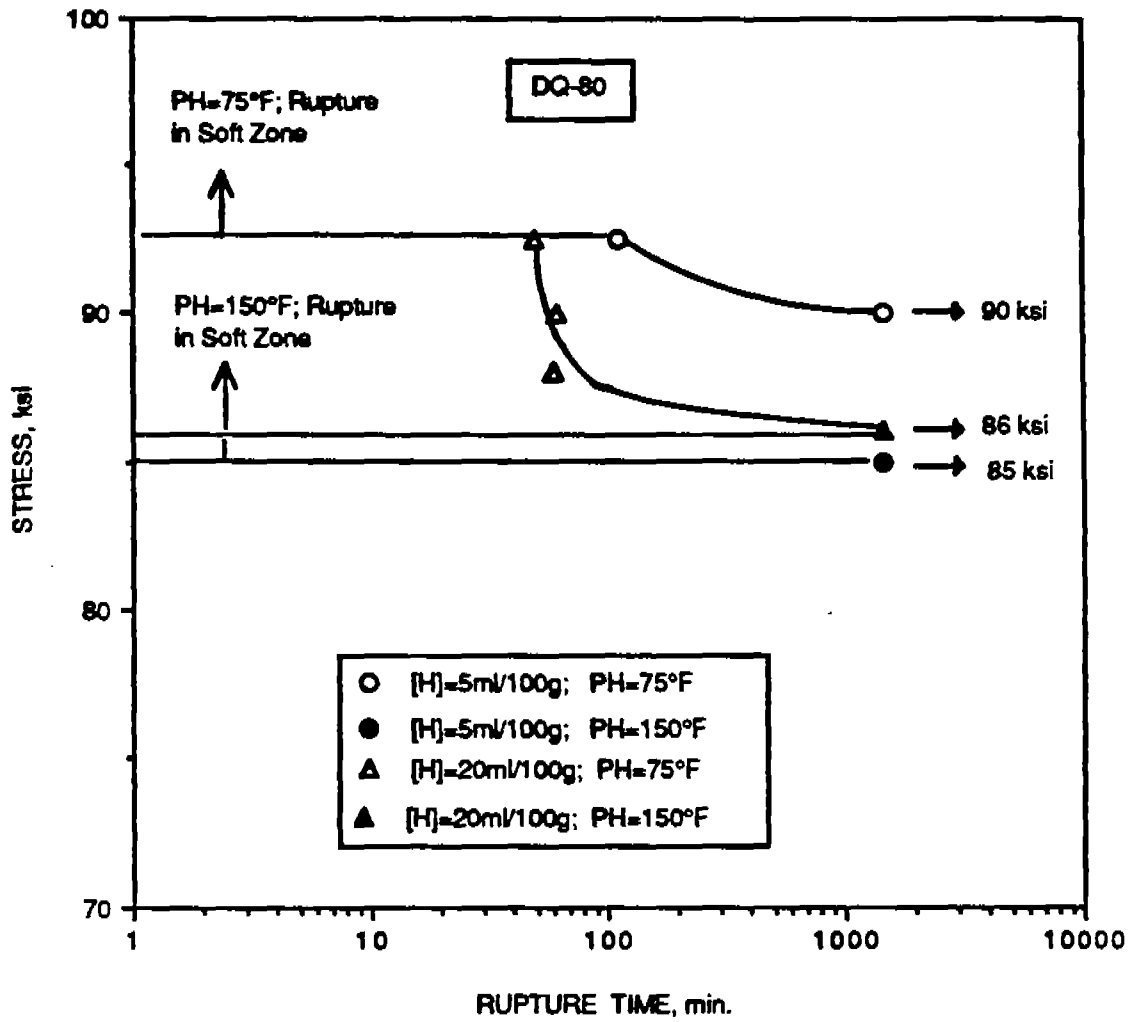
Fig.4.29. Implant cracking test results for DQ-80
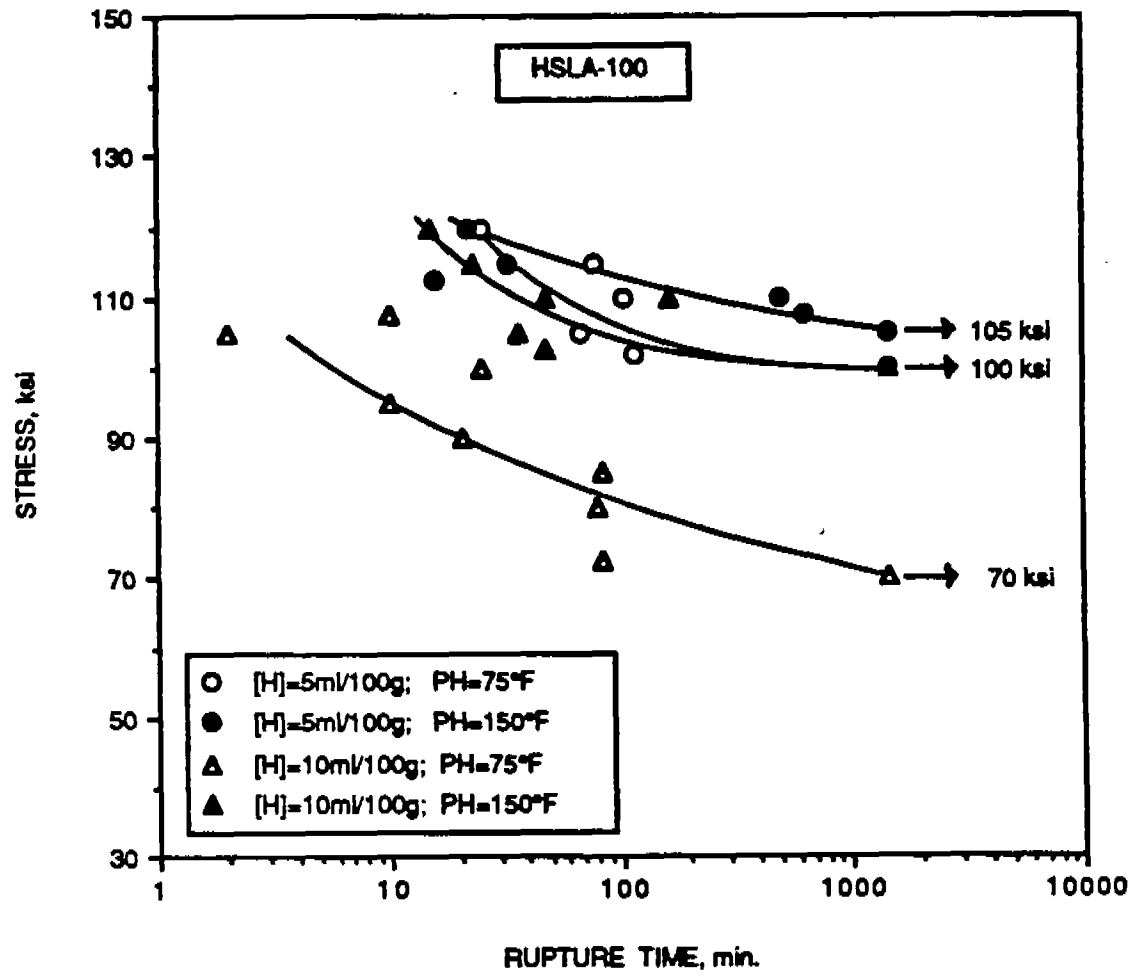
Fig.4.30. Implant cracking test results for HSLA-100
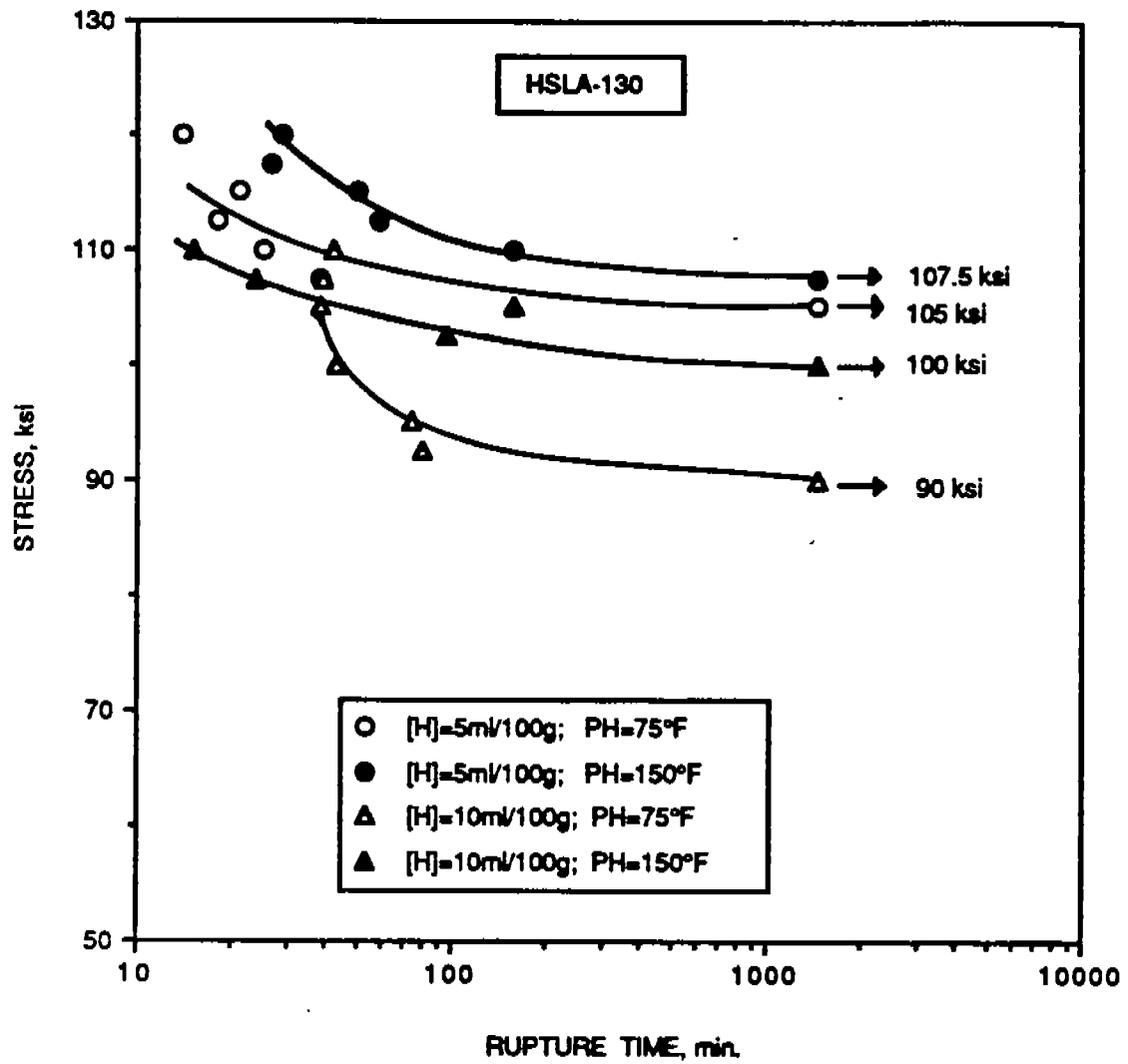
Fig.4.31. Implant cracking test results for HSLA-130
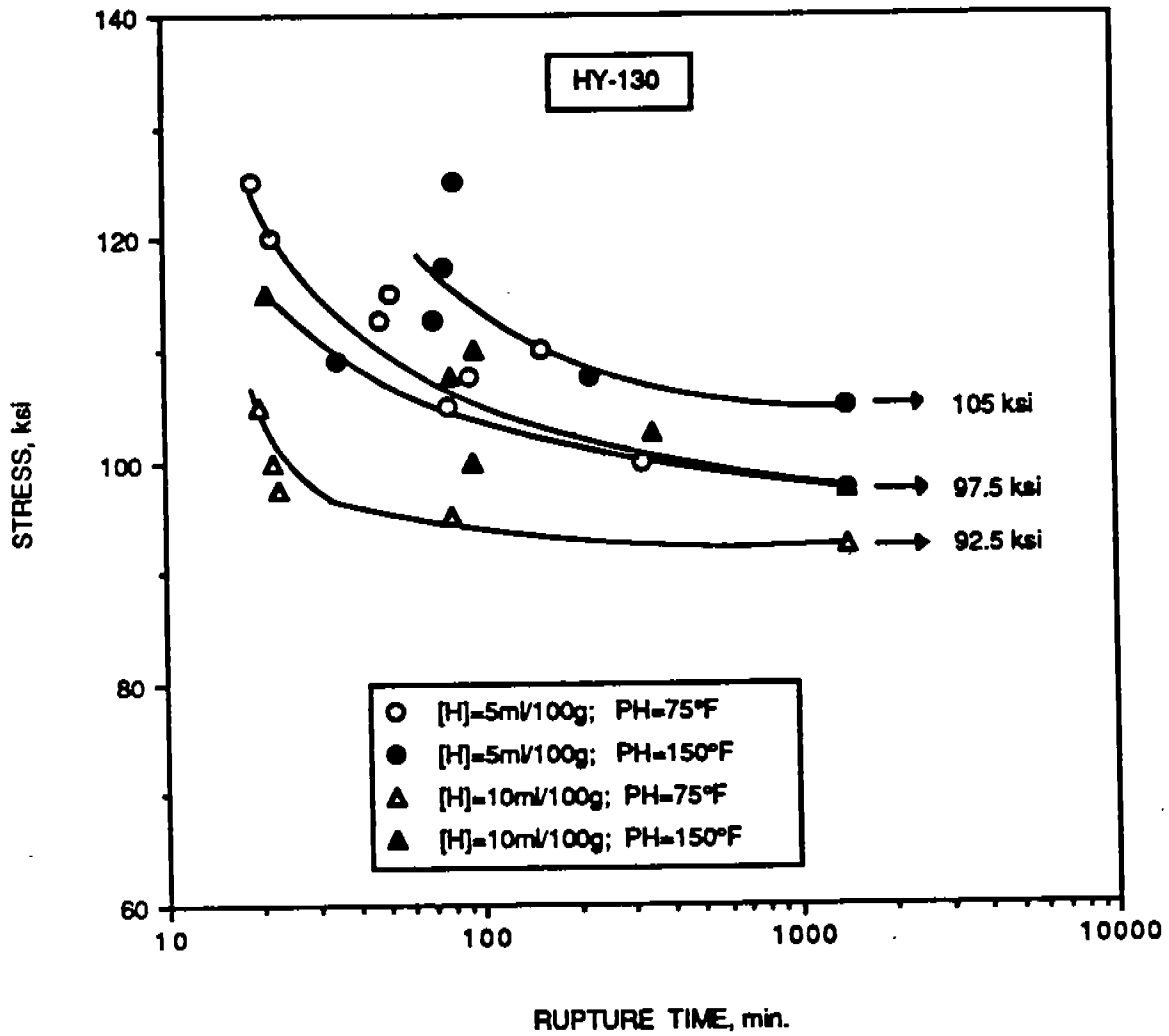
Fig.4.32. Implant cracking test results for HY-130
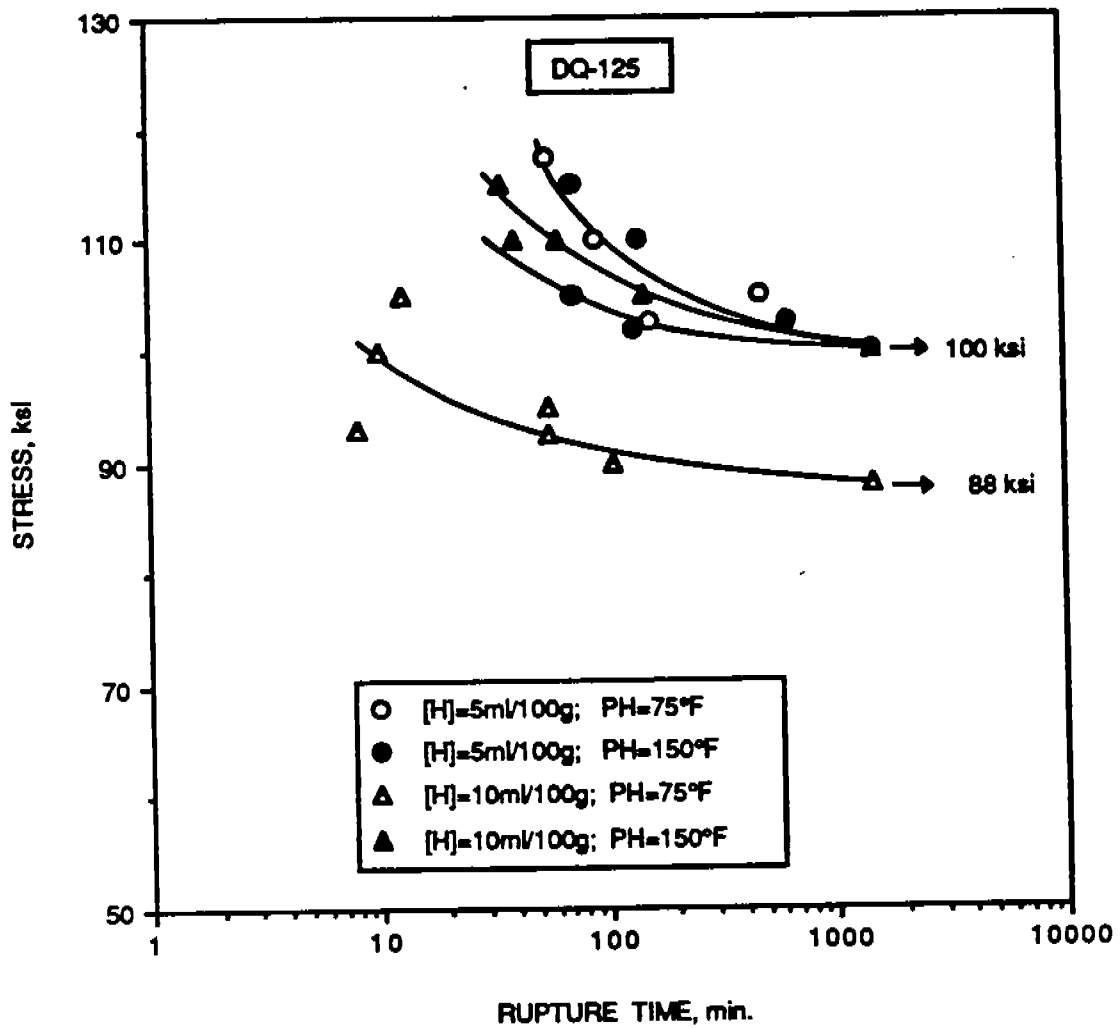
Fig.4.33. Implant cracking test results for DQ-125

Fig.4.34. Fracture of AC-50 in the "soft" zone; 6X

DQ-80 with very low CE (P_{cm} = 0.16 and CE_I = 0.40) behaved in a similar fashion. The stress vs. rupture time variation of DQ-80 is shown in Fig. 4.29. At 75°F preheat and 5 ml/100g hydrogen content, the rupture occurred in "soft" zone at a stress of 92.5 ksi, however, when the stress was decreased to 90 ksi the sample did not fail in 24 hour loading period. But at higher hydrogen level DQ-80 showed "true" HAC behavior. The lower critical stress at 75°F and 20 ml/100g was 86 ksi. When DQ-80 was tested at higher preheat temperatures (150°F), the samples failed in the "soft" zone at a considerably lower stress (86 ksi) as compared to that at 75°F preheat (92.5 ksi). This could be due to an increase in the extent of HAZ softening of samples welded at 150°F as compared to those welded at 75°F preheat temperature. The microhardness scan from the fusion boundary to the base metal in two actual implant samples that did not fail during implant testing, however, could not confirm the above assumption, as shown in Fig. 4.35. The HAZ hardness profile in a bead-on-plate weld (heat input-45 kJ/in) is also shown in the Figure for comparison. In the implant tested sample, the soft zone undergoes strain hardening during testing. That is why a decrease in hardness was not found in the samples after implant testing.

The above results clearly show that in modern TMCP steels which have enhanced resistance to hydrogen assisted cracking in the CGHAZ, the "soft" zone strength may become a critical factor to be given due consideration by the design engineers.

The HSLA-80-1, HSLA-80-2, and HSLA-80M steels, like DQ-80, fall in the 80 ksi strength category and are strengthened by copper precipitation, but unlike DQ-80, they have higher carbon equivalents because of the presence of higher carbon contents. The implant cracking test results for these steels are presented in Figs. 4.26 to 4.28. As expected the LCS decreases when the hydrogen content is increased and the effect of increasing the preheat temperature is to elevate the LCS by increasing the time from 300 to 100°C during the welding thermal cycle and thus providing more time for hydrogen to diffuse out of the weld. The behavior of HSLA-80-1 and HSLA-80-2 is virtually similar in terms of a drop in LCS with an increase in the hydrogen content and an increase in LCS with an increase in preheat temperature. When the hydrogen is increased from 5 to 20 ml/100g at 75°F preheat, the LCS drops from 76 to 65 ksi and 80 to 65 ksi for HSLA-80-1 and HSLA-80-2 respectively. However, there was a significant reduction (77 to 45 ksi) in LCS under the same conditions for HSLA-80M. The loss in LCS at high hydrogen levels is fully recovered when preheat temperature is increased in HSLA-80-1 and HSLA-80-2, but in HSLA-80M the recovery is less complete. The reason for a sharp decrease in the LCS in HSLA-80M could be; (a) the presence of a fully martensitic (estimated % martensite - 100%) structure in the CGHAZ as contrasted to a lower fraction of martensite in both HSLA-80-1 (55%) and HSLA-80-2 (57%), and (b) the differences in the maximum HAZ hardness, e.g. In HSLA-80-1 and HSLA-80-2 H_{max} values are 276 and 312 HV5 respectively, while in HSLA-80M it is 340 HV5. Evans and Christensen [74] and Pavaskar and Kirkaldy [75] in their study on low carbon micro-alloyed steels have shown that in modern steels with reduced carbon equivalents, hardness and /or carbon content are insufficient parameters to describe the susceptibility to HAC. They found that a parameter involving a linear combination of hardness and percentage martensite provided good correlation between the predicted and experimental LCS values. This aspect will be discussed in more detail in the next section.

The results of the implant cracking tests for the higher strength level steels such as HSLA-100, HSLA-130, HY-130 and DQ-125 are illustrated in Figs.

117
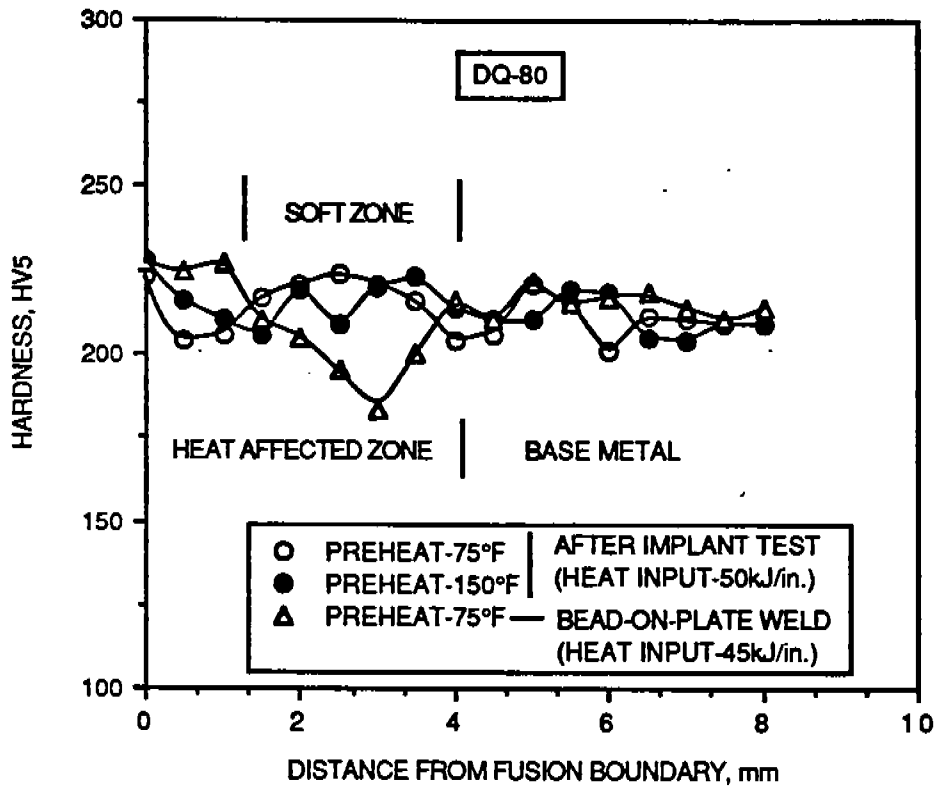
Fig.4.35. HAZ hardness profile in the as-welded bead-on-plate sample and implant samples after testing at 75 and 150°F preheat temperature

4.30 to 4.33 respectively. The carbon equivalent of DQ-125 is the lowest among the steels of this category, while for the other steels the CE lies in a very narrow range. Most of the implant cracking test results of HSLA-100, HSLA-130, and HY-130 are almost identical if normal scatter in implant testing is considered except that a low LCS value for HSLA-100 is obtained when tested at 75°F and 10 ml/100g hydrogen. This difference becomes more obvious when the results from HSLA-130 steel under the same testing conditions are compared. In general, the LCS values for HSLA-130 are higher than HSLA-100. This may be because of the following factors:

(a) HSLA-100 and HSLA-130 have identical chemical composition, but their rolling schedules and aging treatments are different. The presence of a fine initial grain size in the as-received plate should provide a smaller prior austenite grain size in the CGHAZ and thus more grain boundary area where the number of ferrite nucleation sites will be greater. This will decrease the hardenability and thus increase the resistance to HAC. Boron is known to have strong influence on the hardenability of steels. It segregates to the grain boundaries and blocks the sites for ferrite nucleation thereby increasing the hardenability. The boron content in HSLA-100 and HSLA-130 is 4 and 5 ppm respectively (Table 2.2). But due to increased grain size area in the CGHAZ of HSLA-130 the boron concentration per unit grain boundary area may be less as compared to that in HSLA-100 steel and therefore the hardenability of HSLA-130 is expected to be lower than that of HSLA-100.

(b) Although no quantitative analysis was carried out for the distribution of non-metallic inclusions in these steels, the comparison of Figs. A-13(a) and A-17(a) shows that in HSLA-130 the density of inclusions is higher than that in HSLA-100. Therefore, the hardenability of HSLA-130 will be reduced further due to the presence of a higher number density of inclusions which also act as nucleating sites for non-martensitic transformation. The influence of decreased hardenability in HSLA-130 when compared to HSLA-100 is evident in their HAZ hardness responses (Figs. 3.24 and 3.25). The hardness vs cooling time curve of HSLA-130 is slightly lower than that of HSLA-100 for all cooling times.

(c) It is known that the epsilon-copper precipitates do not dissolve completely during a thermal cycle experienced in the CGHAZ [76]. The extent of resolution of copper precipitates, of course, will depend on the energy input and the particle size. The higher the energy input the more will be the extent of precipitate resolution. And if the precipitates are "coarser", a longer time will be needed to completely dissolve them. Since the composition of both HSLA-100 and HSLA-130 is almost the same, and the higher strength in HSLA-130 is achieved because of finer grain size and probably a different aging treatment to exploit maximum strengthening due to copper precipitation. The copper precipitates in HSLA-130, therefore, should be smaller in size than in HSLA-100. Under a similar CGHAZ thermal cycle (as experienced during the implant cracking test) the dissolution of copper precipitates should be comparatively more complete in HSLA-130 as contrasted to that in HSLA-100. By the above argument, the diffusion of hydrogen in HSLA-100 steel should be retarded due to the presence of partly dissolved copper precipitates, and hence at any given time there should be a greater amount of diffusible hydrogen in the CGHAZ of HSLA-100 than that in HSLA-130. This increased amount of hydrogen will result in a lower LCS value. There is some evidence recently provided by Losz and Challenger [77] which shows the presence of discrete pockets of retained austenite in the CGHAZ of HSLA-100. The austenite is believed to be retained in the region where the dissolving copper precipitates enrich the surrounding area in copper. The number and/or size of such

119

packets of retained austenite should be smaller in HSLA-130, because of the presence of the very fine copper precipitate as compared that in HSLA-100. As is well known, the diffusivity of hydrogen is lower and the hydrogen solubility higher in austenite as contrasted to that in ferrite, therefore, the austenite regions may act as barriers to hydrogen diffusion. The net effect of the above two factors either acting individually or in concert will be to provide a higher amount of diffusible hydrogen in the CGHAZ of HSLA-100.

Therefore, a combination of factors such as reduced hardenability in HSLA-130 and the presence of higher amounts of diffusible hydrogen in HSLA-100 CGHAZ may be responsible for the observed implant cracking results. The difference in the hardenability between the two steels is clearly evident in the hardness responses but a detailed study to quantify the microstructural changes taking place in the CGHAZ is required for complete understanding of the phenomenon. It is also very important to observe the extent of copper precipitate dissolution during high temperature excursions in the heat affected zone as a function of initial particle size, and the effect of these undissolved precipitates on hydrogen diffusion. The information derived from such an investigation may lead to a better understanding of the underlying mechanisms and may provide guidelines for an optimum thermomechanical treatment to further enhance the resistance of copper containing steels to HAC.

The fracture surface and cross-sections of the implant tested samples were examined to determine the mode of fracture and the location of crack initiation and propagation. Fig. 4.36 shows a cross-section of an HSLA-80-2 sample tested at 95 ksi and 75°F preheat with 5ml/100g hydrogen content. It is noticed that the cracking initiated in the CGHAZ but propagated into the weld metal. A portion of the weld metal where the implant sample was positioned appears to have ruptured. This type of crack propagation was also observed in all the samples tested except HSLA-80M where the failure was confined mainly to the CGHAZ. An optical micrograph of the cross-section of an HSLA-80-2 sample tested at 80 ksi (5ml/100g hydrogen) for 24 hours is shown in Fig. 4.37. This sample did not rupture under the standard conditions but a long crack was observed traversing the CGHAZ and weld metal. The crack was transgranular in the CGHAZ but the mode and morphology of the crack in the weld metal were similar to that observed in the Battelle test. The fractographic examination of the fractured surface of a sample tested at 82.5 ksi is shown in Fig. 4.38. The hydrogen embrittled region in the CGHAZ has failed in a quasi-cleavage mode. However, the failure in the region away from the CGHAZ took place by the microvoid coalescence mechanism.(Fig. 4.39).

Since the cracks in the implant test propagated through the weld metal after having initiated in the CGHAZ, there was a concern about the possible enhancement of cold cracking susceptibility of the weld metal by dilution from the support plate. This aspect was further examined by calculating the weld metal dilution from the support plate and implant sample. This is illustrated for HSLA-80-2 steel. The chemical compositions and carbon equivalents, CE(IIW), of E 11018M, A 515 (support plate) and diluted weld metal are given below. The chemical composition and CE(IIW) for HSLA-80-2 are provided respectively in Tables 2.1 and 2.3.

E 11018M:
C-0.05%, Mn-1.62%, Si-0.04%, Cr-0.21%, Mo-0.32%, Ni-1.85%, V-0.011%
CE(IIW)-0.55
A 515:
C-0.27%, Mn-0.70%, Si-0.20%, Cr-0.15%, Mo-0.02%, Ni-0.15%, V-0.003%,
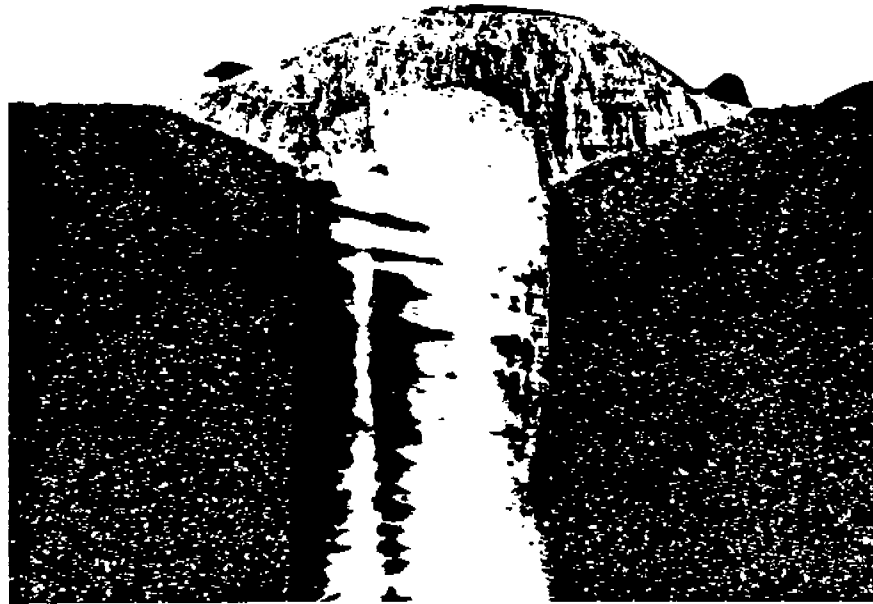
Fig.4.36. Cross-sectional view of an implant sample after rupture; HSLA-80-2; Stress-95ksi; Preheat temp. 75°F; 5X
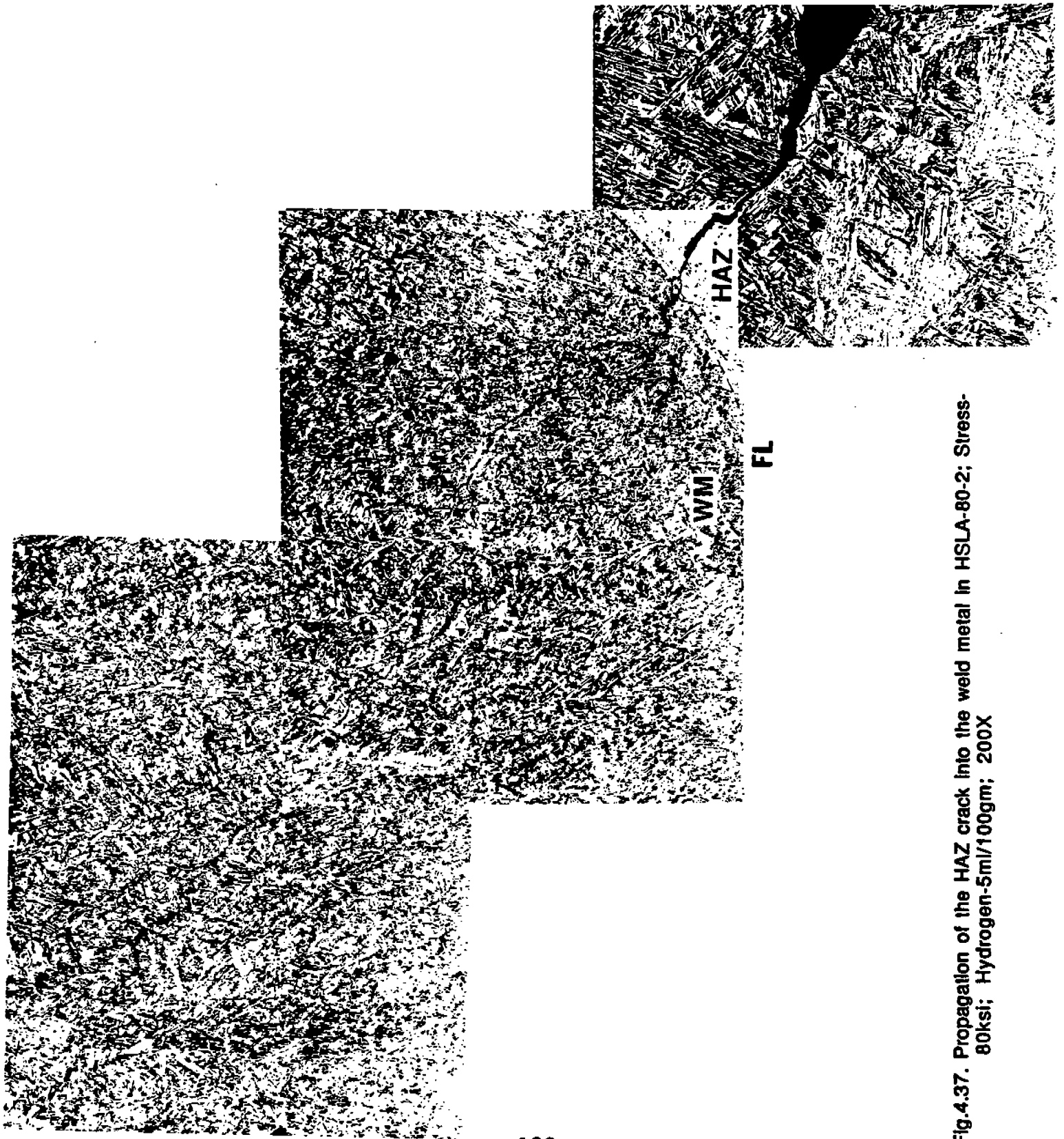
Fig.4.37. Propagation of the HAZ crack into the weld metal in HSLA-80-2; Stress-80ksi; Hydrogen-5ml/100gm; 200X

122
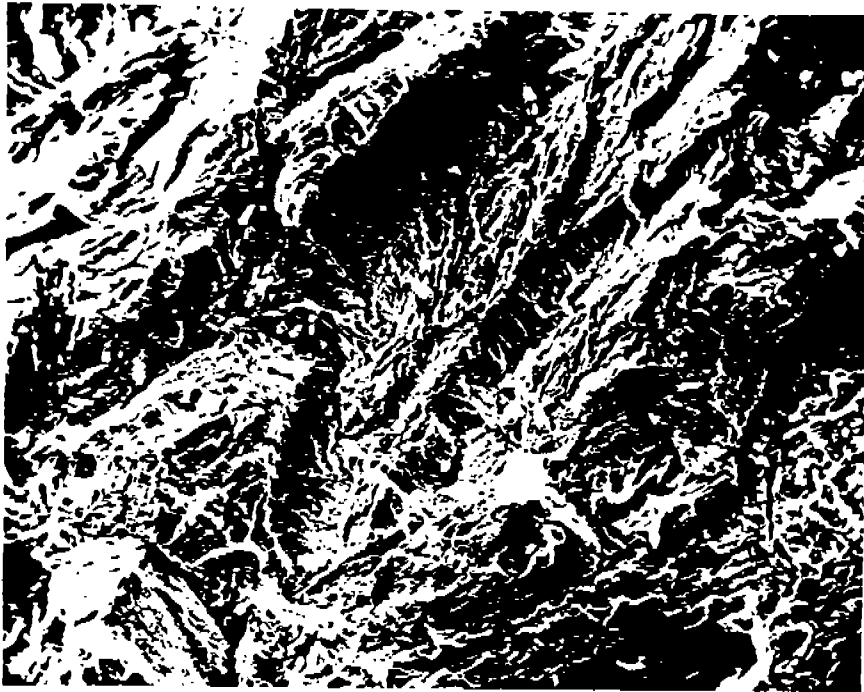
Fig.4.38. Quasi-cleavage mode of fracture in the hydrogen embrittled HAZ of
HSLA-80-2; 500X
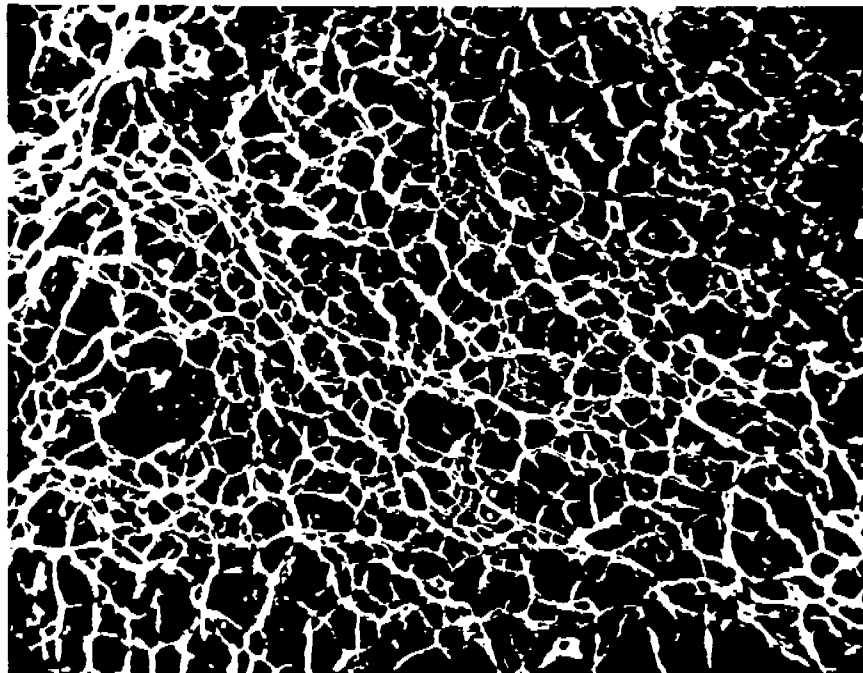
Fig.4.39. Microvoid coalescence failure in the region away from the CGHAZ of
HSLA-80-2; 2000X

Nb-0.001%, Cu-0.11%
CE(IIW)-0.47%
Diluted Weld Metal:
C-0.094%, Mn-1.13%, Si-0.13%, Cr-0.36%, Mo-0.23%, Ni-1.26%, V-0.008%, Cu-
0.40%
CE(IIW)-0.53%

The above exercise indicates that by employing the A 515 support plate, a slight increase in the carbon content of the weld metal is observed, however, since A 515 is a lean steel with respect to the alloying elements other than carbon, there is a slight decrease in the carbon equivalent of the weld metal. The carbon equivalent of the weld metal, if an HSLA-80-2 plate was used as a support plate, would have been 0.52, which is quite close to the CE obtained when A 515 steel is employed as a support plate. Therefore, it appears that the results of implant cracking test may not be affected significantly when A 515 steel is used as a base plate.

Several theories have been proposed to explain the mode of fracture in steels by hydrogen assisted cracking. Thus far the theory proposed by Beachem [78] has been the most successful in explaining hydrogen assisted cracking. This model unifies several other theories proposed in the past and explains the role of diffusible hydrogen content and stress intensity factor in defining the mode of fracture. The interrelationship between these two factors and the type of fracture mode observed is shown in Fig. 4.40. At a given hydrogen level the mode of fracture may vary with the applied stress and may range from intergranular, quasi-cleavage, to microvoid coalescence. Increasing the hydrogen level results in a decrease in the stress intensity factor, therefore, at high hydrogen levels and lower applied stresses, the mode of fracture may be intergranular only and at lower hydrogen levels and high stresses the failure may occur in microvoid coalescence mode. In a given sample all the above mentioned failure modes may be present as the stress intensity factor increases progressively as the crack grows in an implant test because of a constant applied load. The area fraction corresponding to failure due to hydrogen embrittlement increases either due to increase in hydrogen content or because of a longer incubation time for crack initiation.

The regions close to the notch where failure initiated were examined. The intergranular mixed with quasi-cleavage fracture mode was observed only in HSLA-80M as shown in Fig. 4.41 for 5 ml/100g hydrogen and tested at 95 ksi. The fracture modes in DQ-80 tested at two hydrogen levels - 5 and 20 ml/100g - are shown respectively in Figs. 4.42 and 4.43. The fracture in the low hydrogen sample is in the quasi-cleavage mode and when the hydrogen is increased the fracture nature changes and some grain boundary decohesion also appears to occur. The fracture surface morphology in HSLA-100, HSLA-130, HY-130, and DQ-125 is shown in Figs. 4.44 to 4.47 respectively. There is no major difference in the fracture mode in these steels. The failure takes place in the quasi-cleavage mode with well marked river patterns and tear ridges indicating the influence of microstructure on the fracture morphology. The CGHAZ's in these steels are fully martensitic and the well-defined patterns in the fractographs are associated with the presence of martensite. In these steels intergranular secondary cracking was also observed. No detailed quantitative analysis was carried out to estimate the area fractions of different failure modes in the samples. However, qualitative observations made on the present set of steels confirmed the results of the other investigators that the areal fraction of the embrittled region increases both with the rupture time and hydrogen content. This is due to the fact that with longer rupture times,

124
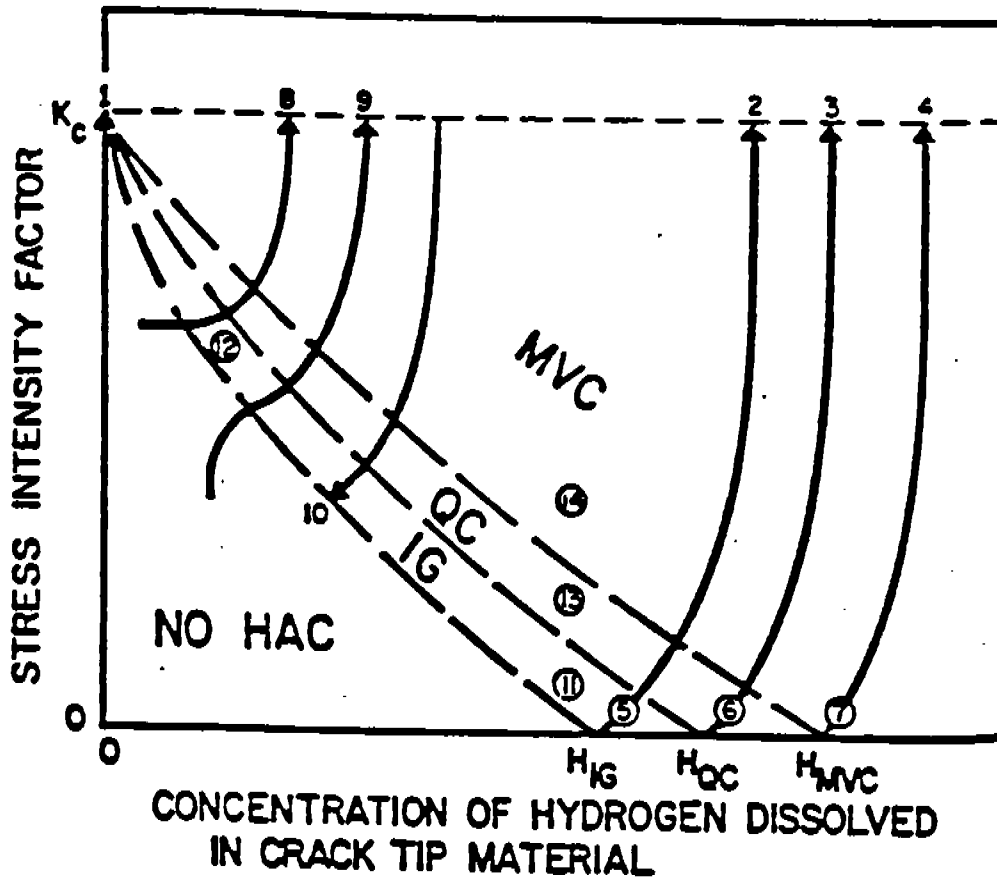
Fig.4.40. Interrelationship between stress intensity factor, diffusible hydrogen content and failure mode (Beachem diagram) [66]

Fig.4.41. Intergranular mixed with quasi-cleavage fracture mode in HSLA-80M; 500X
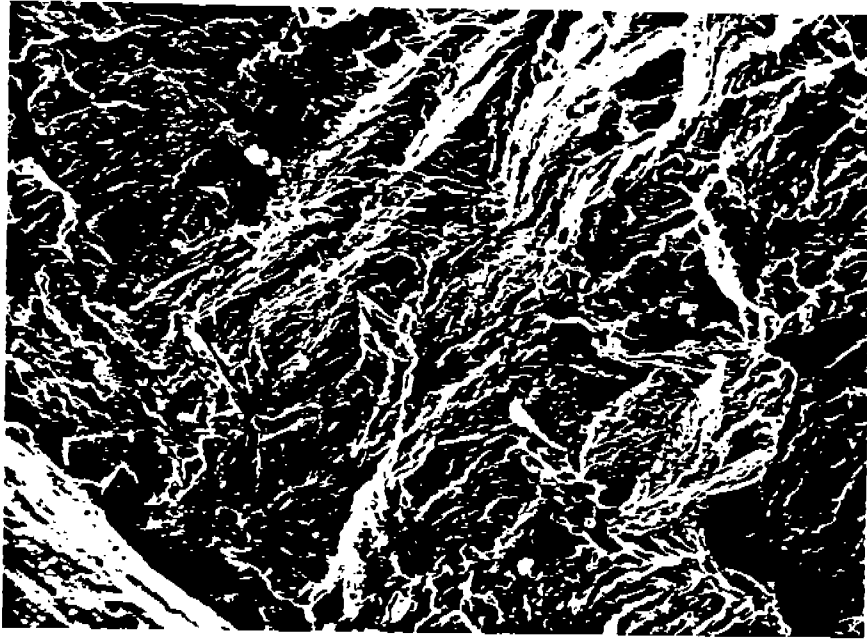
Fig.4.42. Quasi-cleavage mode of rupture observed in DQ-80 when tested at 5ml/100gm hydrogen level; 500X
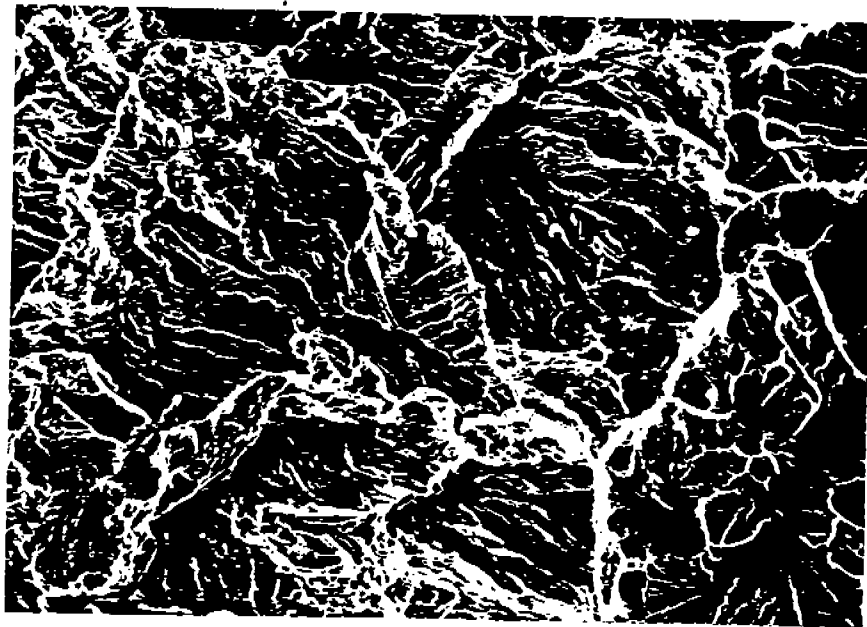
Fig.4.43. Quasi-cleavage with grain boundary decohesion in DQ-80 when tested at 20ml/100gm hydrogen level; 500X
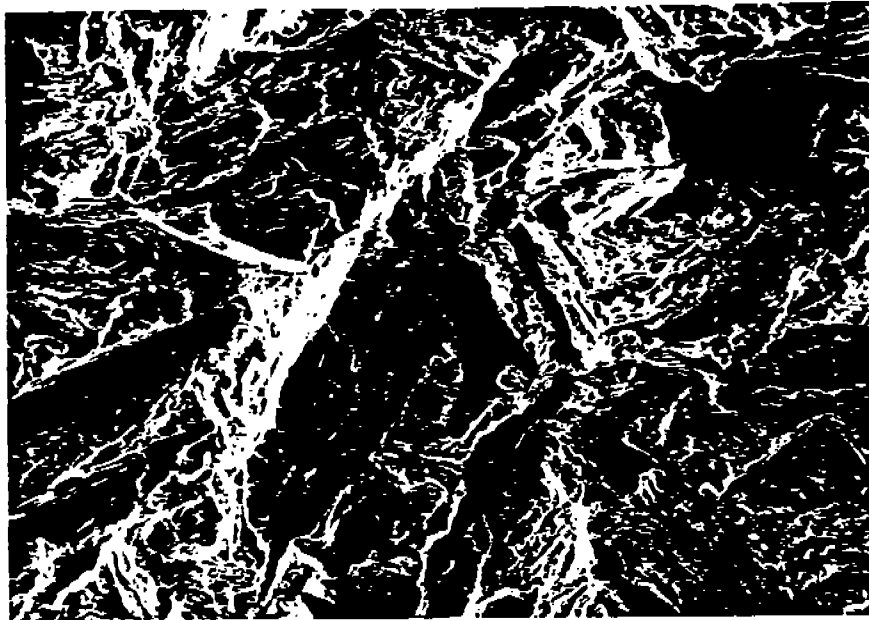
Fig.4.44. Quasi-cleavage fracture mode with river patterns and tear ridges indicating the influence of martensite in HSLA-100; 500X

Fig. 4.45. Quasi-cleavage fracture mode with river patterns and tear ridges indicating the influence of martensite in HSLA-130; 500X

127

Fig.4.46. Quasi-cleavage fracture mode with river patterns and tear ridges indicating the influence of martensite in HY-130; 500X

Fig.4.47. Quasi-cleavage fracture mode with river patterns and tear ridges indicating the influence of martensite in DQ-125; 500X

128

more time is available for hydrogen to diffuse and embrittle the material. The same argument is true when the hydrogen content in the weld metal is increased.

4.3.4. Prediction of the Lower Critical Stress

Several investigators have tried to evolve relationships in order to calculate the lower critical stress from a combination of carbon equivalent, diffusible hydrogen content, maximum HAZ hardness, volume percent martensite in the CGHAZ, cooling time from 800 to 500°C, cooling time from the fusion temperature to 100°C, cooling time from 300 to 100°C, and thermal factors etc. These equations are generally only applicable to the class of steels for which they were developed and thus far no equation of universal applicability has been proposed. Some of the equations to estimate the lower critical stress are described below and their applicability to the data from the steels in this study is discussed. The various parameters determined from the actual thermal cycles recorded during the implant cracking test are given below. These were employed to calculate the LCS using the following equations-

Preheat temperature - 75°F

Cooling time from 800 to 500°C	- 7.5 sec.
Cooling time from 1500 to 200°C	- 23.2 sec.
Cooling time from 1500 to 150°C	- 33.4 sec.
Cooling time from 1500 to 100°C	- 81.4 sec.
Cooling time from 300 to 100°C	- 59 sec.
Calculated thermal factor, $(\Sigma \, D\Delta t)_{100}$	- 175.62 x 10^{-5} cm^2

Preheat temperature - 150°F

Cooling time from 800 to 500°C	- 8.5 sec.
Cooling time from 1500 to 200°C	- 39 sec.
Cooling time from 1500 to 150°C	- 59 sec.
Cooling time from 1500 to 100°C	- 101 sec.
Cooling time from 300 to 100°C	- 77 sec.
Calculated thermal factor, $(\Sigma \, D\Delta t)_{100}$	- 311.87 x 10^{-5} cm^2

(i) **Ito's Formula [79]**

In 1976 Ito et al [79] published the following formula for estimating the LCS in high strength steels:

$$LCS \ (kg/mm^2) = - 242 \, P_{cm} - 22.5 \log [H] + 50 \log t_{100} - 3 \ \ \ ....(4.6)$$

where-

[H] is the content of diffusible hydrogen in ml/100g measured by the JIS method

t_{100} is the cooling time (in sec.) from weld peak temperature to 100°C

P_{cm} is the CE formula proposed by Ito and Bessyo (described earlier)

The Ito's formula was developed based on the steels with the following chemical composition limits-

C - 0.04 to 0.17 %;	Mn - 0.81 to 1.59 %;	Si - 0.24 to 0.42 %;
Ni - 0 to 1 %;	Cr - 0 to 0.48 %;	Mo - 0 to 0.44 %;
Cu - 0 to 0.24 %;	V - 0 to 0.04 %;	Nb - 0 to 0.02 %;
B - 0 to 0.001 %		

P_{cm} of these steels varied from 0.136 to 0.0.271

Diffusible hydrogen content ranged from 0.7 to 3.7 ml/100g (JIS method) and 2.9 to 7 ml/100g (IIW method)

The implant cracking tests were conducted at 23 and 43 kJ/in. heat input and at two preheat temperatures - 75 and 300°F. The implant samples used were of circular notch geometry and the implant samples were positioned in a V-groove in the support plate. When applied to the steels in this program, the validity limit of Ito's formula is violated not only with respect to chemical composition, but also for hydrogen content (when $[H]_D$ = 10 and 20 ml/100g). The comparison of the calculated and actual LCS is shown in Fig. 4.48. It is noticed that Ito's formula considerably underestimates the LCS. However, it is not the exact magnitude of LCS but the ability of a formula to provide a good correlation between calculated and experimental data, which is important because once a good correlation is found, the magnitude of the LCS can be easily calculated from the regression equation.

It is also quite evident from Fig. 4.48 that the data corresponding to steels belonging to the lower strength category (HSLA-80-1, HSLA-80-2, HSLA-80M, and DQ-80) and the higher strength category (HSLA-100, HSLA-130, HY-130, and DQ-125) fall into two distinct groups. The LCS in the higher strength steels is considerably higher than predicted by the formula. This is because of the fact that the higher strength steels have higher CE's and in Ito's formula the critical stress for given welding parameters and hydrogen content decreases with an increase in P_{cm}, which appears to be true only when the data from a similar class of steels are compared. This is also supported by the observations made by Matsuda et al [80] and Christensen and Simonsen [81]. Christensen and Simonsen in their report summarized the results from a program to characterize different types of steels for their susceptibility to HAC. The steels included in the study were-medium strength ship plate, structural and pipeline grades, high strength quenched and tempered steels, and one low alloy wear resistant steel. Based on a detailed data analysis, they concluded that "a fair agreement (between actual and experimental data) has been achieved for the majority of carbon-manganese steels.....the high-strength steels QT1, QT2 and QT3   do not fit into the same pattern. These steels were also found to depart from the general trend of LCS vs. CE". Therefore, the decrease in the LCS with P_{cm} in the lower strength steels cannot be extrapolated to the higher strength steels. The quench hardenable steels are known to have a higher CE as well as a higher resistance to cold cracking. In this context it is not surprising that two linear equations were obtained - one for the lower strength and the other for the higher strength steels in both the Battelle Underbead Cracking and UT-Mod. Hydrogen Sensitivity tests.

The regression equations obtained from Ito's formula are given below. It is seen that there is poor correlation between the actual and estimated values in both type of steels. However, compared to the higher strength steels, the correlation in the lower strength steels is better.

Lower Strength Steels

LCS (act.) = 58.82 + 0.60 LCS (cal.) R^2 = 0.672

Higher Strength Steels

LCS (act.) = 95.32 + 0.20 LCS (cal.) R^2 = 0.100

(ii) Inagaki's Formula [82]

Inagaki et al in 1978 proposed a formula for calculating the LCS in implant cracking tests. The geometry of implant sample and support plate were the same as used by Ito et al [79]. They obtained the following empirical equation for their data-
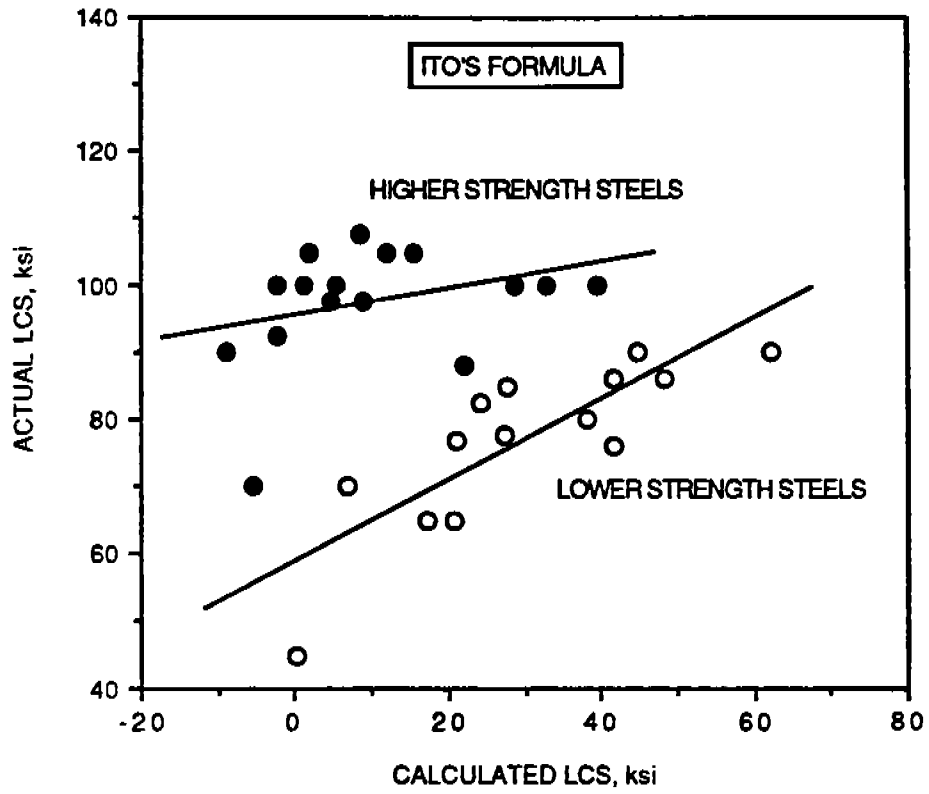
Fig.4.48. Comparison between actual and calculated lower critical stress by Ito's formula for all steels

$$LCS \ (kg/mm^2) = 68.9 - 121 \ P_{cm} - 24 \ log \ ([H] + 1)$$
$$+ \ 1.75 \ \Delta t \ _{800-500} + 1.65 \times 10^{-2} \ \Delta t_{100} \quad ....(4.7)$$

The above equation was derived from data obtained from HT 50 and HT 80 steels with P_{cm} in the 0.16 to 0.282 range. The hydrogen content (JIS method) in this study was varied from 1 to 21 ml/100g and the cooling time from 800 to 500°C from 5 to 20 sec. Inagaki et al found that their data gave a better correlation with log ([H] + 1) as contrasted to log [H] found by several other investigators. Inagaki's formula also included the cooling time from 800 to 500°C in addition to t_{100} as in Ito's formula

The comparison between the experimental data and LCS calculated from Inagaki's formula is shown in Fig. 4.49. The following regression equations were obtained from the correlation-

Lower Strength Steels

LCS (act.) = 34.47 + 0.83 LCS (cal.) $R^2 = 0.629$
Higher Strength Steels

LCS (act.) = 77.30 + 0.46 LCS (cal.) $R^2 = 0.164$
Inagaki's formula also underestimates the LCS in the present set of steels and provides a poor correlation with the experimental data.

(iii) Matsuda's Formula [83]

Matsuda et al compared the applicability of the above two formulae to the data from SM50, HT60, HT80, HY130, 3.5 % Ni, 9 % Ni, 1 1/4 Cr-1/2 Mo, and 2 1/4 Cr-1Mo steels and found that both equations underestimated the LCS in these steels. He attributed the reason for non-applicability of the two predictive equations to the difference in the notch radius of the specimen between his and other studies. Matsuda et al employed a helical notch geometry as against a circular notch used by both Ito et al and Inagaki et al. The main disadvantage in using a circular notch geometry in the implant cracking test samples is the uncertainty associated with the exact positioning of the notch in the CGHAZ, whereas in the helical notch a portion of the notch is always in the CGHAZ. Based on their results, Matsuda et al proposed another formula that allowed calculation of the critical stresses in the above steels-

$$LCS \ (kg/mm^2) = - 268 \ P_{cm} - 23.3 \ log \ [H] + 138 \quad ....(4.8)$$

where the P_{cm} varied from 0.196 to 0.308 and hydrogen content (JIS method) from 1.1 to 28.5 ml/100g.

It should be noted that Matsuda's formula is similar to that proposed by Ito et al but is applicable only for the implant tests conducted with no preheat as this formula does not contain the term corresponding to the effect of preheat on the cooling time from peak temperature to 100°C.

The applicability limit of Matsuda's formula with respect to chemical composition is given below-

C - 0.04 to 0.15 %;	Mn - 0.50 to 0.84 %;	Si - 0.23 to 0.60 %;
Ni - 0.03 to 8.76 %;	Cr -0.04 to 2.25 %;	Mo - 0.01 to 0.96 %;
Cu - 0.01 to 0.23 %;	V - 0 to 0.06 %	

When the calculated LCS at 75°F preheat temperature from this formula are compared with the actual data, the following regression lines (Fig. 4.50) are obtained-
Lower Strength Steels

LCS (act.) = 19.08 + 0.63 LCS (cal.) $R^2 = 0.828$
Higher Strength Steels
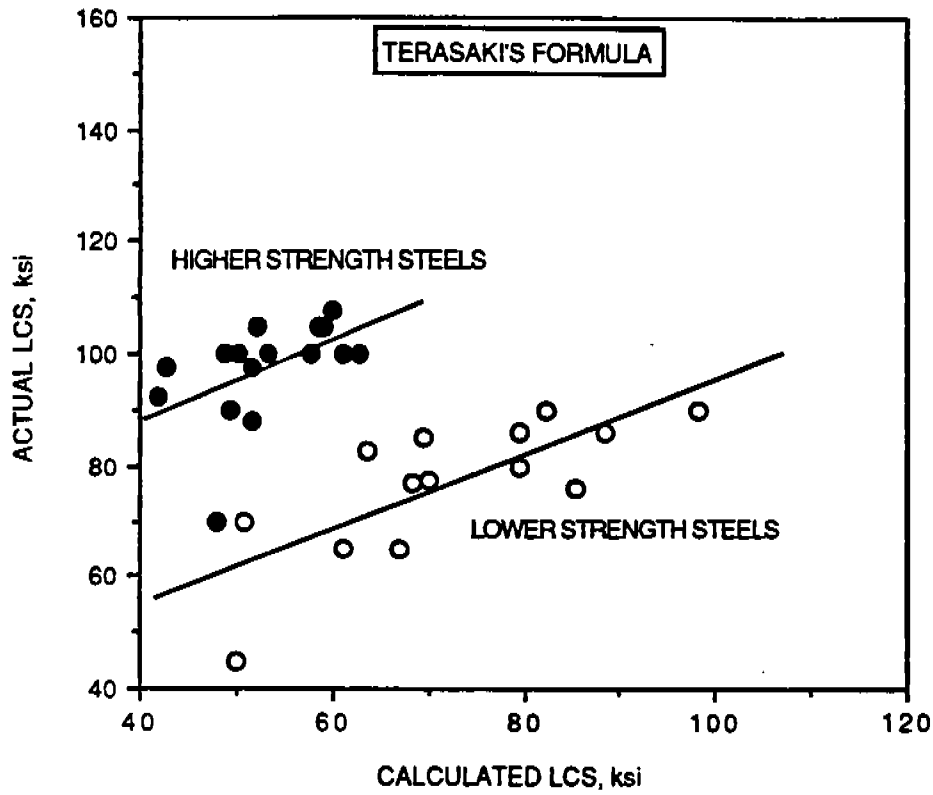
LCS (act.) = 78.98 + 0.23 LCS (cal.) $R^2 = 0.113$
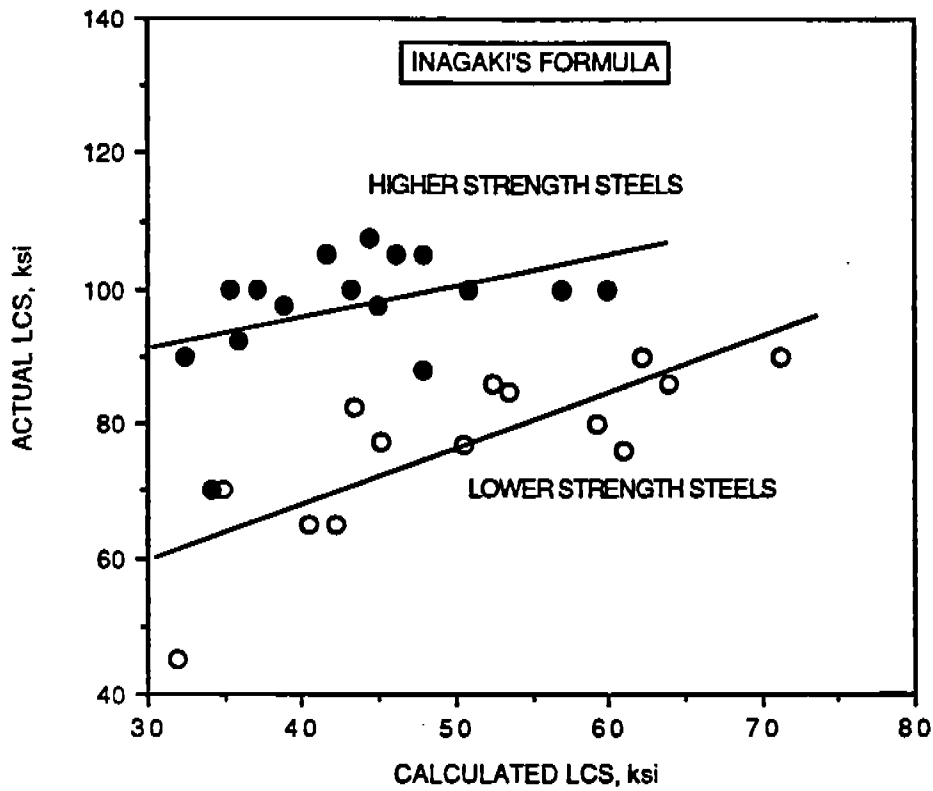
Fig.4.49. Comparison between actual and calculated lower critical stress by Inagaki's formula for all steels
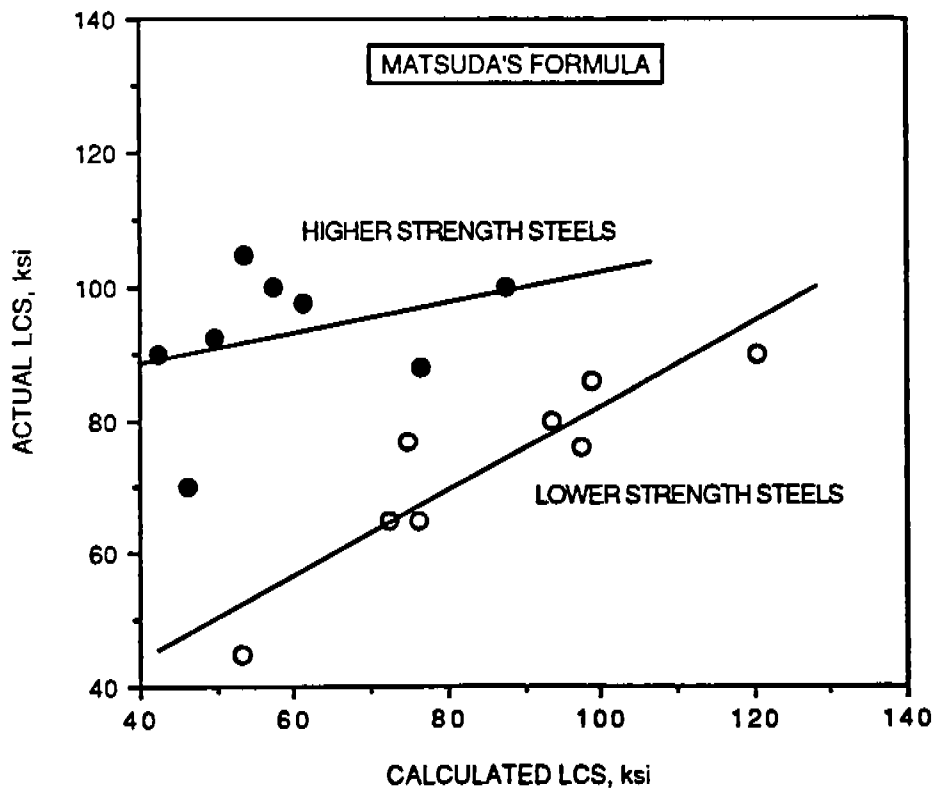
Fig.4.50. Comparison between actual and calculated lower critical stress by Matsuda's formula for all steels

133

It appears that the LCS in the lower strength steels at 75°F preheat can be calculated with a good accuracy by using Matsuda's formula, however, when this formula is applied to the higher strength steels, the coefficient of determination is very poor.

(iv) Terasaki's Formula [84]

Terasaki et al in 1982 proposed the following formula to estimate the lower critical stress in implant cracking tests:

For $(H_R)_{100} \geq 2$ ppm

$$LCS \ (kg/mm^2) = -20 \log (H_R)_{100} - 0.20 \ H_{max} + 125 \qquad \text{..........(4.9)}$$

For $(H_R)_{100} < 2$ ppm

$$LCS \ (kg/mm^2) = -75 \log (H_R)_{100} - 0.20 \ H_{max} + 145 \qquad \text{.............(4.10)}$$

$$(H_R)_{100} = H_0 \exp \{-75 \ (\Sigma \ D\Delta t)_{100}\} \qquad \text{................(4.11)}$$

$$H_0 = 1.26 \ H_F \qquad \text{................(4.12)}$$

where-

$(H_R)_{100}$ is the retained hydrogen content in ppm at 100°C,

H_0 is the hydrogen content in fused metal just after solidification

H_F is the diffusible hydrogen content measured by JIS method

$(\Sigma \ D\Delta t)_{100}$ in cm^2 is the thermal factor for hydrogen diffusion, summed from solidification temperature to 100°C on cooling

H_{max} is the CGHAZ hardness in DPH

Terasaki et al also provided relationships to calculate the thermal factor from different cooling times. They compared the calculated results with the experimental values and arrived at the following regression equations-

$$(\Sigma \ D\Delta t)_{100} = (1.95 \ t_{100} - 20) \ x \ 10^{-5} \qquad (R^2 = 86\%) \qquad \text{...(4.13)}$$

$$= (4.51 \ t_{150} + 41) \ x \ 10^{-5} \qquad (R^2 = 97\%) \qquad \text{....(4.14)}$$

$$= (4.2 \ t_{200} + 2.73 \ t_{150} - 13) \ x \ 10^{-5} \qquad (R^2 = 99.5\%) \qquad \text{....(4.15)}$$

where t_{100}, t_{150}, and t_{200} are the cooling times respectively from fusion temperature to 100, 150, and 200°C

The equation to calculate the thermal factor from t_{150} and t_{200} provides the best correlation with the experimental data. The applicability of this equation was also studied by Karpi et al [85] and they found an excellent correlation with their data from implant and RRC tests.

Terasaki's equations to estimate the lower critical stress were developed for steels with chemical compositions, H_{max} and hydrogen content in the following ranges-

C - 0.07 to 0.42 %;	Mn - 0.42 to 1.47 %;	Si - 0.06 to 0.48 %;
Ni - 0.02 to 9.35 %;	Cr - 0.02 to 2.3 %;	Mo - 0.01 to 1.00 %;
Cu - 0 to 0.39 %;	V - 0 to 0.059 %,	Nb - 0 to 0.042 %;
Al - 0 to 0.58 %;	B - 0 to 0.014 %.	

$1.2 \leq [H] \leq 13$ ppm

$300 \leq H_{max} \leq 500$ DPH

Terasaki et al employed a circular notch geometry to conduct the implant cracking tests. Unlike the formulae described above, the Terasaki equations do not consider carbon equivalent as a variable but instead include the maximum HAZ hardness as a parameter. The effect of preheat is taken care of in the thermal factor which is proportional to the amount of hydrogen remaining in the weldment at 100°C.

Gedeon [86] compared the validity of the relationship between $(H_R)_{100}$ and the thermal factor by analyzing data from his study and that from literature.

134

He found a good correlation between theoretical prediction and experimental data. It appears that it is possible to calculate the thermal factor with greater accuracy by using Terasaki's empirical formulae.

Therefore, while comparing our LCS data with that calculated from Terasaki's equation the value of thermal factors at 75 and 150°F preheat temperatures were calculated from equation (4.15).

The comparison between the experimental and estimated data is shown in Fig. 4.51. The following regression equations were obtained for the lower and the higher strength steels-

Lower Strength Steels

LCS (act.) = 28.46 + 0.67 LCS (cal.) R^2 = 0.571

Higher Strength Steels

LCS (act.) = 59.84 + 0.71 LCS (cal.) R^2 = 0.243

The low values of coefficient of determination indicates that no linear relationship exists between the actual and calculated values.

(v) Pavaskar's Formula [75]

Pavaskar and Kirkaldy in 1982 proposed another formula to estimate the LCS as a function of H_{max} and % martensite content in the CGHAZ. They observed that "hardness alone does not fully characterize the HAZ microstructural condition for assessing the cracking susceptibility.....(instead) LCS correlates very well with the % martensite and the maximum HAZ hardness combined into a linear index".

HAZ Index = [1565 - 10 (% martensite) - H_{max}] ....(4.16)

Pavaskar and Kirkaldy used implant data generated by Evans and Christensen [74] at various hydrogen levels to arrive at the following equation (Evans and Christensen employed a circular notch geometry in their implant samples) -

$$LCS \ (N/mm^2) = \frac{[1565 - 10 \ (\% \ martensite) - H_{max}]^{1/2}}{[31 - 15.5 \ log \ [H]}$$ ....(4.17)

where % martensite and H_{max} can be calculated by the modified Maynier's formulae [51]. The chemical composition of the steels varied in the range-

C - 0.11 to 0.21 %,   Mn - 1.57 to 1.61 %,   Si - 0.43 %,
Al - 0.030 to 0.035 %,   Nb - 0.021 %.

The diffusible hydrogen content ranged from 3 to 30 ppm as measured by the IIW method and the martensite % varied from 30 to 95.

The results of the comparison using Pavaskar's formula is shown in Fig. 4.52. The regression equations are given below-

Lower Strength Steels

LCS (act.) = 55.93 + 0.36 LCS (cal.) R^2 = 0.465

Higher Strength Steels

LCS (act.) = 74.55 + 0.59 LCS (cal.) R^2 = 0.171

(vi) Karpi's Formula [85]

Karpi et al improved upon Terasaki's formula by modifying the following equation for calculating the amount of remaining diffusible hydrogen in the weldments.

$(H_R)_{100} = H_0 \ exp \ [- A \ (\Sigma \ D\Delta t)_{100}]$ ....(4.18)

In Terasaki's formula A = 75, but Karpi et al found that the magnitude of A depends on the type of steel. The following values were assigned to A based on the experimental data by Matsuda et al [87]-

for HT 60 steel   (UTS = 85 ksi)   A is approximately = 83

135

Fig.4.51. Comparison between actual and calculated lower critical stress by Terasaki's formula for all steels
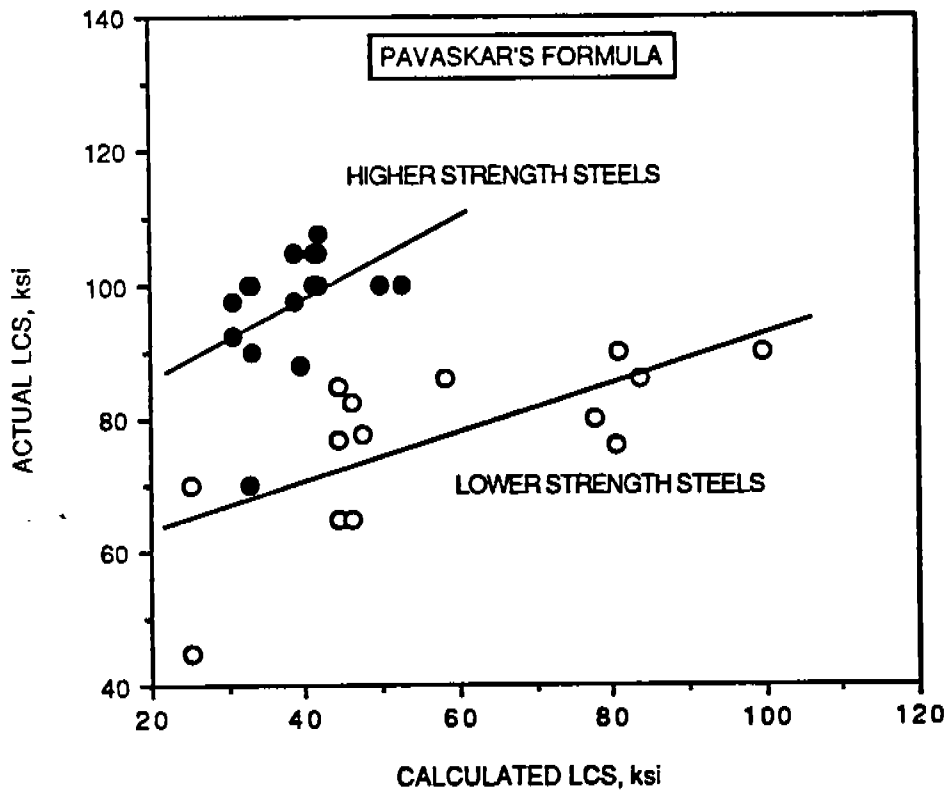
Fig.4.52. Comparison between actual and calculated lower critical stress by Pavaskar's formula for all steels

for HT 80 steel   (UTS = 115 ksi)   A is approximately = 69
for HY 130 steel   (UTS = 145 ksi)   A is approximately = 46
or HY 180 steel   (UTS = 200 ksi)   A is approximately = 41

The dependence of factor A on the type of steel (when welded with a matching filler wire) indicates that under similar welding conditions and hydrogen content, a greater amount of diffusible hydrogen is retained in the weldments of higher strength steels as contrasted to that in the lower strength steels. This appears to be based on the fact that in highly alloyed steels the hydrogen diffusivity is lower than when the alloying content is reduced. In other words, the CGHAZ's of the high strength steels will experience a greater amount of diffusible hydrogen.

Karpi's equation to calculate the lower critical stress in the implant cracking tests is provided below-

$$LCS \ (N/mm^2) = 785 - 1.2 \ H_{max} - 250 \ log \ (H_R)_{100} \qquad ....(4.19)$$

This formula was based on data from steels with the following chemical composition variation-

C - 0.06 to 0.19%	Mn - 0.56 to 1.50%	Si - 0.26 to 0.43%
Cr - 0.02 to 0.80%	Ni - 0.017 to 8.92%	Mo - 0.03 to 0.63%
Cu - 0.013 to 0.17%	V - 0 to 0.04%	Al - 0 to 0.06 %
B - 0.0009 max.		

The steels belonged to two classes; (a) C-Mn steel with 50 ksi strength level, and (b) low alloy steels with 115 ksi strength level. The implant cracking test samples were of helical notch geometry.

The results of correlation between calculated and measured LCS is shown in Fig. 4.53. The data from the lower and higher strength steels fall into two different categories, as also observed with the other formulae. However, using Karpi's formula it was possible to obtain a relatively better R^2 value for the higher strength steels, as shown below-

Lower Strength Steels

LCS (act.) = 53.28 + 0.67 LCS (cal.) R^2 = 0.551

Higher Strength Steels

LCS (act.) = 76.59 + 0.77 LCS (cal.) R^2 = 0.340

It is interesting to compare the capability of various formulae in predicting the lower critical stress for the steels in this study. Although none of the formulae were able to provide the desired accuracy of prediction for all steels, nevertheless comparisons may bring out important factors influencing the crack susceptibility of the steels in this program. The following ranking of different formulae is based on the type of steels.

For the lower strength steels-
    Matsuda > Ito > Inagaki > Terasaki > Karpi > Pavaskar
For the higher strength steels -
    Karpi > Terasaki > Pavaskar > Inagaki > Matsuda ≥ Ito

Matsuda's formula was found to provide maximum R^2 for the lower strength steels but lowest R^2 when applied to the higher strength steels. This is surprising as this formula was developed for C-Mn as well as alloyed steels and represented an improvement over Ito's formula. Both formulae are based on P_{cm}, and it is possible that the hardenability of the present set of steels is not represented adequately by P_{cm}. Karpi's formula did not provide as good a correlation for the higher strength steels as Matsuda's formula did for the lower strength steels. Karpi's formula definitely represents an improvement over Terasaki's formula, at least for the higher strength steels. However,
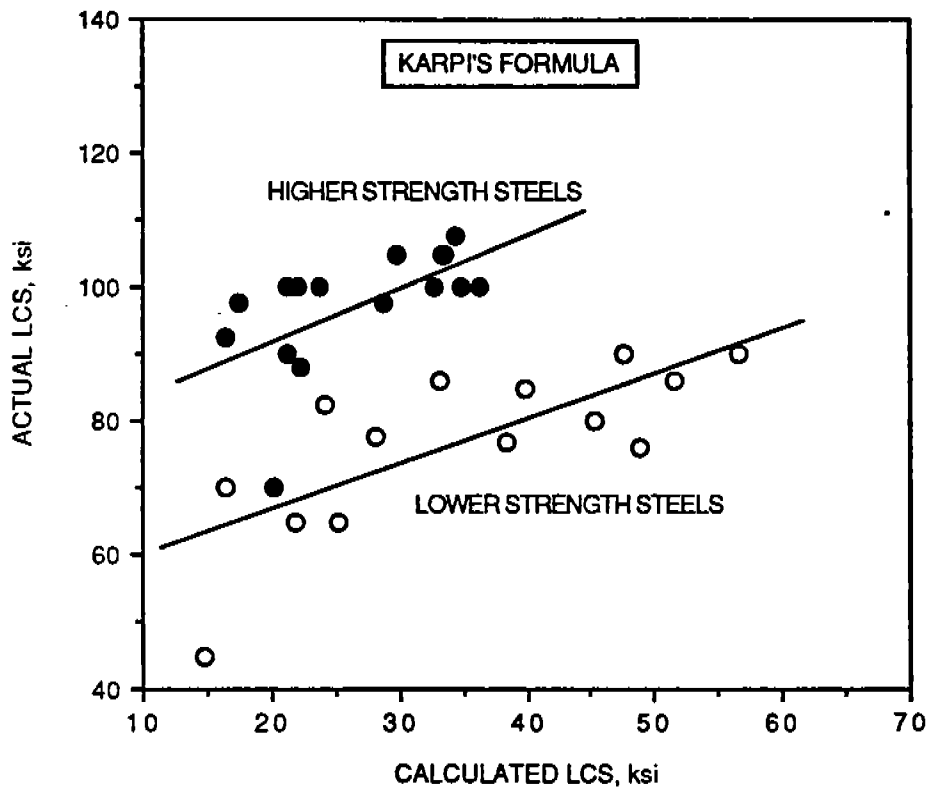
Fig. 4.53. Comparison between actual and calculated lower critical stress by Karpi's formula for all steels

when applied to the lower strength steels the difference in the R^2 values is not appreciable. Since Karpi's formula recognizes the influence of alloying additions on the hydrogen diffusivity coefficient, if a parameter defining the influence of chemical composition on hydrogen diffusivity is incorporated in the formula, it may become possible to explain the results of implant cracking tests from different types of steels. In the present set of steels, Pavaskar's formula (employing % martensite and H_{max}) has not provided satisfactory correlations. This may be due to (a) possible inaccuracy in estimating % martensite and/or (b) non-applicability of the two factors - % martensite and H_{max} - in defining the LCS in the present set of steels. While comparing different formulae, it is also noticed that in the most recent formulae, the carbon equivalent as a parameter to calculate the LCS has been given less importance and instead the maximum HAZ hardness is being preferred as a parameter representing the chemical composition.

Since the calculated and actual LCS values did not show a linear correlation, the implant cracking data were also analyzed for different preheat temperatures. The following regression lines were obtained-

(a) <u>Lower Strength Steels - 75°F preheat temperature:</u>

Terasaki	LCS (act.) = 10.17 + 0.85 LCS (cal.)	$R^2 = 0.810$
Karpi	LCS (act.) = 43.17 + 0.84 LCS (cal.)	$R^2 = 0.708$
Ito	LCS (act.) = 52.29 + 0.68 LCS (cal.)	$R^2 = 0.832$
Matsuda	LCS (act.) = 19.08 + 0.63 LCS (cal.)	$R^2 = 0.828$
Pavaskar	LCS (act.) = 44.96 + 0.47 LCS (cal.)	$R^2 = 0.648$
Inagaki	LCS (act.) = 21.60 + 1.00 LCS (cal.)	$R^2 = 0.793$
Ranking	Ito > Matsuda > Terasaki > Inagaki > Karpi > Pavaskar	

(b) <u>Lower Strength steels - 150°F preheat temperature:</u>

Terasaki	LCS (act.) = 50.24 + 0.45 LCS (cal.)	$R^2 = 0.697$
Karpi	LCS (act.) = 66.43 + 0.44 LCS (cal.)	$R^2 = 0.756$
Ito	LCS (act.) = 69.46 + 0.41 LCS (cal.)	$R^2 = 0.768$
Matsuda	LCS (act.) = 51.78 + 0.38 LCS (cal.)	$R^2 = 0.757$
Pavaskar	LCS (act.) = 67.77 + 0.26 LCS (cal.)	$R^2 = 0.686$
Inagaki	LCS (act.) = 53.46 + 0.56 LCS (cal.)	$R^2 = 0.809$
Ranking	Inagaki > Ito > Matsuda > Karpi > Terasaki > Pavaskar	

When the lower strength steels are considered at different preheat temperatures a considerable improvement in the predictive accuracy of all the formulae is noticed. Figs. 4.54 and 4.55 show the comparisons obtained for Ito's and Inagaki's formulae respectively. The regression lines corresponding to 75 and 150°F preheat temperatures merge at higher LCS values but the difference increases at lower LCS values. The above indicates that (a) the cooling time t_{100} used in these two formulae may not adequately represent the amount of hydrogen remaining at 75 and 150°F temperatures, (b) the increase in hydrogen embrittlement at 75°F is greater at higher hydrogen levels than at 150°F, and (c) the change in embrittlement is not linearly related with preheat temperature.

(c) <u>Higher Strength steels - 75°F preheat temperature:</u>

Terasaki	LCS (act.) = 39.62 + 1.01 LCS (cal.)	$R^2 = 0.361$
Karpi	LCS (act.) = 63.93 + 1.10 LCS (cal.)	$R^2 = 0.507$
Matsuda	LCS (act.) = 78.98 + 0.23 LCS (cal.)	$R^2 = 0.113$
Ito	LCS (act.) = 91.04 + 0.27 LCS (cal.)	$R^2 = 0.124$
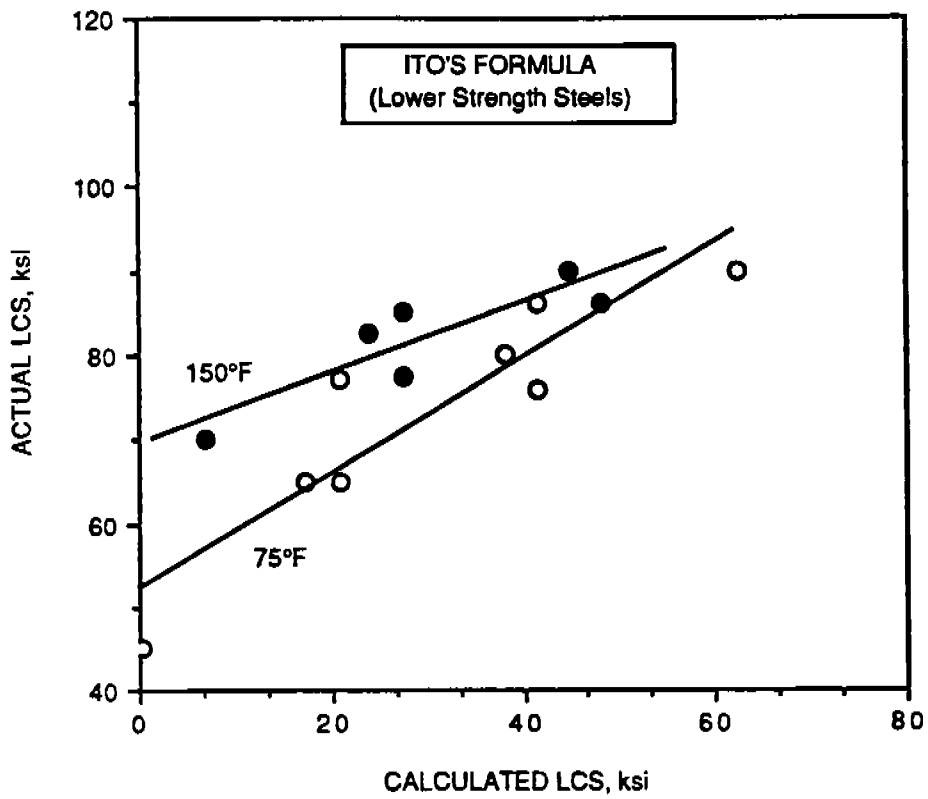
Fig.4.54. Correlation between experimental and calculated lower critical stress for lower strength level steels by Ito's formula when the data are considered individually at 75 and 150°F preheat temperature
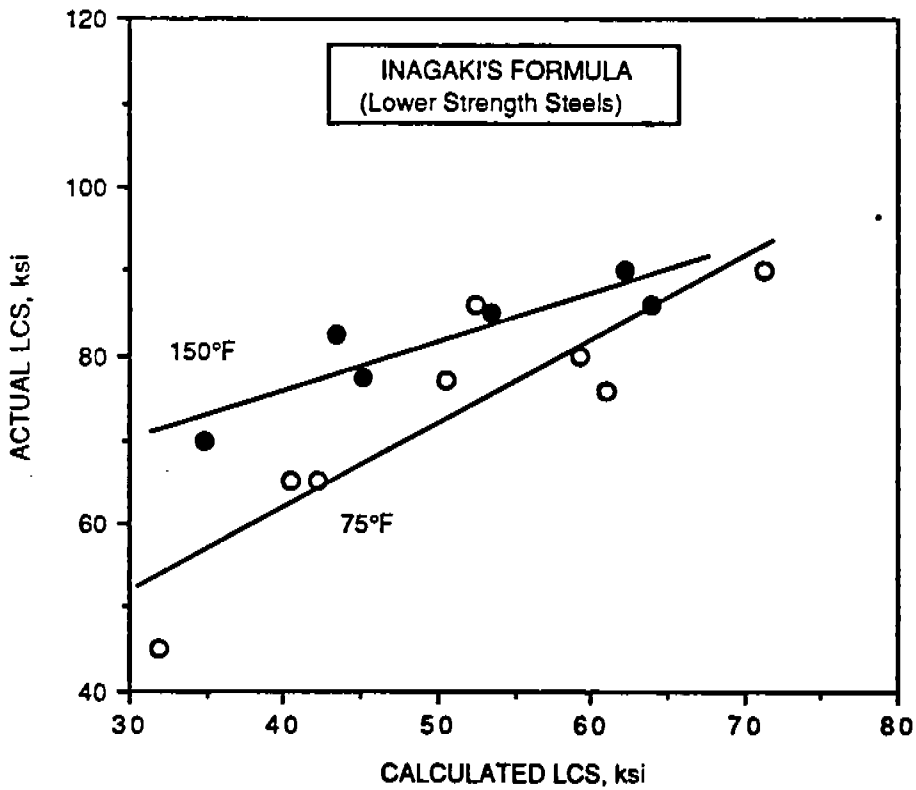
Fig.4.55. Correlation between experimental and calculated lower critical stress for lower strength level steels by Inagaki's formula when the data are considered individually at 75 and 150°F preheat temperature

Pavaskar   LCS (act.) = 51.20 + 1.08 LCS (cal.) $R^2 = 0.374$
Inagaki   LCS (act.) = 64.99 + 0.66 LCS (cal.) $R^2 = 0.243$
Ranking   Karpi > Pavaskar > Terasaki > Inagaki > Ito > Matsuda

(d) Higher Strength Steels - 150°F preheat temperature:

Terasaki   LCS (act.) = 85.37 + 0.31 LCS (cal.) $R^2 = 0.343$
Karpi   LCS (act.) = 92.35 + 0.35 LCS (cal.) $R^2 = 0.500$
Matsuda   LCS (act.) = 102.6 - 0.02 LCS (cal.) $R^2 = 0.003$
Ito   LCS (act.) = 102.0 - 0.01 LCS (cal.) $R^2 = 0.001$
Pavaskar   LCS (act.) = 96.20 - 0.14 LCS (cal.) $R^2 = 0.086$
Inagaki   LCS (act.) = 98.91 + 0.06 LCS (cal.) $R^2 = 0.024$
Ranking   Karpi > Terasaki > Pavaskar > Inagaki > Matsuda > Ito

Although Karpi's formula provided the best R^2 between the experimental and measured values, however, there does not appear to be any linear relationship between measured and calculated LCS. Therefore, the data were further analyzed by categorizing steels into Cu-containing (HSLA-100 and HSLA-130) and non Cu-containing (HY-130 and DQ -125) steels. The following regression equations were obtained:

HSLA-100 and HSLA-130 steels - 75°F preheat temperature:

Terasaki   LCS (act.) = -40.68 + 2.45 LCS (cal.) $R^2 = 0.805$
Karpi   LCS (act.) = 40.50 + 1.88 LCS (cal.) $R^2 = 0.758$
Matsuda   LCS (act.) = 18.73 + 1.45 LCS (cal.) $R^2 = 0.418$
Ito   LCS (act.) = 94.01 + 1.55 LCS (cal.) $R^2 = 0.435$

Pavaskar   LCS (act.) = -10.14 + 2.71 LCS (cal.) $R^2 = 0.750$

Inagaki   LCS (act.) = 10.10 + 2.14 LCS (cal.) $R^2 = 0.547$
Ranking   Terasaki > Karpi > Pavaskar > Inagaki > Ito > Matsuda
HSLA-100 and HSLA-130 steels - 150°F preheat temperature:

Terasaki   LCS (act.) = 67.70 + 0.65 LCS (cal.) $R^2 = 0.960$
Karpi   LCS (act.) = 88.88 + 0.51 LCS (cal.) $R^2 = 0.946$
Matsuda   LCS (act.) = 80.02 + 0.46 LCS (cal.) $R^2 = 0.724$
Ito   LCS (act.) = 100.7 + 0.49 LCS (cal.) $R^2 = 0.739$
Pavaskar   LCS (act.) = 75.50 + 0.74 LCS (cal.) $R^2 = 0.948$
Inagaki   LCS (act.) = 77.06 + 0.64 LCS (cal.) $R^2 = 0.829$
Ranking   Terasaki > Pavaskar = Karpi > Inagaki > Ito > Matsuda

Terasaki's formula provides the best correlation parameters when data from HSLA-100 and HSLA-130 are considered separately at 75 and 150°F preheat temperatures. The comparison for Terasaki's equation is shown in Fig. 4.56. As observed in the lower strength steels, the regression lines for 75 and 150°F preheat temperatures in HSLA-100 and HSLA-130 steels also converge when tests are conducted at lower hydrogen content. The difference increases as the hydrogen content is increased.

When data for HY-130 and DQ-125 are compared at 75 and 150°F preheat temperatures, no correlation was observed among the experimental and calculated LCS values. Therefore, HY-130 and DQ-125 steels are considered separately.

HY-130 Steel (75 and 150°F preheat temperature)

Terasaki   LCS (act.) = 65.36 + 0.69 LCS (cal.) $R^2 = 0.567$
Karpi   LCS (act.) = 85.49 + 0.55 LCS (cal.) $R^2 = 0.569$

141
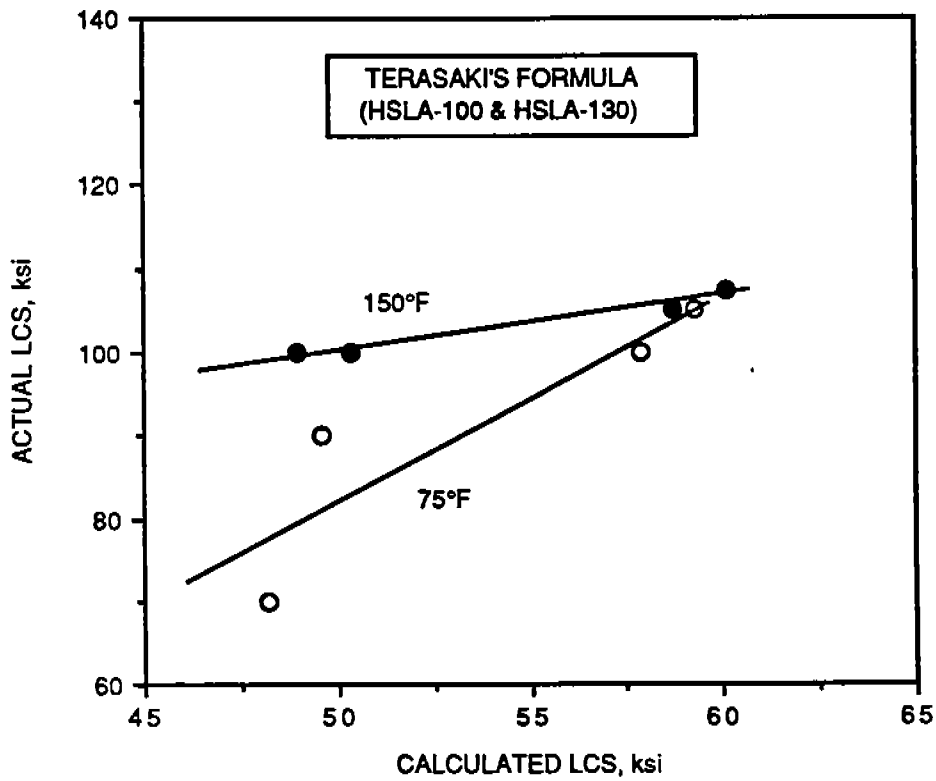
Fig.4.56. Terasaki's formula predicts accurate lower critical stress for HSLA-100 and HSLA-130 steels when data are analyzed separately at 75 and 150°F preheat

Ito	LCS (act.) = 93.62 + 0.67 LCS (cal.)	$R^2 = 0.928$
Pavaskar	LCS (act.) = 70.86 + 0.78 LCS (cal.)	$R^2 = 0.490$
Inagaki	LCS (act.) = 63.45 + 0.83 LCS (cal.)	$R^2 = 0.778$
Ranking	Ito > Inagaki > Karpi > Terasaki > Pavaskar	

Matsuda's formula was not considered as it is applicable to room temperature preheat only. Ito's formula provided the best correlation with the experimental results.

DQ-125 Steel (75 and 150°F preheat temperature)

Terasaki	LCS (act.) = 56.31 + 0.71 LCS (cal.)	$R^2 = 0.448$
Karpi	LCS (act.) = 81.31 + 0.53 LCS (cal.)	$R^2 = 0.413$
Ito	LCS (act.) = 77.13 + 0.64 LCS (cal.)	$R^2 = 0.631$
Pavaskar	LCS (act.) = 67.04 + 0.65 LCS (cal.)	$R^2 = 0.465$
Inagaki	LCS (act.) = 54.29 + 0.79 LCS (cal.)	$R^2 = 0.525$
Ranking	Ito > Inagaki > Pavaskar > Terasaki > Karpi	

The reason that none of the formulae provided good correlation with the actual data appears to be the constant LCS values (100 ksi) obtained for low diffusible hydrogen content at both the preheat temperatures and for high diffusible hydrogen content at 150°F preheat temperature. Taking this aspect into consideration Ito's formula appears to calculate the LCS in DQ-125 with the best accuracy.

The applicability of the above formula to the steels in this program can be summarized as below:

For the lower strength steels tested at 75°F Ito's formula allowed accurate determination of the LCS and the following equation can be used to calculate the critical stress-

$$LCS \text{ (act.)} = 52.29 + 0.68 \text{ LCS (cal.)}$$

For the lower strength steels tested at 150°F, the following equation derived from Inagaki's formula can be employed for calculating the LCS-

$$LCS \text{ (act.)} = 53.46 + 0.56 \text{ LCS (cal.)}$$

For HSLA-100 and HSLA-130 steels Terasaki's equation provided the best correlation coefficients for both 75 and 150°F preheat temperatures.

75°F preheat temperature-

$$LCS \text{ (act.)} = -40.68 + 2.45 \text{ LCS (cal.)}$$

150°F preheat temperature-

$$LCS \text{ (act.)} = 67.70 + 0.65 \text{ LCS (cal.)}$$

For HY-130 steel tested at 75 and 150°F, Ito's equation can be employed to estimate the lower critical stress-

$$LCS \text{ (act.)} = 93.62 + 0.67 \text{ LCS (cal.)}$$

For DQ-125 steel tested at 75 and 150°F, Ito's equation provided the best coefficient of determination-

$$LCS \text{ (act.)} = 77.13 + 0.64 \text{ LCS (cal.)}$$

It is evident from the above that no single formula is able to estimate the lower critical stress in all steels in this study. The steels strengthened by copper precipitation behave differently from the remaining steels. In addition two regression lines are obtained for two preheat temperatures in copper containing steels. This implies that the existing parameter defining the remaining diffusible hydrogen content in the weldment (t_{100} in the case of Ito's and Inagaki's formulae) as a function of preheat temperature does not adequately represent the real situation. However, in the non copper strengthened steels such as DQ-125 and HY130 the cooling time from fusion temperature to 100°C appears to be sufficiently accurate. The reason for this anomaly may lie in the difference in the CGHAZ microstructures of Cu-

containing and non Cu-containing steels. It is possible that the presence of fully or partly dissolved copper precipitates and their effect on the retention of austenite pockets in the CGHAZ may enhance the actual hydrogen level in the CGHAZ thus leading to increased embrittlement of the HAZ. The above can be confirmed by carefully planned experimentation designed to provide specific information on the role of copper precipitates and their associated microstructural features. These investigations were outside the scope of the present study. Unless the underlying mechanisms are clarified it appears difficult to evolve a single formula to calculate the lower critical stress in all steels in this investigation.

4.3.5. Applicability of Carbon Equivalent Formulae

When the existing formulae to calculate the LCS are applied to the data from steels under study, Ito's and Inagaki's formulae based on P_{cm} provide the best correlations for the lower strength, and HY-130 and DQ-125 steels. However, the results from HSLA-100 and HSLA-130 are best explained by employing Terasaki's formula. Terasaki's formula is not based on any CE but the chemistry is indirectly represented by the maximum HAZ hardness. The results of the implant cracking test were also analyzed with respect to-

(a) LCS vs Carbon equivalents, P_{cm} and CE_I

(b) LCS vs Maximum HAZ Hardness, H_{max}

(c) Susceptibility Index (SI) vs CE's and H_{max}

The variation of LCS and SI with carbon equivalent, [CEN], is not presented herein as it reveals a trend similar to that observed with P_{cm}. This is due to the fact that CEN approaches P_{cm} for low carbon steels.

The variation of LCS with P_{cm} for the lower strength steels is shown Fig. 4.57. When the diffusible hydrogen content is high (20 ml/100g) and the preheat temperature is low (75°F), there is a linear decrease in the LCS with P_{cm}. At 5 ml/100g hydrogen and 75°F preheat temperature, an initial decrease in the LCS with P_{cm} is noticed, however the LCS becomes constant with a further increase in P_{cm}. The LCS does not decrease appreciably with P_{cm} at 150°F, as shown in Fig. 4.57. It should be noted that results for DQ-80 at 150°F preheat could not be obtained as the rupture occurred in the soft zone instead in the CGHAZ. No clear relationship among LCS and CE's was apparent for the lower strength steels, therefore, these results are not shown.

Fig. 4.58 illustrates the change in the LCS with CE_I for the lower strength steels. The relationship between the LCS and CE_I is essentially similar to that obtained for LCS vs P_{cm}. However, it appears that LCS and CE_I are better related than LCS and P_{cm}. The above, however, cannot be supported based on statistical parameters, as the scope of the present study included testing only at two preheat temperatures and two hydrogen levels. Any attempt to conclude the validity of one CE over the other for the steels under study based on limited data will be misleading.

Figs. 4.59 and 4.60 show the change in the LCS with H_{max} for the lower and higher strength steels respectively. It was found that in case of the higher strength steels, no definite relationship between the LCS and P_{cm} and CE_I was observed. But when the LCS is plotted as a function of H_{max}, it was possible to obtain a somewhat better correlation, as shown in Fig. 4.60. There was a slight increase in the LCS with an increase in the hardness of CGHAZ. This type of behavior, however, was not observed for the lower strength steels. In the
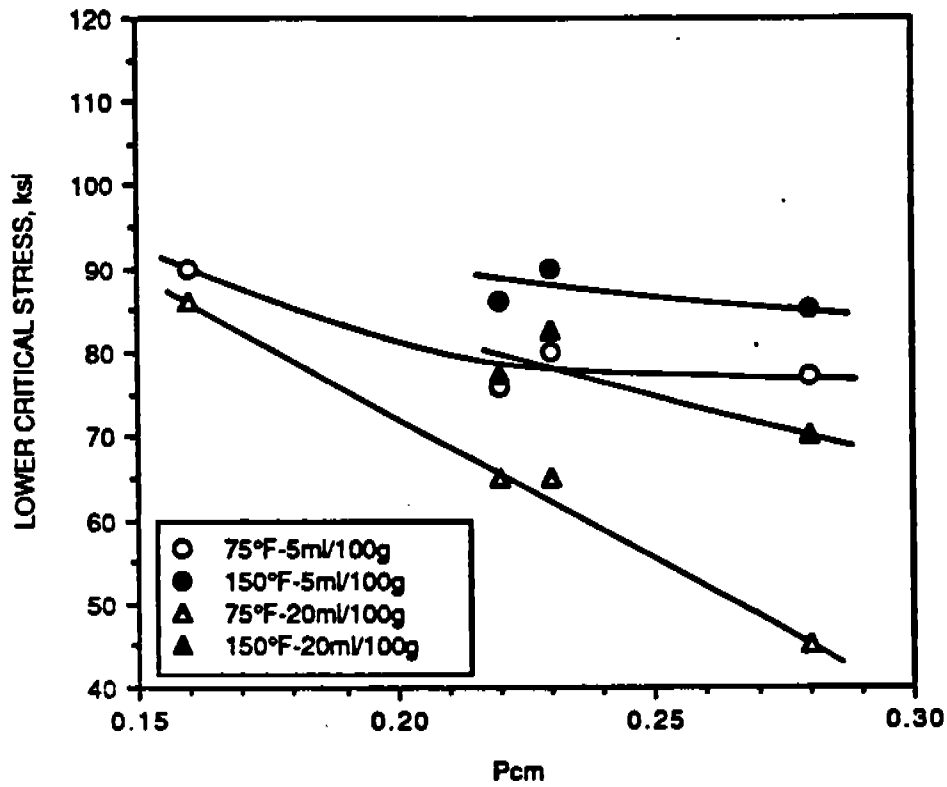
Fig.4.57. Variation of lower critical stress with P$_{cm}$ for lower strength level steels
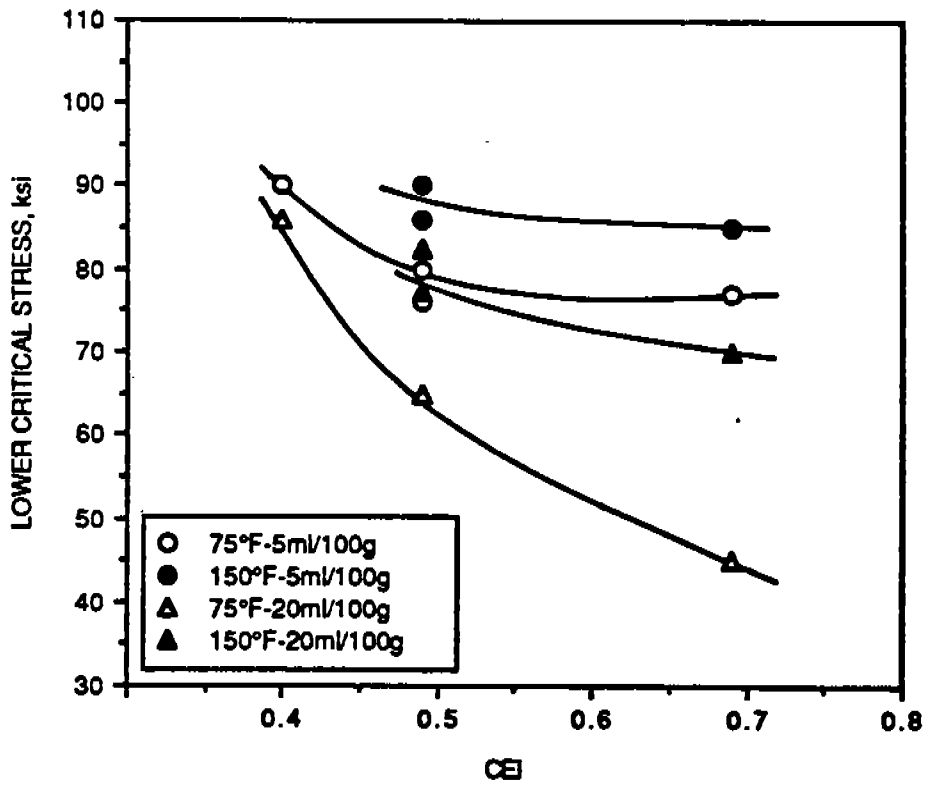
Fig.4.58. Variation of lower critical stress with CE$_I$ for lower strength level steels
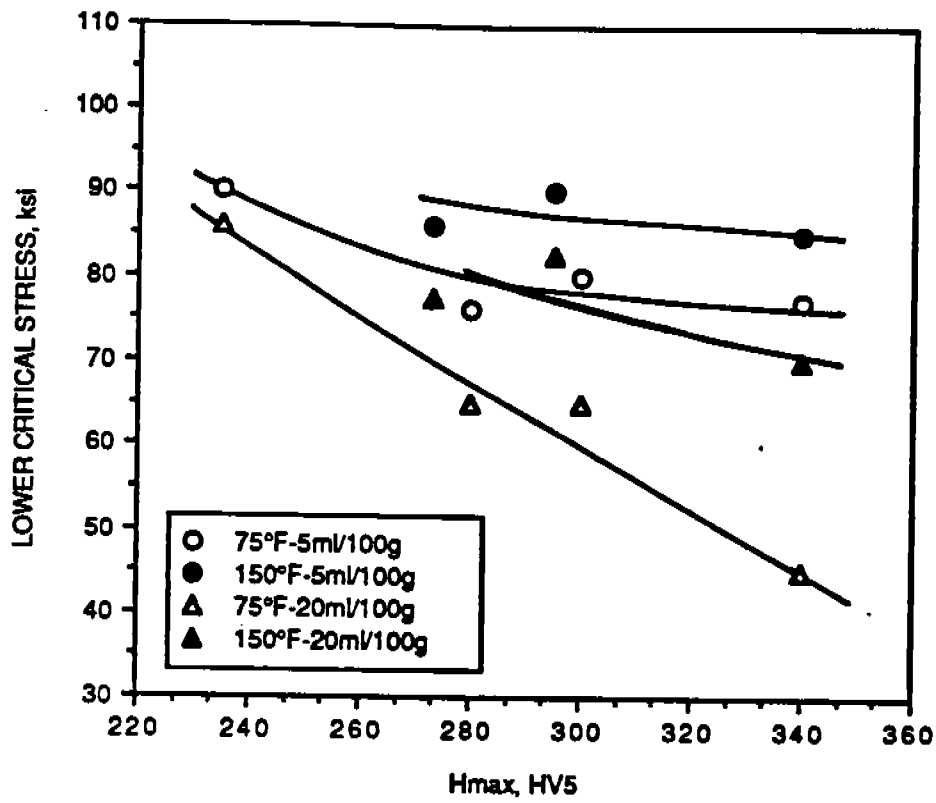
Fig.4.59. Variation of lower critical stress with H_{max} for lower strength level steels
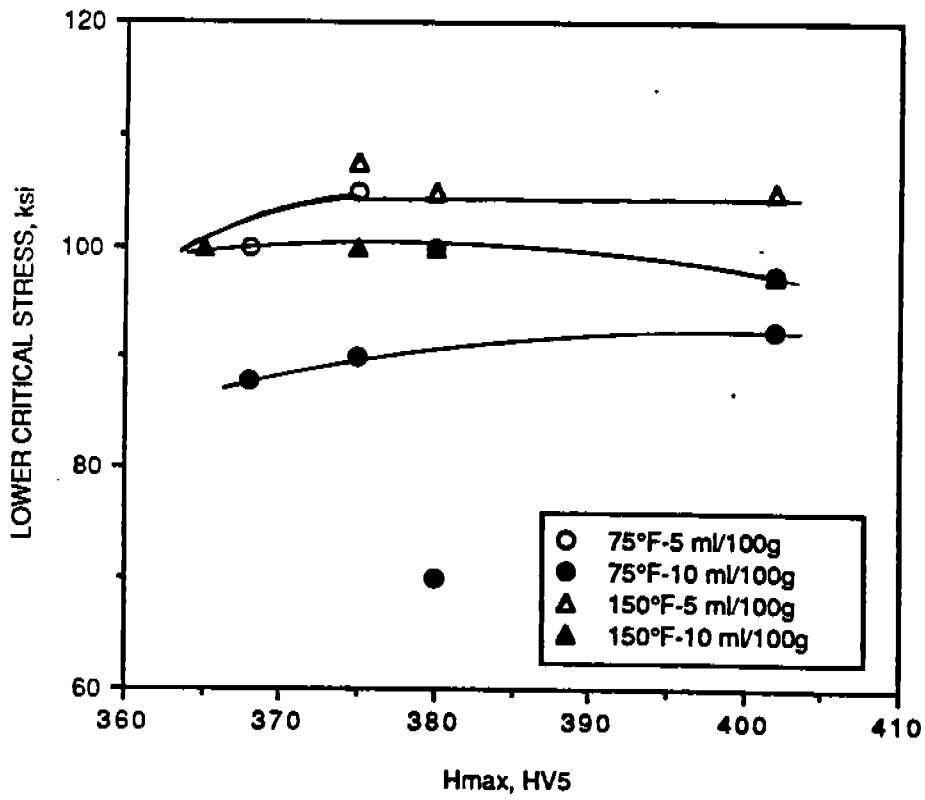
Fig.4.60. Variation of lower critical stress with H_{max} for higher strength level steels

lower strength steels, the LCS decreased with an increase in H_{max}, as shown in Fig. 4.59.

The susceptibility index (SI) is defined as-

$$SI=(NTS-LCS)/NTS$$

Table 4.4 gives the values of notched tensile strength (NTS) in the coarse grained HAZ and SI for all steels in this program. The SI represents the embrittlement of a steel to HAC, higher the SI more susceptible the steel will be to HAC. The variation of SI with P_{cm}, CE_I, and H_{max} is shown in Figs. 4.61 to 4.63 respectively. Like in the LCS vs CE's behavior, no definite relationship was observed in the SI vs CE's variation for the higher strength steels. For the lower strength steels the SI increased with CE's and H_{max} when data for 75°F at 5 and 20 ml/100g hydrogen contents were plotted. There was no significant change in the SI with either CE's or H_{max} when results at 150°F were analyzed. Fig. 4.63 shows that when the SI variation with H_{max} is considered, the SI for all conditions except 75°F-10 ml/100g shows a slight initial decrease with H_{max} and then an increase. This implies that, in general, steels DQ-125, HSLA-100, and HSLA-130 show lower SI than HY-130.

From the above discussion, it appears that no single CE can explain the results of the implant cracking test for all steels. However, CE_I was found to correlate with the observed data slightly better than P_{cm} for the lower strength steels. When the higher strength steels are considered, the use of H_{max} in explaining the experimental data was found to be better than CE's. An almost similar trend was also observed in the Battelle Underbead cracking test. However, the UT-Mod. HST provided results which are at slight variance from that observed in the implant cracking and Battelle underbead cracking tests. As mentioned earlier, the results from the Battelle and UT-Mod HS tests should not be considered conclusive because of the reasons discussed in Sections 4.3.1 and 4.3.2.

To apply the results from the implant cracking test to actual welding conditions, it is necessary to obtain a stress field parameter responsible for crack initiation. Some investigators have been successful in determining stress field parameter from theory and experiments. If the lower critical stress from the implant cracking test is greater than the stress field parameter, the probability of hydrogen assisted cracking is greatly reduced. The parameter is still difficult to calculate with a great deal of confidence as it depends on the groove geometry, bead length, yield strength of the material etc. In this study, the steels are ranked approximately by considering the ratio of the lower critical stress and yield strength. The magnitude of maximum residual stress in a welded geometry attains a value equal to the yield strength of the material, therefore, the data from the implant cracking test can also be used to compare various steels based on the ratio of LCS and YS. If the ratio of LCS to YS is one or greater than one, the steel can be safely welded under the welding conditions and hydrogen levels employed during the implant test. The variation of LCS/YS ratio with hydrogen content at 75 and 150°F preheat temperatures for all the steels in this program are shown in Figs. 4.64 and 4.65 respectively. It may be noticed that in DQ-80 tests at 150°F, rupture during the implant cracking test occurred in the soft zone rather than in the CGHAZ, therefore, the LCS under this condition is taken as the rupture strength of the soft zone, as it approximately represents the lower limit of potential hydrogen assisted cracking. The LCS/YS ratio for DQ-80 at 75°F preheat temperature is greater than that at both hydrogen levels, thus implying that this steel can be easily welded at room temperature even with a diffusible hydrogen content up

147

Table 4.4 Susceptibility Index of Steels

Steel	NTS (ksi)	Preheat Temp(°F)	Hydrogen Content (ml/100g)	Susceptibility Index
HSLA-80-1	213	75	5	0.643
		150	5	0.596
		75	20	0.695
		150	20	0.636
HSLA-80-2	224	75	5	0.643
		150	5	0.598
		75	20	0.710
		150	20	0.632
HSLA-80-M	213	75	5	0.638
		150	5	0.601
		75	20	0.789
		150	20	0.671
HSLA-100	246	75	5	0.593
		150	5	0.573
		75	10	0.715
		150	10	0.593
HSLA-130	257	75	5	0.591
		150	5	0.582
		75	10	0.650
		150	10	0.611
HY-130	275	75	5	0.645
		150	5	0.618
		75	10	0.664
		150	10	0.645
DQ-125	259	75	5	0.614
		150	5	0.614
		75	10	0.660
		150	10	0.614
DQ-80	145	75	5	0.379
		150	5	*
		75	20	0.407
		150	20	*

* Not Determined
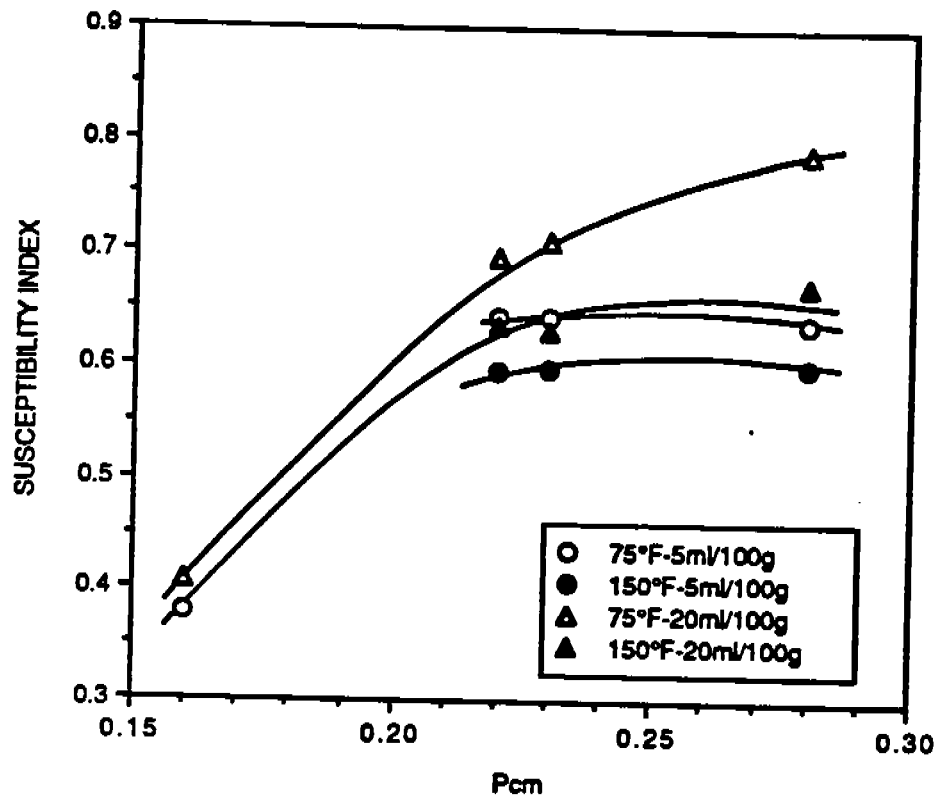
Fig.4.61. Variation of susceptibility index with P_{cm} for lower strength level steels
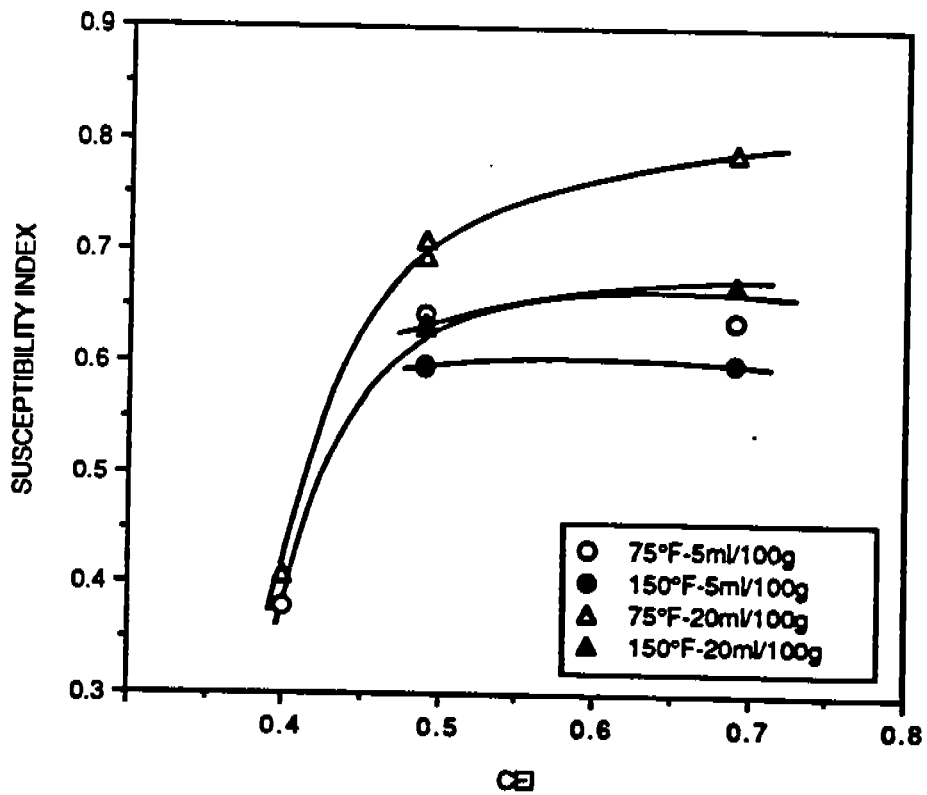
Fig.4.62. Variation of susceptibility index with CE_I for lower strength level steels
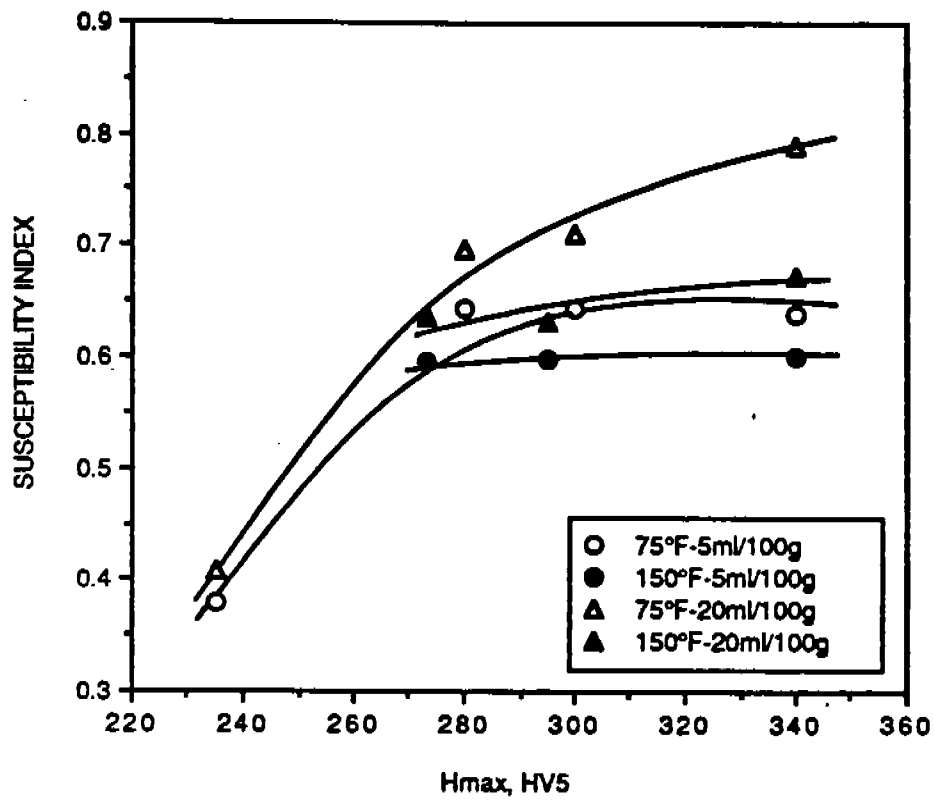
Fig.4.63. Variation of susceptibility index with H_{max} for lower strength level steels
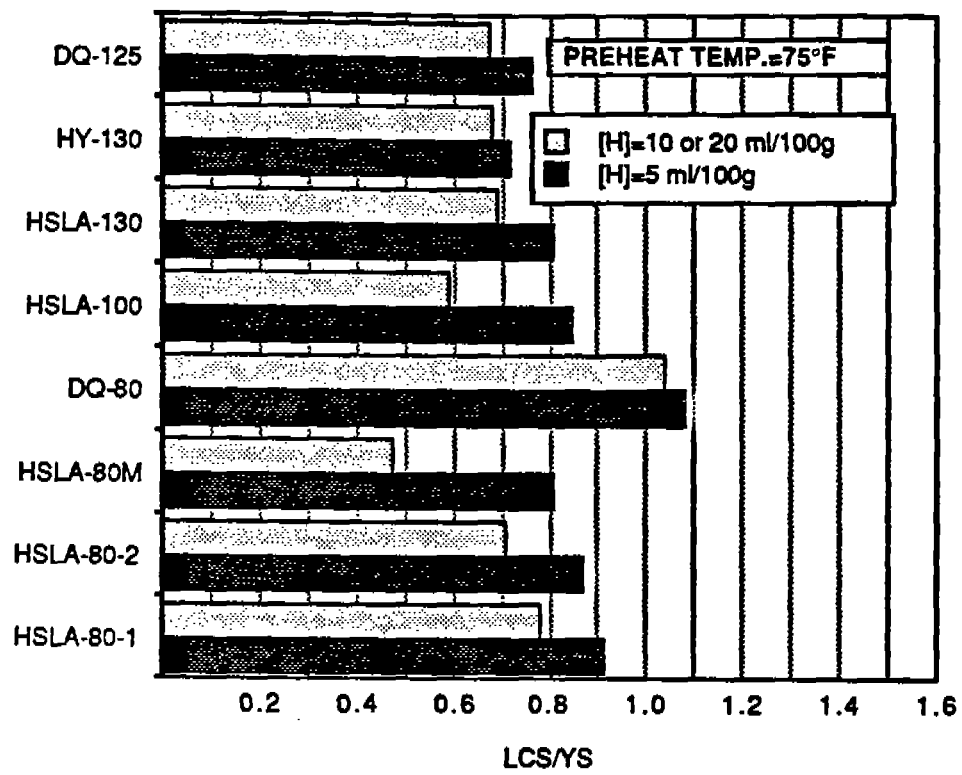
Fig.4.64. Comparison of LCS/YS ratio for different steels at 75°F preheat temperature
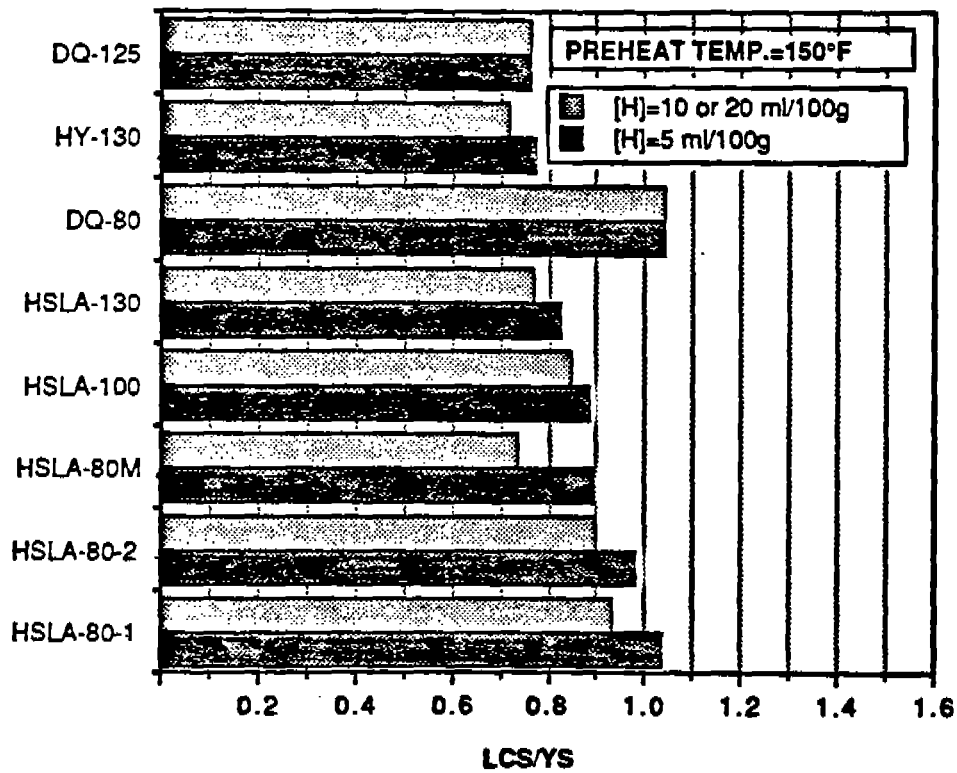
Fig.4.65. Comparison of LCS/YS ratio for different steels at 150°F preheat temperature

151

to 20 ml/100g. However, for all the remaining steels, the LCS/YS ratio is less than one, therefore, precautions must be taken by way of either reducing the diffusible hydrogen or increasing the preheat temperature. At 150°F preheat temperature and 5 ml/100g diffusible hydrogen content, LCS/YS ratio for HSLA-80-1 becomes greater than one and therefore, can be welded safely at 150°F only when the hydrogen content is about 5 ml/100g. But under similar conditions steels HSLA-80-2 and HSLA-80M may be prone to cold cracking. It is interesting to note that the LCS/YS ratio for low CE steels (lower strength level steels) generally shows a significant improvement when the preheat temperature is increased, but the ratio in the higher strength level steels (higher CE's) remains relatively insensitive to both hydrogen content and preheat temperature. On the face of it the above observation implies that it is more difficult to obtain crack-free welds in the higher strength steels. However, on the contrary it is found that these steels have greater resistance to cold cracking despite having higher CE's. It is experimentally observed than in highly alloyed steels the residual stresses may remain appreciably lower than the yield strength and therefore, even at apparent LCS/YS ratios less than one, the steels can be welded safely. Karpi et al [85] also observed a similar phenomenon and attributed this to the lower austenite to martensite transformation temperature and larger transformation expansion in steels containing higher amounts of alloying elements

4.3.6. Preheat Requirement to Avoid Hydrogen Assisted Cracking

The ranking of all steels based on susceptibility index and LCS/YS ratio is similar. However, when the steels are compared with respect to LCS/YS ratio, it becomes possible to roughly estimate the preheat temperature to prevent cold cracking in a highly restraint weld joint. These estimates are approximate as the scope of the investigation was to evaluate the implant cracking data at only 75 and 150°F preheat temperatures. Further confirmation of the estimates can only be possible by generating data at more preheat temperatures and hydrogen levels.

The AC-50 steel did not show any hydrogen assisted cracking in both the UT-Modified and Implant Cracking tests, therefore, it can be inferred that AC-50 would be weldable at room temperature even with high hydrogen electrodes.

The DQ-80 steel can be safely welded at room temperature (probably the lowest preheat temperature could be as low as 32°F-indicated by the UT-Modified test results) and up to 20 ml/100g hydrogen. However, to prevent the hydrogen assisted cracking in HSLA-80-1, a preheat temperature of 150°F at 5 ml/100g hydrogen appears to be required. At greater than 5ml/100g hydrogen content, a preheat temperature higher than 150°F should be used. For HSLA-80-2 and HSLA-80M a preheat temperature higher than 150°F at 5ml/100g hydrogen is indicated by the present data.

Since HSLA-130 is being considered for certain structures as a replacement for HY-130, it is interesting to compare these two steels in terms of preheat temperature requirement. The required preheat temperature to avoid cold cracking in HY-130, according to Bailey [88], is 300°F when the hydrogen content of the weldment is 14 ml/100g. The comparison of LCS/YS for HSLA-130 and HY-130 at 10 ml/100g hydrogen level with 75 and 150°F preheat, reveals that HSLA-130 is less sensitive to cracking than HY-130, thus a preheat temperature lower than 300°F will be required to safely weld HSLA-130. At lower hydrogen contents (e.g. 5ml/100g), the sensitivity of HSLA-130 is significantly reduced as compared to HY-130, therefore, a preheat temperature considerably less than 300°F would be required to obtain crack-free welds in HSLA-130. The preheat temperature requirement for HSLA-100 is lower than

HSLA-130 except when HSLA-100 is welded at higher hydrogen contents. The DQ-125 is less sensitive to HAC than HY-130 but it is more susceptible than HSLA-130 and HSLA-100.

In summary, the following ranking of steels in this program can be derived in terms of preheat temperature requirement to prevent hydrogen assisted cracking:

If the critical preheat temperatures for DQ-80 and HSLA-80-1 are taken as 75 and 150°F at hydrogen contents up to 20 ml/100g, then the remaining steels in the lower strength steels can be qualitatively ranked as below-

DQ-80<HSLA-80-1<HSLA-80-2<HSLA-80M

If the critical temperature of HY-130 at high hydrogen content is considered as 300°F, the ranking for the higher strength steels in terms of preheat temperature required to avoid cold cracking is given below-

HSLA-100<HSLA-130=DQ-125<HY130

In order to determine the exact critical preheat temperatures for steels in this program, further testing at different preheat temperatures is required.

4.4 CONCLUSIONS

The following main conclusions can be derived from the results presented in this Section-

(1) The Hardness Control and Hydrogen Control approaches to estimate the preheat temperature for crack-free welds cannot be used for steels in this program because of inherent limitations. These approaches do not take into account the influence of finer grain size (due to TMCP) and shape controlled non-metallic inclusions in decreasing the hardenability. Therefore, the estimated preheat temperatures from the approaches may be overly conservative for modern steels.

(2) The steels in this program were tested for their susceptibility to hydrogen assisted cracking by the Battelle Underbead Cracking, UT-Modified Hydrogen Sensitivity, and Implant Cracking tests. In the Battelle test no true hydrogen assisted underbead cracking was observed in any of the steels. The cracks appeared to initiate in the weld metal and propagate into the heat affected zone. The cracks in the HAZ were transverse to the fusion line. On the other hand, in the UT-Modified test, no cracks were observed in the fused zone but cracking occurred in the HAZ. The cracking was intergranular in nature. Steels DQ-80, AC-50, DQ-125 and HSLA-80M did not show cracking even at 32°F preheat temperature and 4% strain. In general, the results of the two tests agreed in terms of ranking of the materials.

(3) The trend observed in the Battelle and UT-Modified tests was also evidenced in the Implant Cracking tests. The AC-50 steel did not rupture in the CGHAZ but the failure took place in the soft zone. A similar behavior was also noticed for DQ-80 when tested at 150°F preheat temperature. However, DQ-80 ruptured in the CGHAZ at 75°F preheat temperature. The lower critical stress in HSLA-80M and HSLA-100 dropped appreciably when tested at 75°F and 20 and 10 ml/100g hydrogen content respectively. This was believed to be due to the presence of a susceptible microstructure in the CGHAZ containing retained austenite or austenite-martensite packets in a predominantly martensitic structure. The secondary constituents may retard the diffusion of hydrogen and thus lead to increased susceptibility. The HSLA-130 steel having almost the same composition as HSLA-100 did not show a rapid drop in the LCS under similar conditions of testing. This was attributed to the presence of a finer grain size in the base plate and a finer distribution of epsilon-copper precipitate as contrasted to that in HSLA-100.

153

(4) The cracking in the Implant test initiated in the CGHAZ and propagated into the weld metal in all steels except HSLA-80M, where the cracking was confined to the CGHAZ. The fracture surface examination revealed that the cracks propagated in an intergranular fashion in HSLA-80M, while in the remaining steels the cracks followed a mixed mode-intergranular and quasi-cleavage.

(5) Several published formulae to calculate the lower critical stress in the Implant tests were analyzed and their applicability to the data from steels in this study assessed. None of the formulae predicted LCS with acceptable accuracy. However, when data were categorized according to the lower strength and the higher strength steels, and considered individually at 75 and 150°F preheat temperatures, some of the formulae allowed calculation of LCS with acceptable accuracy. Two separate regression lines, converging at higher LCS (i.e. low hydrogen content) and corresponding to 75 and 150°F, were obtained. This indicated that for copper containing steels, thermal factor for hydrogen diffusion may be at variance from the conventional steels. Therefore, there is a need to determine the thermal factor for copper-containing steels.

(6) From the implant tests, the variation of LCS and susceptibility index (SI) with CE's (P_{cm} and CE_I) and H_{max} was evaluated. Carbon equivalent, CE_I, was found better than P_{cm} for the lower strength steels, whereas, H_{max} was better than CE's for the higher strength steels. A similar trend was also observed for the Battelle and UT-Modified test results.

(7) The data from the present investigation is limited and not sufficient to calculate the critical preheat temperature to avoid cold cracking . However, an approximate estimation can be provided when the ratio LCS/YS is compared for different steels. If LCS/YS ratio is equal or greater than one, the steel can be welded safely under the test conditions. The AC-50 and DQ-80 steels can be welded safely at room temperature preheat and hydrogen level up to 20 ml/100g. A minimum preheat temperature of 150°F will be required for HSLA-80-1 to prevent risk of cracking. The HSLA-80-2 and HSLA-80M will require a preheat temperature greater than 150°F.

Since a preheat temperature of 300°F is required (obtained from literature) for sound welds in HY-130 at high hydrogen levels, the other steels belonging to the higher strength category will require significantly lower preheat temperature than 300°F, as indicated by the ratio LCS/YS. The higher strength steels can be ranked in the order of increasing critical preheat temperature-
HSLA-100<HSLA-130<DQ-125<HY-130

Thus using HY-130 in place of HSLA-130 will result in a definite improvement by decreasing the preheat temperature for safe welding.

5. HAZ SOFTENING

5.1. INTRODUCTION

The introduction of the TMCP in steel production has enhanced the resistance of the weld HAZ in such steels to hydrogen assisted cracking by reducing the carbon equivalent while maintaining or even improving mechanical properties when compared to conventional steels. The attractive properties in such steels are obtained by controlled rolling and/or accelerated cooling. These manufacturing operations leave the material with considerable stored energy. This energy is released and the effect of TMCP is partly or fully erased when the steels are either welded and/or heat treated.

In a weldment, the HAZ consists of several sub-zones. Each sub-zone in the HAZ is characterized by a different microstructure and hence different mechanical properties. The zone immediately adjacent to the fusion boundary experiences the highest peak temperature and austenite grain growth takes place. Austenite grain growth depends on the amount and type of micro-alloying addition. Easterling has compiled a time/temperature precipitate dissolution diagram for the commonly used micro-alloy carbides and nitrides (Fig. 5.1) [22]. TiC appears to be the most stable and VC the least during a welding thermal cycle. The HAZ zone nearest to the fusion line is referred as the coarse grained HAZ and corresponds to an average peak temperature of 2400°F. The microstructure in this zone is controlled by the chemical composition (represented by carbon equivalent) and welding parameters. The CGHAZ is of paramount importance not only from the point of view of mechanical properties such as strength and toughness but also for its susceptibility to hydrogen assisted cracking and stress relief cracking.

The region corresponding to an average peak temperature of 1750°F represents the fine grain HAZ (FGHAZ). During the on-heating portion of a FGHAZ thermal cycle, ferrite transforms to austenite and sufficient time is not available for the austenite grains to grow, therefore, the grain size in this zone remains small or is refined. Consequently during the austenite transformation in the on-cooling portion of the cycle, a fine grained microstructure results. In micro-alloyed steels the FGHAZ is quite wide because of more effective grain boundary pinning as the carbides and nitrides present do not dissolve at these temperatures. From Fig. 5.1, it is clear that most of the carbides and nitrides are thermodynamically stable in the FGHAZ. Therefore, the width of the FGHAZ will depend on the number density of precipitates and not on the type of carbides or nitrides.

A thermal cycle with peak temperature of 1450°F defines the HAZ heated between the critical temperatures (A_1-A_3) and is known as the intercritical HAZ (ICHAZ) or partly refined zone. Thermal cycles with temperatures less than the A_1 temperature represent subcritical HAZ (SCHAZ) exposure. Unlike in CGHAZ, FGHAZ, and ICHAZ, no transformation takes place in the SCHAZ. However, during intercritical and subcritical exposures, the recovery and recrystallization processes occur and the completeness of these processes depends mainly on the type of steel, thermomechanical processing and welding heat input. For example, recrystallization behavior during a thermal cycle is affected by whether the original material was cold rolled, and cold rolled and control cooled, or is in the annealed condition.

A region in the HAZ having a lower hardness than the base metal is termed the "soft" zone. The soft zone has been shown to possess poor tensile properties (Fig. 5.2) [89]. Increased fatigue crack growth rate in the HAZ is also directly related to the presence of a soft zone [89]. Moreover, the presence

155
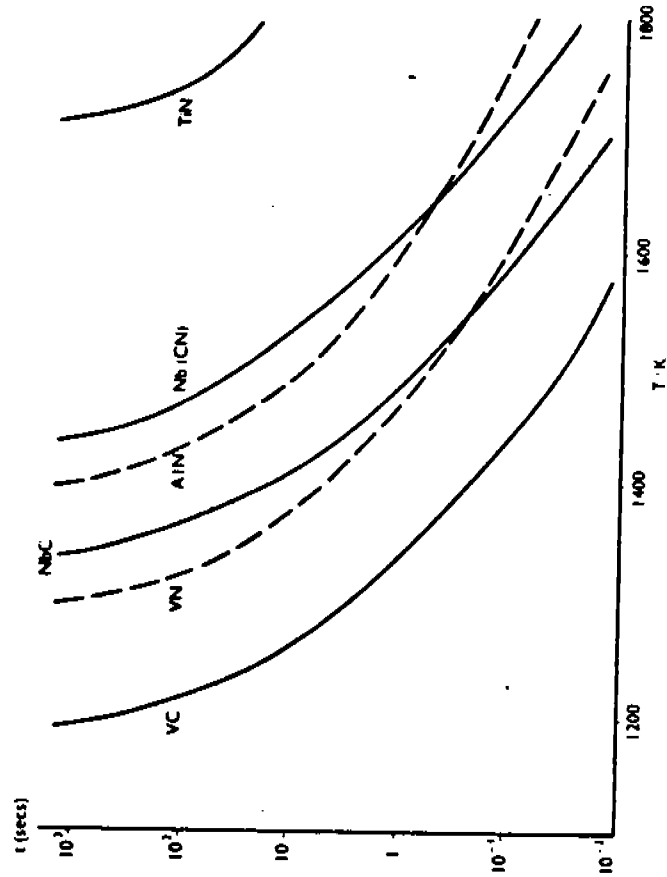
Fig.5.1. Time-Temperature-Precipitate dissolution diagram for commonly used microalloyed carbides and nitrides [22]
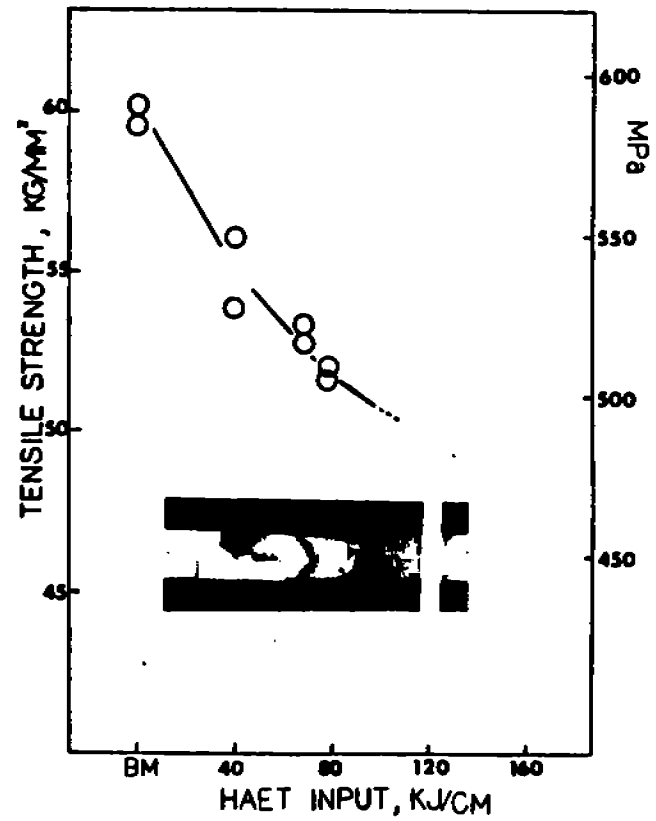
Fig.5.2. Decrease in the tensile strength of the "soft" zone with increase in heat input
[77]

of a soft zone in a welded structure may limit the design strength to a lower value and influence strain distribution during subsequent fabrication or in service. In the copper containing steels the complete of partial dissolution of epsilon copper precipitates may also contribute to a decrease in hardness in addition to that due to recrystallization.

Since the steels in this program are thermo-mechanically control processed and five of them derive their strength from copper precipitation, it was decided to investigate the effect of heat input on the soft zone characteristics.

5.2. EXPERIMENTAL PROCEDURE

The bead-on-plate welds employed for measuring the maximum HAZ hardness as described in Section 3 were used to determine the hardness profile across the HAZ. Only data for welds deposited by the shielded metal arc process were analyzed. Therefore, the variation in heat input is from 15 to 154 kJ/in. Samples were heat treated at 1000°F for one hour to study the effect of postweld heat treatment on the soft zone in steels strengthened by epsilon-copper and non-copper containing steels. Samples were also examined for microstructural changes brought about by increasing heat input.

5.3. RESULTS AND DISCUSSION

The HAZ hardness profiles in HSLA-80-1(Fig. B-1 to B-6), HSLA-80-2 (Fig. B-9 to B-14), DQ-80 (Fig. B-17 to B-22), DQ-125 (Fig. B-25 to B-31), AC-50 (Fig. B-34 to B-39), and HSLA-100 (Fig. B-42 to B-48) as a function of heat input are given in Appendix B. The bead shape and location of hardness measurement is also provided as an inset.

In the present set of steels a soft zone was observed in HAZ's of HSLA-80-1, HSLA-80-2, DQ-80, DQ-125, and AC-50 only. The remaining steels such as HSLA-80M, HSLA-100, HSLA-130, and HY-130 did not show any softening in the HAZ. The HAZ in these latter steels is characterized by the presence of a fully martensitic structure and any effect of recrystallization, recovery, or dissolution of copper precipitate on the HAZ hardness seems to be overshadowed by the dominant influence of martensite.

Typical microhardness distribution across the HAZ from fusion boundary to the unaffected base metal for HSLA-80-1 at three different heat inputs is shown in Fig. 5.3. It is noted that for longer cooling times (e.g. 39.6 sec. for HSLA-80-1) even the CGHAZ tends to becomes softer than the base metal. This was observed in all the steels prone to HAZ softening except AC-50. The reason for this anomalous behavior will be discussed later.

In order to define the characteristics of the soft zone two parameters were determined from the HAZ hardness profiles-(a) soft zone width, defined as the linear distance in mm over which the hardness is less than the base metal hardness, (b) ΔH, the difference between the base metal hardness and the minimum HAZ hardness.

The increase in the width of the soft zone with $t_{8/5}$ for the five susceptible steels is shown in Fig. 5.4. The soft zone width increases linearly with $t_{8/5}$ in all steels. However, the rate of increase in the soft zone width depends on the type of steel and may reflect the differences in stored energy, initial grain size, chemical composition, amount and distribution of inclusions. All of these factors influence recovery and recrystallization kinetics.

The variation of ΔH with $t_{8/5}$ is shown in Fig. 5.5. ΔH increases rapidly with cooling time and tends to approach a saturation value, ΔH_S, at longer cooling times. The saturation value of ΔH does not appear to be a simple function of carbon equivalent, as DQ-80 (P_{cm}-0.16) shows a much higher ΔH_S than AC-50

158
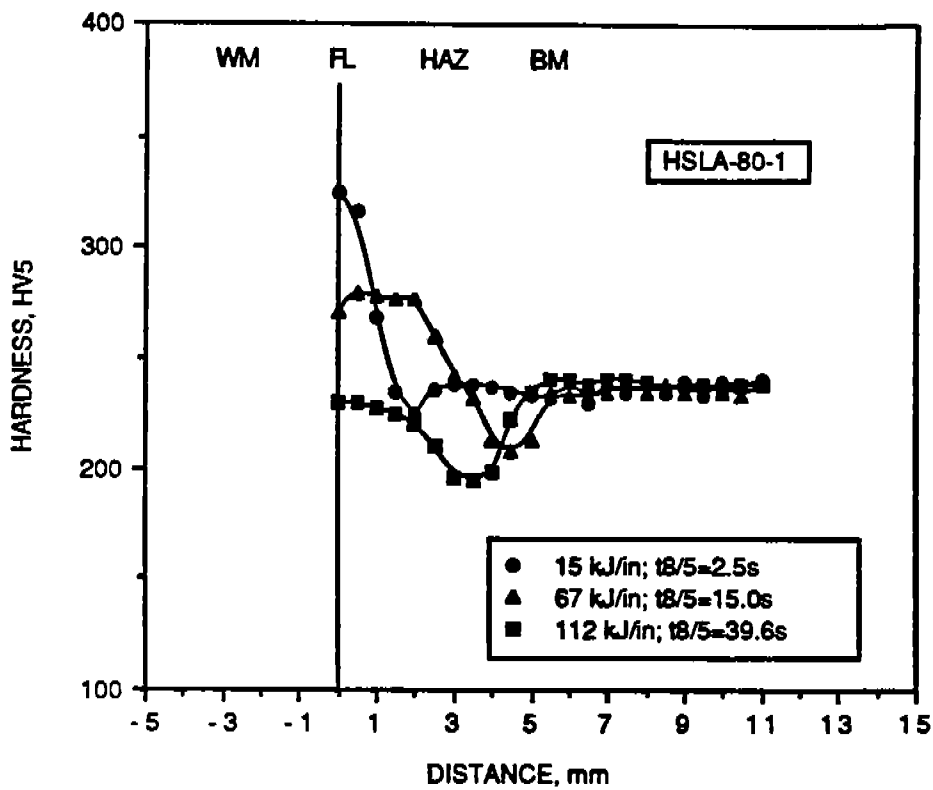
Fig.5.3. Typical microhardness distribution across HAZ from fusion line to the unaffected base metal for HSLA-80-1 at three different cooling times (800 to 500°C)
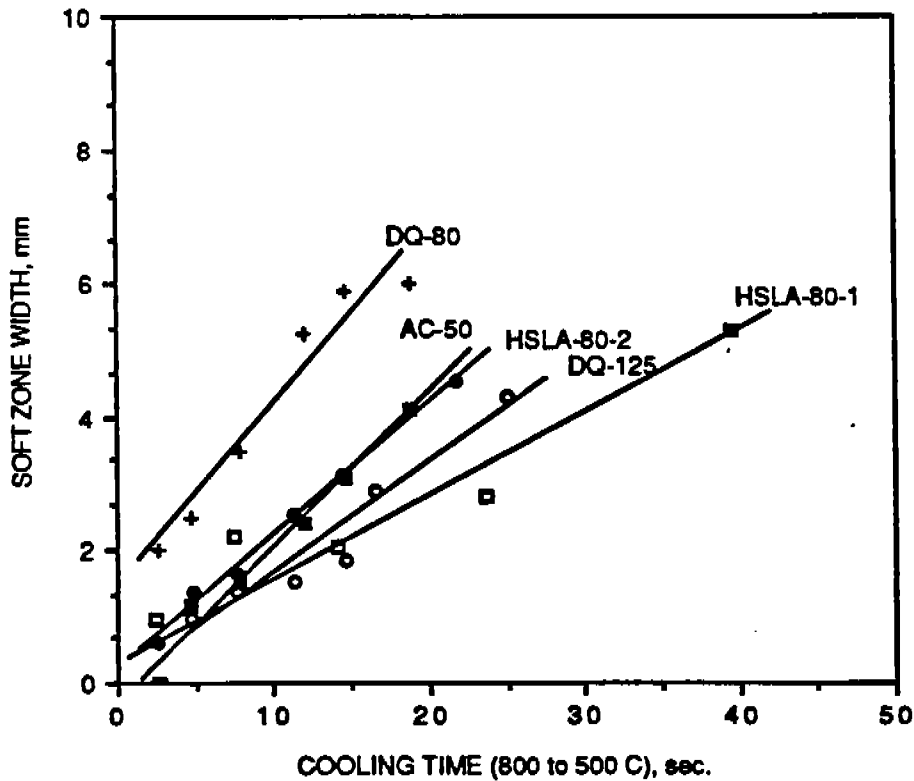
Fig.5.4. Linear increase in the "soft" zone width with cooling time

159
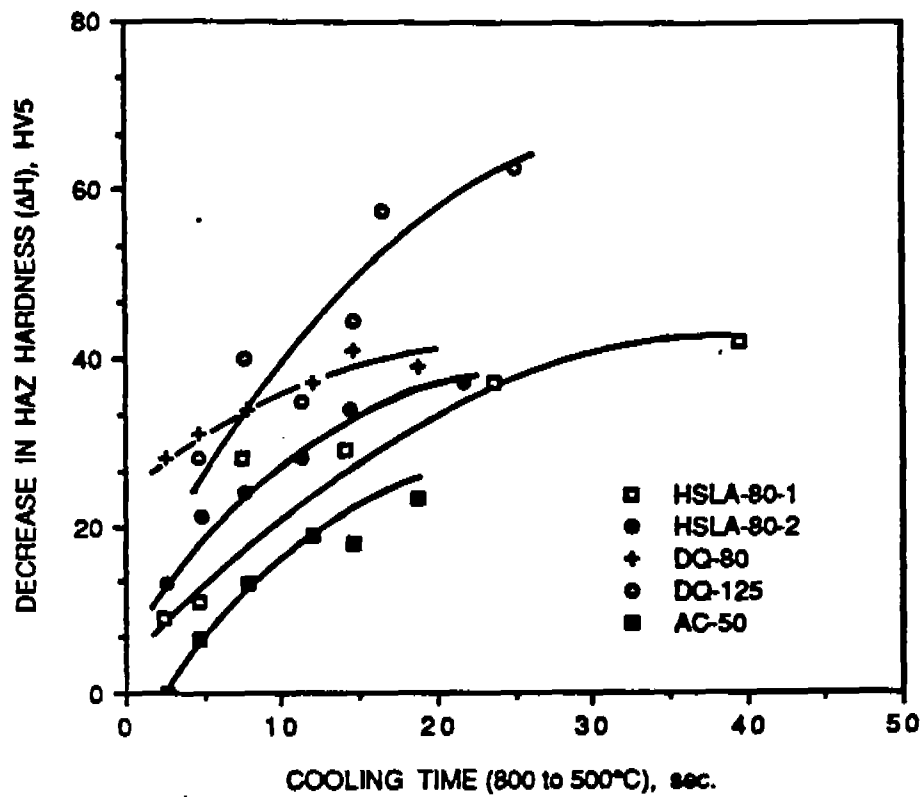
Fig.5.5. Variation of ΔH with cooling time for the five steels susceptible to HAZ softening
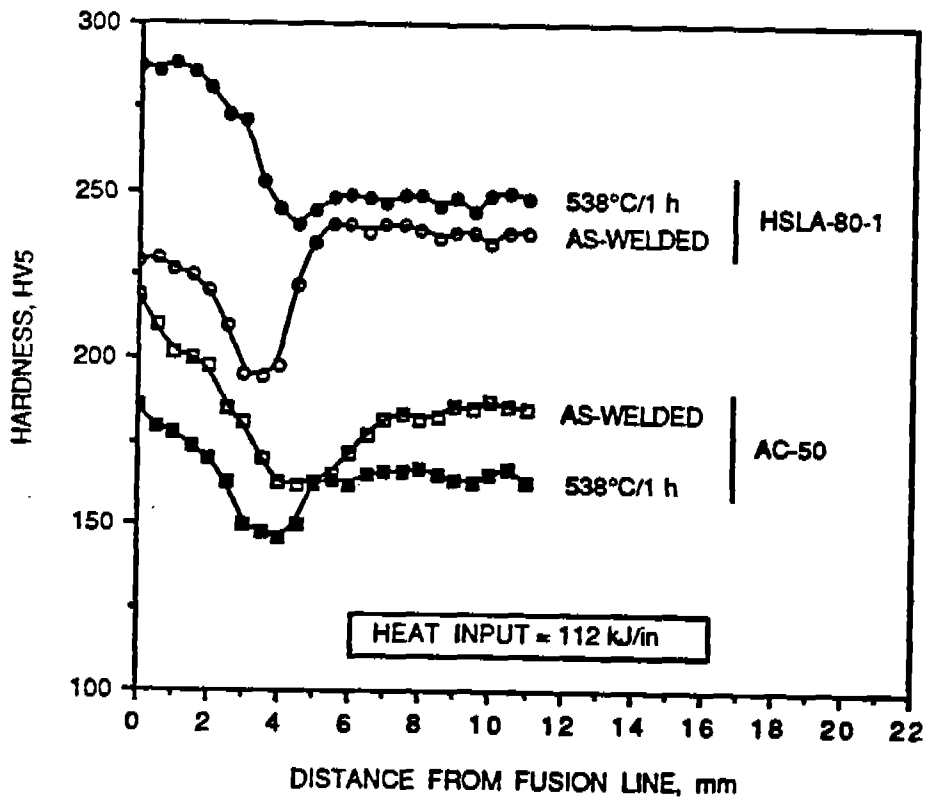
Fig.5.6. HAZ hardness profiles for HSLA-80-1 and AC-50 in the as-welded and PWHT condition

160

(P_{cm}-0.16), HSLA-80-1 (P_{cm}-0.22) and HSLA-80-2 (P_{cm}-0.23). However, as reported by other investigators [89], the minimum HAZ hardness achieved in the soft zone is directly proportional to the carbon equivalent, and increases with an increase in the carbon equivalent. Prior thermo-mechanical history of the steel also seems to play an important role along with carbon equivalent in defining ΔH_S. In the copper-added steels there appears to be an additional contribution to ΔH from precipitate dissolution besides recrystallization. Therefore, it is appropriate to discuss separately the steels containing copper and the copper-free steels. For example, when ΔH vs $t_{8/5}$ behaviors for non-age hardenable steels, DQ-125 and AC-50, are compared it is found that DQ-125 with the higher CE softens more rapidly than AC-50 having a lower CE and achieves a much higher ΔH_S value than AC-50. However, the same is not true when copper strengthened steels are compared. DQ-80 with a lower CE softens more quickly than HSLA-80-1 and HSLA-80-2 with higher CE's. This implies that the TMCP employed in the production of DQ steels leaves the steel matrix with more stored energy than either quenching (in HSLA steels) or accelerated cooling (in AC-50). Therefore, ΔH_S appears to be directly proportional to the magnitude of stored energy in the steel.

In AC-50, the CGHAZ hardness (Fig. 3.29) even at long cooling times remains significantly above the base metal hardness contrary to the observations in the other steels prone to softening. This anomalous behavior can be explained on the basis of ΔH_S and carbon equivalent. The CGHAZ hardness in the lower shelf of the hardness vs $t_{8/5}$ curve is controlled by the carbon equivalent whereas the base metal hardness is a function of microstructure (due to TMCP) and CE. If the CE of a steel is low and its strength (or hardness) is increased considerably by the application of TMCP, the CGHAZ hardness will eventually become lower than the base metal, as is the case with the other four steels in which HAZ softening was detected. The lowest value of ΔH, obtained for AC-50 (Fig. 5.5) confirms the above argument.

In the copper strengthened steels, it is possible to eliminate the soft zone by PWHT at elevated temperatures. Fig. 5.6 shows a typical HAZ hardness distribution in HSLA-80-1 in the as-welded and aged condition. The soft zone disappears almost completely and there is an increase in hardness throughout the HAZ and unaffected base metal in HSLA-80-1. Fig. 5.6 also illustrates the HAZ hardness profiles in AC-50. It is observed that the softening becomes more pronounced and the hardness decreases throughout the HAZ and base metal in AC-50 as opposed to HSLA-80-1 where the opposite was noticed. In the HSLA steels the hardness increase upon PWHT is due to the reprecipitation of epsilon-copper, but the absence of a similar phenomenon in AC-50 leads to a decrease in hardness because of the release of stored energy at elevated temperatures.

Another interesting observation is made when comparing the behaviors of HSLA-80-1 and AC-50. In AC-50, the hardness curve is shifted to lower hardness values by a constant amount throughout the HAZ and base metal, but this is not true in HSLA-80-1. A significant increase in the hardness was observed in the CGHAZ adjacent to the fusion boundary upon heat treatment but the difference in hardness from the as-welded condition decreases gradually as the distance increases from the fusion boundary until it becomes constant in the unaffected base metal. This can be understood on the basis of the extent of dissolution of copper precipitate during a welding thermal cycle experienced in different regions of the HAZ. In the CGHAZ, complete dissolution of epsilon-copper precipitate is expected but away from the fusion

161

boundary the dissolution may not be complete. This is why the maximum increase in hardness is observed in the CGHAZ region after PWHT. If the aging treatment is continued for a longer period, the hardness of the CGHAZ should decrease. This was observed by some investigators [90] when they found an improvement in the SRC susceptibility for an overaged CGHAZ as opposed to CGHAZ which was heat treated for shorter durations. A similar improvement in the toughness is also noticed in the overaged CGHAZ of the copper containing steels [90]. In the ICHAZ and SCHAZ, a partial dissolution of the copper precipitate is expected as the peak temperature is not high. Therefore, on PWHT a smaller increase in hardness is observed. In the base metal the hardness may increase or decrease on PWHT depending on whether the copper precipitate are underaged or overaged. In the HSLA-80-1 steels the copper precipitates appear to be underaged as a further increase in the base metal hardness was observed on aging.

The PWHT of copper strengthened steels should be used with caution as these steels have been shown to posses considerable susceptibility to reheat cracking and may suffer HAZ toughness degradation [2].

5.4. CONCLUSIONS

(1) Low carbon equivalent TMCP steels exhibited HAZ softening. However, high CE quench hardenable steels do not show a soft zone in the HAZ.

(2) The width of the soft zone increases linearly with an increase in cooling time from 800 to 500°C. The difference between the base metal hardness and the minimum HAZ hardness in the soft zone was found to be a function of steel making process and carbon equivalent.

(3) The soft zone disappeared in HSLA-80-1 on PWHT due to the reprecipitation of epsilon-copper, but a further decrease in HAZ hardness was observed in AC-50, a steel not precipitation strengthened.

(4) The hardness of a specific region in the HAZ of epsilon-copper strengthened steel after PWHT was found to depend on the state of the copper precipitate after the welding thermal cycle in the as-welded condition. A maximum increase in hardness after PWHT was observed in the CGHAZ, as in this region complete resolution of the epsilon-copper precipitate is expected upon thermal cycling during welding.

162

6. SUMMARY

The program to investigate the weldability of low carbon micro-alloyed steels for marine structures was instituted with a view to studying the following nine steel:

(1)	HSLA-80-1	(C-0.044%;	CE(IIW)-0.46;	P_{cm}-0.22)
(2)	HSLA-80-2	(C-0.062%;	CE(IIW)-0.48;	P_{cm}-0.23)
(3)	HSLA-80M	(C-0.057%;	CE(IIW)-0.64;	P_{cm}-0.28)
(4)	HSLA-100	(C-0.072%;	CE(IIW)-0.75;	P_{cm}-0.33)
(5)	HSLA-130	(C-0.070%;	CE(IIW)-0.77;	P_{cm}-0.34)
(6)	DQ-80	(C-0.032%;	CE(IIW)-0.31;	P_{cm}-0.16)
(7)	DQ-125	(C-0.11%;	CE(IIW)-0.56;	P_{cm}-0.25)
(8)	HY-130	(C-0.12%;	CE(IIW)-0.78;	P_{cm}-0.32)
(9)	AC-50	(C-0.079%;	CE(IIW)-0.32;	P_{cm}-0.16)

The carbon content of the steels ranged from 0.032 (DQ-80) to 0.12% (HY-130) and the yield strength varied from 64 (AC-50) to 136 ksi (HY-130). The range of variation in carbon equivalent, CE(IIW), was 0.31 (DQ-80) to 0.78 (HY-130) and that for P_{cm} was 0.16 (AC-50 and DQ-80) to 0.34 (HSLA-130). The first six steels contained copper greater than 1 wt% and the strength in these steels was derived in part from the precipitation of epsilon copper. The remaining three steels; DQ-125, HY-130, and AC-50, were not precipitation strengthened.

The HSLA steels were austenitized, rolled and quenched. A subsequent heat treatment was provided to precipitation strengthen these steels. The base plate microstructures in HSLA-80-1 and HSLA-80-2 was predominantly ferritic with granular bainite as the minor constituent. However, granular bainite was the major constituent in the HSLA-80M steel. The granular bainite is differentiated from bainite based on the microstructural differences. Granular bainite consists of packets of ferrite laths with non-cementite, interlath, second phase particles. These have been identified as retained austenite or austenite-martensite. The base plate microstructure of HSLA-100 and HSLA-130 was essentially similar and consisted of a predominantly martensitic structure. The DQ steels were produced by a direct quench process and DQ-80 was subsequently aged to precipitate epsilon-copper. However, DQ-125 did not undergo a similar heat treatment but the strength in this steel was achieved by an optimum combination of microstructure and carbon content. The Direct Quench process, in principle, consists of rapid quenching of steel to a temperature below the martensite transformation temperature after controlled rolling. The AC-50 steel had undergone controlled rolling and controlled cooling to provide a banded ferritic-pearlitic microstructure. The HY-130 is a conventional quenched and tempered steel and the strength is achieved mainly by a tempered martensitic structure. The HSLA-100, HSLA-130, and HY-130 steels contain higher amounts of nickel which is intentionally added to provide good low temperature toughness. In copper containing steels, nickel addition also prevents the incidence of hot-shortness during rolling.

The work scope of this program included a detailed literature survey to critically review the approaches employed to estimate the preheat temperatures for safe welding and their applicability to steels in this program, maximum HAZ hardness determination as a function of cooling time, and testing of the steels for hydrogen assisted cracking by the Battelle Underbead Cracking test, UT-Modified Hydrogen Sensitivity test, and Implant Cracking test. The data analysis from these tests was carried out with a view to validate

one or more carbon equivalents applicable to the steels under study. In addition, preliminary investigations were also conducted to document the occurrence of a soft zone in the HAZ. The following is a summary of the literature review and results of testing presented in this report:

(1) The application of thermo-mechanical controlled processing (TMCP) in modern steel-making has enabled the production of steels with higher strength and toughness while keeping the carbon content at the same level or lowering the carbon content. The reduction in carbon content and thus carbon equivalent has enhanced the resistance of steels to hydrogen assisted cracking. The TMCP steels are characterized by the presence of a fine grain size and the amount and type of micro-alloying elements are carefully controlled to retard the growth of austenite grains in the HAZ. The modern steels also contain a low sulfur level and the non-metallic inclusions are shape-controlled. The inclusions in the shape-controlled steels are spherical in nature as contrast to an elongated morphology in the conventional steels. Therefore, for the same amount of sulfur the density of inclusions will be higher in the modern steels than in the conventional steels. The net effect of increased grain boundary area, and higher inclusion density in the TMCP steels is to decrease the hardenability by providing greater number of sites for ferrite nucleation. This implies that the application of carbon equivalent formulae to define the hardenability of conventional steels may over estimate the hardenability of modern steels. This appears to be due to the fact that in conventional steels the hardenability was fully defined by the chemistry alone and any effect of metallurgical factors was overshadowed by the dominant influence of chemical composition.

(2) In order to estimate the preheat temperature two approaches are in wide use-Hardness Control and Hydrogen Control. In the Hardness Control approach, the hardness of the CGHAZ is controlled below a certain critical level by suitably adjusting the welding parameters. In this approach the hardenability is defined by CE(IIW). In developing this approach it was assumed that the critical hardness remains constant with CE. However, now it is known that the critical hardness decreases with a decrease in the CE, thus implying that steels with CGHAZ hardness below the critical level may also show a tendency to crack in the CGHAZ. Most of the modern low carbon steels develop lower CGHAZ hardness and, therefore, the Hardness Control approach in its present form may not be suitable for estimating the preheat temperature for crack-free welding. The Hydrogen Control approach is based on the observation that the preheated welds do not show HAC even though the hardness is higher than the critical hardness. This approach emphasizes the importance of the diffusible hydrogen content in the weldment rather than the maximum HAZ hardness. In the Hydrogen Control approach, the welding parameters are selected to provide a cooling time (from 300 to 100°C) greater than the critical cooling time, which is a function of weld restraint. It is found that more hydrogen diffuses out of the weld when the cooling time (300 to 100°C) is increased by increasing the preheat temperature, thus reducing the tendency for HAC without significantly changing the CGHAZ hardness. The composition characterizing parameter employed in this approach is P_{cm}, a carbon equivalent proposed by Ito and Bessyo. The validity limits of P_{cm} is violated by all steels in this program except AC-50. Therefore, its applicability to the steels under study or other low carbon TMCP steels is in doubt. In the literature, it is reported that the Hydrogen Control approach is overly conservative in predicting preheat temperature when applied to the modern steels.

164

(3) In recent years another method, the Critical Stress Control approach, to obtain sound welds was developed as an alternative to the two approaches described above. In this approach the critical stress below which cracking does not take place is determined based on laboratory tests, such as the Implant Cracking test, as a function of hydrogen content and preheat temperature. If the lower critical stress under given conditions of welding is greater than the intensity of restraint in an actual weld joint, the probability of HAC is greatly reduced. In the literature several predictive equations are available to calculate the lower critical stress in the Implant Cracking test, and the intensity of restraint in an actual joint. However, the formulae available to calculate the lower critical stress are applicable only to; (i) the class of steels for which they were developed, (ii) a narrow range of diffusible hydrogen content, and (iii) the specific implant sample geometry particularly the notch radius. Thus far no single formula has been found to be applicable to all classes of steels. Since the Hardness Control and Hydrogen Control approaches have limitations when considering their application to modern steels, the Stress Control approach has been examined in detail in this report.

(4) The literature review provided information on the type of microstructures desirable in the CGHAZ for obtaining sound welds. The CGHAZ microstructure containing internally twinned martensite followed by martensite without twins has been described as the most sensitive to the HAC. Among the less sensitive microstructures, a mixture of martensite and a softer constituent such as bainite or ferrite and nonmartensitic structures such as bainite or ferrite. It was shown by several investigators that the hydrogen permeation rate in a martensitic structure is considerably slower than in a bainitic structure. Thus, a combination of a hard and brittle microconstituents and the presence of a higher amount of diffusible hydrogen makes CGHAZ's containing martensite more prone to hydrogen assisted cracking as compared to bainitic structures.

The hydrogen sensitivity of CGHAZ's containing retained austenite or austenite-martensite (expected to be present in the steels strengthened with epsilon-copper) has not been investigated in detail. However, this type of microstructure is expected to be deleterious to hydrogen assisted cracking by retarding the diffusivity of hydrogen.

(5) The CGHAZ microstructure can also be characterized by monitoring the variation of maximum HAZ hardness (H_{max}) with either cooling rate or cooling time. The CGHAZ hardness response curve consists of three distinct regions. A typical hardness curve consists of two plateaus-one at shorter cooling time and the other at longer cooling time. The plateau at shorter cooling time represents the hardness of a fully martensitic structure, whereas the plateau corresponding to longer cooling time is due to the presence of a fully bainitic structure. In between these two shelves, the hardness decreases rapidly as the martensite is replaced by bainite and/or ferrite. This report presents several formulae for calculating the hardness of fully martensitic and fully bainitic structures. The martensite hardness is a direct linear function of the carbon content, but the hardness of bainitic structure varies linearly with the carbon equivalent.

(6) In this study all steels were tested for HAZ hardness behavior as a function of cooling time (800 to 500°C), $t_{8/5}$. The cooling time was varied by changing the heat input during bead-on-plate weld deposition by employing both the SMAW and SAW processes. In order to obtain all three regions of the hardness curve, $t_{8/5}$ was varied from 2.5 to 140 sec. It was considered necessary to select a formula or a nomogram to calculate $t_{8/5}$ for different

165

welding heat inputs. The literature search provided three nomograms and two equations to determine $t_{8/5}$ which were simple and at the same time accurate. The experimental data obtained from the cooling portions of the weld thermal cycles on two steels were compared with the calculated cooling times from these five methods. All the nomograms and equations allowed accurate determination of $t_{8/5}$. However, the Uwer and Degenkolbe equation is preferred over the other methods as it is applicable over a wider heat input range, different joint geometries and various welding processes. This equation was also used to compare a large body of data from the published literature. The data from this study and from literature confirmed the predictive superiority of the Uwer and Degenkolbe equation. After validating the equation for calculating $t_{8/5}$ for two steels, the cooling times for the remaining steels were determined using this equation.

(7) The H_{max} vs $t_{8/5}$ behavior has been documented for all steels in this program. The steels with lower carbon equivalents such as HSLA-80-1, HSLA-80-2, DQ-80, DQ-125, and AC-50 showed typical hardness response curves with three distinct regions. The hardness of a fully martensitic HAZ was found to be proportional to the carbon content, and the hardness of the bainitic structure was related to the carbon equivalent. In all of the above steels, except HSLA-80-1 and AC-50, the hardness of the HAZ bainitic constituent was lower than that of the base metal structure. This indicates the effect of TMCP and copper-precipitation in enhancing the strength and thus hardness of the base plate while keeping the carbon equivalent low. The CGHAZ hardness did not decrease appreciably with $t_{8/5}$ in the quench hardenable steels such as HSLA-100, HSLA-130, and HY-130. The CGHAZ consisted of a fully martensitic structure for all cooling times. A gradual decrease in the hardness with $t_{8/5}$ was observed which could be ascribed to auto-tempering of the martensitic constituent. The hardness behavior of HSLA-80M was found to lie between the quench hardenable steels and the steels with lower carbon equivalents. The CGHAZ microstructures obtained were found to correlate very well with the measured hardness. An Atlas of Microstructures was prepared and is presented in Appendix A.

(8) In order to select a carbon equivalent applicable to the class of steels under investigation, the experimental H_{max} data were compared with the hardness calculated from several formulae available in literature. Suzuki recently analyzed various available H_{max} formulae and found that these were not applicable to modern steels. He proposed five equations to calculate H_{max} in steels with composition varying over a wide range. The formulae were based on P_{cm}, CE(IIW) and CE_m (modified version of CE(IIW)). In his evaluation the maximum copper and nickel contents were 0.26% and 2.09% respectively. Therefore, steels in this study were outside the scope of the formulae proposed by Suzuki with respect to Cu and Ni. Yurioka also proposed three formulae to calculate the maximum HAZ hardness in modern steels namely; Yurioka-1, Yurioka-2, and Yurioka-3. Yurioka-3 is a simplified version of Yurioka-2 and is applicable to steels with C<0.3%, Ni<5%, Cu<0.9% and Cr<1%. The steels in this study, therefore, lie within the scope of the Yurioka-3 formula for all elements except copper. The results of comparison between the experimental and calculated H_{max}, when Suzuki's five formulae and Yurioka's two formulae (Yurioka-1 and Yurioka-3) were considered, indicated that Yurioka-3 formula provided the best correlation parameters followed by

166

Suzuki's formulae based on CE(IIW) and CE_m. The H_{max} equations derived from P_{cm} did not yield accurate predictions of the hardness.

(9) The carbon equivalent employed in the Yurioka-3 formula, CE_I, is given below-

$$CE_I=C+Si/24+Mn/6+Cu/15+Ni/12+Cr/8+Mo/4+\Delta H$$

where ΔH represents the effect of free boron on the hardenability. A comparison of CE_I, CE(IIW) and CE_m with P_{cm}, revealed that in defining the hardenability of steels, the contribution of C and Cu to the overall CE is greatly reduced in CE_I, CE(IIW) and CE_m whereas the weightage of Mn, Ni, Cr, Mo, and B has been increased, when compared to that in P_{cm}. This implies that in the modern low carbon steels the alloying elements (other than carbon and copper) exert more influence on the hardenability than was the case in the conventional C-Mn steels. The effect of copper (in amounts >0.50%) does not appear to increase linearly with increase with content and therefore, in CE_I valid for the steels in this program its weightage has been reduced appreciably. The evaluation of the H_{max} data analysis provided a basis for the selection of a carbon equivalent applicable to the steels under study. CE_I may be considered to best represent the hardenability of steels in this investigation.

(10) All steels in this program were tested for their susceptibility to hydrogen assisted cracking using three different methods namely; the Battelle Underbead Cracking test, UT-Modified Hydrogen Sensitivity test, and Implant Cracking test. In the Battelle test an E 8010 (high hydrogen) electrode was employed to deposit bead-on-plate welds. The preheat temperature was varied to obtain a critical preheat temperature above which the probability of HAC is greatly reduced. The data thus generated was analyzed as a function of CE's and H_{max}. It was found that the lower strength steels (AC-50, DQ-80, and HSLA-80) showed a different behavior than the higher strength steels (HSLA-100, HSLA-130, DQ-125 and HY-130). A better correlation between the critical preheat temperature vs carbon equivalent was observed for CE_I when data for the lower strength level steels were considered. However, the correction for the higher strength steels was optimum when H_{max} was considered. The data from the Battelle test cannot be considered conclusive as no true underbead HAC was observed in any of the steels. The cracks generally originated in the weld metal and propagated into the HAZ. Moreover, an undermatched electrode was employed for the higher strength steels, which could also give misleading results.

(11) In the UT-Modified Hydrogen Sensitivity test, the steels DQ-80, AC-50, DQ-125 and HSLA-80M did not show cracking even when the tests were conducted at 32°F and at 4% strain. These steels, except HSLA-80M, were also found to be the least susceptible to HAC in the Battelle test. The remaining steels showed intergranular HAC in the CGHAZ. No cracking, however, was observed in the fused zone in the UT-Modified test. The critical preheat temperature vs CE's (P_{cm} and CE_I)and H_{max} behavior revealed a slight superiority of CE_I over P_{cm} and H_{max} in explaining the results from the UT-Modified test. The gradient of critical preheat temperature vs CE_I was steeper for the lower strength steels than for the higher strength steels, thus indicating a weaker dependence of critical preheat temperature on the carbon equivalent for the higher strength steels as compared to that for the lower strength steels.

(12) The steels in this program were also tested employing the Implant Cracking test at two preheat temperatures (75 and 150°F) and at two diffusible hydrogen contents. The diffusible hydrogen content for HSLA-80-1, HSLA-80-2, HSLA-80M and DQ-80 steels was 5 and 20 ml/100g, and for HSLA-100, HSLA-130, DQ-125 and HY-130 steels was 5 and 10 ml/100g. The AC-50 steel tested at 5 and 40 ml/100g diffusible hydrogen content did not show any HAC in the CGHAZ, and the rupture always occurred in the soft zone. DQ-80 steel also behaved in a similar fashion when tested at 150°F preheat temperature, however, the rupture occurred in the CGHAZ when tests were conducted at 75°F preheat temperature. In all the remaining steels, except HSLA-80M, the cracks originated in the CGHAZ but propagated into the weld metal. In HSLA-80M an intergranular mode of failure in the CGHAZ was observed as contrasted to a predominantly quasi-cleavage mode in the other steels. Moreover, a sudden drop in the lower critical stress was also observed when HSLA-80M was tested at 20 ml/100g hydrogen and 75°F preheat temperature. A similar significant drop was also evident in HSLA-100 at high hydrogen content and 75°F preheat. This phenomenon is explained on the basis of microstructural differences expected in these steels. The CGHAZ microstructure may contain a large fraction of retained austenite or austenite-martensite in the otherwise martensitic HAZ. The presence of packets of secondary phases in the CGHAZ may act trapping sites for the diffusible hydrogen, thus increasing the susceptibility to HAC. This phenomenon was more pronounced at high hydrogen levels. Though the chemistry of HSLA-100 and HSLA-130 is identical, an appreciable difference in the HAC behavior particularly at high hydrogen level was observed. This was attributed to the differences in the size and distribution of epsilon-copper in these steels in addition to a finer grain size in HSLA-130. The presence of second phase packets in the CGHAZ of HSLA-100 have been observed by other investigators, but the effect of such packets on the diffusivity of hydrogen has not been investigated thus far. Probably because of the same reasons the lower critical stress in HSLA-130 was slightly lower than in HY-130 at high hydrogen content and at 75°F preheat, otherwise HSLA-130 was found superior to HY-130. In the UT-Modified test the critical preheat temperature for HSLA-130 and HY-130 was found to be the same. However, HSLA-100 showed a higher tendency to crack than HSLA-130 and HY-130.

(13) In order to recommend a formula to calculate the lower critical stress for steels in this program, various formulae published were analyzed and the experimental data compared with the calculated LCS. This exercise also provided a comparison of these steels with the conventional steels on which most of the formulae were based. It is evident that copper containing steels behave differently from the non-copper containing steels such as HY-130 and DQ-125. While acceptable single regression equations could be obtained for HY-130 and DQ-125 at 75 and 150°F preheat temperatures, for the copper-containing steels two regression equations with different slopes were found to represent the data at 75 and 150°F temperatures. This indicates that in the copper added steels, parameters such as the thermal factor and cooling time from peak temperature to 100°C, which represent the amount of diffusible hydrogen remaining at 100°C, are at variance with the non-Cu-precipitation strengthened steels. This further confirms the conclusions derived from the implant test results about the differences in the CGHAZ microstructures between steels with and without a copper addition. Further work in this direction is required to correlate the CGHAZ microstructure with diffusivity of hydrogen and derive a parameter such as the thermal factor for HSLA steels.as a function of preheat temperature.

(14) The following equations can be employed to approximately calculate the lower critical stress-

(a) For HSLA-80-1, HSLA-80-2, HSLA-80M, and DQ-80 at 75°F preheat temperature, the LCS can be calculated from the Ito's formula using the following regression equation-

$$LCS\ (actual) = 52.29 + 0.68\ LCS\ (calc.) \quad R^2 = 0.832$$

Implant data for the lower strength level steels tested at 150°F showed good correlation when Inagaki's formula was employed and the following regression equation was used-

$$LCS\ (actual) = 53.46 + 0.56\ LCS\ (calc.) \quad R^2 = 0.809$$

(b) For HSLA-100 and HSLA-130, Terasaki's formula provided the best regression coefficients at 75 and 150°F-

At 75°F preheat temperature

$$LCS\ (actual) = -40.68 + 2.45\ LCS\ (calc.) \quad R^2 = 0.805$$

At 150°F preheat temperature

$$LCS\ (actual) = 67.70 + 0.65\ LCS\ (calc.) \quad R^2 = 0.960$$

(c) Ito's equation was found adequate in providing accurate LCS for HY-130 at both 75 and 150°F preheat temperatures-

$$LCS\ (actual) = 93.62 + 0.67\ LCS\ (calc.) \quad R^2 = 0.928$$

(d) DQ-125 did not show any variation in the LCS with the test conditions except for high hydrogen and 75°F preheat temperature. Therefore, none of the formulae provided acceptable correlation with the experimental data. However, Ito's formula was found to be the best among all other formulae. The regression equation is given below-

$$LCS\ (actual) = 77.13 + 0.64\ LCS\ (calc.) \quad R^2 = 0.631$$

If the thermal parameter or cooling time to 100°C is modified for the steels under study and if the tests are conducted at more hydrogen levels and preheat temperatures, to provide a statistically significant data base, it will become possible to derive an equation to calculate the lower critical stress in the steels under study.

(15) Variation of the Implant Cracking test data (LCS and Susceptibility Index) were also analyzed with respect to CE's (P_{cm} and CE_I) and H_{max}. It was found that the carbon equivalent CE_I allowed better evaluation of the implant data than P_{cm} for the lower strength level steels. And H_{max} was found superior to CE's for the higher strength level steels. A similar trend was also observed in the Battelle test and UT-Modified test results. In order to estimate the critical preheat temperature to prevent cold cracking in steels under investigation, the ratio LCS/YS was compared for all steels. Since AC-50 did not show true CGHAZ rupture but instead failed in the soft zone, it can be welded safely at 75°F preheat temperature and at higher hydrogen contents. A similar behavior was also observed for DQ-80 at 150°F, however, at 75°F preheat temperature, the CGHAZ rupture was observed. Therefore, DQ-80 can be welded at 75°F up to a hydrogen content of 20 ml/100g. On the other hand a minimum of 150°F preheat temperature is required for HSLA-80-1. The critical preheat temperature for HSLA-80-2 and HSLA-80M is higher than 150°F.

The critical preheat temperature required for HY-130 is reported to be 300°F. The remaining steels in the higher strength category are less susceptible than HY-130, therefore, the preheat temperature requirement will be appreciably lower than 300°F. The higher strength level steels are ranked in terms of critical preheat temperature requirement for crack-free welding-

HSLA-100<HSLA-130<DQ-125<HY-130 ·

(16) Some of the steels showed the presence of a soft zone in the heat affected zone. Therefore, the bead-on-plate welds employed for CGHAZ hardness determination were used to investigate the variation of soft zone width and the decrease in the HAZ hardness ΔH when compared to the base metal, as a function of heat input. The steels HSLA-80-1, HSLA-80-2, DQ-80, DQ-125 and AC-50 showed the presence of a soft zone. In the remaining steels no HAZ softening was observed. The width of the soft zone increased linearly with the cooling time from 800 to 500°C, and ΔH showed an initial abrupt increase but tended to approach a saturation value with increased cooling time. These parameters were found to depend on the type of steel. (ΔH is proportional to the amount of retained energy in the steel and carbon equivalent.) · In the copper containing steels the dissolution of epsilon-copper precipitate during the thermal cycle also contributed to the softening in addition to recovery and recrystallization. The soft zone disappeared in the copper containing steels on PWHT due to the reprecipitation of epsilon-copper, but in the non-copper containing steels softening became more pronounced.

REFERENCES

(1) Lundin, C.D., Welding Research and Engineering Group, The University of Tennessee, unpublished results

(2) Lundin, C.D., Menon, R. and Chen, Z., (1986); "Post Weld Heat Treatment Cracking in a A 710 HSLA Precipitation Strengthened Steel", Proc. Int. Conf. on Trends in Welding Research, May 18-22, Gatlinburg, TN, pp 559-570

(3) Cordea, J.N., (1975); "Niobium- and Vanadium-Containing Steels for Pressure Vessel Service", WRC Bulletin No. 203, pp 1-37

(4) Gray, J.M., (1976); "Weldability of Niobium-Containing High Strength Low Alloy Steels", WRC Bulletin No. 213, pp 1-19

(5) Levine, E. and Hill, D.C., (1976); "A Review of Structure and Properties of Welds in Columbium or Vanadium High Strength Low Alloy Steels", WRC Bulletin No. 213, pp 20-35

(6) Lundin, C.D. and Eftekar, A.R., (1977); Welding Journal Research Supplement, 57, pp 113s-118s

(7) Dolby, R.E., (1976); "The Effect of Niobium on the HAZ Toughness of High Heat Input Welds in C-Mn Steels", Proc. International Conference on Welding of HSLA (Microalloyed) Structural Steels", Ed. A.B. Rothwell and J. Malcolm Gray, Nov. 1976, Rome, Italy, pp 212-234

(8) Sawhill, J.M. Jr., Boussel, P. and Morrow, J.W., ibid., pp 235-256

(9) Watanabe, I., Suzuki, M., Tsukada, K., Yamazaki, Y. and Tokunaga, T., (1984); Welding Research Abroad, 31(1), pp 2-10

(1 0) Suzuki, H., Sogo, Y., Iwanaga, K., Yamaba, R., Maeda, K. and Ohno, Y., (1984); "New HT 50 Steels for Marine and Offshore Constructions with Superior Weldability", IIW Doc. IX-1314-84

(1 1) Yurioka, N., Koike, M., Mori, N. and Nagano, K., (1984); "Impact of Welding Research on Steel Composition Development", IIW Doc. IX-1313-84

(12) BS 5135:1984, "Process of Arc Welding of Carbon and Carbon-Manganese Steels", British Standards Institute

(1 3) Ito, Y. and Bessyo, K., (1968); "Weldability Formula of High Strength Steels Related to Heat Affected Zone Cracking", IIW Doc. IX-567-68

(1 4) AWS D1.1-86, (1986); "Structural Welding Code-Steel", American Welding Society

(1 5) Yurioka, N., Ohshita, S. and Tamehiro, H., (1981); "Study on Carbon Equivalents to Assess Cold Cracking Tendency and Hardness in Steel Welding", Conference on Pipeline Welding in 80's, AWRA, Melbourne

(1 6) Yurioka, N., Okumura, M., Kasuya, T. and Cotton, H.J.U., (1987); Metal Construction, 19(4), pp 217R-223R

(1 7) Graville, B.A., (1976); "Cold Cracking in Welds in HSLA Steels", Proc. International Conference on Welding of HSLA (Microalloyed) Structural Steels", Nov. 9-12, Rome, Italy, pp 85-101

(1 8) Wilson, A.D., Hamburg, E.G., Colvin, D.J., Thompson, S.W. and Krauss, G., (1988); "Properties and Microstructures of Copper Precipitation Aged Plate Steels", Proc. Microalloying '88, Sept. 24-30, Chicago, Illinois, pp 259-275

(1 9) Thompson, S.W., Colvin, D.J., and Krauss, G., (1988); Scripta Met., 22, pp 1069-1074

(2 0) Scoonover, T.M., Lukens, W.E. and Pande, C.S., "Correlation of Heat Affected Zone Microstructure with Peak Heating Temperature in HSLA 80 Steel Weldments", unpublished results, David Taylor Naval Ship Research and Development Center, Bethesda, MD

(2 1) Kirkwood, P.R., (1987); "A Viewpoint on the Weldability of Modern Structural Steels", Proc. International Symposium on Welding Metallurgy of Structural Steels, Feb. 22-26, Denver, Colorado, pp 21-45

(2 2) Easterling, K., (1983); Introduction to the Physical Metallurgy of Welding , Butterworths Monographs in Metals, Butterworths and Co. Ltd.

(2 3) Christensen, N., Davies, V. de L., and Gjermundsen, K., (1965); Br. Welding Journal, 12 , pp 54-75

(2 4) Ion, J.C., Easterling, K., Ashby, M.F., (1984); Acta Metall., 32, pp 1949-1962

(2 5) Welding Handbook, Ed. C. Weisman, American Welding Society, Miami

(2 6) Huber, R.A., Bradway, D., Weidmann, C.M., and Turner, P.W., (1968); "Computer Programs for Calculating Peak Temperature Distribution in Welding", ORNL Report No. Y-1927

(2 7) Ronningen, J.A., Simonsen, T., and Christensen, N., (1973); Scandinavian Journal of Metallurgy, 2, pp 87-90

(2 8) Easterling, K., (1987); "Modelling the Weldability of Structural Steels", Proc. International Symposium on Welding Metallurgy of Structural Steels", Feb. 22-26, Denver, Colorado, pp 45-62

(2 9) Rosenthal, D., (1941); Welding Journal Research Supplement, 20, pp 220s-234s

(3 0) Rosenthal, D., (1946); Trans. ASME, 68, pp 819-866

(3 1) Adams, C.M., Jr., (1958); Welding Journal Research Supplement, 37, pp 210s-215s

(32) Rykalin, N.N., (1974); "Calculation of Heat Flow in Welding", Translated by Zvi Paley and C.M. Adams, Jr., IIW Doc. 212-350-74

(33) Tsai, C.L., (1981); "Modeling of Thermal Behaviors of Metals during Welding", Proc. Conf. Trends in Welding Research in the United States, Nov. 16-18, New Orleans, LA, pp 91-108

(34) Solomon, H.D., and Levy, S., (1981); "HAZ Temperatures and Cooling Rates as Determined by a Simple Computer Program", ibid., pp 173-205

(35) Papazoglou, V.J., (1981); "Analytical Techniques for Determining Temperatures, Thermal Strain, and Residual Stresses during Welding", Ph.D. Thesis, M.I.T.

(36) Mangonon, P.L. and Mahimkar, M.A., (1986); "A Three Dimensional Heat Transfer Finite Element Model of Submerged Arc Welding of HSLA Steels", Proc.1st International Conf. Trends in Welding Research, May 18-22, Gatlinburg, TN, pp 35-46

(37) Tekriwal, P. and Majumdar, J., (1986); "Finite Element Modeling of Arc Welding Process", ibid., pp 71-82

(38) Tekriwal, P. and Majumdar, J., (1988); Welding Journal Research Supplement, 67, pp 150s-156s

(39) Inagaki, M. and Sekiguchi, H., (1960); Trans. Natn. Res. Inst. Metals (Japan), 2, pp 102-125

(40) Berkhout, C.F. and van Lent, P.H., (1968); Schweissen u. Schneiden, 20, pp 256-260

(41) De Fourny, J. and Bragard, A., (1975); Rev. de la Soudure, 31, pp 124-132

(42) Uwer, D. and Degenkolbe, J., (1976); "Thermal Cycles in Arc Welding-Calculation of Cooling Times", IIW Doc. IX-987-76

(43) Suzuki, H., (1985); "A New Formula for Estimating HAZ Maximum Hardness in Welded Steels", IIW Doc. IX-1315-85

(44) Kohno, R. and Jones, S.B., (1978); "An Initial Study of Arc Energy and Thermal Cycles in the Submerged Arc Welding of Steels", TWI Report No. 81/1978/PE

(45) Bernard, G., (1975); "A Viewpoint on the Weldability of C-Mn and Micro-alloyed Structural Steels", Micro Alloying '75, pp 552-596

(46) Lorenz, K., and Duren, C., (1981); C-equivalent for Weldability of Large Diameter Pipe Steels", Conf. on Steels for Pipe and Pipeline Fittings, Oct. 21-23, London, Paper 37

(47) Satoh, K. and Terasaki, T., (1979); General Assembly of JWS, No. 25, p98

173

(4 8) Lorenz, K. and Duren, C., (1982); IIW Doc. IX-B-II-82

(4 9) Beckert, M. and Holz, R., (1973); Schweisstechnik, 23, No. 8. p 344

(5 0) Leshie, W.C., (1982); The Physical Metallurgy of Steels, Mcgraw-Hill, New York

(5 1) Maynier, P., Dollet, J. and Jungmann, B., (1977); "Creusot-Loire System for the Prediction of the Mechanical Properties of Low Alloy Steel Products. Hardenability Concepts with Applications to Steel", Proc. of AIME Symposium, Oct. 24-26, pp 518-544

(5 2) Terasaki, T., Akiyama, T. and Serino, M., (1984); "Chemical Compositions and Welding Procedure to Avoid Cold Cracking", Proc. International Conf. Joining of Metals, April 15-18, Helsingor, Denmark, pp 381-386

(5 3) Kaup, K. and Mikula, W., (1980); "Entwicklung der Rohrstahle", Proc. of Pipeline Technik, Verlag TUV-Rheinland, Vol. 3, p225

(5 4) Yurioka, N., (1985); Materials and Design, VI(4)

(5 5) Hart, P.H.M., (1984); "The Influence of Steel Cleanliness on HAZ Hydrogen Cracking: The Present Position", IIW Doc. IX-1308-84

(5 6) Hart, P.H.M., (1978); "Low Sulphur Levels in C-Mn Steels and Their Effects on HAZ Hardenability and Hydrogen Cracking", International Conf. Trends in Steels and Consumables for Welding, London

(5 7) Coe, F.R., (1973); "Welding Steels without Hydrogen Cracking", The Welding Institute Report, Abington

(5 8) Coe, F.R., (1973); "The Avoidance of Hydrogen Cracking in Welding", The Welding Institute Report, Abington

(5 9) Masubuchi, K., (1980); "Analysis of Welded Structures", Pergamon Press, New York

(6 0) Klein, K.M., (1971); "Investigation of Welding Thermal Strains in Marine Structures", M.S. Thesis, M.I.T.

(6 1) Yurioka, N., Suzuki, H., Oshita, S. and Saito, S., (1983); Welding Journal Research Supplement, 62(6), pp 147s-153s

(6 2) Ito, Y. and Bessyo, K., (1969); "A Prediction of Welding Procedure to Avoid Heat Affected Zone Cracking", IIW Doc. IX-631-69

(6 3) Suzuki, H., (1984); "Revised Cold Cracking Parameter P_{HA} and its Applications", IIW Doc. IX-1311-84

(6 4) Satoh, K., Matsui, S., Horikawa, K., Bessyo, K. and Okumura, T., (1973); "JSSC Guidance Report on Determination of Safe Preheating Conditions without Weld Cracks in Steel Structures", IIW Doc. IX-834-73

(6 5) Ito, Y., and Bessyo, K., (1971); Sumitomo Search, 6, pp 10-20

(6 6) Suzuki, H., (1980); "Cold Cracking and its Prevention in Steel Welding (III), Effects of Heat Input and Restraint", IIW Doc. IX-1157-80

(6 7) Suzuki, H. and Terasaki, T., (1986); "Estimating Critical Stress and Preheat Temperature to Avoid Cold Cracking in Implant and JIS-Y (Tekken) Tests", IIW Doc. IX-1417-86

(6 8) Graville, B.A., (1986); "Determining Preheat Requirements for Structural Steels", Presented at the 67th AWS Annual Convention, Atlanta

(6 9) Savage, W.F., Nippes, E.F. and Szekers, E.S., (1976); Welding Journal Research Supplement, 57, pp 276s-283s

(7 0) Savage, W.F., Nippes, E.F., Homma, H., (1976); ibid, 57, pp 376s-386s

(7 1) Savage, W.F., Nippes, E.F., and Husa, E.S., (1982); ibid., 63, pp 223s-242s

(7 2) "Cold Cracking Test Methods using Implants", (1984); IIW Doc. 802-84

(7 3) Signes, E.G. and Howe, P., (1988); Welding Journal Research Supplement, 67(8), pp 163s-170s

(7 4) Evans, G.M. and Christensen, N., (1973); Scandinavian Journal of Metallurgy, 2, pp 91-94

(7 5) Pavaskar, V. and Kirkaldy, J.S., (1982); ibid., 11, pp 256-262

(7 6) Todd, J., UCLA, Private Communication

(7 7) Losz, J.M.B. and Challenger, K.D., (1989); "Microstructural Characterization of Gas-Metal-Arc Weldments in Copper-Precipitation Strengthened HSLA Steels", 2nd International Conf. Trends in Welding Research, May 14-18, Gatlinburg, TN

(7 8) Beachem, C.D., (1972); Metallurgical Transactions, 3(2), pp 437-451

(7 9) Ito, Y., Ikeda, M., and Nakanishi, M., (1976); J. Japanese Welding Soc., 45(12), pp 1029-1036

(8 0) Matsuda, F., Nakagawa, H., Tsuji, T. and Tsukamoto, M., (1978); Trans. JWRI, 7(1), pp 71-85

(8 1) Christensen, N. and Simonsen, T., (1981); Scandinavian Journal of Metallurgy, 10, pp 120-126

(82) Inagaki, M., Satoh, K., Matsui, S. and Ohkuma, Y., (1978); "Application of Implant Test on Cold Cracking", IIW Doc. IX-1078-78

(83) Matsuda, F., Nakagawa, H., Tsuji, T., and Tsukamota, M., (1978); Trans. JWRI, 7(2), pp 47-53

(84) Terasaki, T. and Satoh, K., (1982); ISIJ, 68(1), pp140-146

(85) Karpi, R.A.J., Ruusila, J., Toyoda, M., Satoh, K., and Vartiainen, K., (1984); Scandinavian Journal of Metallurgy, 13, pp 66-74

(86) Gedeon, S.A., (1988); "Hydrogen Assisted Cracking of High Strength Steel Welds", US Army Materials Technology Laboratory Report MTL TR 88-12

(87) Matsuda, F., (1981); Trans. JWRI, 10, pp 55-63

(88) Bailey, N., (1970); British Welding Journal, 2(8), pp 339-344

(89) Youn, J.G. and Kim, H.J., (1987); "Characteristics of the TMCP Steel and its Softening", Proc. Int. Sym. on Welding Metallurgy of Structural Steels, Feb. 22-26, Denver, Colorado, pp 157-168

(90) Bolliger, W., Varughese, R., Kaufmann, E., Qin, W.F., Pense, A.W., and Stout, R.D., (1988); "The Effect of Welding and Fabrication Operation on the Toughness of A 710 Steel", Proc. of Microalloying '88, Sept. 24-30, Chicago, Illinois, pp 277-290

APPENDIX-A

ATLAS OF MICROSTRUCTURES

(a)

200μm

(b)

20μm
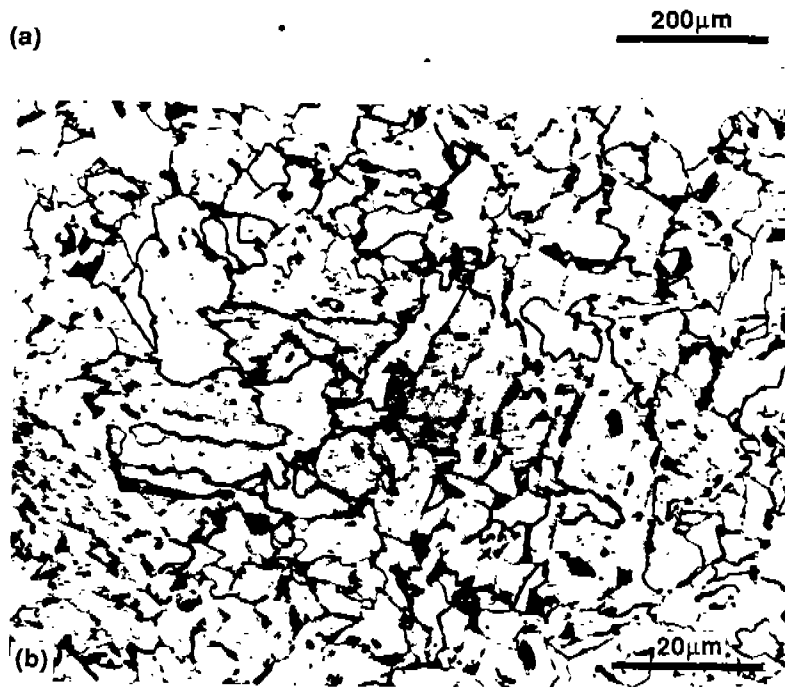
Fig. A-1.(a)   Distribution of inclusions, 100X, as-polished.

Fig. A-1.(b)   Base metal microstructure containing ferrite and granular bainite,
1000X, 2% nital etched.

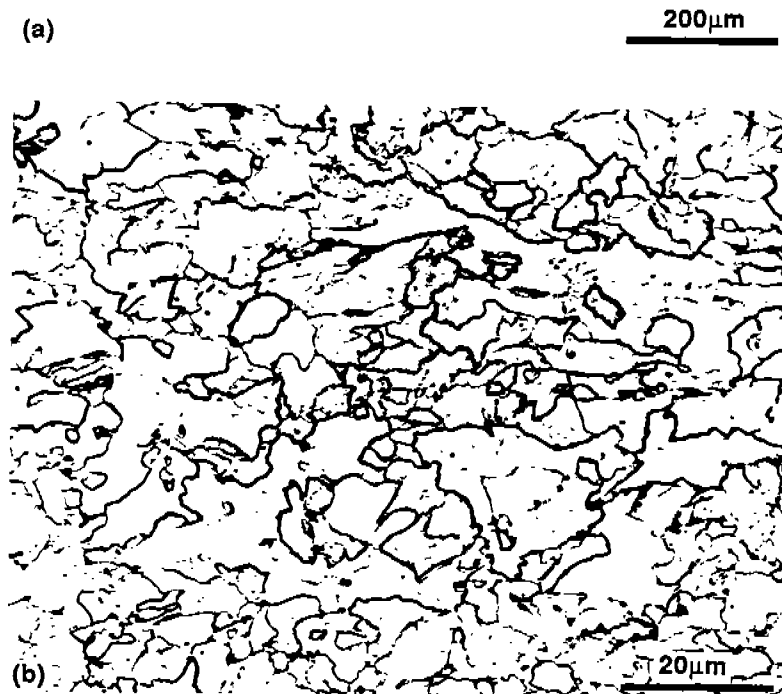Condition :   As-received.
Grain Size :   ASTM No. 5-6   (5.6μm,   1000X)
Hardness :   220 DPH.

178
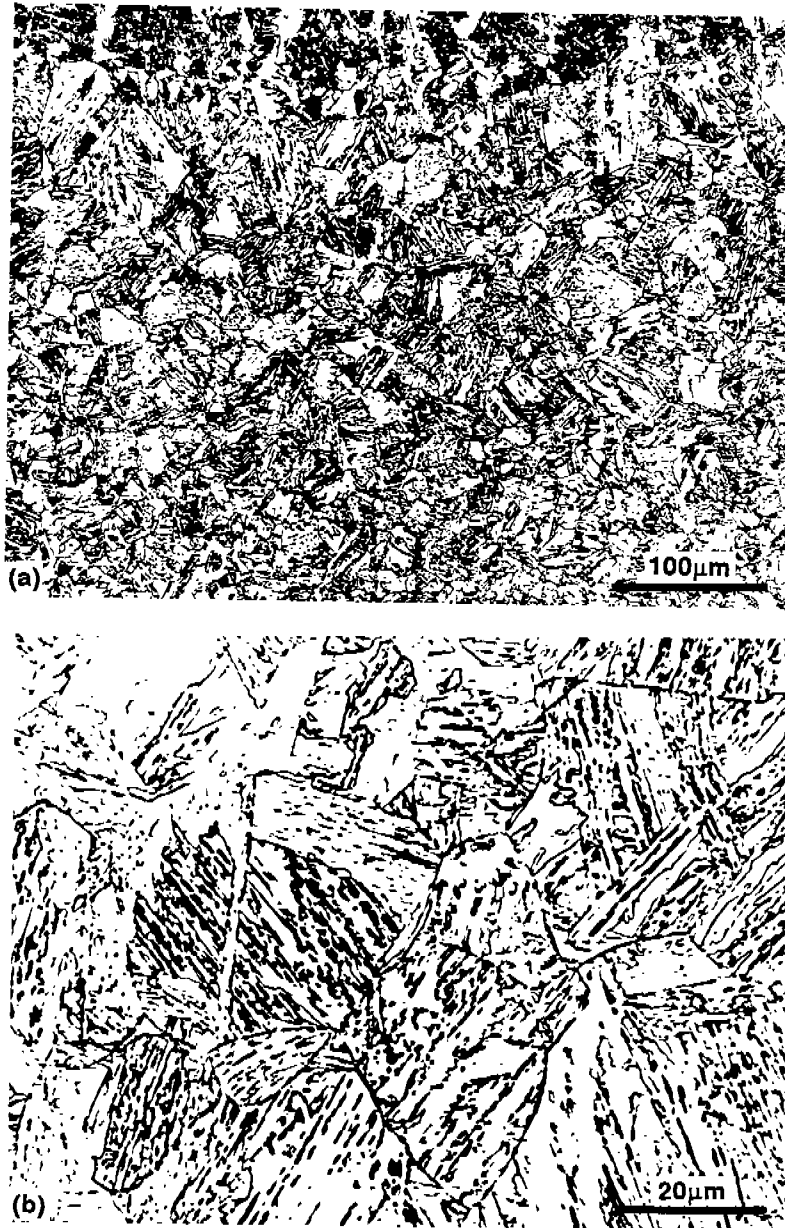
Fig. A-2.   Microstructure of the coarse grained HAZ contains a predominantly
martensitic structure, (a) 200X, (b) 1000X.

Etchant: 2% nital.
Welding Process: SMAW.
Heat Input: 15 kJ/in.
Cooling Time(800-500°C):   2.5 sec.
Grain Size: ASTM No.7   (32μm).
Estimated Martensite Percentage: 89%.
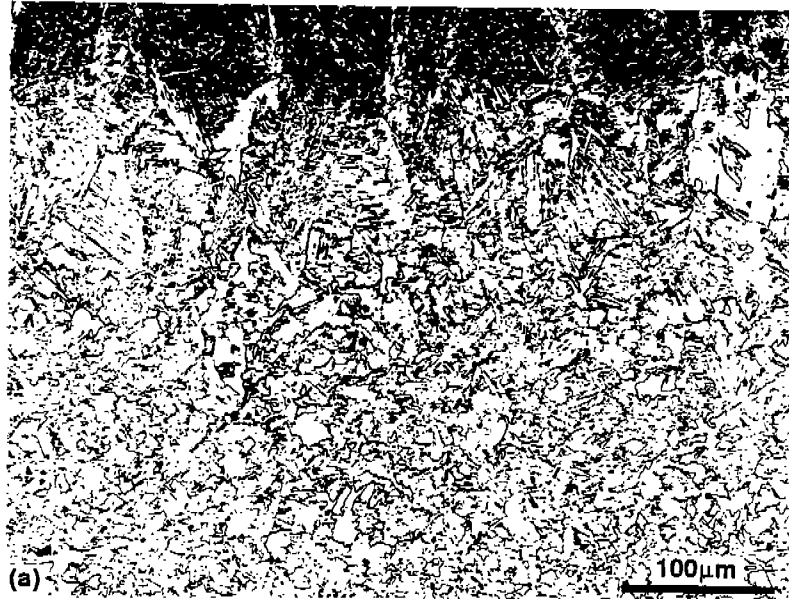Hardness: 321 DPH.

179

Fig. A-3. Microstructure of the coarse grained HAZ containing a mixture of martensite and bainite; (a) 200X, (b) 1000X.

Etchant: 2% nital.
Welding Process: SMAW.
Heat Input: 67 kJ/in.
Cooling Time(800-500°C): 14 sec.
Grain size: ASTM No.4 (90μm).
Estimated Martensite Percentage: 28%.
Hardness: 267 DPH.

180
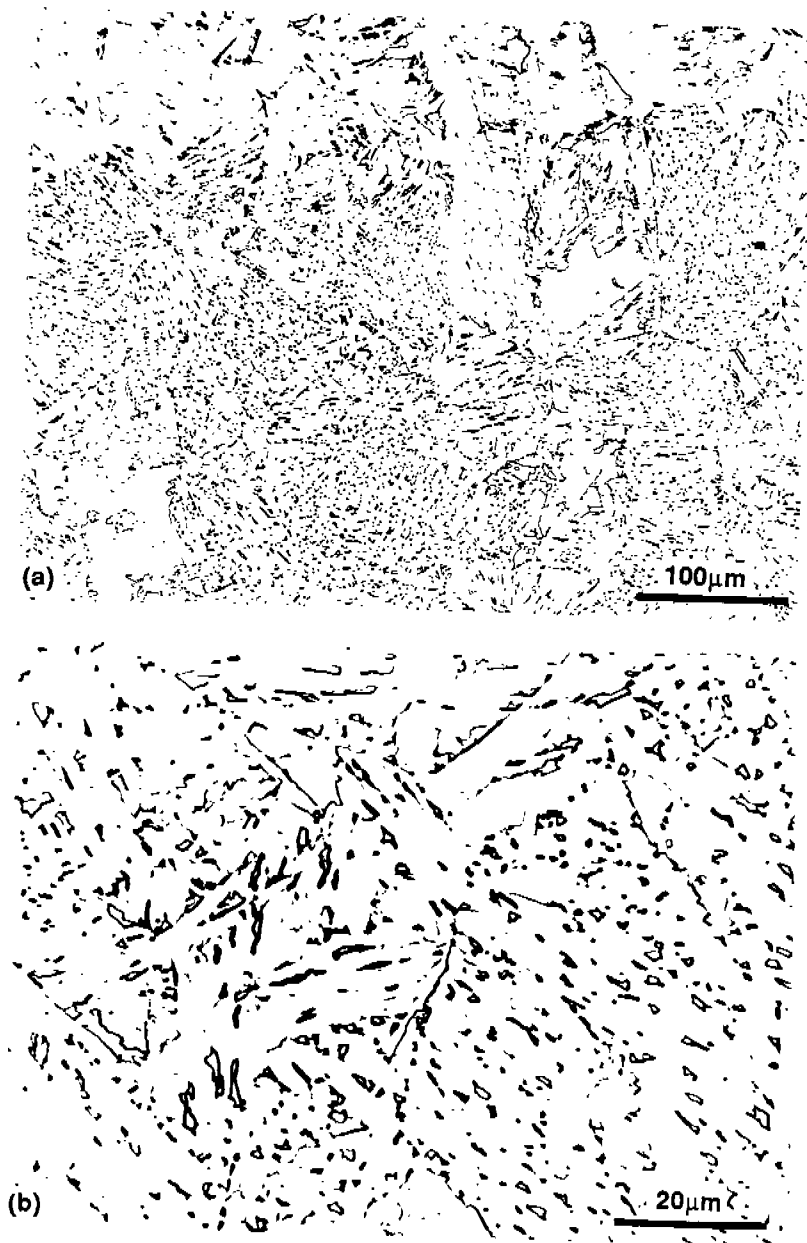
Fig. A-4.   Microstructure of the fully bainitic coarse grained HAZ. (a) 200X, (b)1000X.

Etchant: 2% nital.
Welding Process: SAW.
Heat Input: 134 kJ/in
Cooling Time (800-500°C): 90 sec.
Grain Size: ASTM No.3 (125μm).
Estimated Martensite Percentage: 0%.
Hardness: 227 DPH.

181

(a)

200μm

(b)

20μm
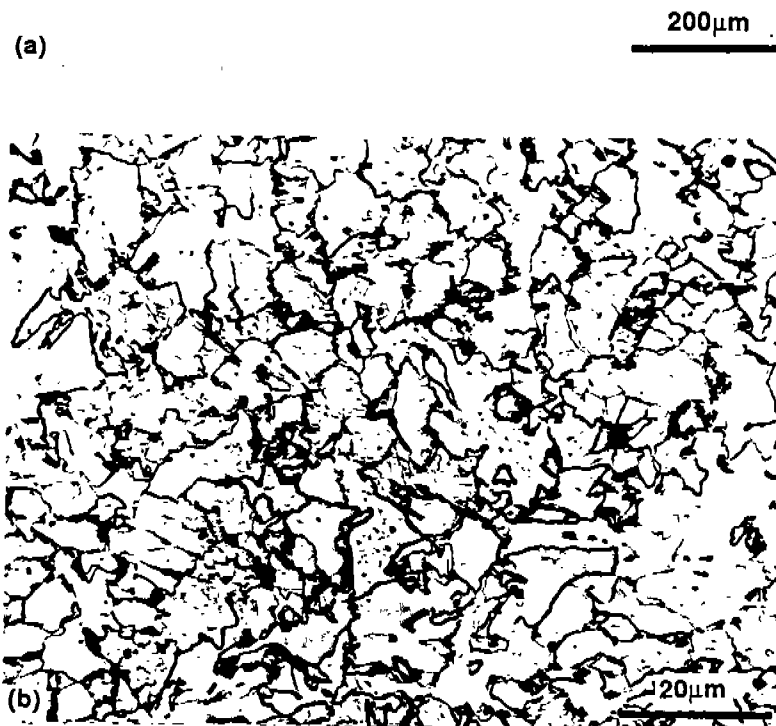
Fig. A-5.(a)   Distribution of inclusions, 100X, as-polished.

Fig. A-5.(b)   Base metal microstructure containing ferrite and small amount of granular bainite, 1000X, 2% nital etched.

Condition: As-received.
Grain Size: ASTM No.5 (6.7μm, 1000X)
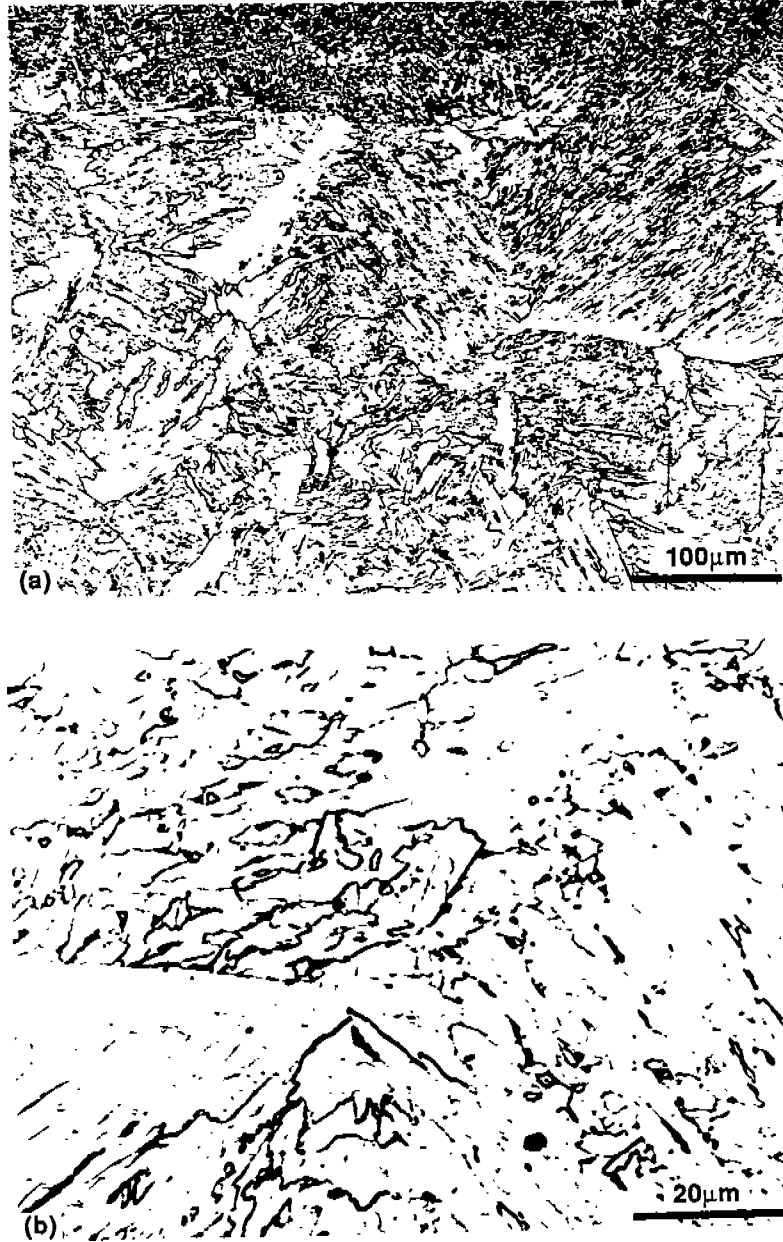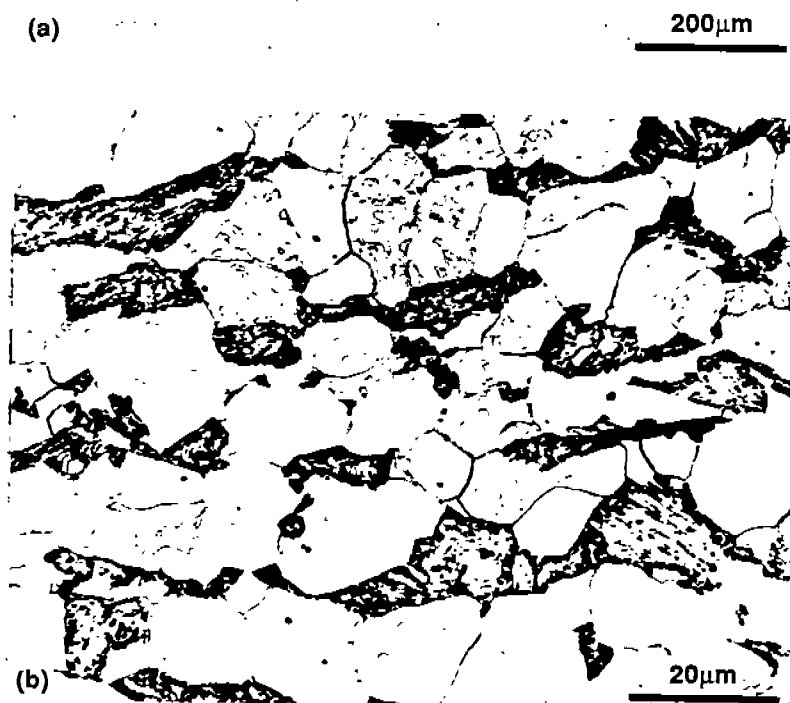Hardness: 244 DPH.

182

(a)

100μm

(b)

20μm
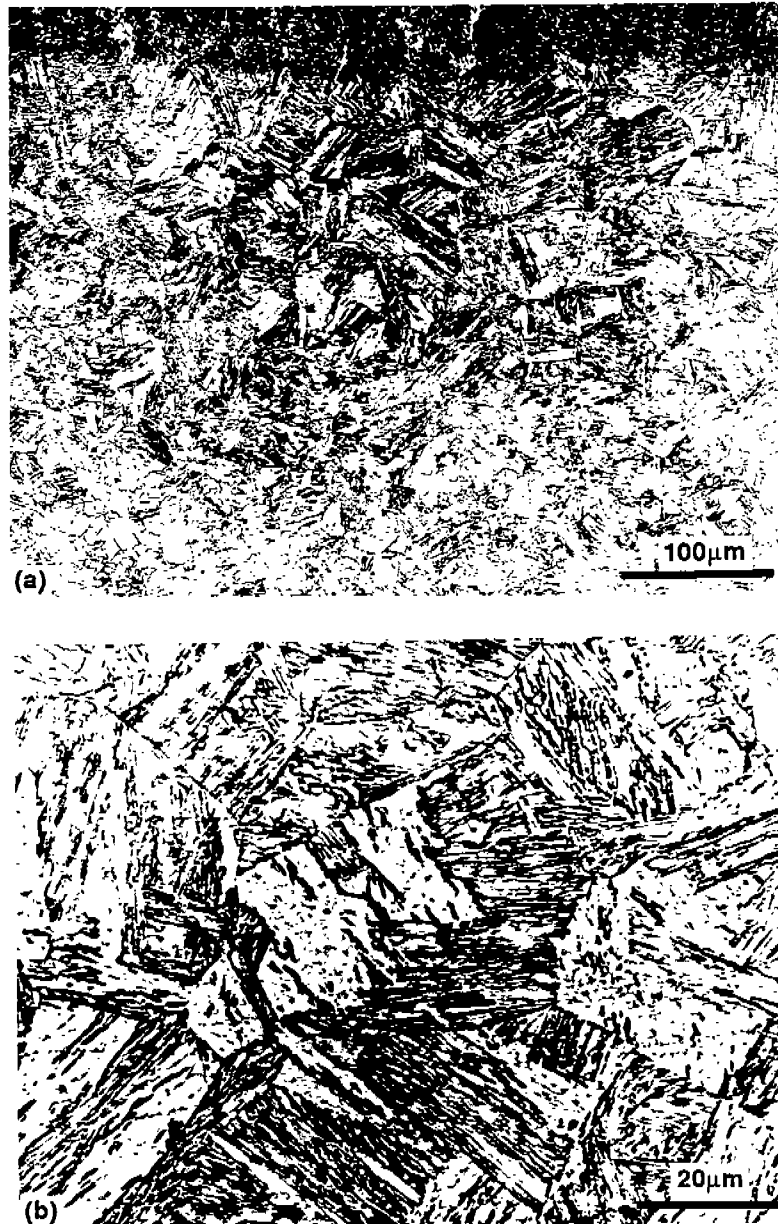
Fig. A-6. Microstructure of the coarse grained HAZ containing a large fraction of martensite, (a) 200X, (b) 1000X.

Etchant: 2% nital.
Welding Process: SMAW.
Heat Input: 15 kJ/in.
Cooling Time (800-500°C): 2.5 sec.
Grain Size: ASTM No.5-6 (55μm).
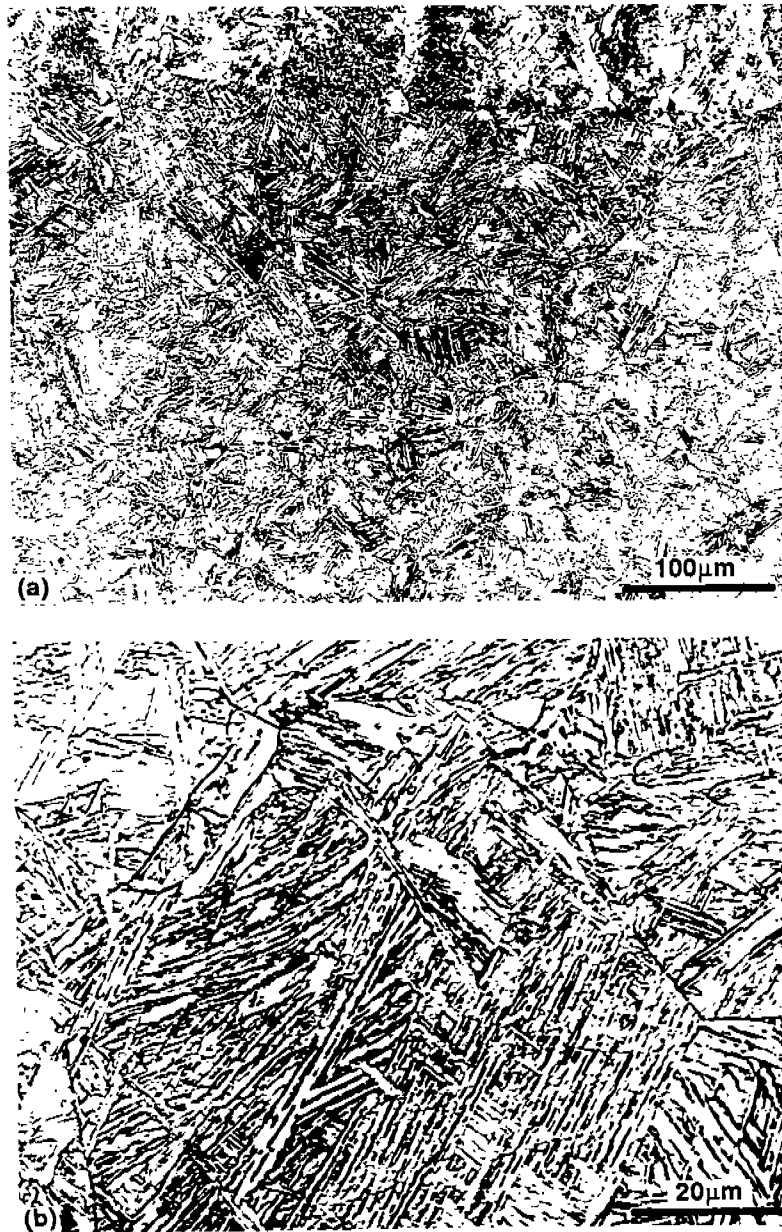Estimated Martensite Percentage: 90%.
Hardness: 359 DPH.

183
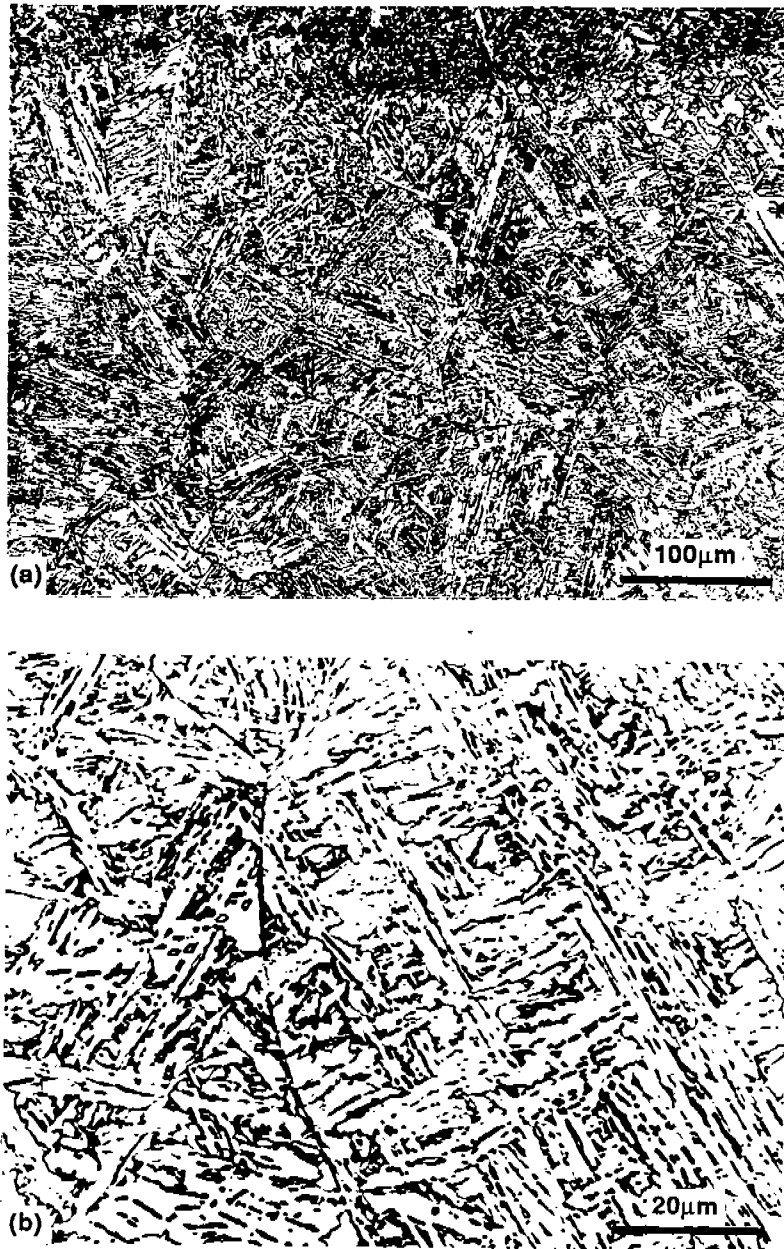
Fig. A-7. Microstructure of the coarse grained HAZ containing bainite and martensite; (a) 200X, (b) 1000X.

Etchant: 2% nital.
Welding Process: SMAW.
Heat Input: 67 kJ/in
Cooling Time (800-500°C): 11sec.
Grain Size: ASTM No.4 (90µm).
Estimated Martensite Percentage: 40%.
Hardness: 276 DPH.

184

Fig. A-8   Microstructure of the fully bainitic coarse grained HAZ;
(a) 200X, (b) 1000X.

Etchant: 2% nital.
Welding Process: SAW.
Heat Input: 224 kJ/in.
Cooling Time (800-500°C): 140 sec.
Grain Size: ASTM No.2 (180 μm).
Estimated Martensite Percentage: 0%.
Hardness: 227 DPH.

185

MATERIAL: HSLA-80M
Base Metal

(a)

200μm

(b) 20μm
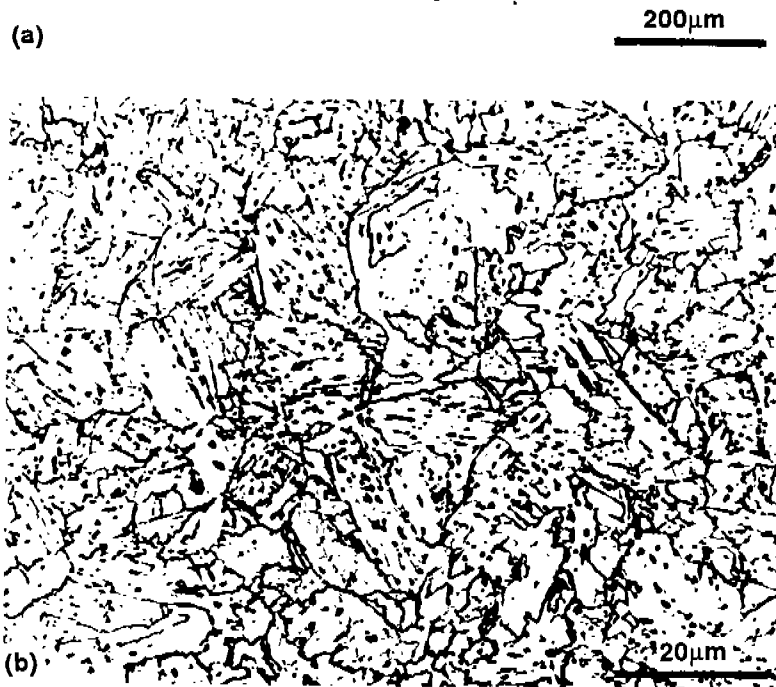
Fig. A-9.(a)   Distribution of inclusions, 100X, as-polished.

Fig. A-9.(b)   Base metal microstructure containing granular bainite,
1000X, 2% nital etched.

Condition: As-received.
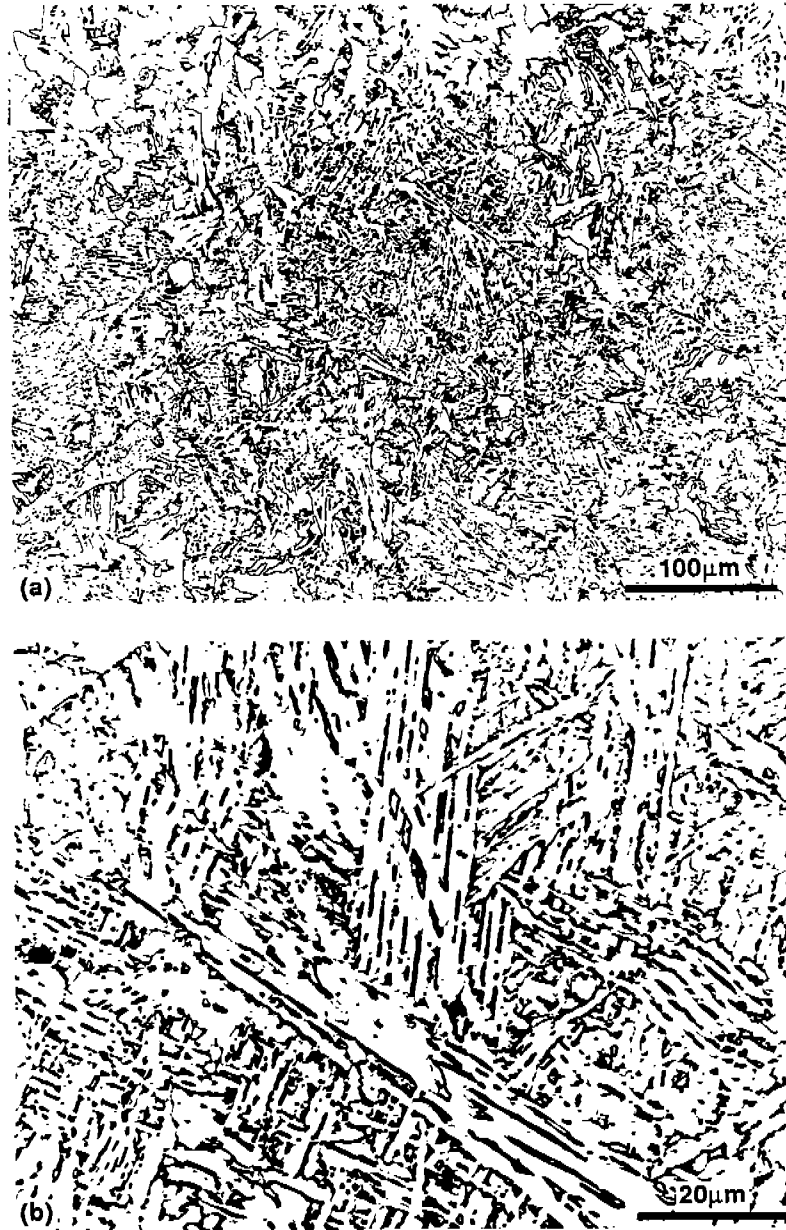Grain Size: ASTM   No.4 (9.4μm, 1000X).
Hardness: 248 DPH.

Fig. A-10.   Microstructure of the coarse grained HAZ containing 100% martensite;
(a) 200X, (b) 1000X.

Etchant: 2% nital.
Welding Process: SMAW.
Heat Input: 15 kJ/in.
Cooling Time (800-500°C): 2.5 sec.
Grain Size: ASTM No.5-6 (55µm).
Estimated Martensite Percentage: 100%.
Hardness: 353 DPH.

187
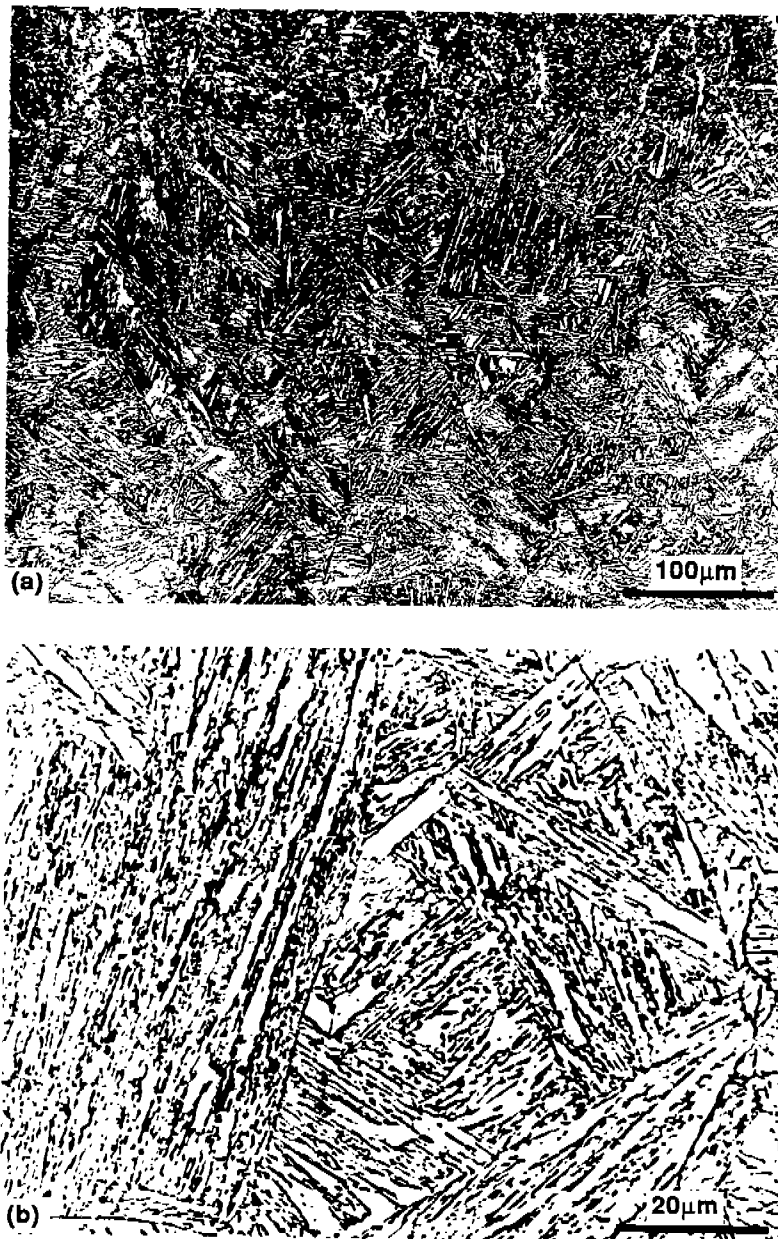
Fig. A-11.   Microstructure of the coarse grained HAZ containing martensite;
(a) 200X, (b) 1000X.

Etchant: 2% nital.
Welding Process: SMAW.
Heat Input: 67 kJ/in.
Cooling Time (800-500°C):   11 sec.
Grain Size: ASTM No.4 (90μm).
Estimated Martensite Percentage: 100%.
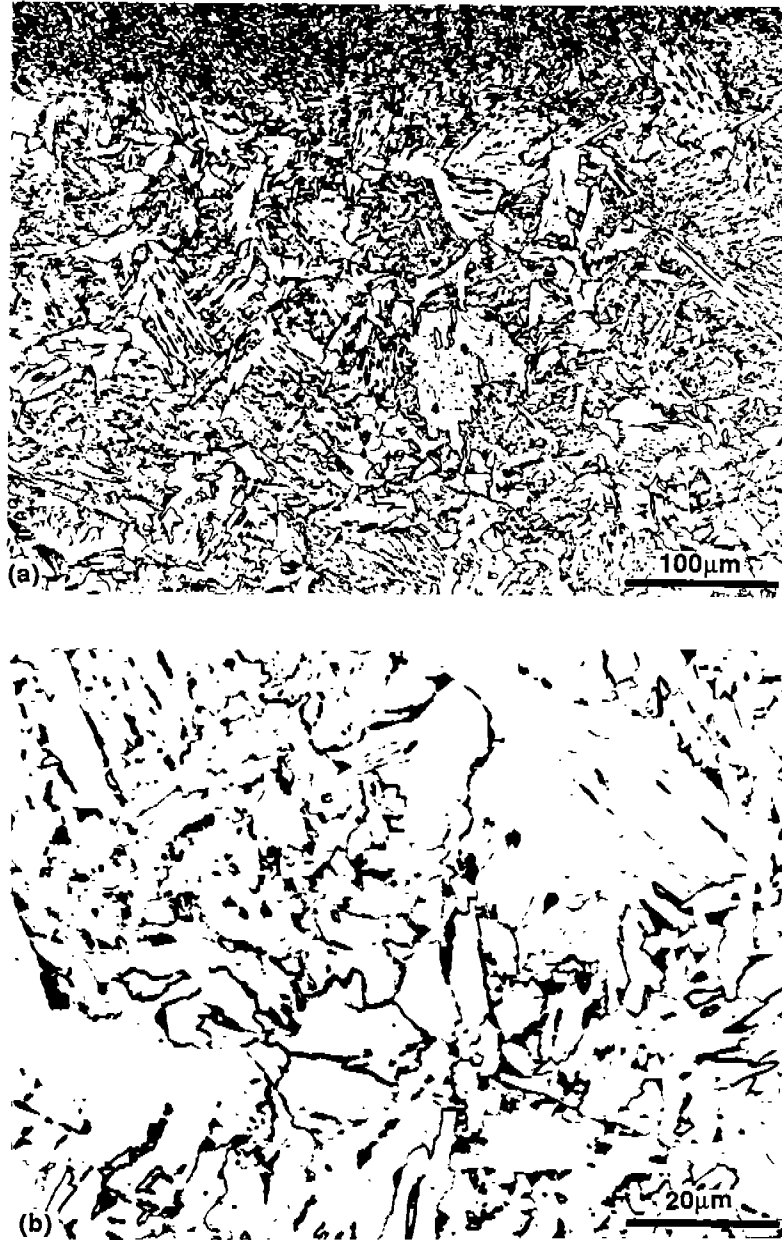Hardness: 322 DPH.

188
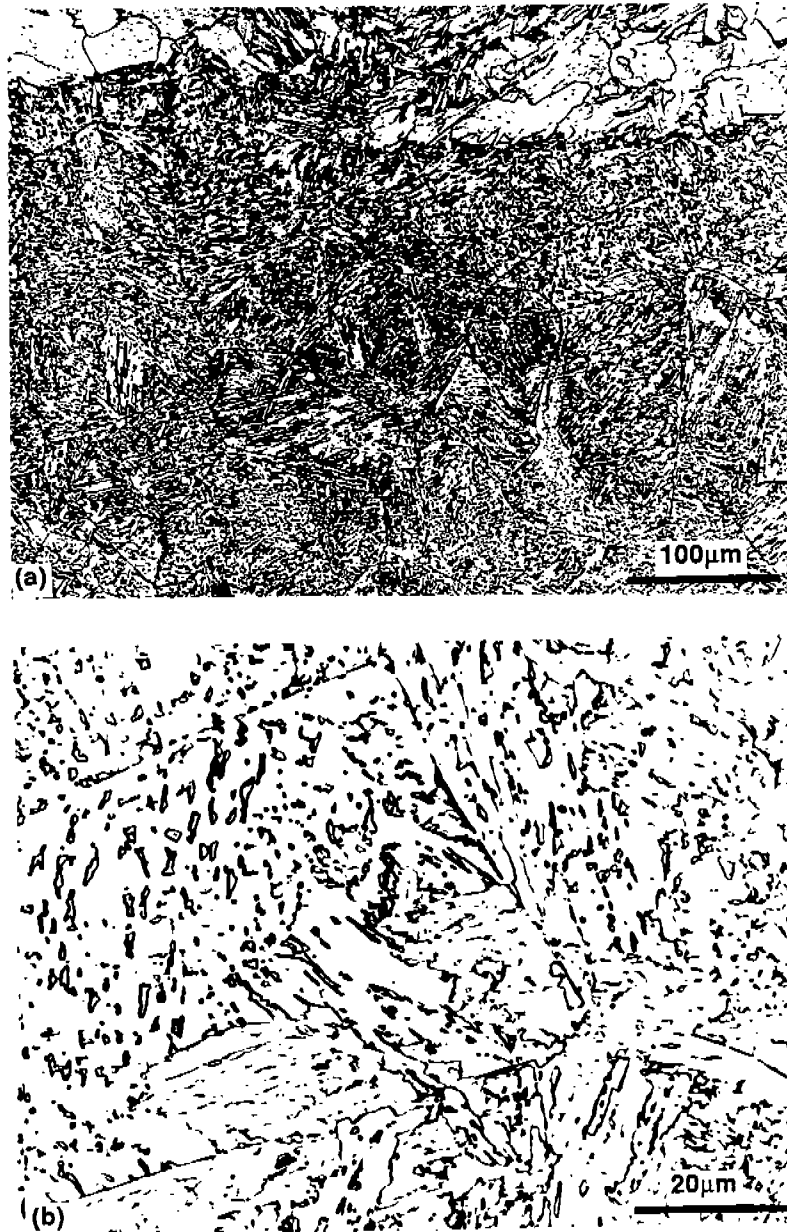
Fig.   A-12.   Microstructure of the coarse grain HAZ containing martensite
and bainite; (a) 200X, (b) 1000X.

Etchant: 2% nital.
Welding Process: SAW.
Heat Input: 224 kJ/in.
Cooling Time (800-500°C):   90 sec.
Grain Size: ASTM No.3 (125μm).
Estimated Martensite Percentage: 30%.
Hardness: 308 DPH.

189

200μm

(a)

(b)
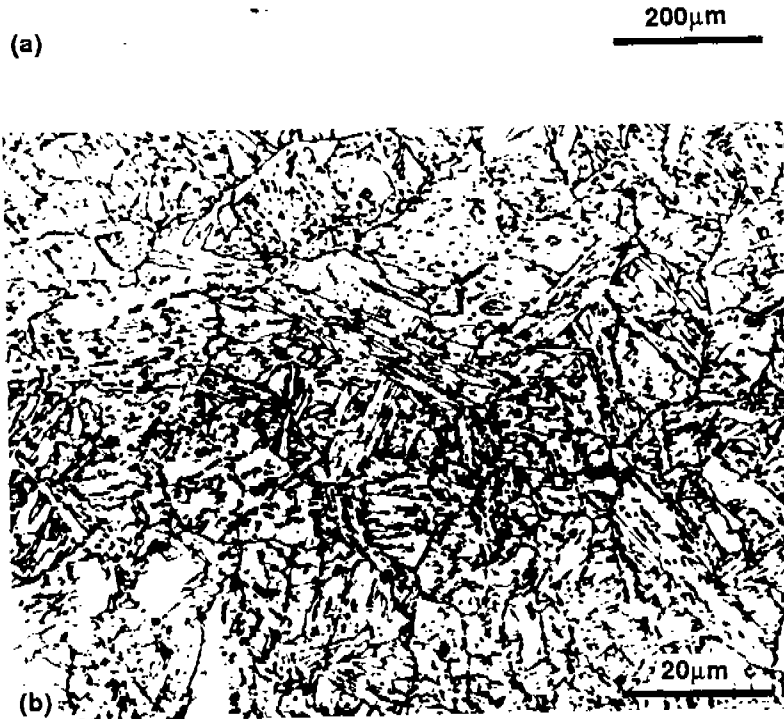
Fig. A-13.(a)   Distribution of Inclusions, 100X, as-polished.

Fig. A-13.(b)   Base metal microstructure containing martensite,1000X,
2% nital etched.

Condition: As-received.
Grain Size: ASTM No.5 (6.7 μm, 1000X).
Hardness: 272 DPH.

190

Fig. A-14. Microstructure of the fully martensitic coarse grained HAZ; (a) 200X, (b) 1000X.

Etchant: 2% nital.
Welding Process: SMAW.
Heat Input: 15 kJ/in.
Cooling Time (800-500°C): 2.5 sec.
Grain Size: ASTM No.7 (32μm).
Estimated Martensite Percentage: 100%.
Hardness: 388 DPH.

191
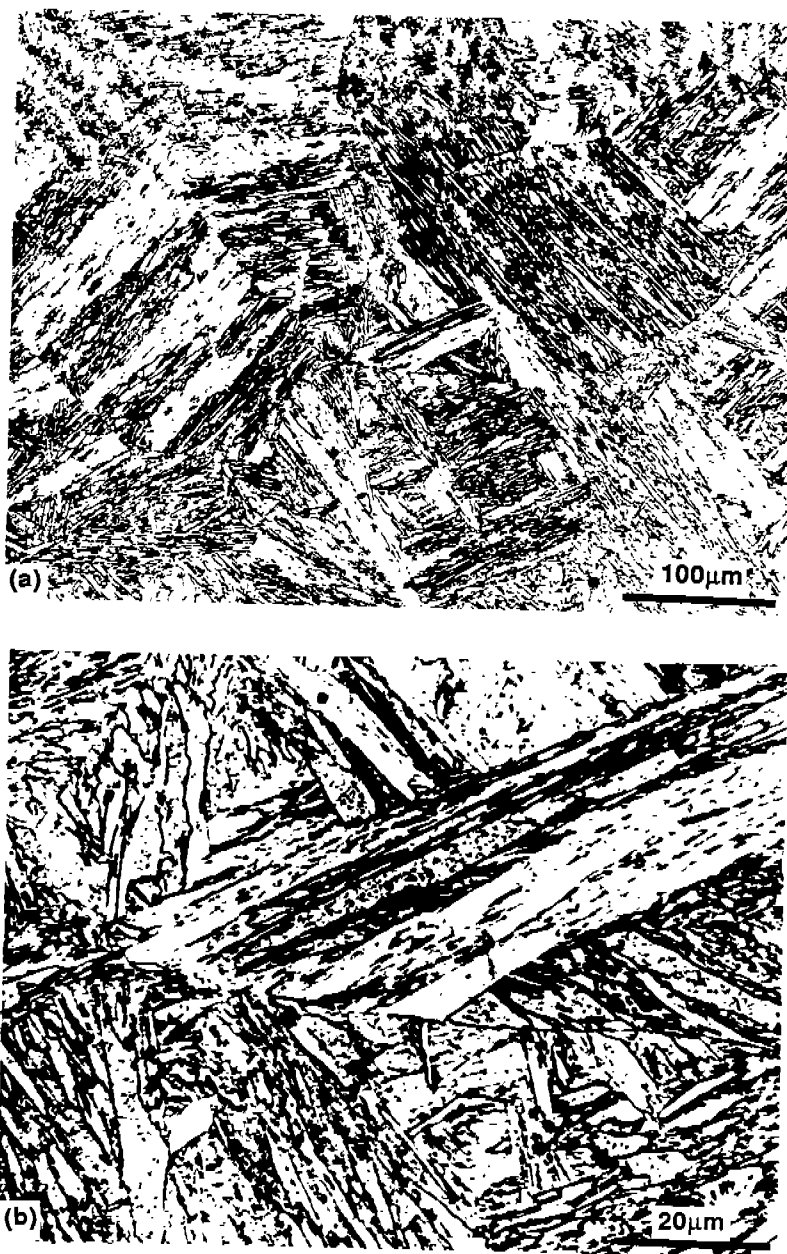
Fig. A-15.   Microstructure of the coarse grained HAZ with 100% martensite; (a) 200X, (b) 1000X.

Etchant: 2% nital.
Welding Process: SMAW.
Heat Input: 67 kJ/in.
Cooling Time (800-500°C):   11 sec.
Grain Size: ASTM No.4 (90 μm).
Estimated Martensite Percentage: 100%.
Hardness: 372 DPH.

192
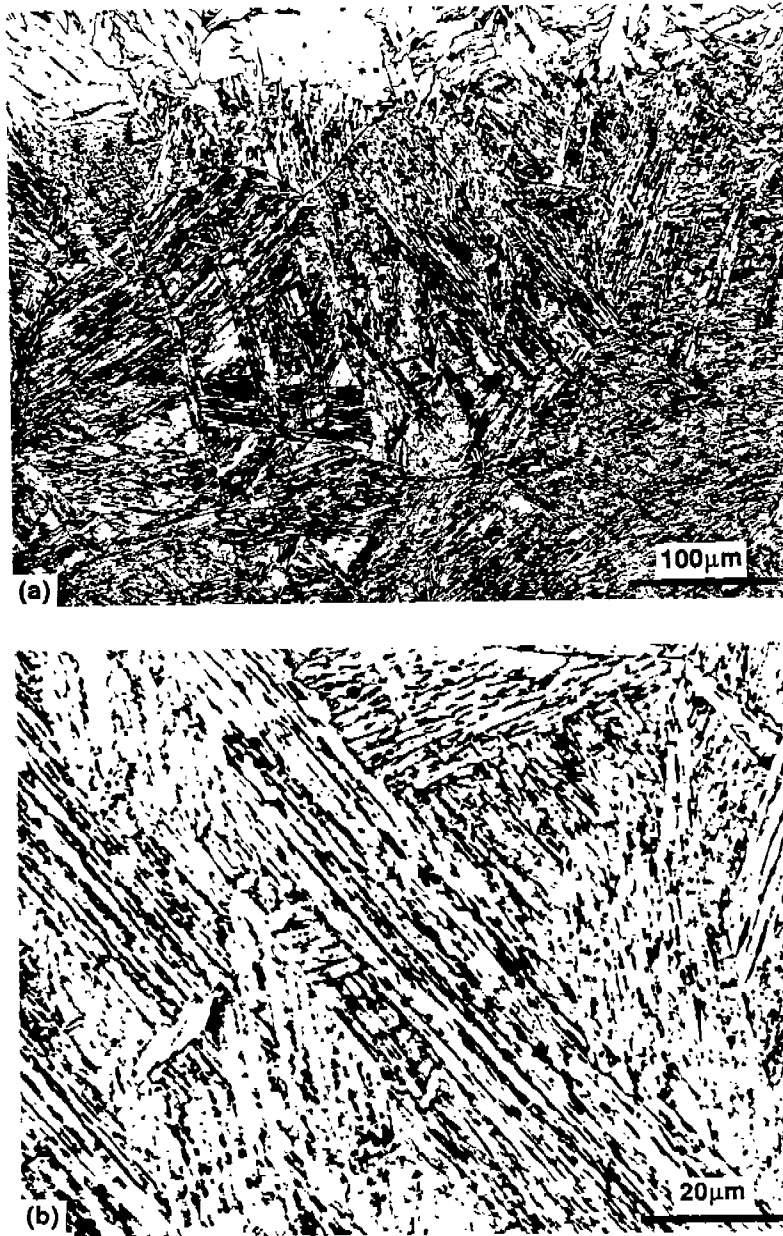
Fig. A-16. Microstructure of the coarse grained HAZ containing mostly martensite; (a) 200X, (b) 1000X.

Etchant: 2% nital.
Welding Process: SAW.
Heat Input: 336 kJ/in.
Cooling Time (800-500°C): 71 sec.
Grain Size: ASTM No.3 (125 μm).
Estimated Martensite Percentage: 93%.
Hardness: 359 DPH.

193

(a)

200μm

(b)

20μm
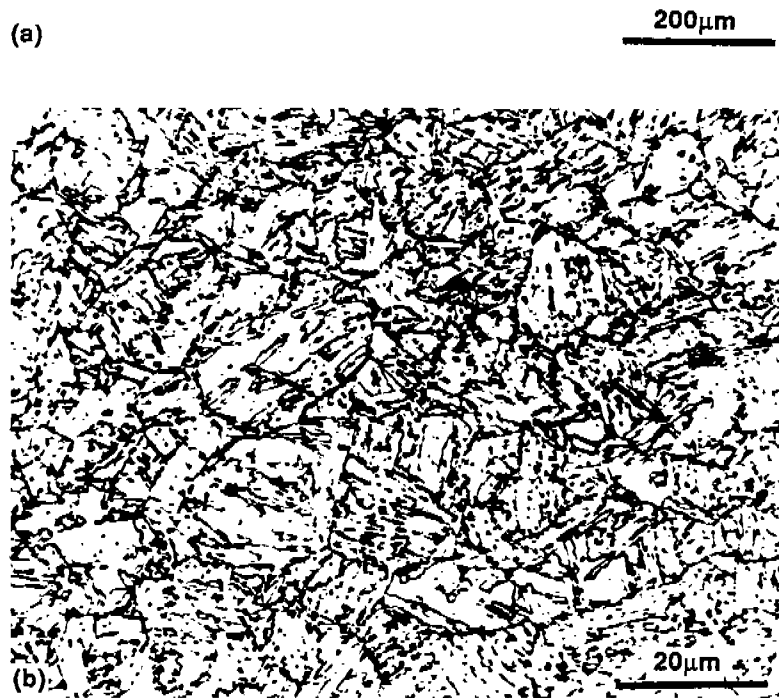
Fig. A-17.(a)   Distribution of Inclusions, 100X, as-polished.

Fig. A-17.(b)   Base metal microstructure containing martensite, 1000X, 2% nital etched.

Condition :   As-received.
Grain Size :   ASTM No. 5 (6.7μm, 1000X)
Hardness :   303 DPH.

194
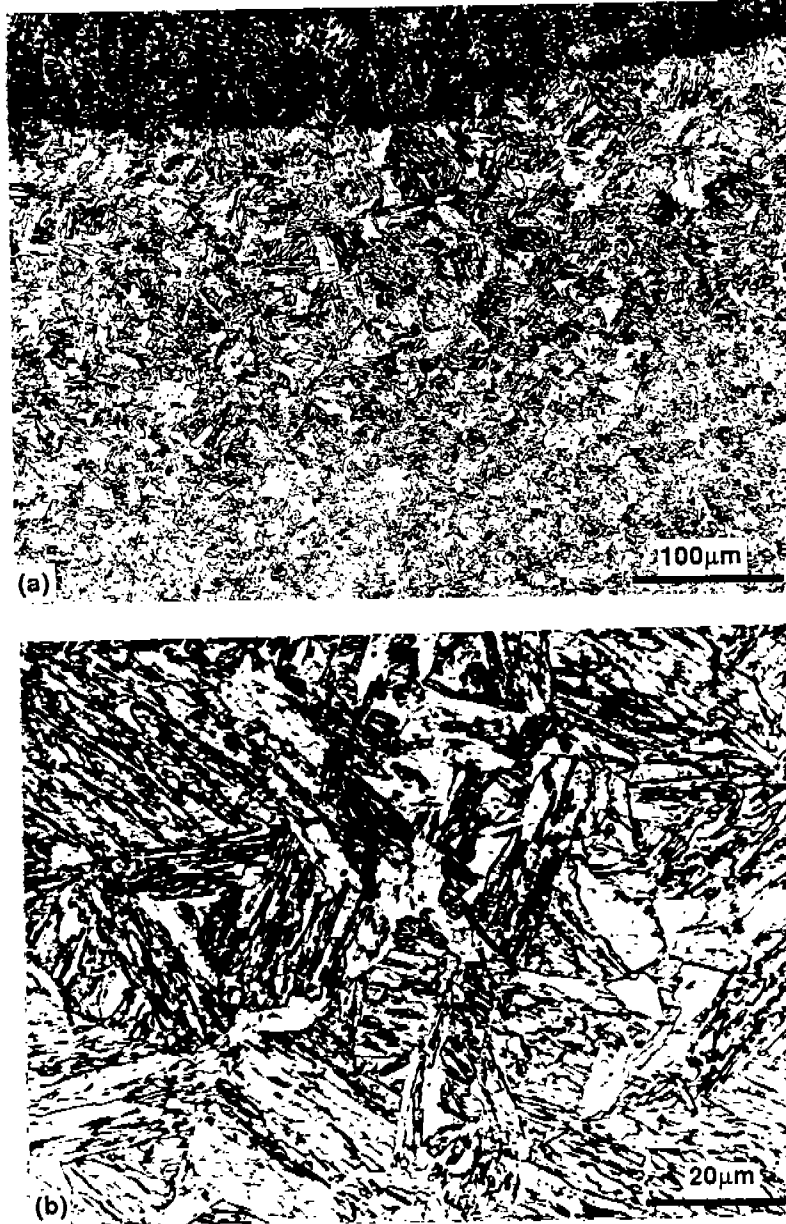
Fig. A-18.   Microstructure of the coarse grained HAZ containing martensite;
(a) 200X, (b) 1000X.

Etchant: 2% nital.
Welding Process: SMAW.
Heat Input: 15 kJ/In.
Cooling Time(800-500°C): 2.5 sec.
Grain Size: ASTM No. 7 (32μm).
Estimated Martensite Percentage: 100%.
Hardness: 387 DPH.

195

Fig. A-19. Microstruture of the fully martensitic coarse grained HAZ;
(a) 200X, (b) 1000X.

Etchant: 2% nital.
Welding Process: SMAW.
Heat Input: 67 kJ/in.
Cooling Time(800-500°C): 11 sec.
Grain size: ASTM No.4 (90μm).
Estimated Martensite Percentage: 100%.
Hardness: 370 DPH.

196
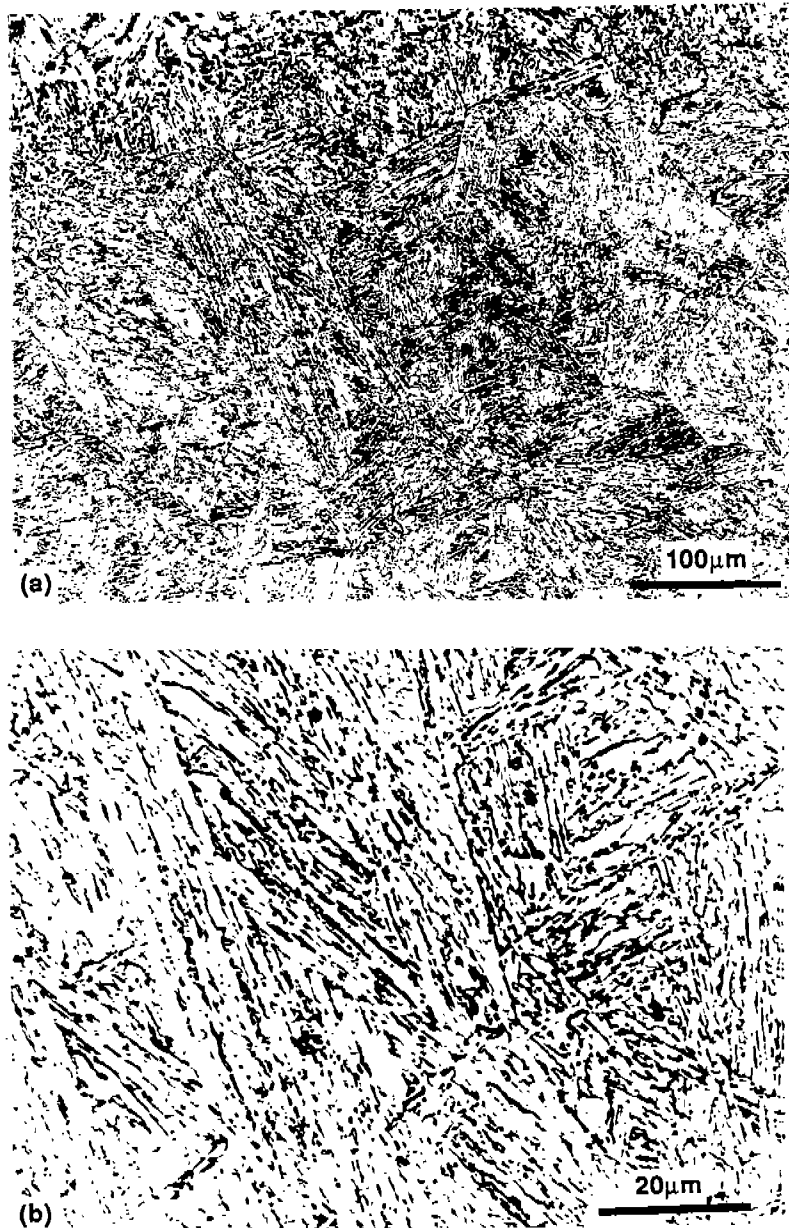
Fig. A-20.   Microstructure of the coarse grained HAZ containing a predominant amount of martensite; (a) 200X, (b)1000X.

Etchant: 2% nital.
Welding Process: SAW.
Heat Input: 224 kJ/in
Cooling Time (800-500°C):   90 sec.
Grain Size: ASTM No.3 (125μm).
Estimated Martensite Percentage: 93%.
Hardness: 355 DPH.

(a)

200μm

(b)
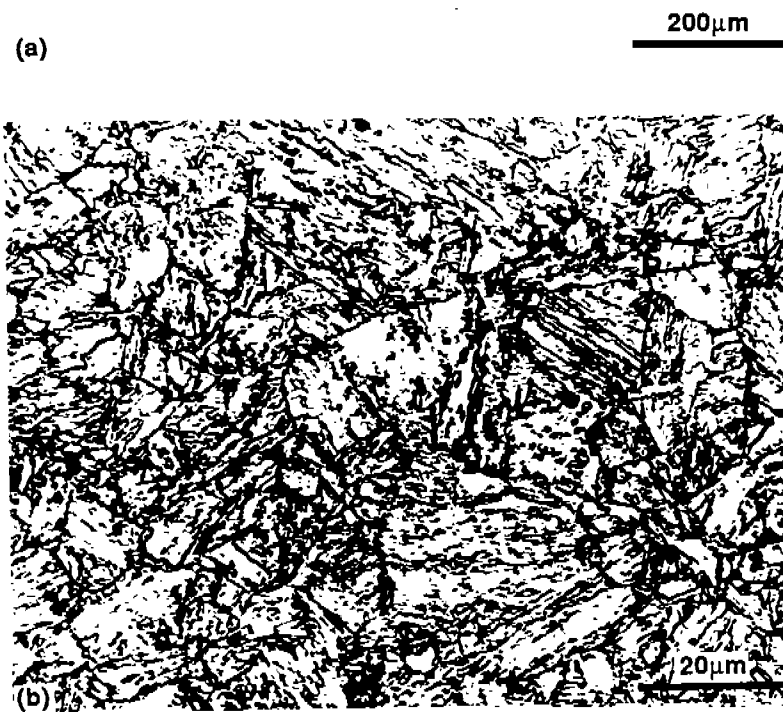
Fig. A-21.(a)   Distribution of inclusions, 100X, as-polished.

Fig. A-21.(b)   Base metal microstructure containing tempered martensite, 1000X, 2% nital etched.

Condition: As-received.
Grain Size: ASTM No. 4 (9.4 μm, 1000X).
Hardness: 327 DPH.

198

MATERIAL: HY-130
Coarse Grained HAZ
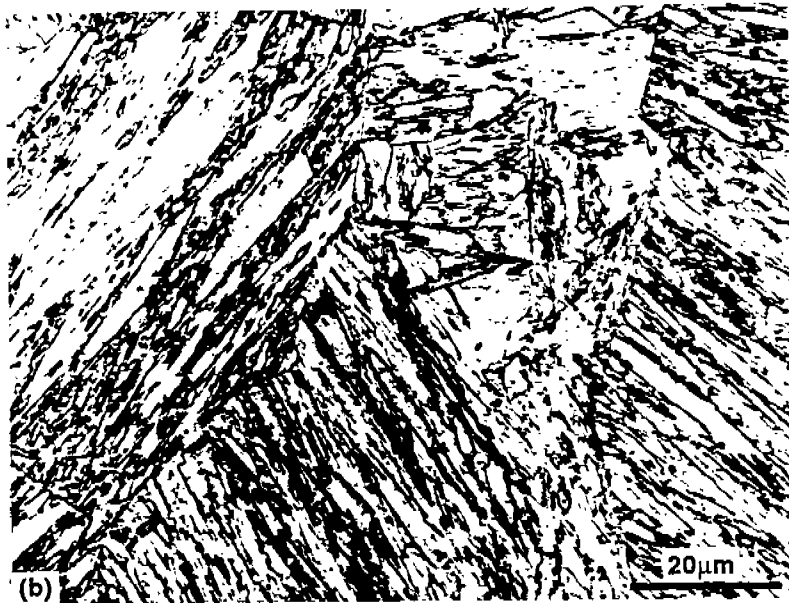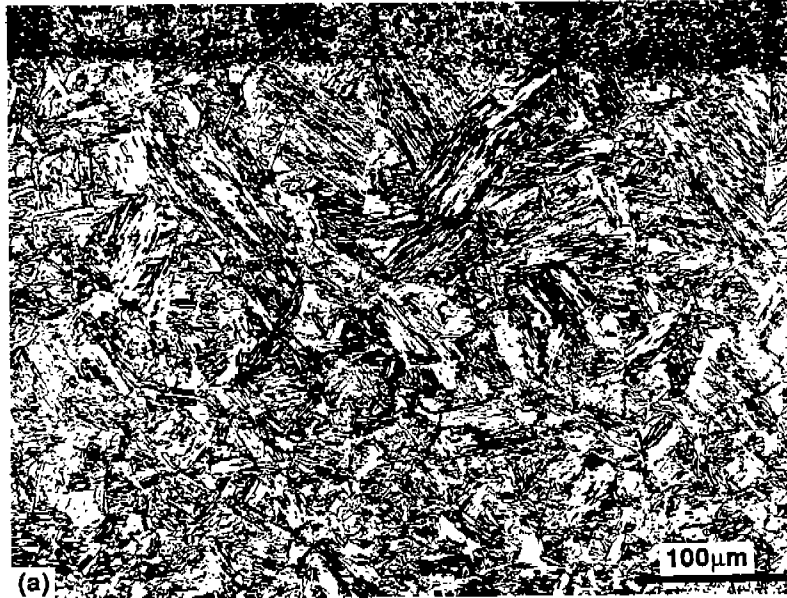
Fig. A-22.   Microstructure of the fully martensitic coarse grained HAZ;
(a) 200X, (b) 1000X.

Etchant: 2% nital.
Welding Process: SMAW.
Heat Input: 15 kJ/in.
Cooling Time (800-500°C): 2.5 sec.
Grain Size: ASTM No.5 (65μm).
Estimated Martensite Percentage: 100%.
Hardness: 419 DPH.
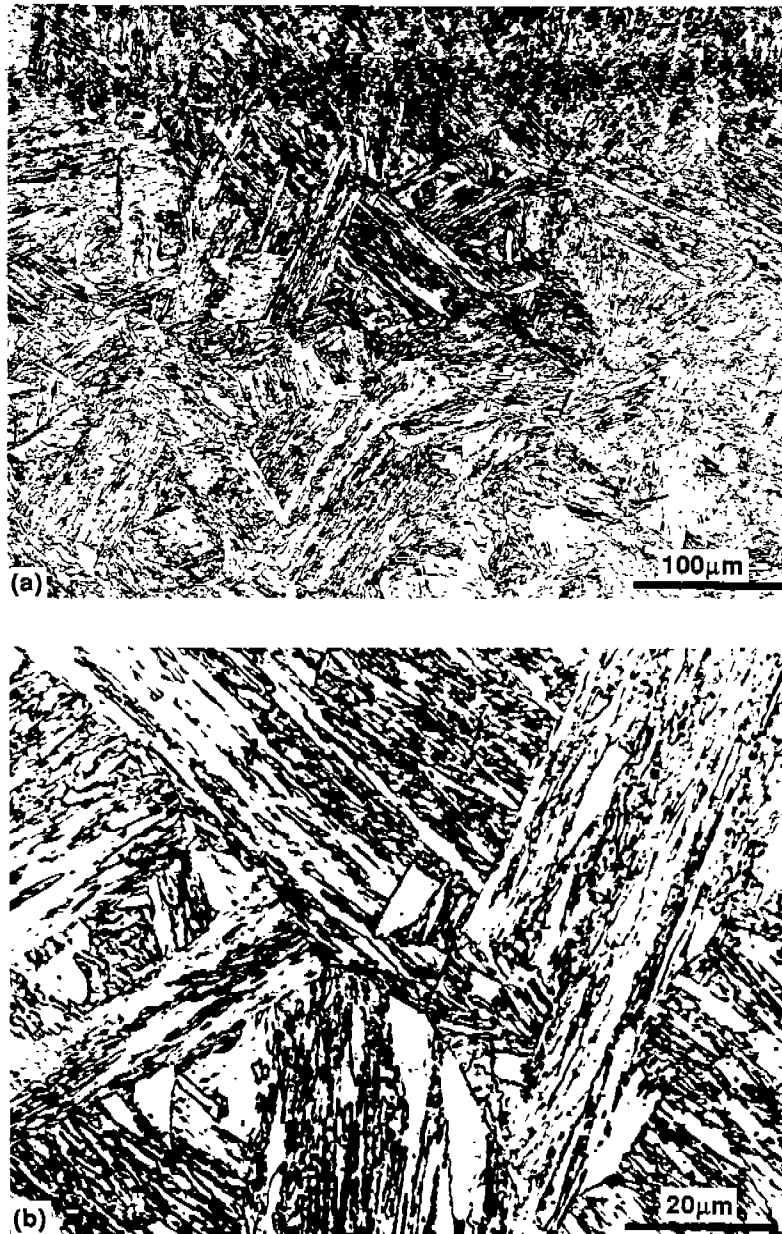
Fig. A-23. Microstructure of the coarse grained HAZ containing almost all the martensite; (a) 200X, (b) 1000X.

Etchant: 2% nital.
Welding Process: SMAW.
Heat Input: 67 kJ/in.
Cooling Time (800-500°C): 11 sec.
Grain Size: ASTM No.4 (90 μm).
Estimated Martensite Percentage: 100%.
Hardness: 378 DPH.

200

Fig. A-24.   Microstructure of the coarse grained HAZ containing predominant amount of martensite; (a) 200X, (b) 1000X.

Etchant: 2% nital.
Welding Process: SAW.
Heat Input: 224 kJ/in.
Cooling Time (800-500°C):   140 sec.
Grain Size: ASTM No.3 (125 μm).
Estimated Martensite Percentage: 85%.
Hardness: 385 DPH.

(a)

200μm

(b)
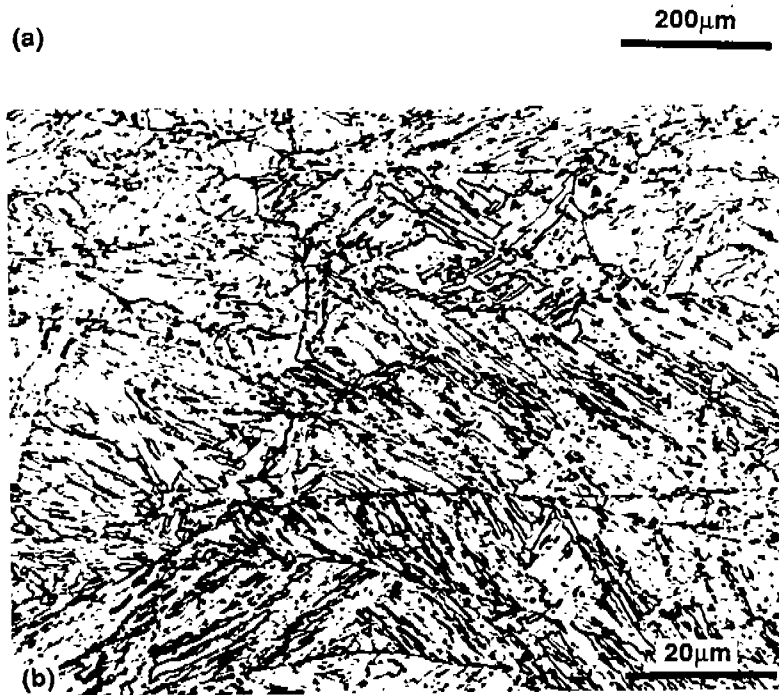
Fig. A-25.(a)   Distribution of inclusions, 100X, as-polished.

Fig. A-25.(b)   Base metal microstructure containing martensite and bainite,
1000X, 2% nital etched.

Condition :   As-received.
Grain Size :   ASTM No. 7 (32μm, 1000X)
Hardness :   321 DPH.

202
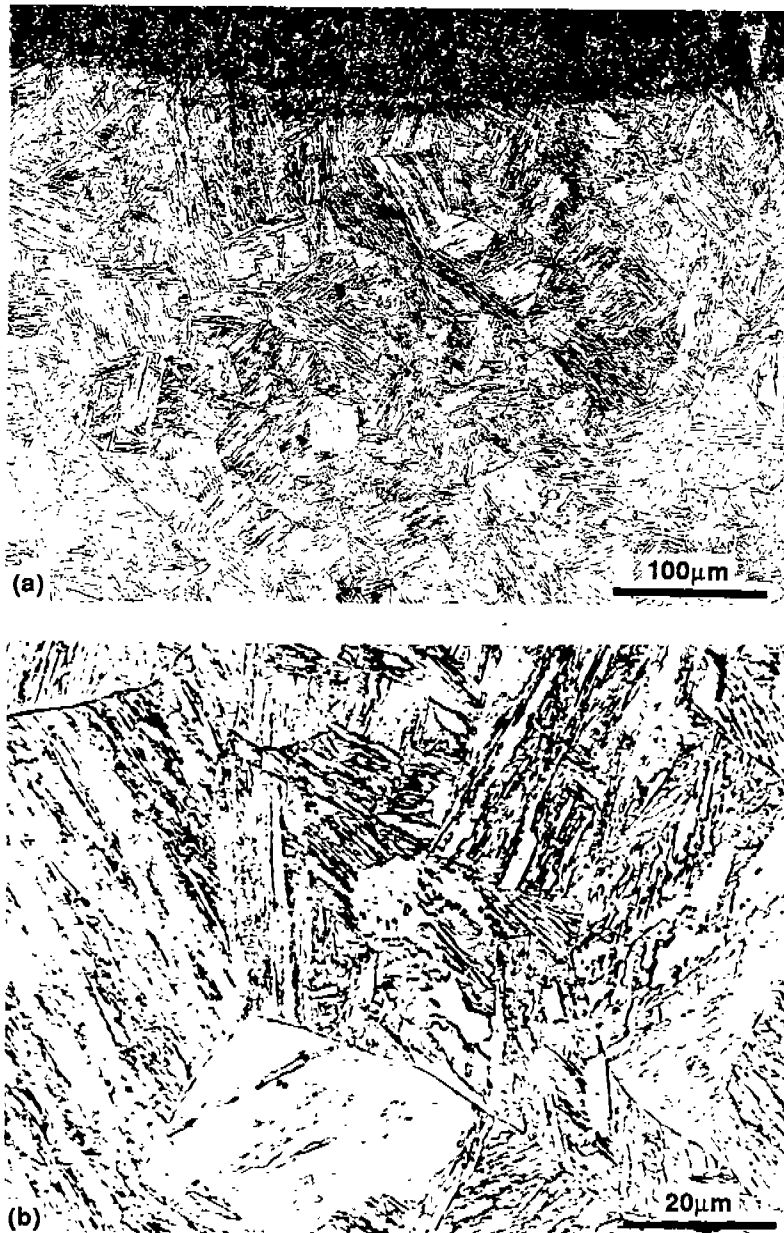
Fig. A-26.   Microstructure of the coarse grained HAZ containing martensite;
(a) 200X, (b) 1000X.

Etchant: 2% nital.
Welding Process: SMAW.
Heat Input: 15 kJ/in.
Cooling Time(800-500°C): 2.5 sec.
Grain Size: ASTM No. 6-7 (40μm).
Estimated Martensite Percentage: 100%.
Hardness: 399 DPH.
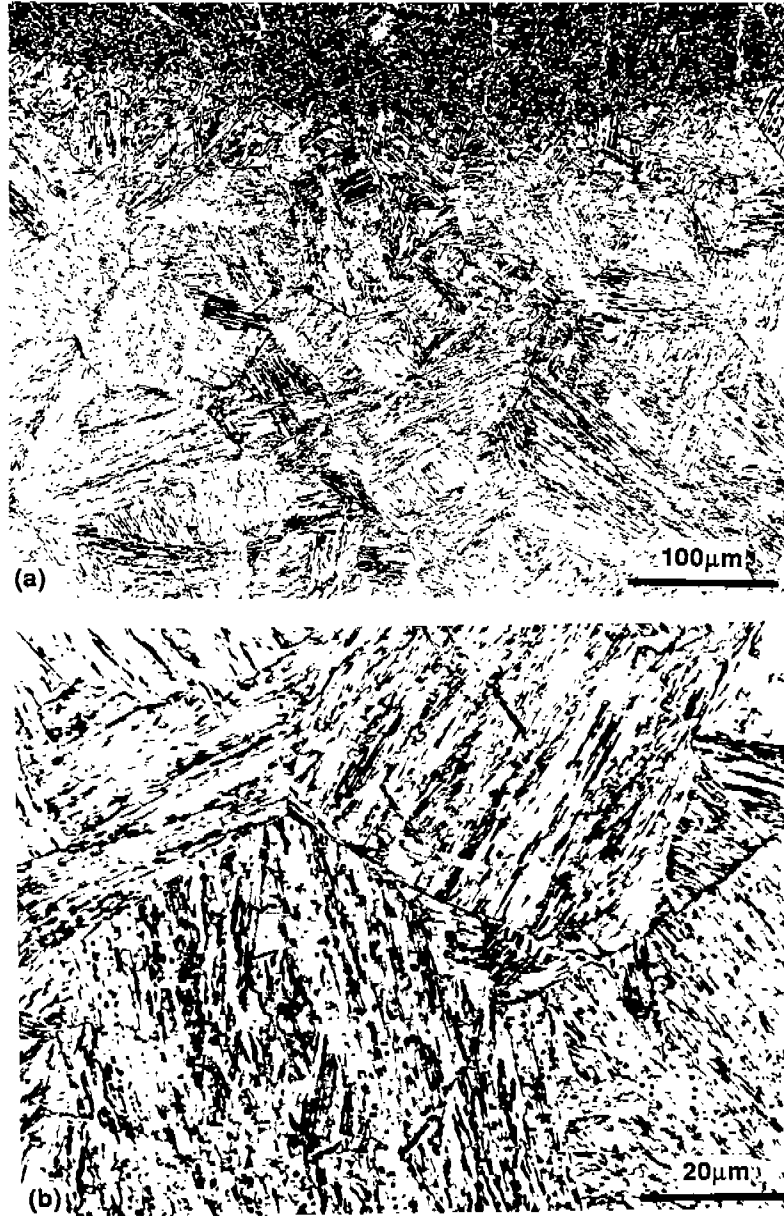
Fig. A-27.   Microstructure of the coarse grained HAZ containing predominant
amount of martensite; (a) 200X, (b) 1000X.

Etchant: 2% nital.
Welding Process: SMAW.
Heat Input: 67 kJ/in.
Cooling Time(800-500°C): 11 sec.
Grain size: ASTM No.4 (90μm).
Estimated Martensite Percentage: 85%.
Hardness: 355 DPH.

204
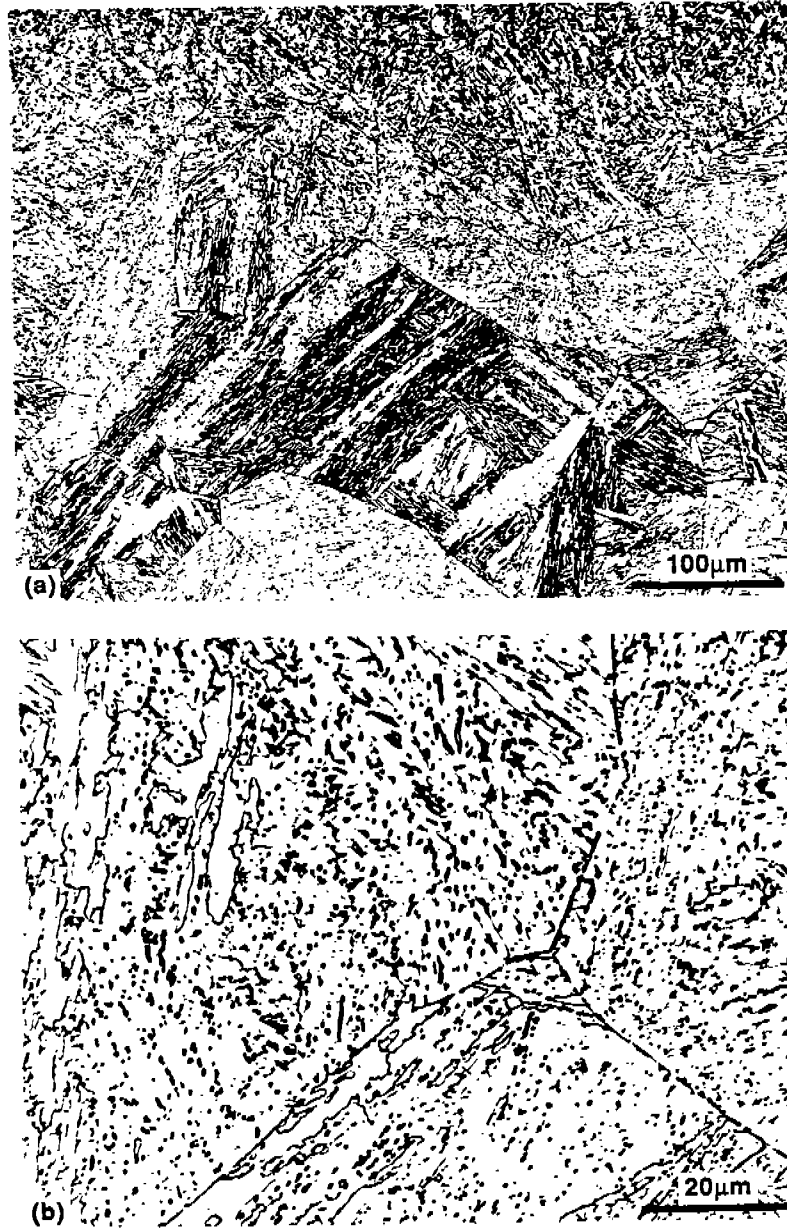
Fig. A-28.   Microstructure of the coarse grained HAZ containing mostly bainite and small amount of martensite; (a) 200X, (b)1000X.

Etchant: 2% nital.
Welding Process: SAW.
Heat Input: 336 kJ/in
Cooling Time (800-500°C):   80 sec.
Grain Size: ASTM No.3 (125μm).
Estimated Martensite Percentage: 12%.
Hardness: 289 DPH.

205

(a)

200μm

(b)

20μm

Fig. A-29.(a)   Distribution of Inclusions, 100X, as-polished.

Fig. A-29.(b)   Base metal microstructure containing ferrite, 1000X, 2% nital etched.

Condition: As-received.
Grain Size: ASTM No.6 (5μm, 1000X)
Hardness: 221 DPH.

206
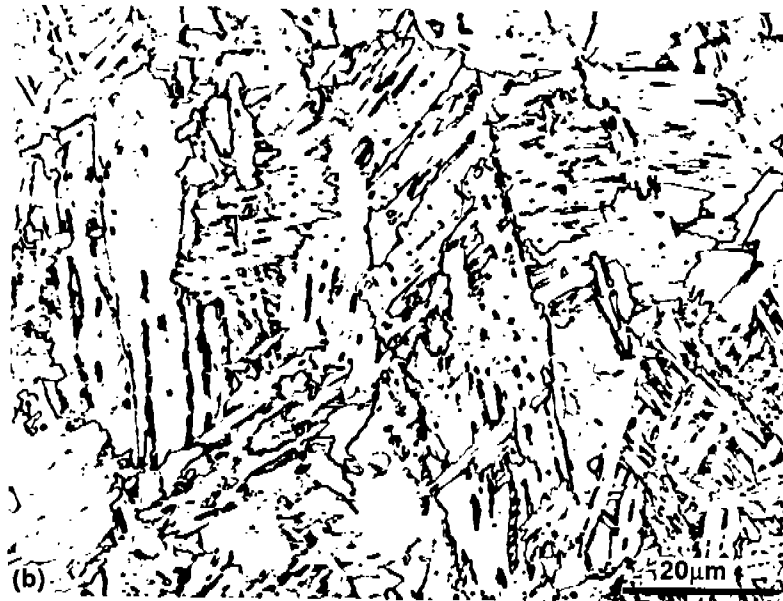
Fig. A-30.   Microstructure of the coarse grained HAZ containing bainite and
                  martensite; (a) 200X, (b) 1000X.

Etchant: 2% nital.
Welding Process: SMAW.
Heat Input: 15 kJ/in.
Cooling Time (800-500°C):   2.5 sec.
Grain Size: ASTM No.7 (30μm).
Estimated Martensite Percentage: 55%.
Hardness: 250 DPH.
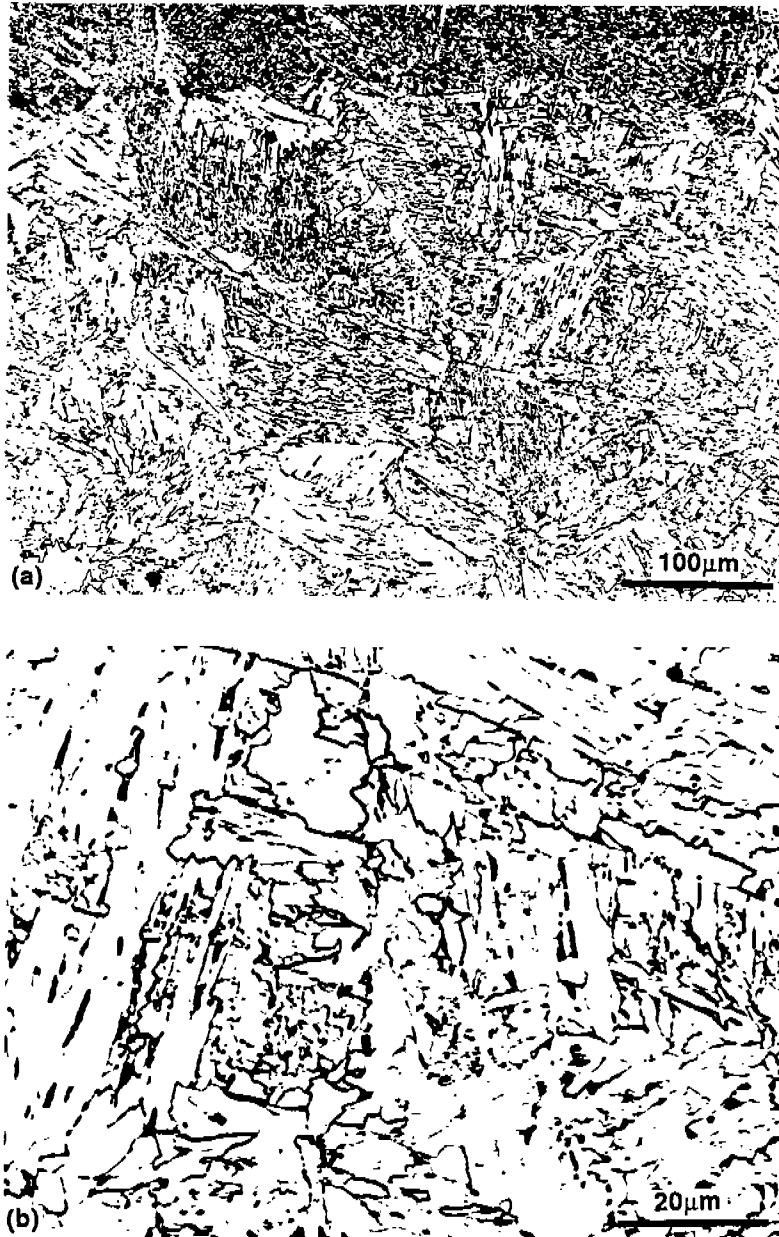
Fig. A-31. Microstructure of the coarse grained HAZ with almost fully bainite structure; (a) 200X, (b) 1000X.

Etchant: 2% nital.
Welding Process: SMAW.
Heat Input: 87 kJ/in
Cooling Time (800-500°C): 14.6 sec.
Grain Size: ASTM No. 2.5 (150μm).
Estimated Martensite Percentage: 6%.
Hardness: 225 DPH.

208

Fig. A-32   Microstructure of the coarse grained HAZ containing bainite and ferrite;
(a) 200X, (b) 1000X.

Etchant: 2% nital.
Welding Process: SAW.
Heat Input: 275 kJ/in.
Cooling Time (800-500°C):   90 sec.
Grain Size: ASTM No. 1-2 (200μm).
Estimated Martensite Percentage: 0%.
Hardness: 205 DPH.

(a)

200μm

(b)

20μm

Fig. A-33.(a)   Distribution of inclusions, 100X, as-polished.

Fig. A-33.(b)   Base metal microstructure containing a banded structure ferrite and pearlite; 1000X, 2% nital etched.

Condition: As-received.
Grain Size: ASTM No. 9-10 (12.5μm, 1000X).
Hardness: 172 DPH.

Fig. A-34.   Microstructure of the coarse grained HAZ containing bainite and; martensite; (a) 200X, (b) 1000X.

Etchant: 2% nital.
Welding Process: SMAW.
Heat Input: 15 kJ/in.
Cooling Time (800-500°C): 2.5 sec.
Grain Size: ASTM No. 6-7 (40μm).
Estimated Martensite Percentage: 68%.
Hardness: 300 DPH.

Fig. A-35. Microstructure of the coarse grained HAZ containing ferrite and small amount of martensite; (a) 200X, (b) 1000X.

Etchant: 2% nital.
Welding Process: SMAW.
Heat Input: 67 kJ/in.
Cooling Time (800-500°C): 11 sec.
Grain Size: ASTM No.4 (90μm).
Estimated Martensite Percentage: 17%.
Hardness: 242 DPH.

212

MATERIAL: AC-50
Coarse Grained HAZ

Fig. A-36. Microstructure of the coarse grain HAZ containing ferrite and bainite; (a) 200X, (b) 1000X.

Etchant: 2% nital.
Welding Process: SAW.
Heat Input: 224 kJ/in.
Cooling Time (800-500°C): 90 sec.
Grain Size: ASTM No.3 (125μm).
Estimated Martensite Percentage: 0%.
Hardness: 207 DPH.

213

APPENDIX-B

HAZ SOFTENING DATA
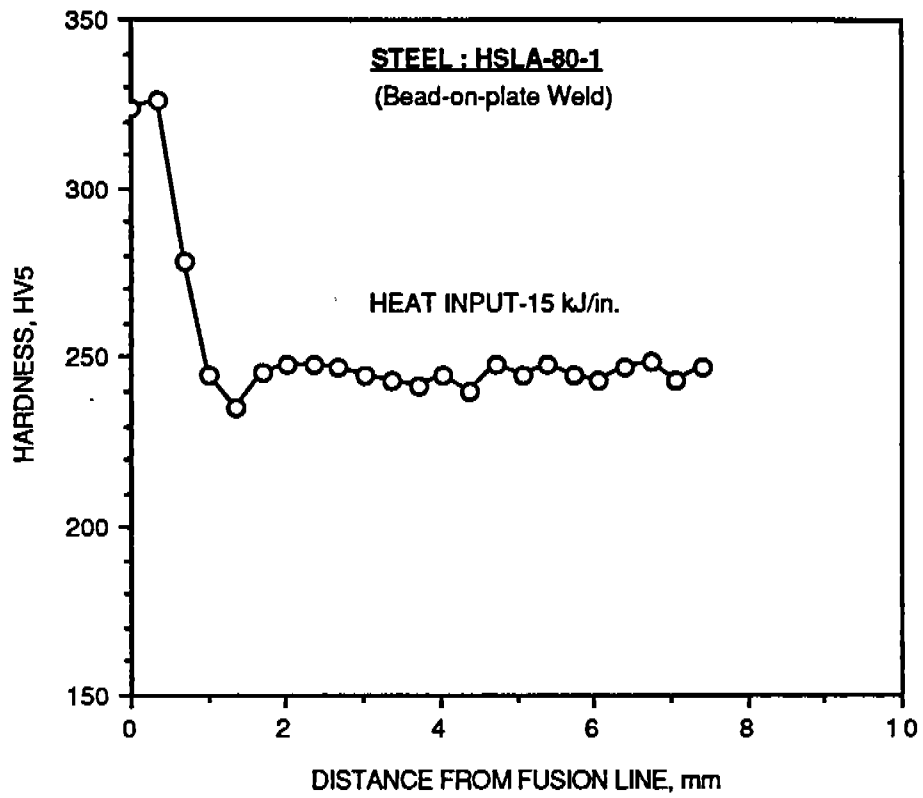
Fig. B-1. HAZ hardness profile. Steel : HSLA-80-1 . Heat Input : 15 kJ/in
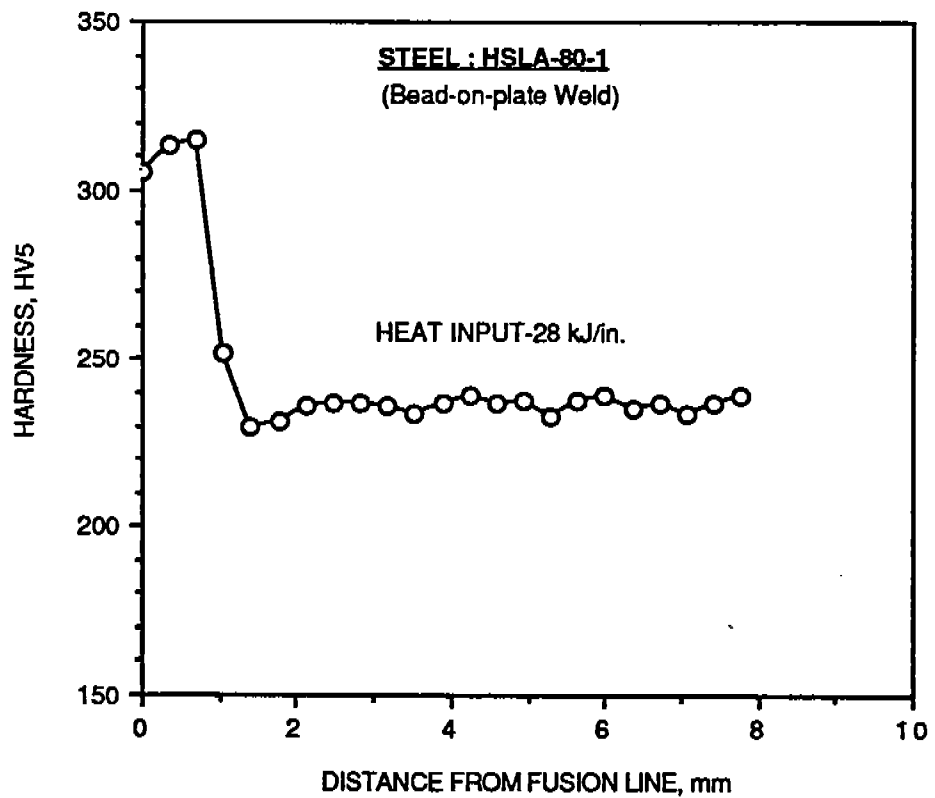
Fig. B-2. HAZ hardness profile. Steel : HSLA-80-1. Heat Input : 28 kJ/in
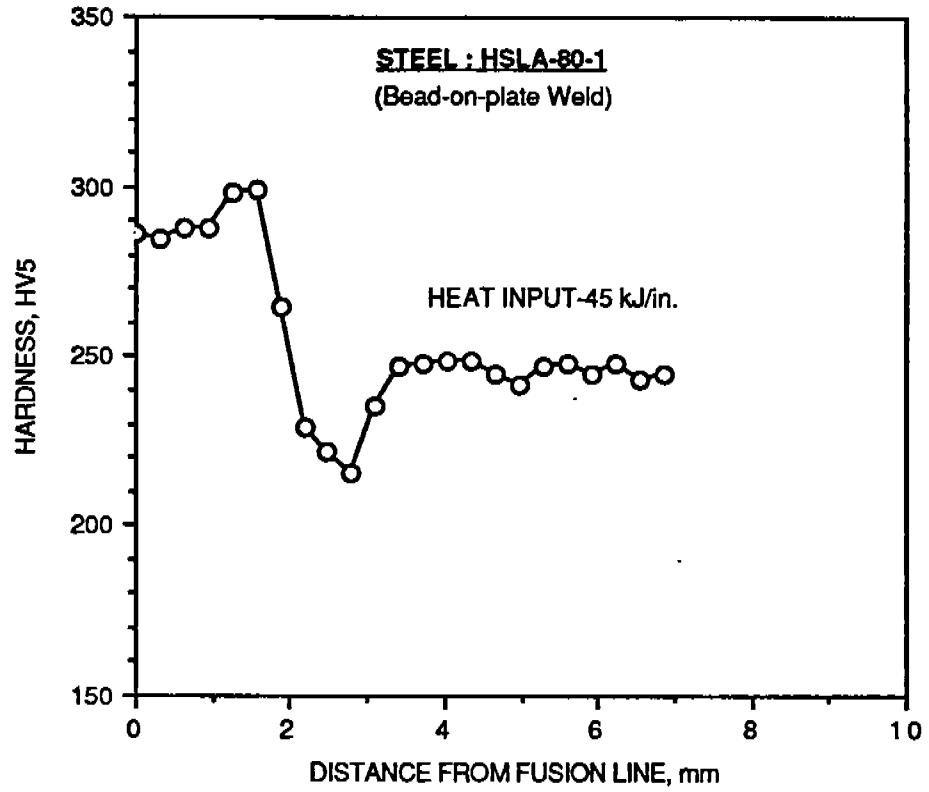
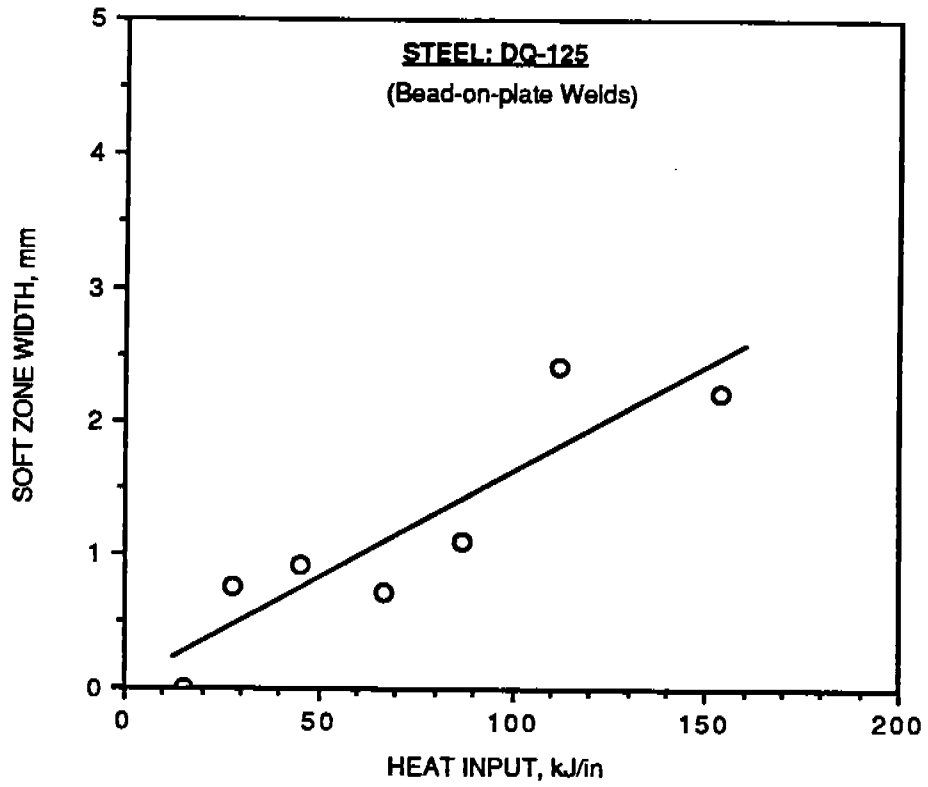Fig. B-3.   HAZ   hardness   profile. Steel :   HSLA-80-1 . Heat Input : 45 kJ/in
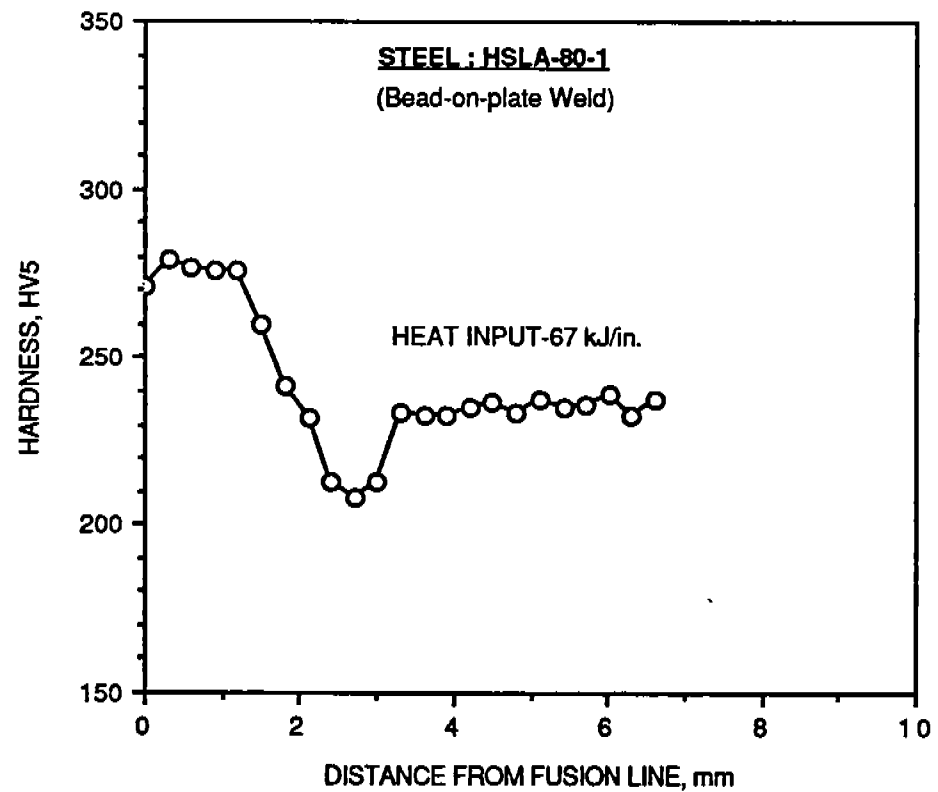
Fig. B-4.   HAZ   hardness   profile. Steel :   HSLA-80-1 . Heat   Input : 67 kJ/in

217
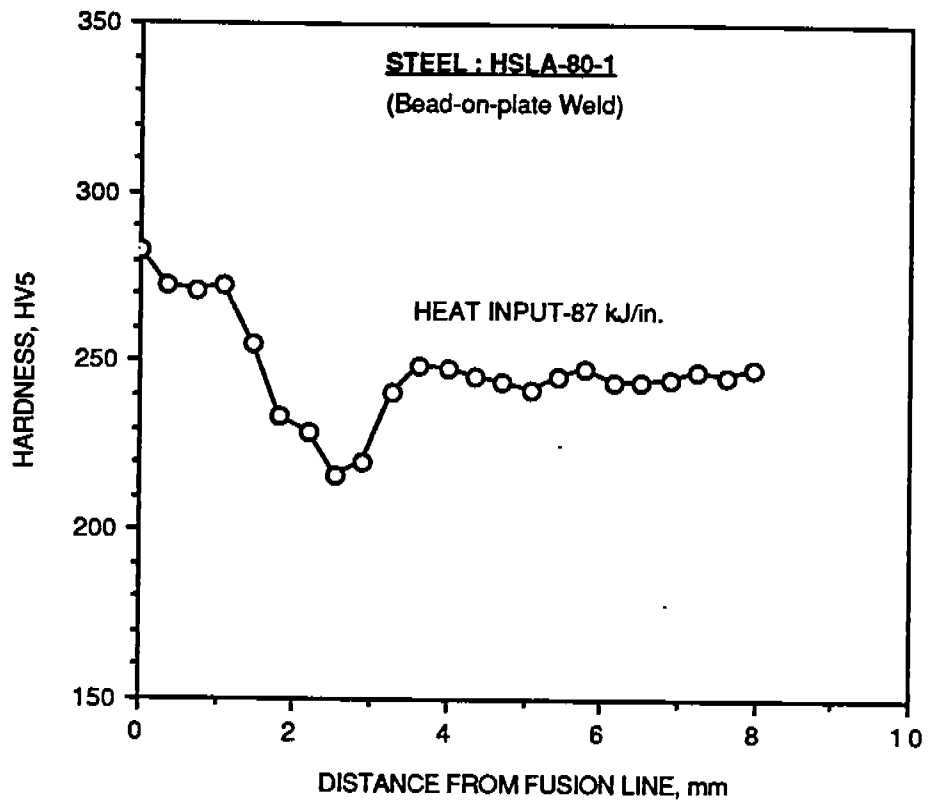
Fig. B-5. HAZ hardness profile. Steel : HSLA-80-1 . Heat Input : 87 kJ/in
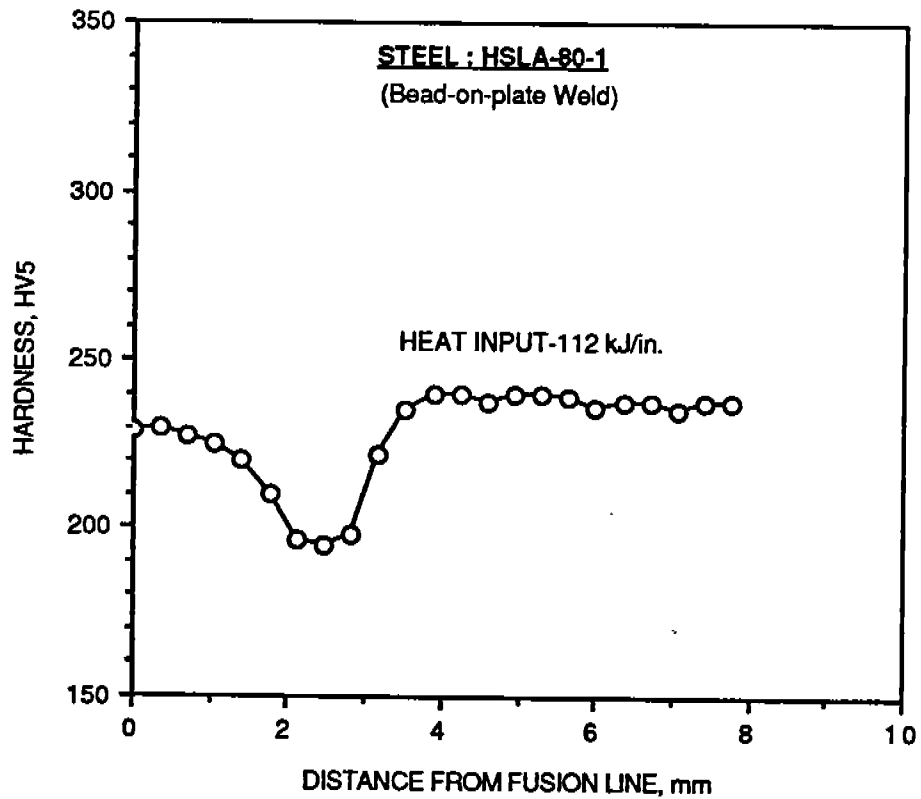
Fig. B-6. HAZ hardness profile. Steel : HSLA-80-1 . Heat Input : 112 kJ/in

218
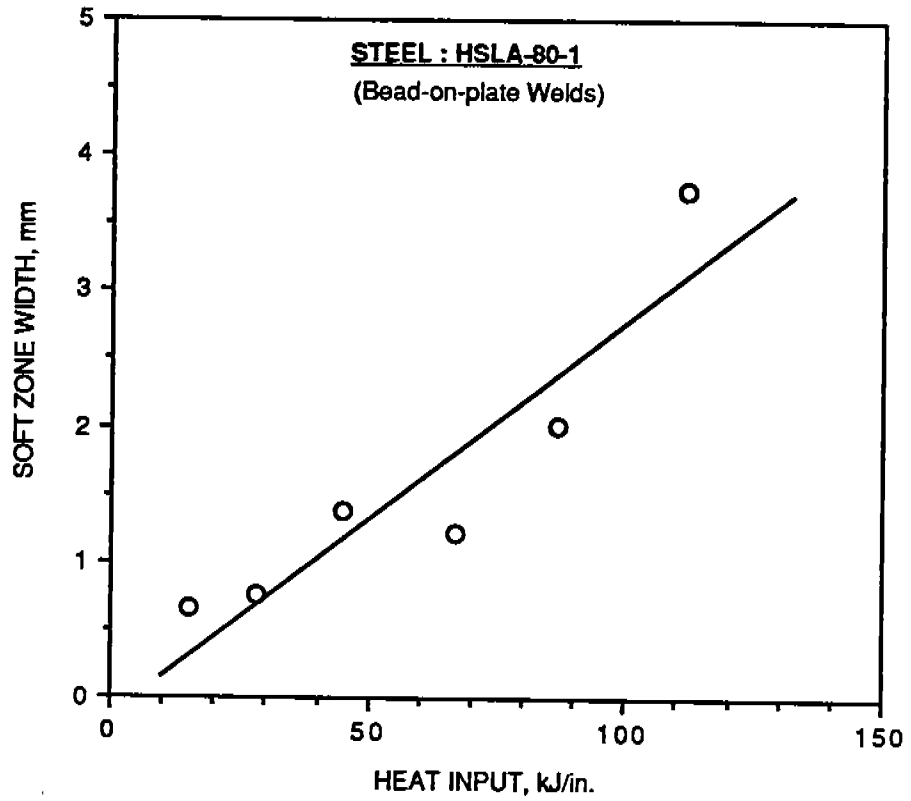
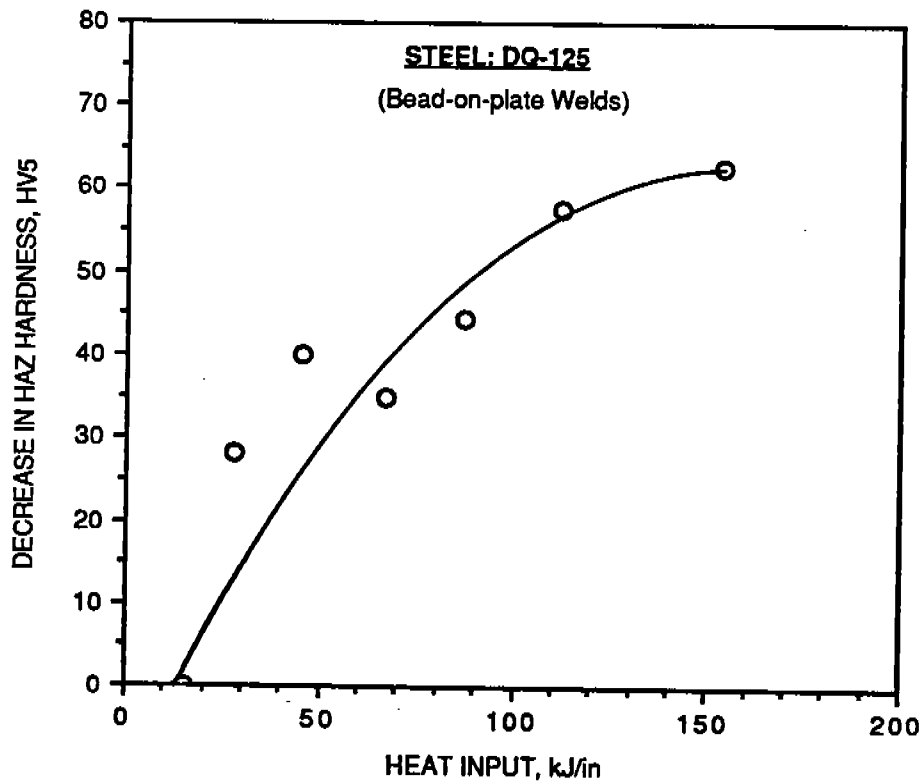Fig. B-7.   Variation of soft zone width with heat input for   HSLA-80-1
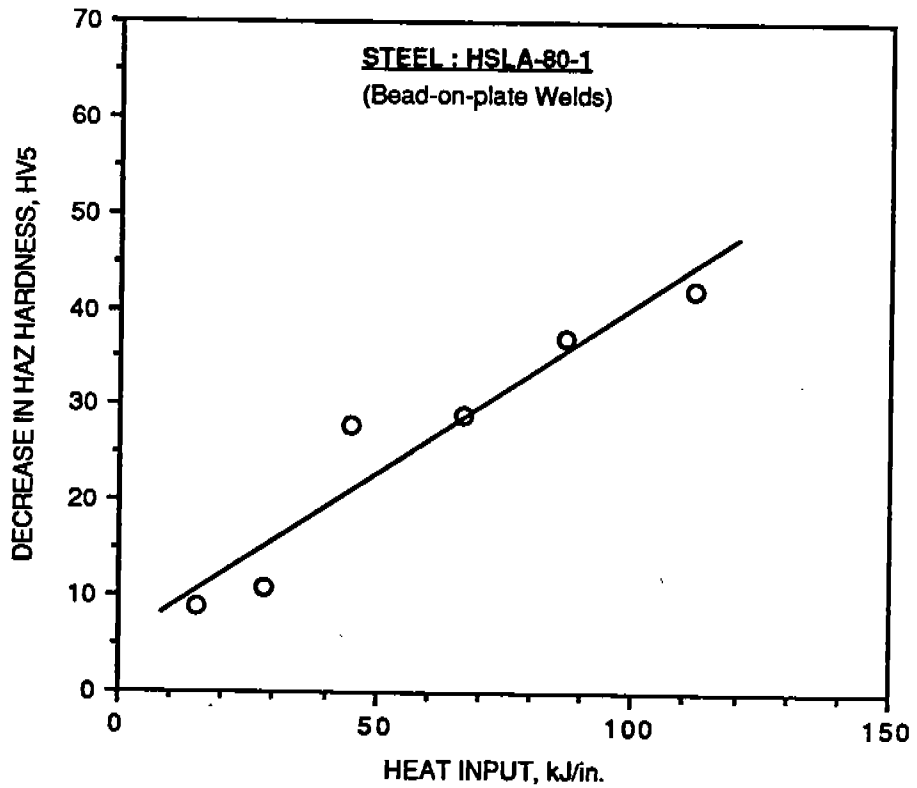
Fig.   B-8.   Variation of decrease in HAZ hardness with heat input for   HSLA-80-1
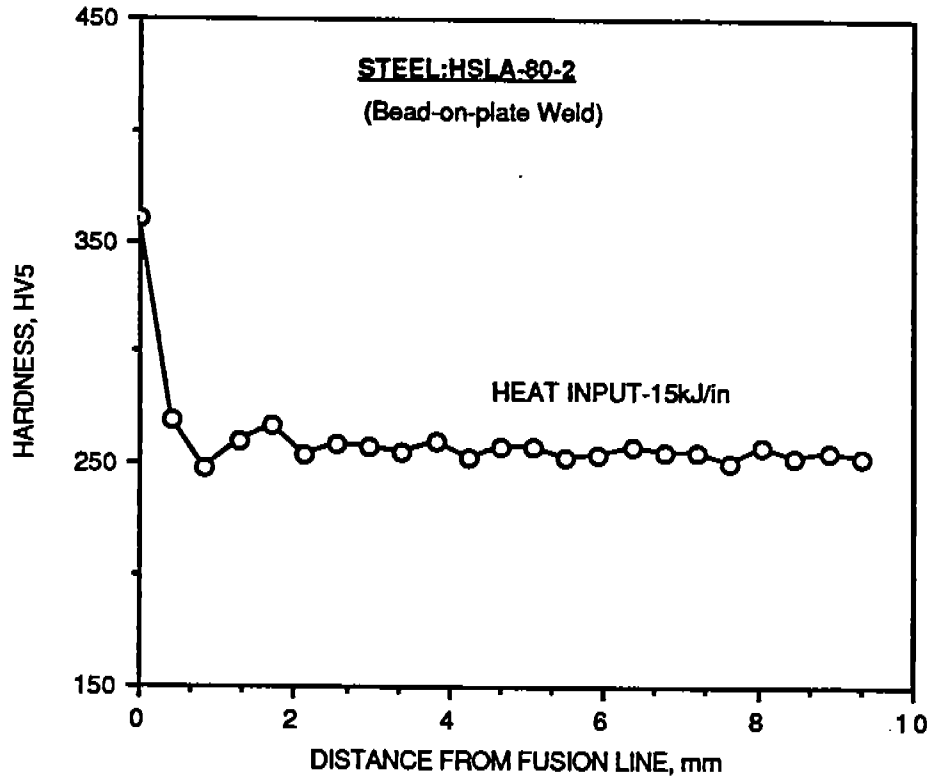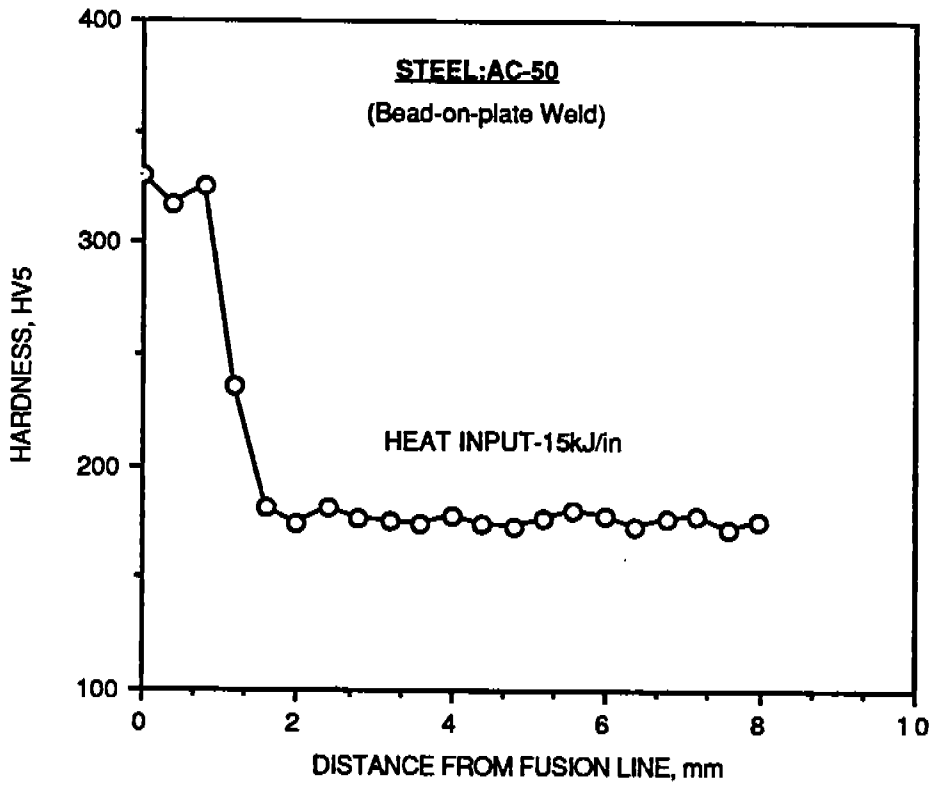
Fig. B-9.   HAZ   hardness   profile. Steel :   HSLA-80-2 . Heat   Input : 15kJ/in
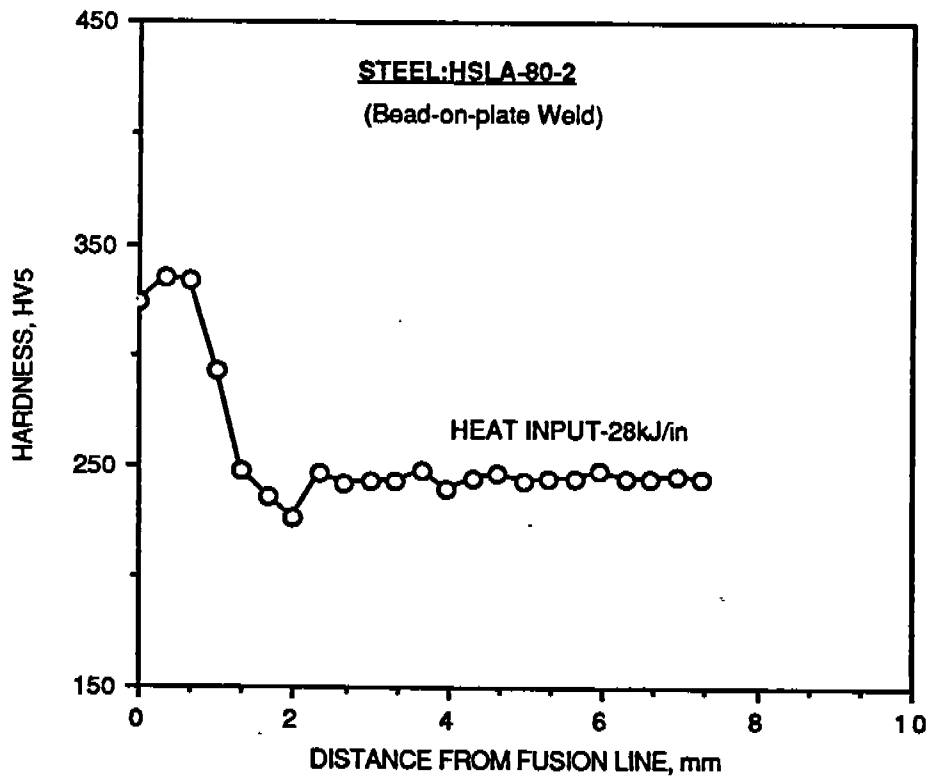

Fig. B-10.   HAZ   hardness   profile. Steel :   HSLA-80-2. Heat   Input : 28 kJ/in

220
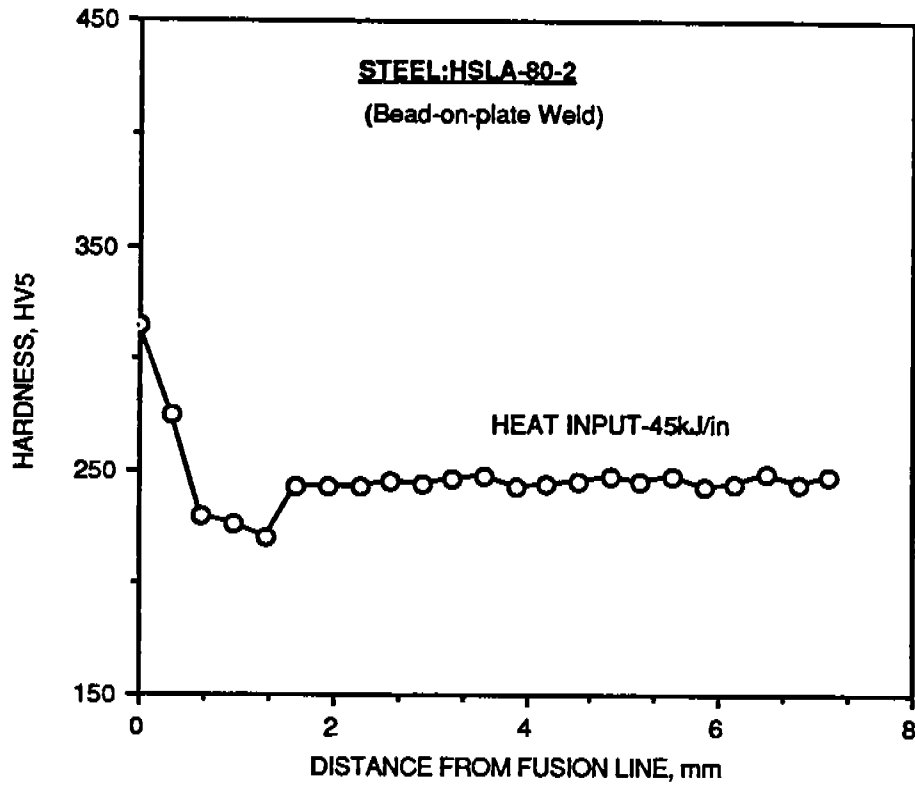
Fig. B-11.   HAZ hardness profile. Steel :   HSLA-80-2. Heat Input : 45 kJ/in
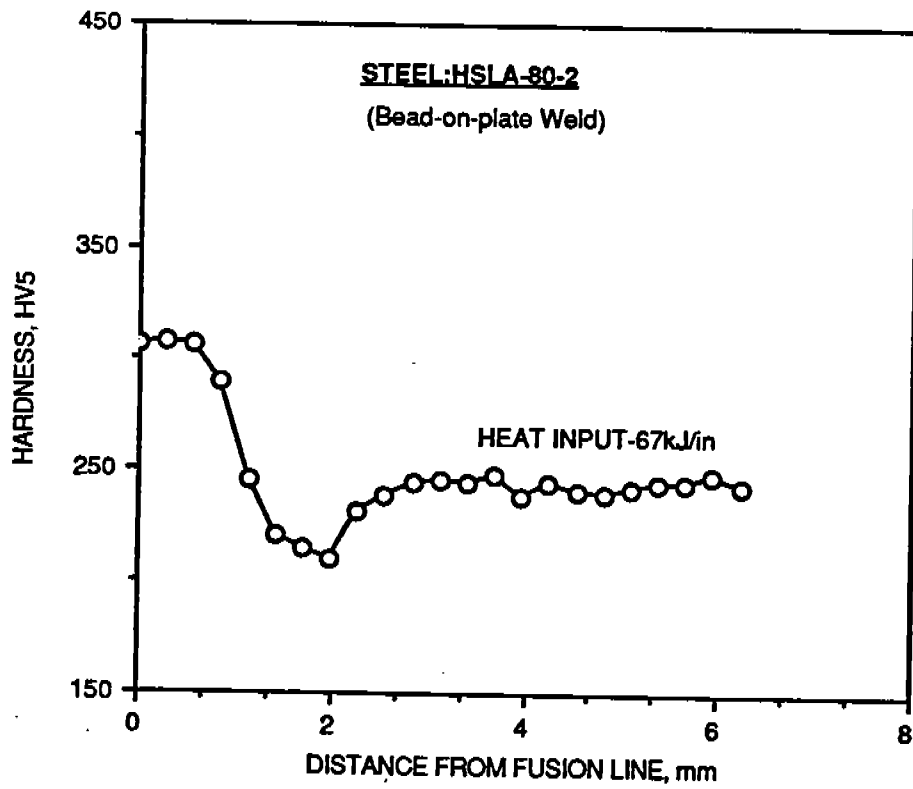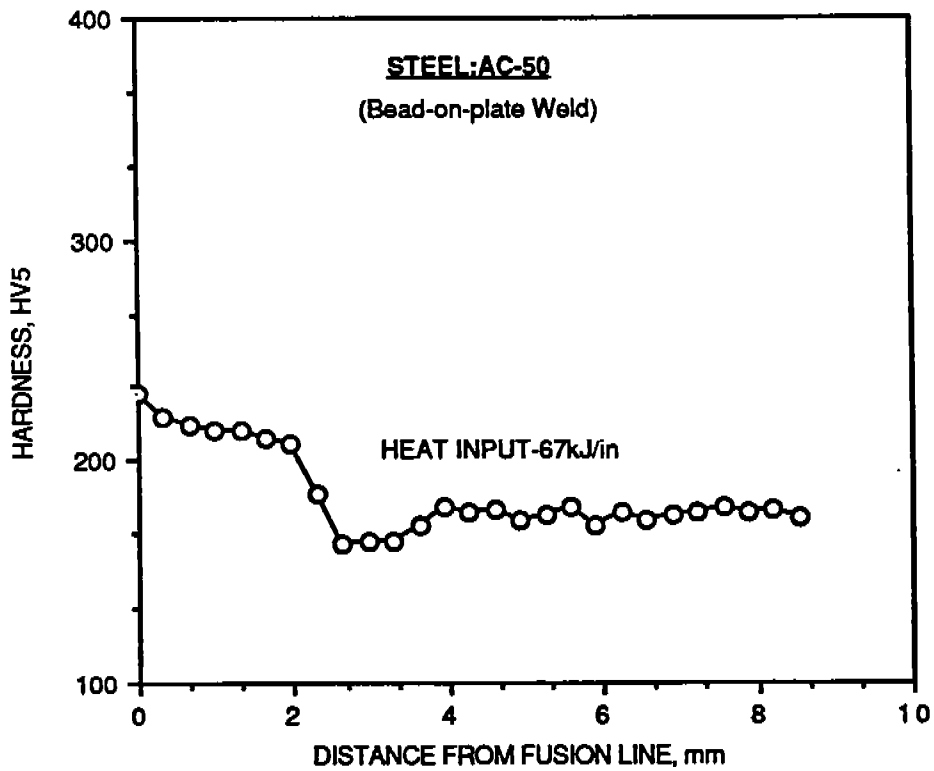

Fig. B-12.   HAZ hardness profile. Steel :   HSLA-80-2. Heat Input : 67 kJ/in
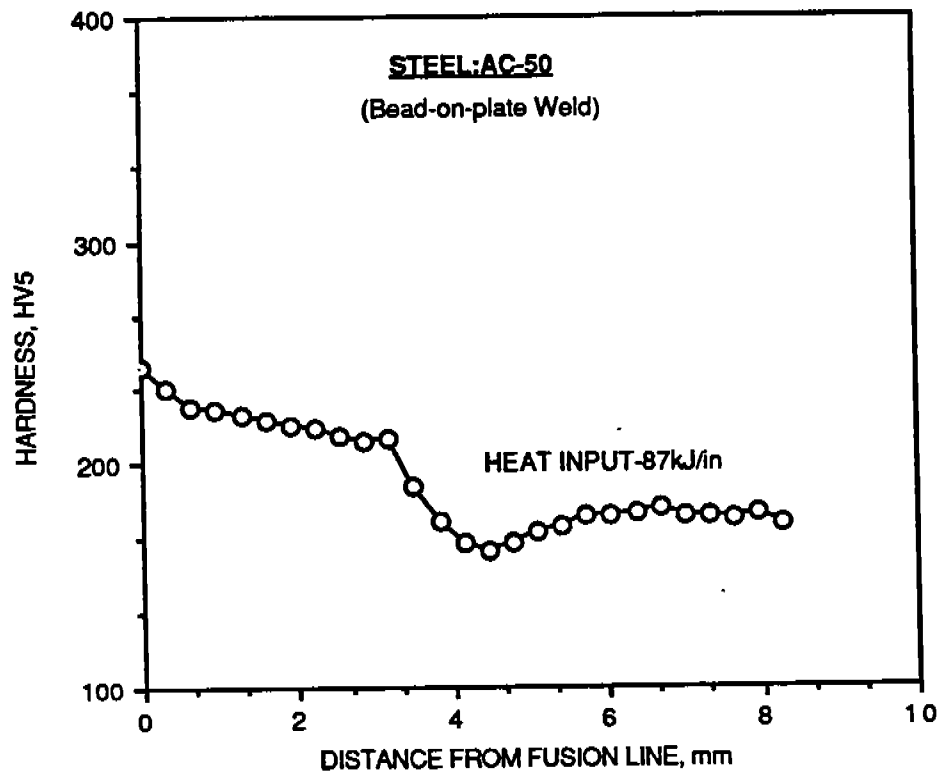
221
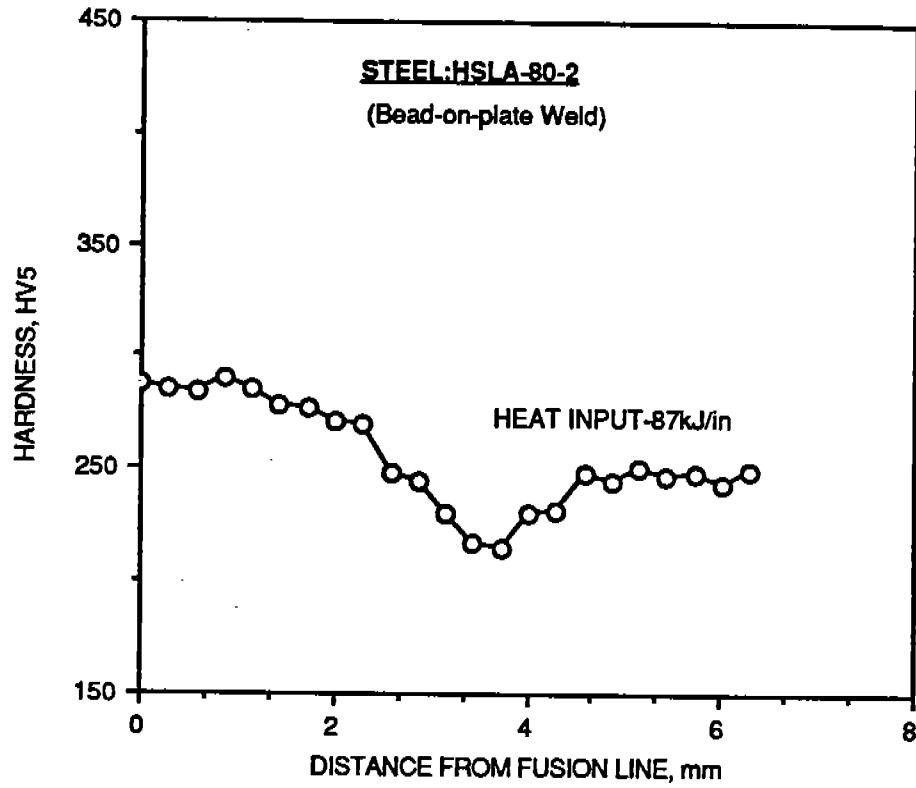
Fig. B-13.   HAZ hardness profile. Steel :   HSLA-80-2. Heat Input : 87 kJ/in
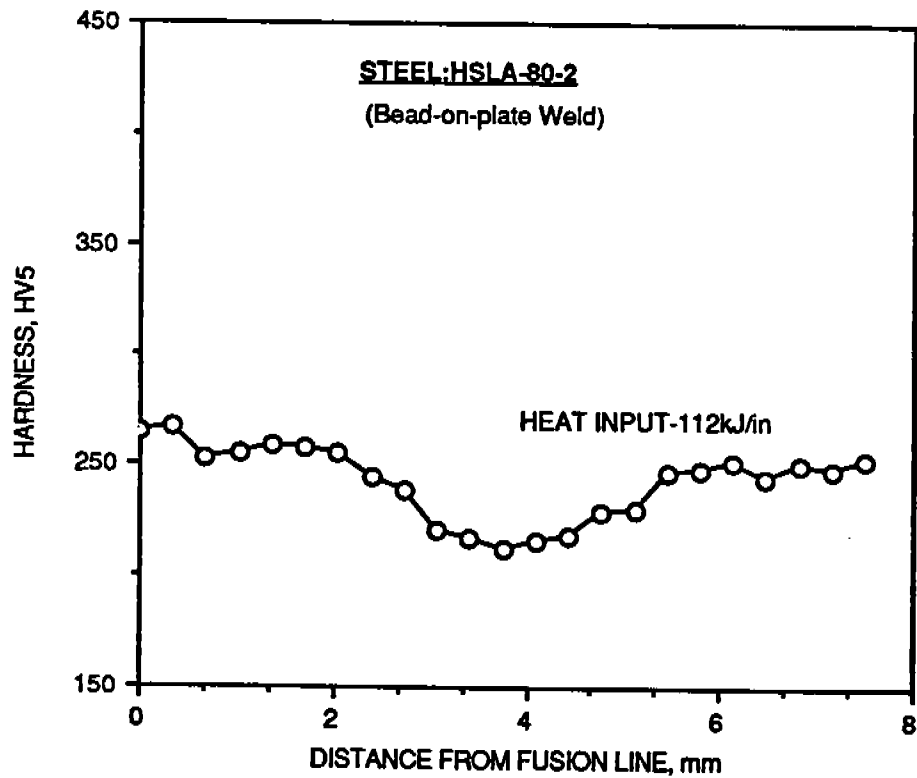
Fig. B-14.   HAZ hardness profile. Steel :   HSLA-80-2. Heat Input : 112 kJ/in

222
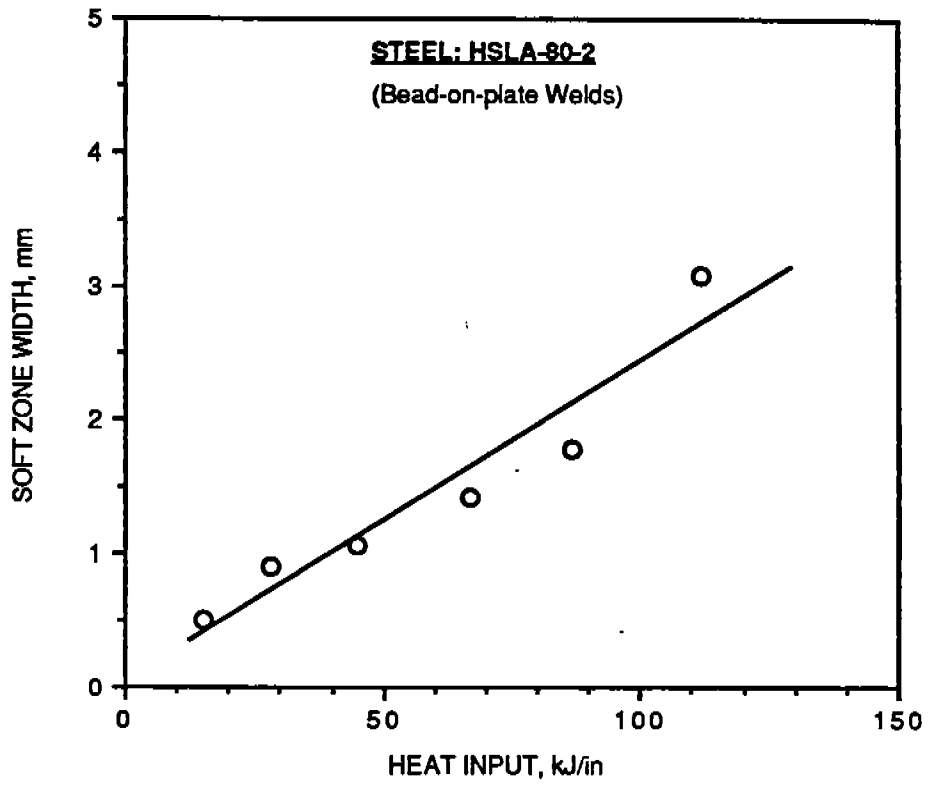
Fig. B-15. Variation of soft zone width with heat input for HSLA-80-2
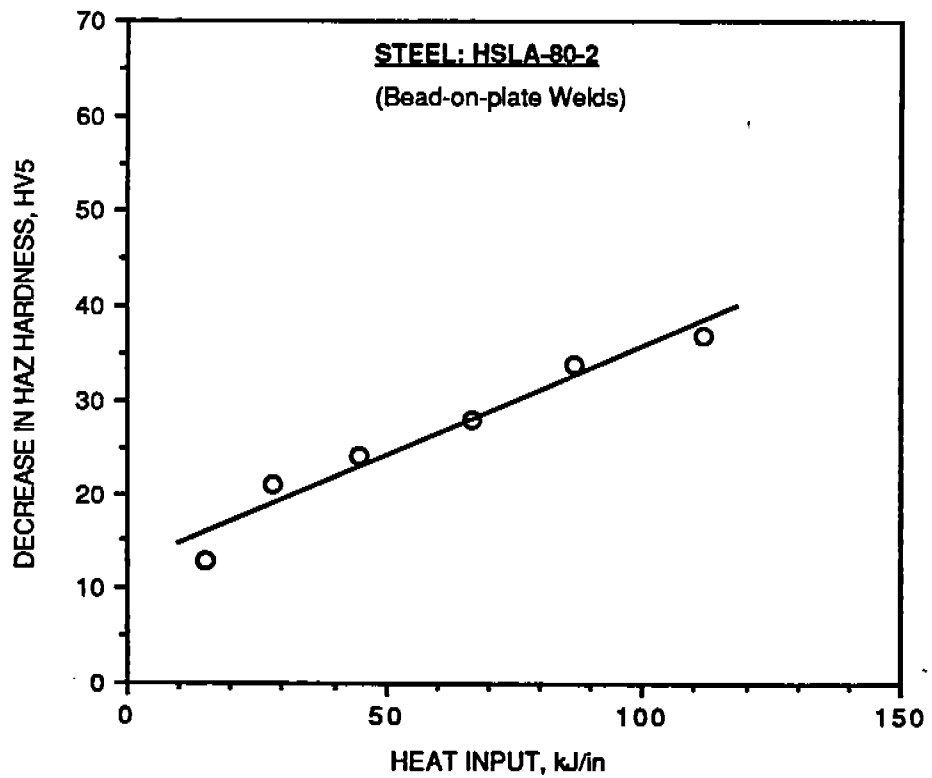
Fig. B-16. Variation of decrease in HAZ hardness with heat input for HSLA-80-2

223
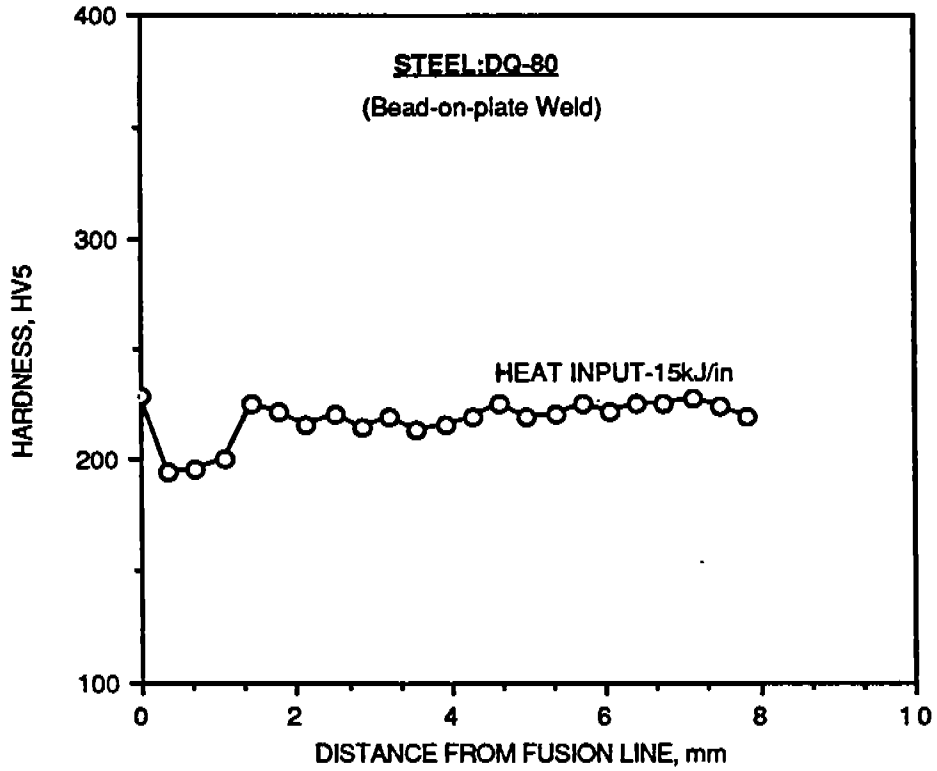
Fig. B-17.   HAZ hardness profile. Steel :   DQ-80 . Heat Input : 15 kJ/in
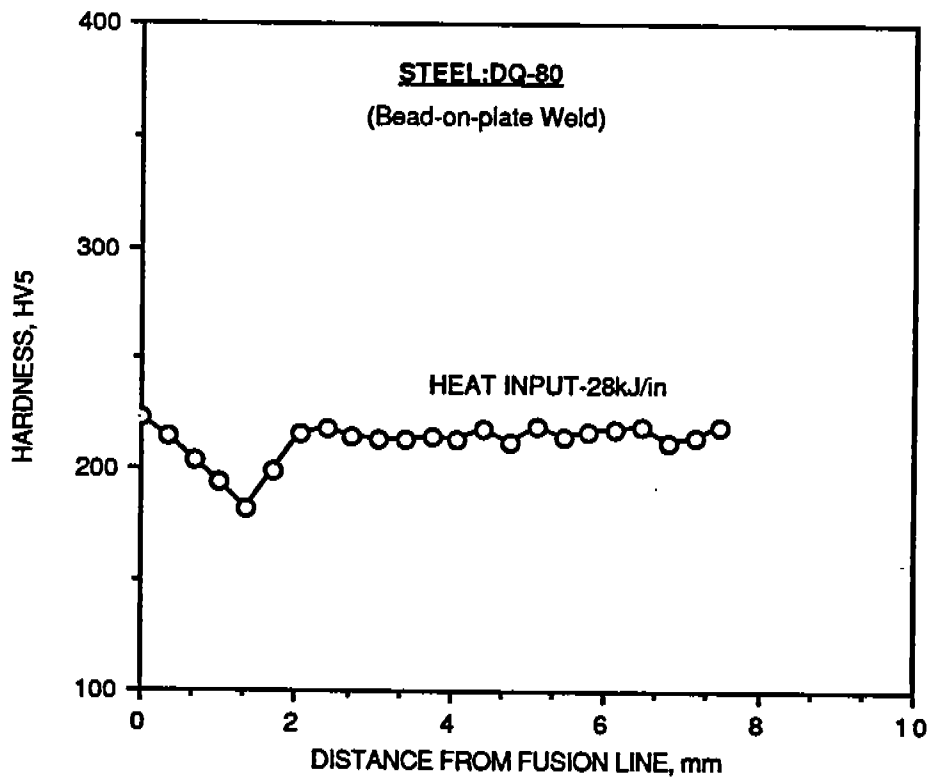
Fig. B-18.   HAZ hardness profile. Steel :   DQ-80. Heat Input : 28 kJ/in

224
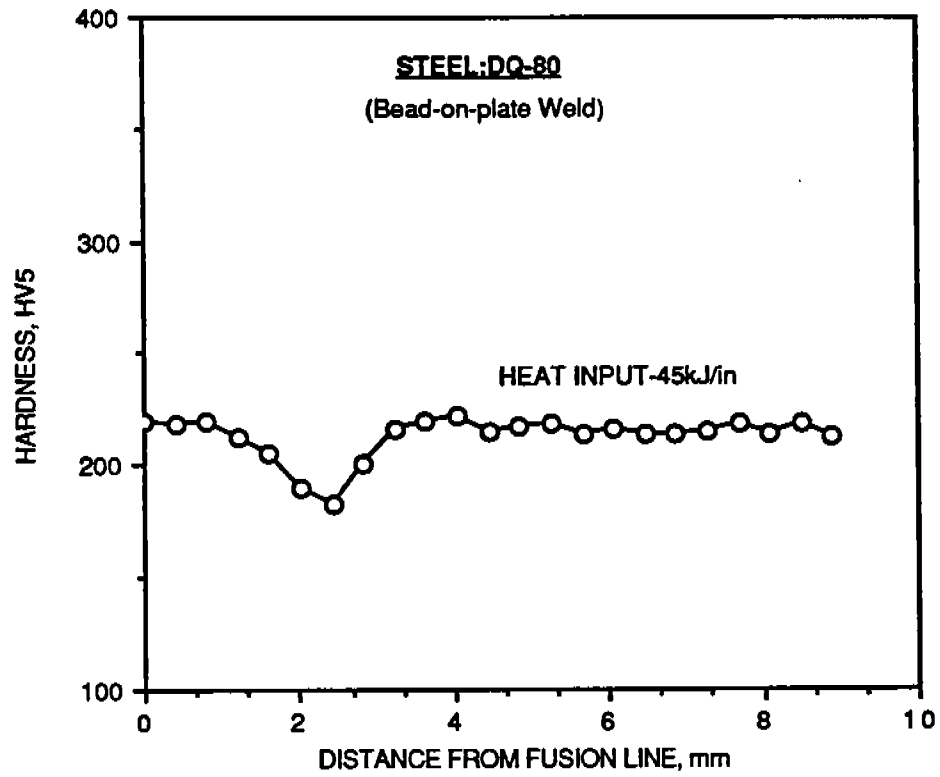
Fig. B-19.   HAZ hardness profile. Steel :   DQ-80. Heat   Input : 45 kJ/in
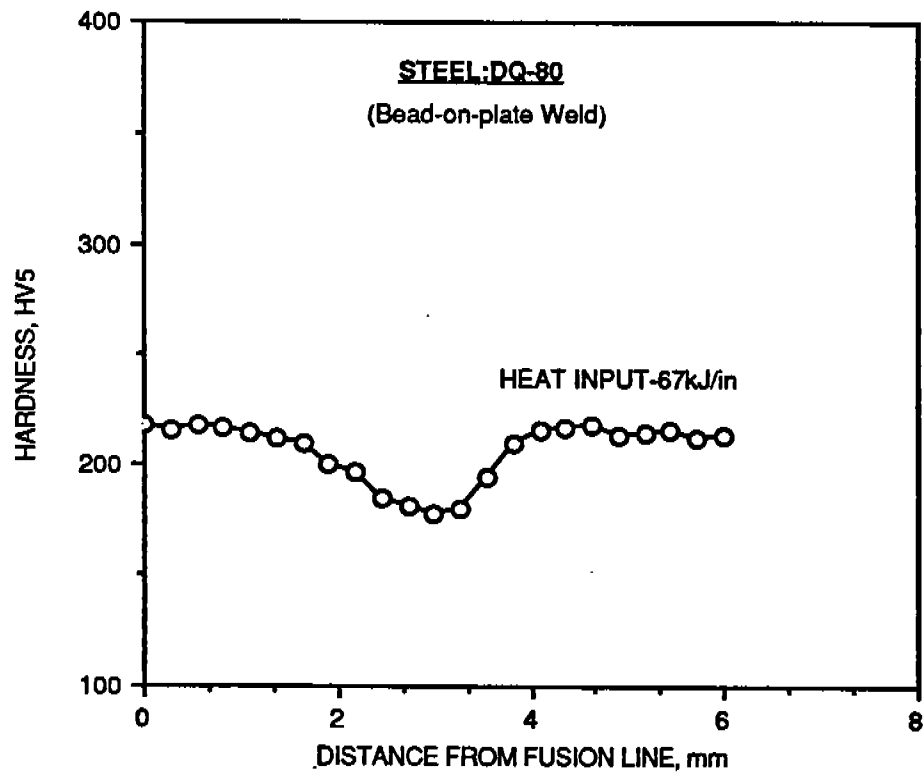
Fig. B-20.   HAZ hardness profile. Steel :   DQ-80. Heat   Input : 67 kJ/in

225
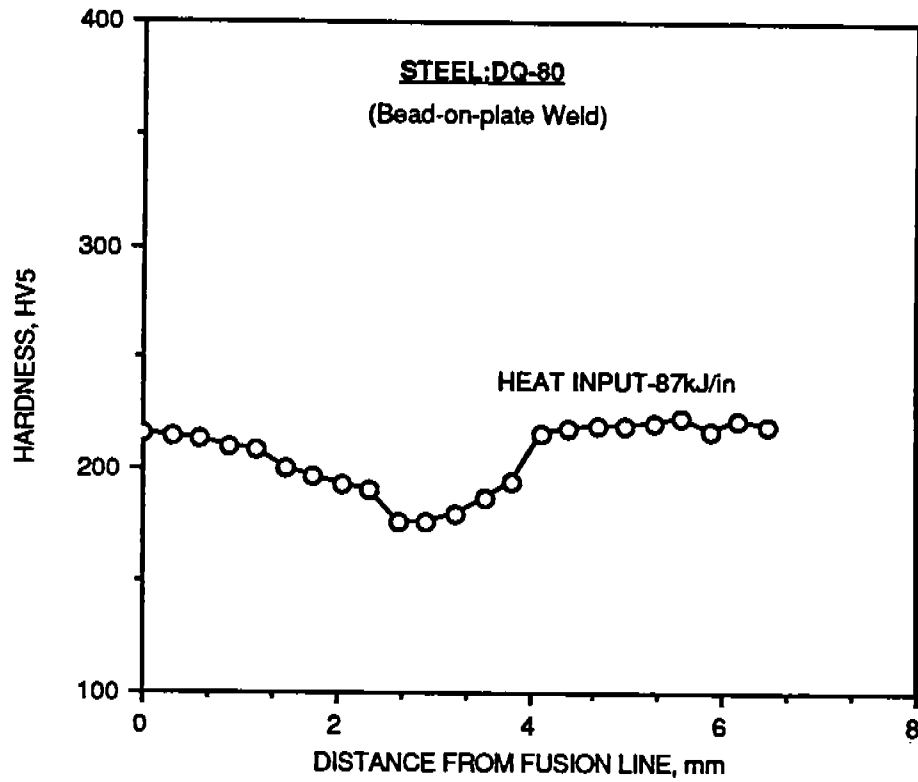
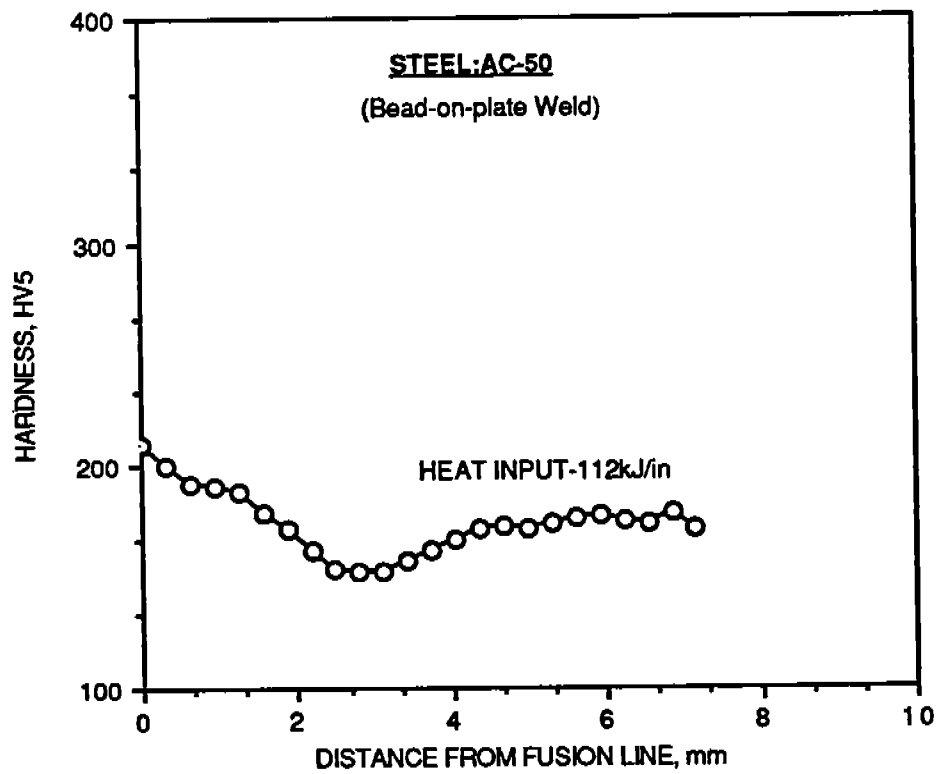Fig. B-21.   HAZ hardness profile. Steel :   DQ-80. Heat Input : 87 kJ/in
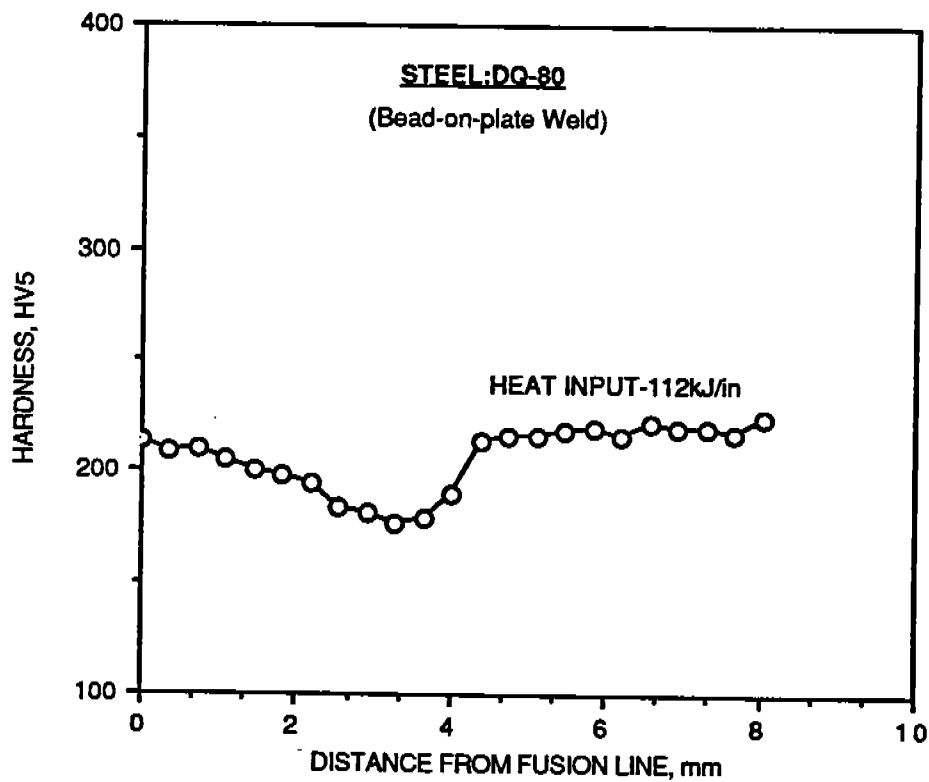
Fig. B-22.   HAZ hardness profile. Steel :   DQ-80. Heat Input : 112 kJ/in
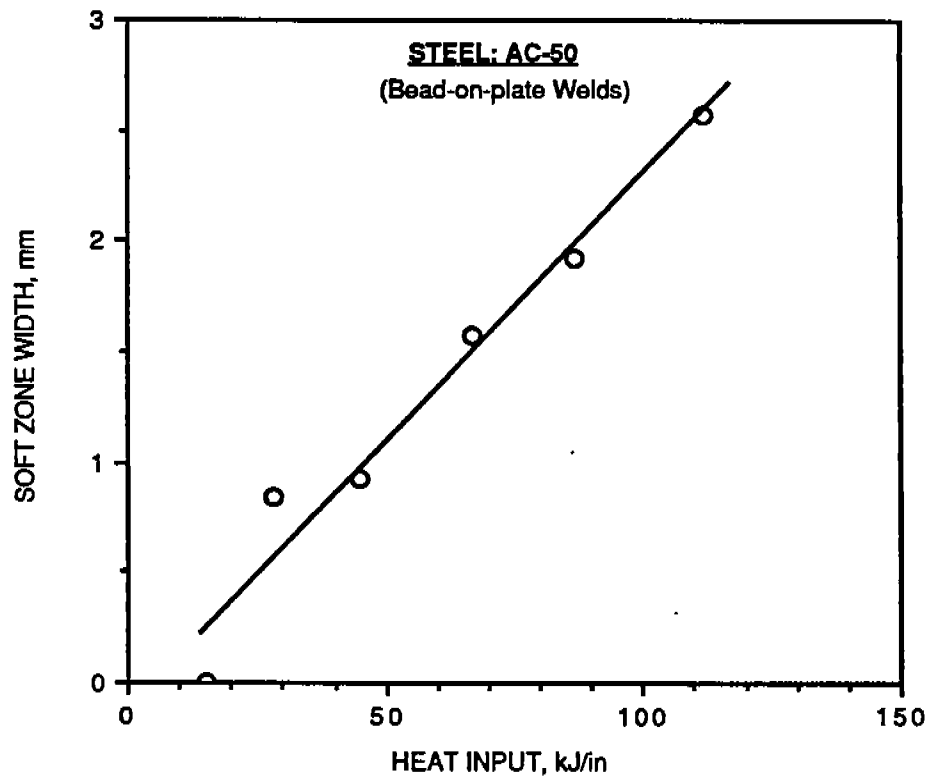
226
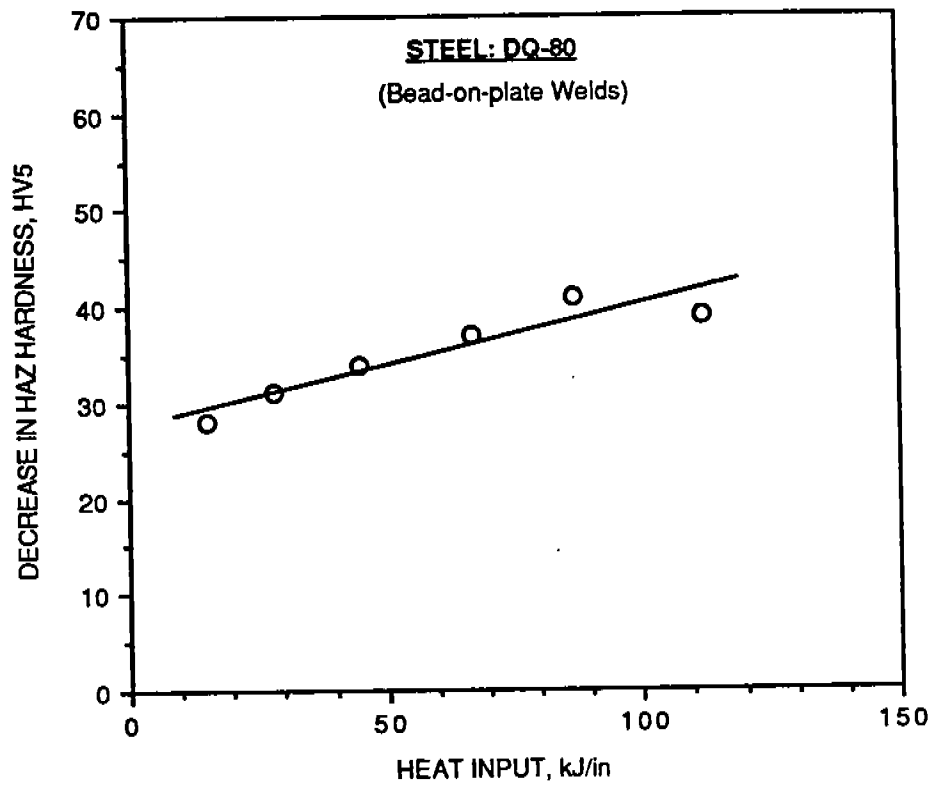
Fig. B-23.   Variation of soft zone width with heat input for   DQ-80
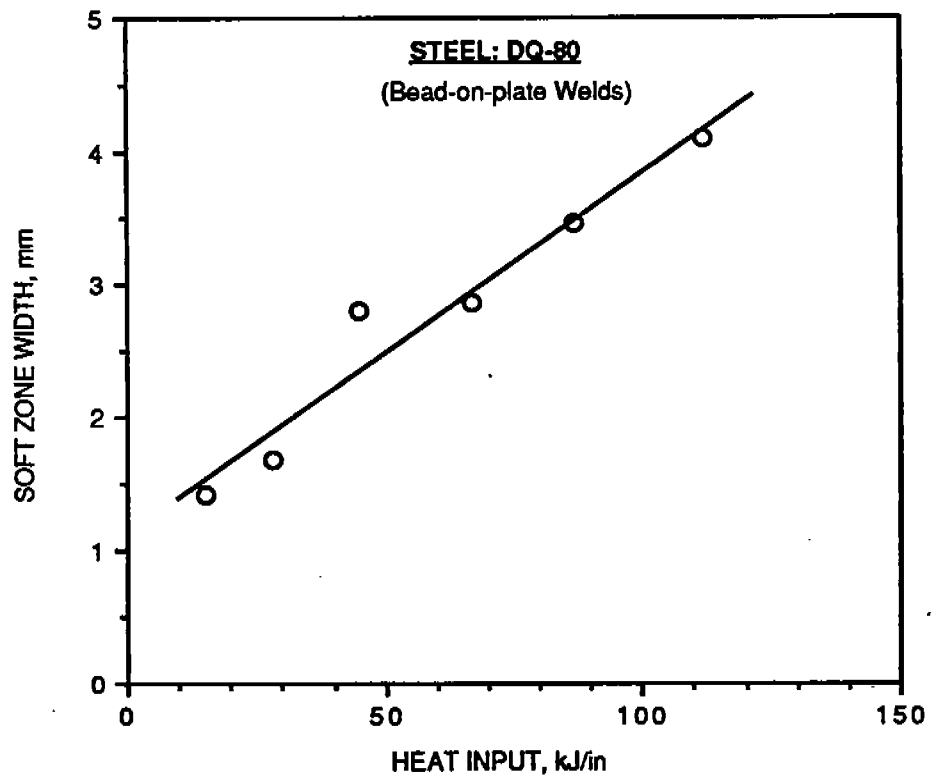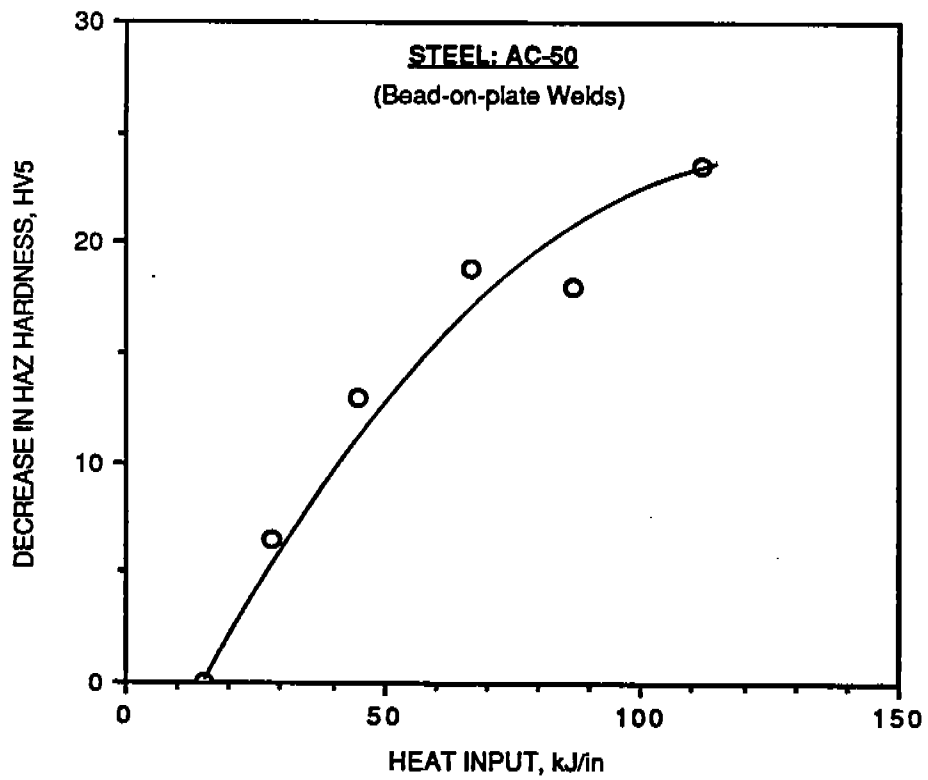

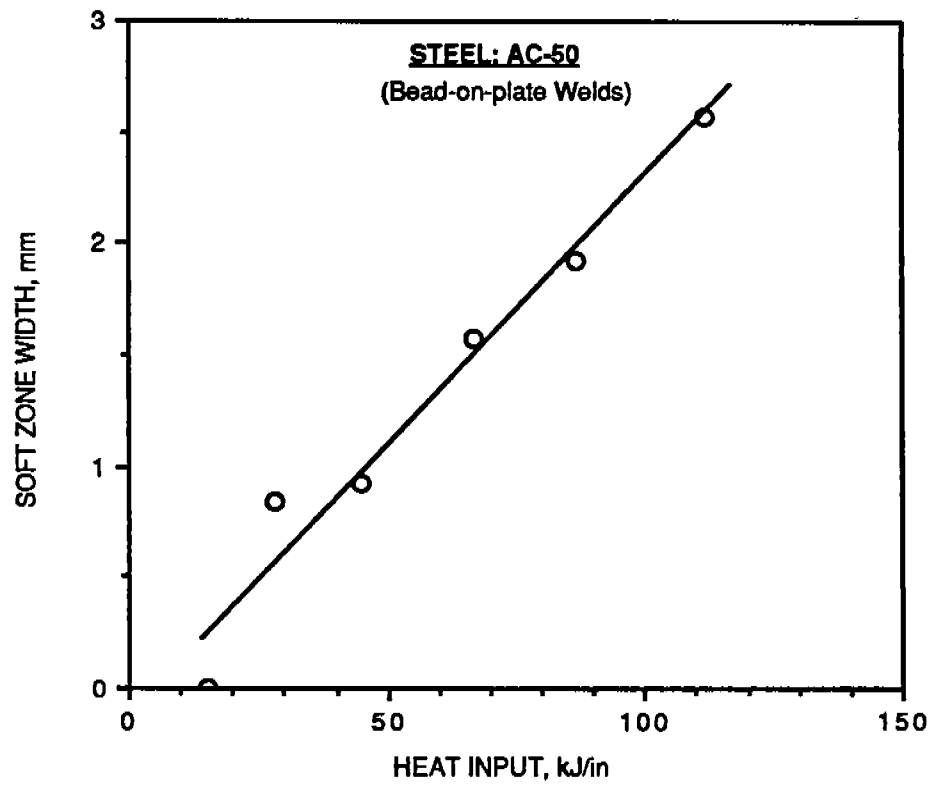Fig. B-24.   Variation of decrease in HAZ hardness with heat input for DQ-80

227
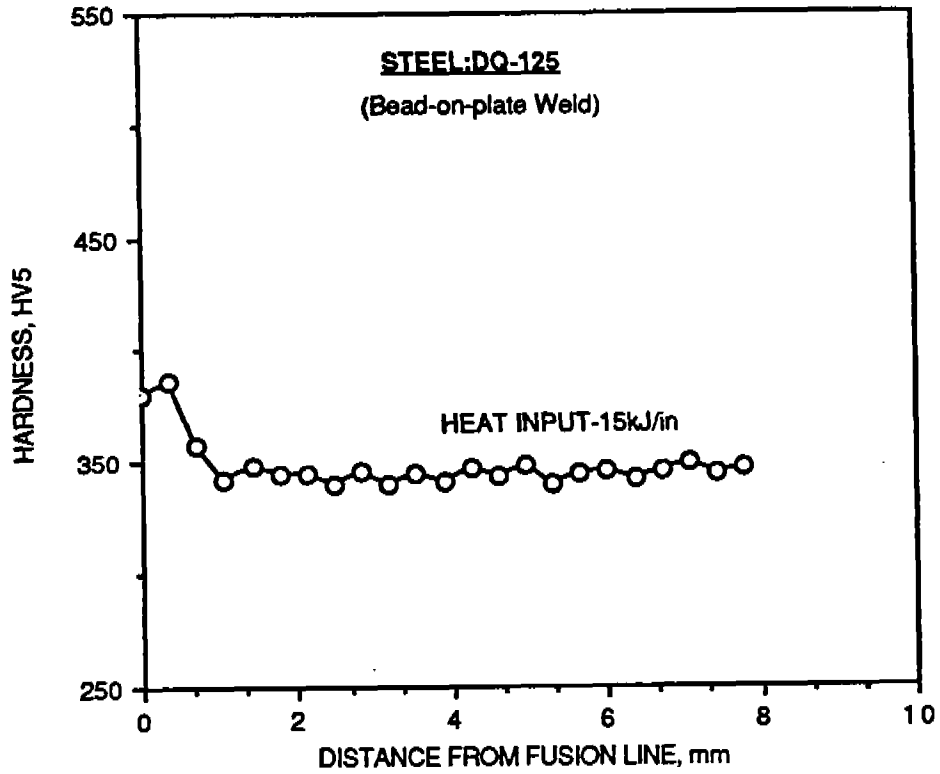
Fig. B-25.   HAZ hardness profile. Steel :   DQ-125. Heat Input : 15 kJ/in
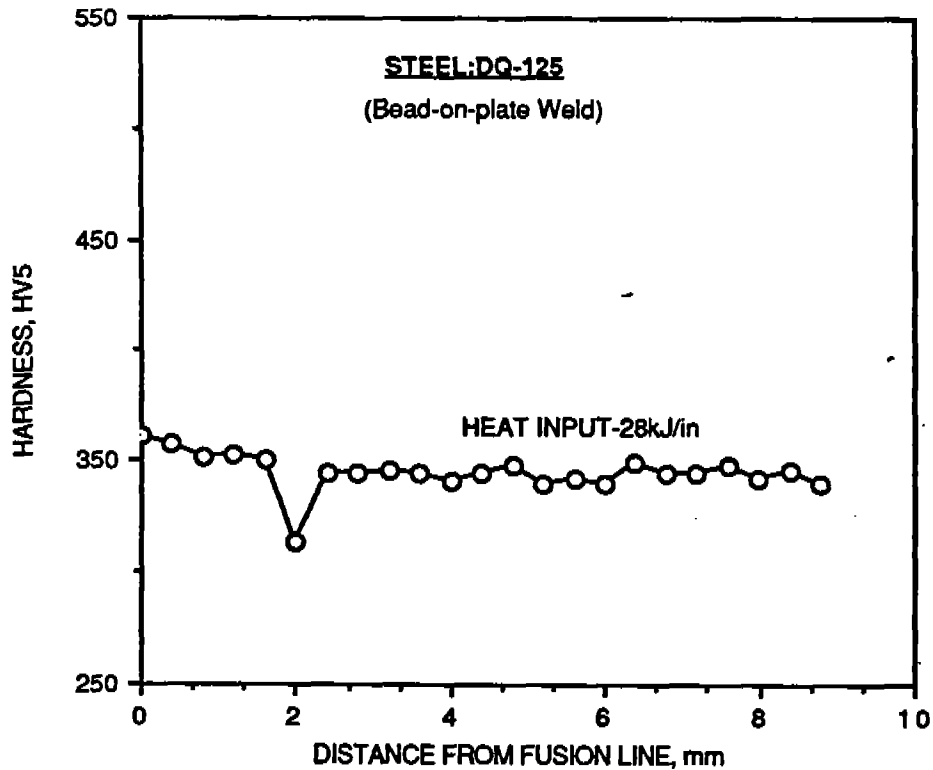
Fig. B-26.   HAZ hardness profile. Steel :   DQ-125. Heat Input : 28 kJ/in

228
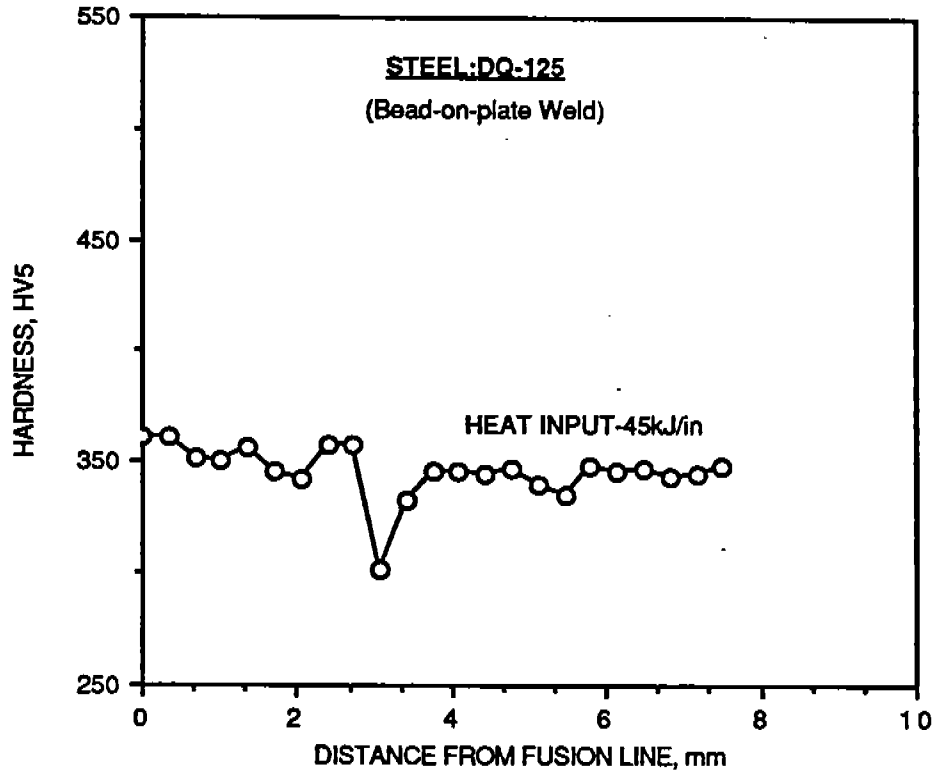
Fig. B-27.   HAZ   hardness   profile. Steel :   DQ-125. Heat   Input : 45 kJ/in
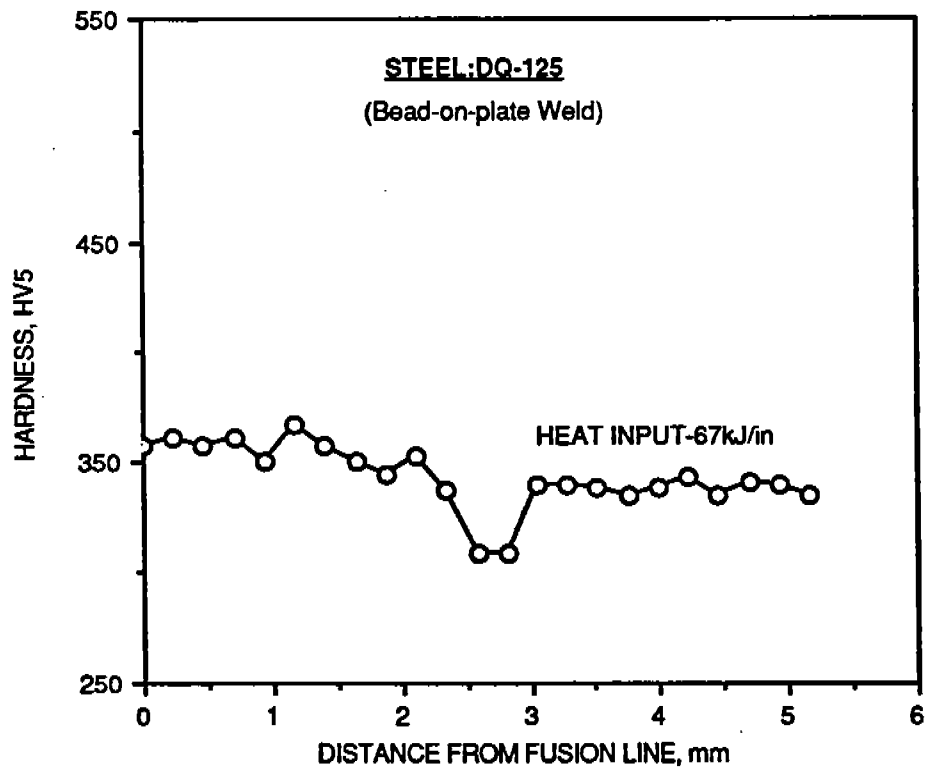
Fig. B-28.   HAZ   hardness   profile. Steel :   DQ-125. Heat   Input : 67 kJ/in

229
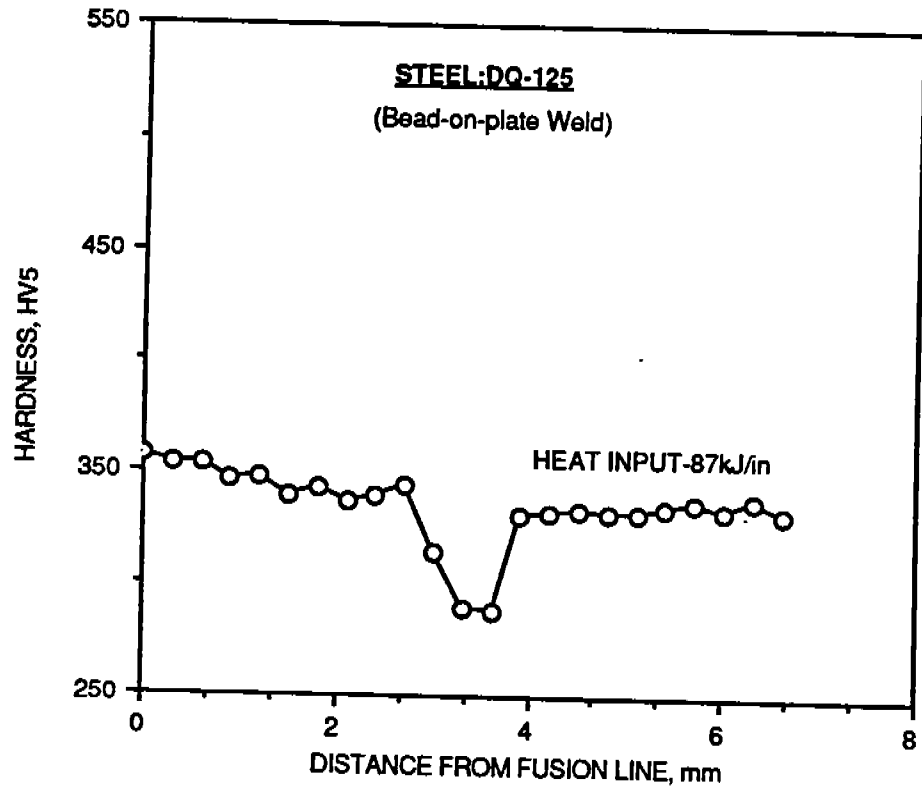
Fig. B-29. HAZ hardness profile. Steel : DQ-125 Heat Input : 87 kJ/in
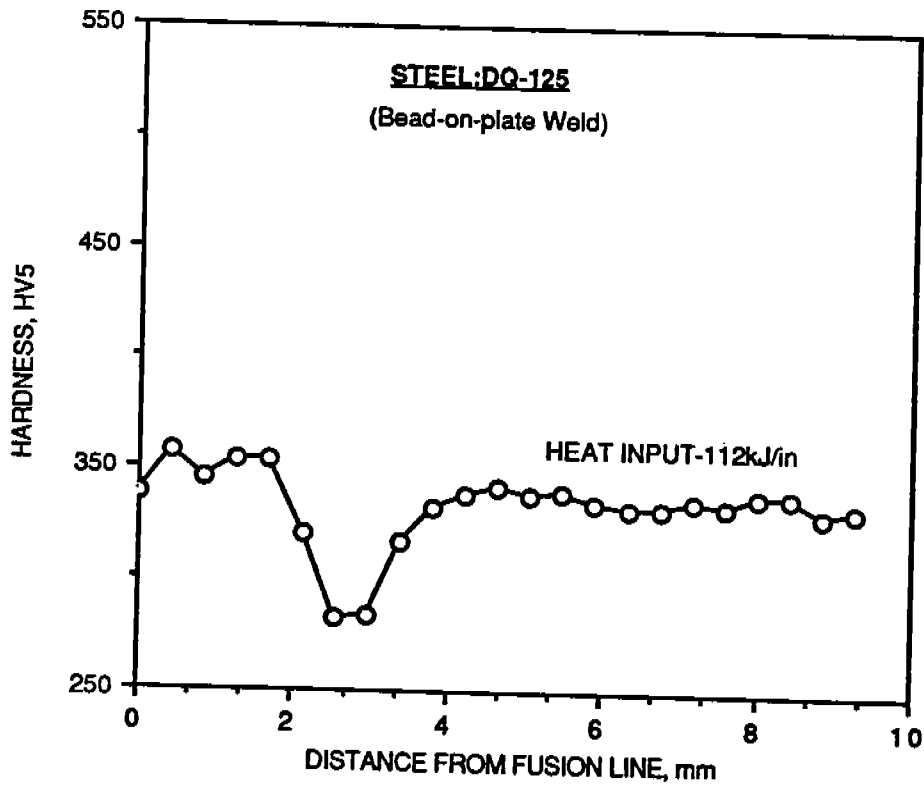
Fig. B-30. HAZ hardness profile. Steel : DQ-125. Heat Input : 112 kJ/in

230
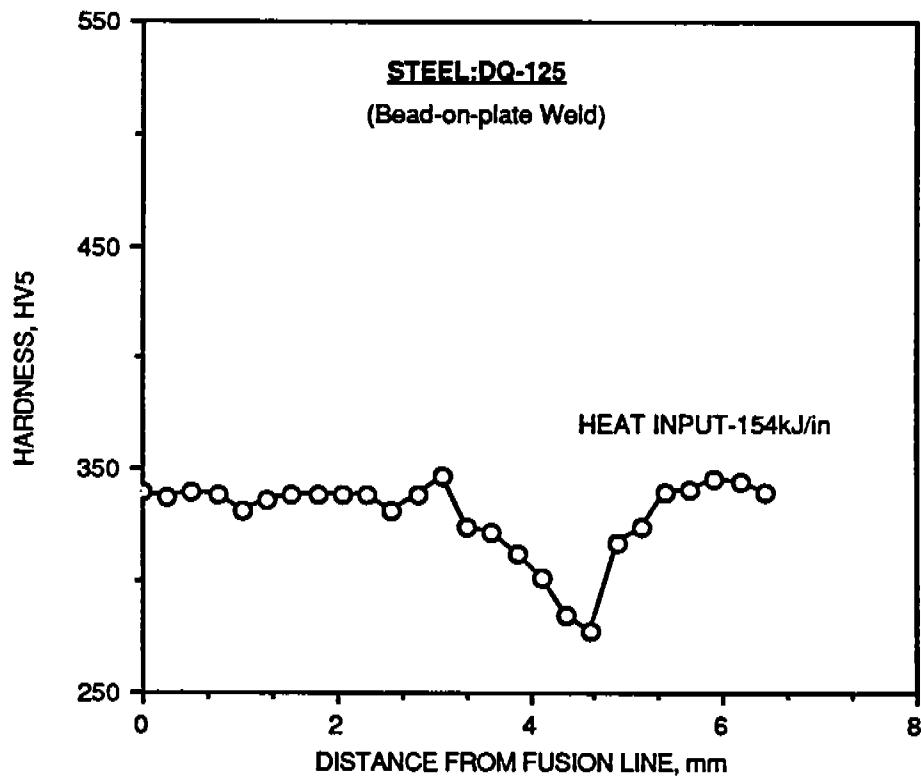
Fig. B-31.   HAZ hardness profile. Steel :   DQ-125. Heat Input : 154 kJ/in

Fig. B-32.   Variation of soft zone width with heat input for   DQ-125

Fig. B-33.   Variation of decrease in HAZ hardness with heat input for DQ-125

232

Fig. B-34.   HAZ   hardness   profile. Steel :   AC-50. Heat   Input : 15 kJ/in
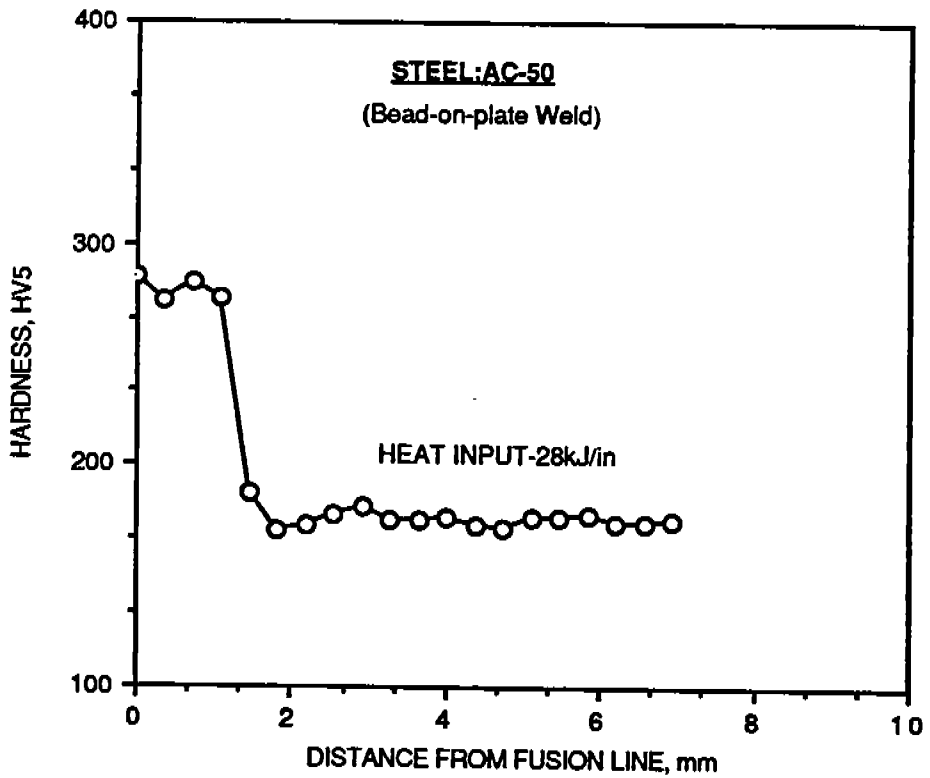
Fig. B-35.   HAZ   hardness   profile. Steel :   AC-50. Heat   Input : 28 kJ/in
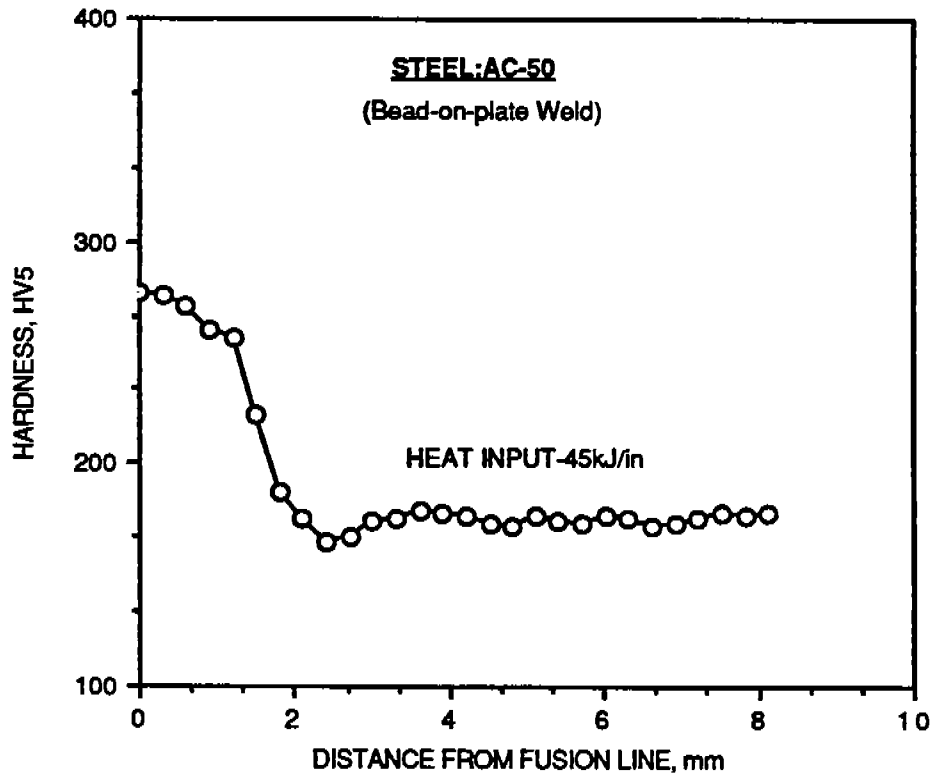
Fig. B-36.   HAZ hardness profile. Steel :   AC-50. Heat Input : 45 kJ/in

Fig. B-37.   HAZ hardness profile. Steel :   AC-50. Heat Input : 67 kJ/in

Fig. B-38. HAZ hardness profile. Steel : AC-50. Heat Input : 87 kJ/in

Fig. B-39. HAZ hardness profile. Steel : AC-50. Heat Input : 112 kJ/in

235

Fig. B-40. Variation of soft zone width with heat input for AC-50

Fig. B-41. Variation of decrease in HAZ hardness with heat input for AC-50

236

Fig. B-40.   Variation of soft zone width with heat input for   AC-50

Fig. B-41.   Variation of decrease in HAZ hardness with heat input for AC-50

237

SHIP STRUCTURE COMMITTEE PUBLICATIONS

SSC-341   Global Ice Forces and Ship Response to Ice by P. Minnick,
           J. W. St. John, B. Cowper, and M. Edgecomb   1990

SSC-342   Global Ice Forces and Ship Response to Ice - Analysis of
           Ice Ramming Forces by Yung-Kuang Chen, Alfred L. Tunik,
           and Albert P-Y Chen   1990

SSC-343   Global Ice Forces and Ship Response to Ice - A Second
           Season by P. Minnick and J. W. St. John   1990

SSC-344   Development of an Onboard Strain Recorder by Eric Greene
           and William A. Wood   1987

SSC-345   Elastic-Plastic Fracture Mechanics by T. L. Anderson   1990

SSC-346   Fatigue Characterization of Fabricated Ship Details -
           Phase 2 by K. K. Park and F. V. Lawrence, Jr.   1988

SSC-347   Strategies for Nonlinear Analysis of Marine Structures by
           Subrata K. Chakrabarti   1988

SSC-348   Corrosion Experience Data Requirements by Karl A.
           Stambaugh and John C. Knecht   1988

SSC-349   Development of a Generalized Onboard Response Monitoring
           System (Phase I) by F. W. DeBord, Jr. and B. Hennessy
           1987

SSC-350   Ship Vibration Design Guide by Edward F. Noonan   1989

SSC-351   An Introduction to Structural Reliability Theory by
           Alaa E. Mansour   1990

SSC-352   Marine Structural Steel Toughness Data Bank by J. G.
           Kaufman and M. Prager   1990

SSC-353   Analysis of Wave Characteristics in Extreme Seas by
           William H. Buckley   1989

SSC-354   Structural Redundancy for Discrete and Continuous Systems
           by P. K. Das and J. F. Garside   1990

SSC-355   Relation of Inspection Findings to Fatigue Reliability by
           M. Shinozuka   1989

SSC-356   Fatigue Performance Under Mulotiaxial Load by Karl A.
           Stambaugh, Paul R. Van Mater, Jr., and William H. Munse
           1990

None   Ship Structure Committee Publications - A Special
           Bibliography   1983